Construction, Monitoring, and Performance of Two Soil Liners

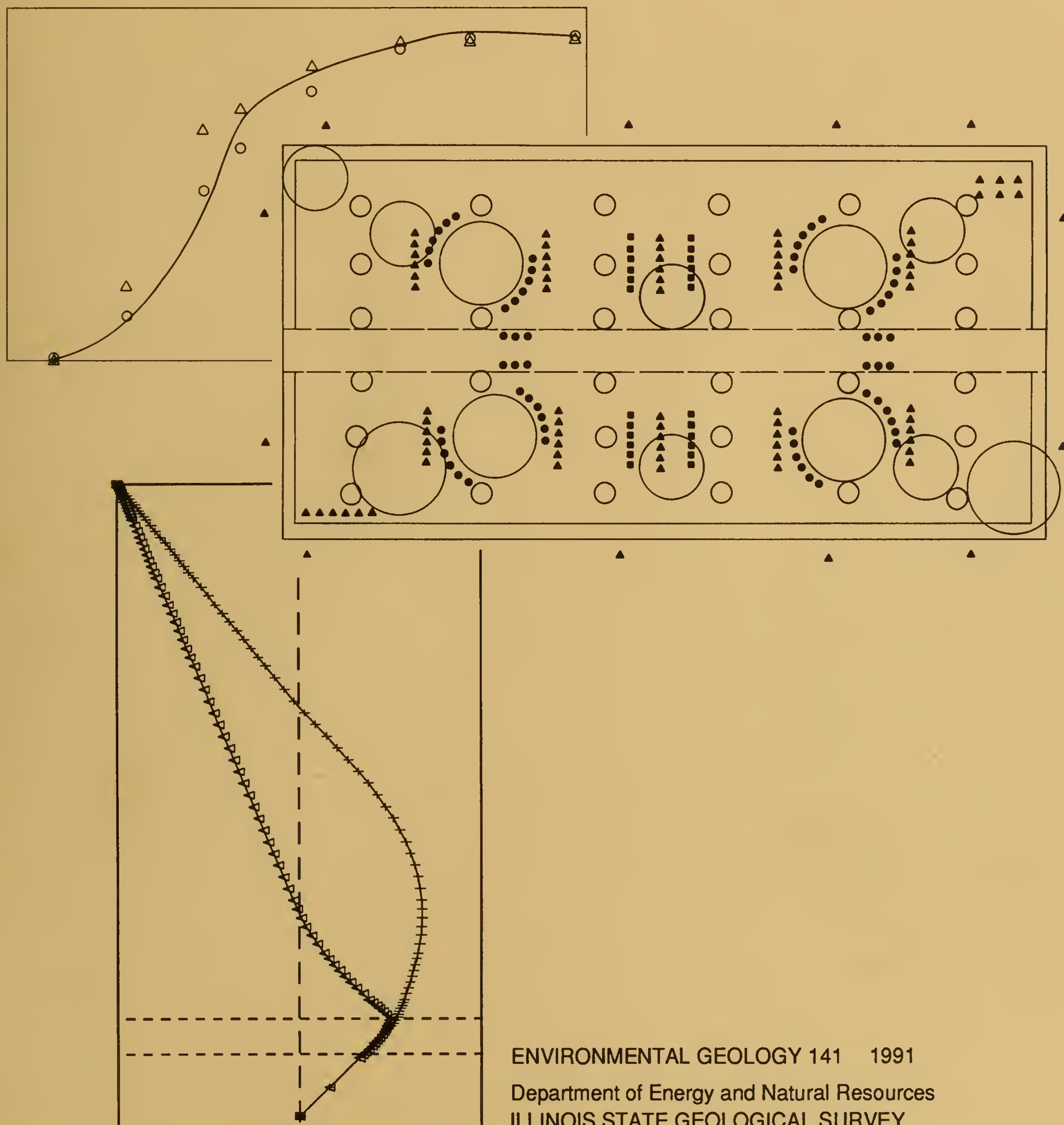

ENVIRONMENTAL GEOLOGY 141 1991

Department of Energy and Natural Resources
ILLINOIS STATE GEOLOGICAL SURVEY

Construction, Monitoring, and Performance of Two Soil Liners

Ivan G. Krapac
Keros Cartwright
Bruce R. Hensel
Beverly L. Herzog
Timothy H. Larson
Samuel V. Panno
James B. Risatti
Wen-June Su
Illinois State Geological Survey
Kenneth R. Rehfeldt
Illinois State Water Survey

Prepared in cooperation with

U. S. Environmental Protection Agency,
Risk Reduction Engineering Laboratory, Cincinnati, OH
(contract EPA-CR-812650)

Illinois Hazardous Waste Research
and Information Center, Champaign, IL

ENVIRONMENTAL GEOLOGY 141 1991

ILLINOIS STATE GEOLOGICAL SURVEY
Morris W. Leighton, Chief

Natural Resources Building
615 East Peabody Drive
Champaign, IL 61820

CONTENTS

CONTENTS *continued*

CONTENTS *continued*

TABLES

TABLES *continued*

FIGURES

FIGURES *continued*

Printed by authority of the State of Illinois / 1991 / 1200

ABSTRACT

A prototype and large-scale soil liner were constructed to test whether compacted soil barriers in cover and liner systems could be built to meet the standard set by the U.S. Environmental Protection Agency for saturated hydraulic conductivity ($\leq 1 \times 10^{-7}$ cm/s). In situ ponded infiltration rates into the prototype liner were measured using two large (1.5 m in diameter) sealed double-ring infiltrometers. A steady flux, averaging 1.5×10^{-7}, was achieved 2 to 3 weeks after the infiltration experiment began. The saturated hydraulic conductivity of the liner was estimated from the infiltration data to be no more than 3.6×10^{-8} cm/s.

Water containing fluorescein and rhodamine WT dyes was allowed to infiltrate into the prototype liner for 46 days. Dye patterns observed during excavation of the liner indicated that lateral flow occurred between lifts and along soil clod-clod interfaces. Although the liner met the USEPA conductivity requirement, the dye flow paths indicated a need for better bonding between lifts and a reduction in soil clod sizes. These observations suggested that if soil liners are to perform according to design specifications, soil processing prior to construction and rigid construction QA/QC are necessary.

The large-scale liner ($7.3 \times 14.6 \times 0.9$ m) consisted of six 15-cm compacted lifts. Full-scale equipment was used for compaction, and construction practices were modified on the basis of experience gained from the prototype liner study. The liner was compacted at an average moisture content of 11.5 percent, which was 1.5 percent wet of optimum, as determined by the Standard Proctor test. The mean dry density of the liner was 1.84 g/cm^3, which was 93 percent of the maximum Standard Proctor density.

After 1 year, initial estimates of saturated hydraulic conductivities were 3.3×10^{-9}, 5.3×10^{-8}, and 6.7×10^{-8} cm/s, based on measurements of water infiltration into the liner by large-ring and small-ring infiltrometers and a water-balance analysis, respectively. Measurements of soil tension by pressure-transducer tensiometers indicated that the wetting front had reached a depth greater than 20 cm.

Small variances in infiltration flux, as measured using small-ring infiltrometers, suggest that the liner is homogeneous with respect to infiltration fluxes. The predictions of water and tracer breakthrough at the base of the liner range from 2.4 to 12.6 years, depending upon the method of calculation and assumptions made. To date, water breakthrough has not been confirmed. The work conducted so far indicates that compacted soil barriers can be constructed to meet the saturated hydraulic conductivity requirement established by the USEPA.

Questions regarding methodologies to collect in situ infiltration data have arisen from the research. Differences have been noted in infiltration fluxes, as measured by different types of infiltrometers. Perturbations in measurements of infiltration rates and soil tensions have been correlated with barometric pressure fluctuations and/or temperature changes in the liner. Continued monitoring of the liner and further laboratory and field research may explain these observations.

ACKNOWLEDGMENTS

The U.S. Environmental Protection Agency, Risk Reduction Engineering Laboratory (cooperative agreement CR812650), and the Illinois Hazardous Waste Research and Information Center (contracts HWR 88-047 to 91-047) provided partial support for this study. We are grateful to staff members of the Illinois State Geological Survey who assisted during the construction and provided technical support throughout the project. Dr. David Daniel and Dr. Andrew Rogowski donated the infiltrometers and furnished helpful advice on the installation and operation of instruments. Waste Management of North America, American Colloid Company, Gundle Lining Systems Inc., and Clem Environmental Corporation generously donated personnel, materials, and equipment.

DISCLAIMER

This report was prepared by the Illinois State Geological Survey (ISGS) and the Illinois State Water Survey, Champaign, Illinois. The project was funded in part by the U.S. Environmental Protection Agency (USEPA) under assistance agreement (CR812650). The USEPA provided administrative and peer review and approved this document for publication by the ISGS. Mention of trade names or commercial products does not constitute endorsement or recommendation for use.

INTRODUCTION

Compacted soil liners are widely used at landfill and waste lagoon facilities for containing leachates and liquid wastes. The liner functions as a barrier between the hydrogeologic environment and the wastes by limiting seepage from these waste facilities. The USEPA requires that landfills or lagoons containing hazardous wastes have a double liner system, a leachate collection and leak detection system, and two flexible membrane liners, all underlain by a compacted soil liner. Disposal requirements for municipal refuse are less stringent than those applying to hazardous waste: naturally occurring or recompacted soil materials usually are permitted to be used as the sole liner in municipal landfills. However, more rigorous landfilling requirements for municipal wastes may be adopted by individual states in the near future. The Resource Conservation and Recovery Act (RCRA) requires that the earthen part of the liner must be at least 0.9 meters thick and have a saturated hydraulic conductivity of no more than 1×10^{-7} cm/s (USEPA 1987).

Little research has been conducted to evaluate the performance of field-scale compacted soil liners (USEPA 1988a). Detailed field-scale experiments of soil liners were conducted by Rogowski (1990) and Elsbury et al. (1990). Rogowski studied the spacial variability of a soil liner's hydraulic properties, Elsbury focused on soil properties, construction equipment, and laboratory testing conditions in building soil liners. (The emphasis of these studies was not on constructing a soil liner with the lowest possible hydraulic conductivity.) The liners constructed during the studies failed to meet the minimum USEPA requirement for hydraulic conductivity; measurements yielded hydraulic conductivities of 5×10^{-7} (Rogowski 1990) and 1×10^{-4} cm/s (Elsbury et al. 1990). Currently used full-scale equipment was not used in one fo the studies, and recommended liner construction guidelines were not implemented in the other study. However, these studies have provided useful information about soil clod size, moisture content, and the size of construction equipment—information currently being used in the construction of liners.

Daniel and Brown (1988) compiled a table of 14 case studies of earthen liners constructed throughout the United States and Canada. Only two met the USEPA hydraulic conductivity requirement of 1×10^{-7} cm/s or less. The two successful liners were the Keele Valley Landfill in Ontario (Daniel and Trautwein 1986) and a test liner in California (Chen and Yamamoto 1987). A rigorous quality assurance program was followed during the construction of both liners. Daniel and Brown (1988) suggested five common causes for the failure of liners to meet the hydraulic conductivity criteria: (1) the liners were too thin; 2) they were constructed improperly (i.e., poor material selection and/or inadequate design; (3) inadequate quality assurance was maintained during construction; (4) desiccation and freezing occurred during construction; and (5) chemical constituents in the waste affected the permeability of the soil.

In some of the studies, laboratory tests indicated that liner materials could be compacted to the required hydraulic conductivity. Increasing evidence shows that laboratory measurements of hydraulic conductivity tend to be lower than the values based on field data (Daniel 1984, Herzog and Morse 1986, USEPA 1988a).

Sources of potential error in laboratory tests of hydraulic conductivity, as discussed by Olsen and Daniel (1979), include (1) compaction and water content greater in laboratory samples than in field samples; (2) air trapped in laboratory samples; (3) excessive hydraulic gradients used in the laboratory, causing particle migration; and (4) the size of laboratory samples being too small. Other researchers have also been concerned with the issue of confidence in laboratory-derived results of hydraulic conductivity of soils related to size and number of samples (Mason et al. 1957, Anderson and Bouma 1973, Daniel 1981). The importance of hydraulic gradient in laboratory tests of hydraulic conductivity has been investigated by Mitchell and Younger (1967), Daniel (1981), Zimmie et al. (1981), Brown and Anderson (1982), Acar and Field (1983), and

Foreman (1984). Another long-standing concern has been the difficulty of achieving saturation of samples (Smith and Browning 1942).

Studies by Dunn and Mitchell (1984) suggested that present laboratory methods may yield variations of hydraulic conductivity up to several orders of magnitude for a single soil type. They proposed a test procedure that would yield consistent results. Daniel et al. (1984) described a method using a flexible-wall permeameter to eliminate problems of sidewall leakage, and discussed the relative merits of flexible- and fixed-wall permeameters.

In September 1985, in response to concerns about the safety of landfills and the lack of data on the performance of landfill liners, the Illinois State Geological Survey (ISGS) began a multiyear study to develop a database on the performance of a field-scale soil liner using in situ measurements made during construction (e.g., soil density, moisture content) and hydrogeologic parameters (e.g., infiltration rates, moisture movement). Specific overall objectives of this study, being conducted under a cooperative agreement (EPA-CR812650-01) with the USEPA, are to

- determine whether the USEPA requirement for a saturated hydraulic conductivity (measured in situ) of 1×10^{-7} cm/s or less can be achieved;
- quantify the areal variability of liner hydraulic properties;
- determine the transit times of water and tracers through a compacted soil liner (that is, when breakthrough of contaminants will occur);
- test the accuracy of methods to predict the transit time of water and tracers through the liner.

The study was divided into three phases. Phase 1, which began in September 1985, included (1) an evaluation of the properties that make soils suitable for use in landfill liners, and (2) the characterization and selection of a soil for use in this project. Phase 2, which began in October 1986, provided for the construction of a prototype liner to test construction practices and determine whether the hydraulic conductivity requirement could be met using the soil selected. Phase 3, which began in October 1987, involved the construction and monitoring of a field-scale soil liner. This extensively instrumented liner continues to be monitored.

Chapters 1 and 2 of this report incorporate the results of the Phase 1 and 2 studies. Chapters 3 and 4 detail the construction of the field-scale liner, and Chapters 5 to 9 report the results of the first year of monitoring the field-scale liner.

Literature reviews and information sources pertaining to construction and evaluation of liners are available in USEPA (1979, 1988a, 1988b, 1990), Ely et al. (1983), Rogowski (1990), Rowe (1990), and Quigley (1990).

SUMMARY AND RECOMMENDATIONS

Although the study has been in progress since October 1985, the main phase—monitoring of the field-scale soil liner to determine the time required for water to break through—is not yet complete. The pond above the liner was filled on April 12, 1988; current data and observations and model projections indicate that monitoring will have to continue for a minimum of 2 more years before water breakthrough occurs in the field-scale liner. It is therefore premature to draw many conclusions or make recommendations. The findings from Phases 1, 2, and 3 can be summarized, however, and the implications and recommendations derived from these findings can be presented.

Results

■ Soil Selection

Qualitative selection criteria were established to evaluate three tills from five locations as potential materials from which to construct soil liners. Numerical criteria were assigned to these soil properties: hydraulic conductivity, Atterberg limits, particle-size distribution, natural moisture content, and dry density. The hydraulic conductivity criterion eliminated one potential soil material. The Atterberg limits (plasticity index) was relaxed because none of the materials achieved a plasticity index greater than 10 percent. However, subsequent sampling and testing of the actual soil (Batestown till) used in construction showed that the soil did achieve a plasticity index greater than 10 percent. Monitoring of the soil densities and infiltration fluxes indicated that relaxation of this criterion did not result in problems for liner construction or performance. The soils satisfied the remaining criteria. Other soil properties evaluated (dispersivity, clay mineralogy, specific gravity, cation exchange capacity) were not significantly different in the three tills, and thus were inconclusive as selection criteria. The final selection decision was based on economic factors because of the similarity in soil properties.

■ Prototype Liner

Full-scale equipment was used to construct the prototype liner. Engineering properties (moisture content and density) of the liner appeared to be relatively homogeneous. Coefficients of variation indicated that moisture content varied more than density in the liner. Densities of 90 percent of maximum, as determined by Standard Proctor tests, were achieved at moisture contents approximately 1 to 2 percent above optimum.

Double-ring infiltrometers, pressure-vacuum lysimeters, and tensiometers were used to monitor the prototype liner. Infiltration rates measured by two 1.5-m diameter double-ring infiltrometers for a 50-day period produced the following results (assuming a Green-Ampt infiltration model).

- The saturated hydraulic conductivity of the prototype liner was no greater than 3.6×10^{-8} cm/s, meeting the USEPA hydraulic conductivity requirement for soil liners (no greater than 1×10^{-7} cm/s).

- An average constant infiltration flux of 1.5×10^{-7} cm/s was achieved 2 to 3 weeks after the infiltration experiments began.

- Wetting-front depths of 7.3 and 9.6 cm were calculated from infiltration volumes for each infiltrometer after 46 days of infiltration.

- Transit time for the wetting front to reach the bottom of the liner was predicted, on the basis of infiltrometer data, to be about 3 years.

- Fluorescein and rhodamine WT dye patterns in the liner indicated that lateral flow had occurred between lifts as well as along clod-clod interfaces. The dye tracer front observed when the prototype liner was excavated showed a sharp front at 4 cm.

- Morphological studies indicated that variable compaction (hard and soft layers of soil) had occurred within lifts.

- Horizontally installed instruments may create preferential flow paths that allow seepage of water at lift interfaces. These instruments may be damaged during compaction.

- **Field-Scale Liner**

The field-scale liner (7.3 × 14.6 × 0.9 m) was constructed with full-scale equipment, and construction practices were modified on the basis of experience gained from the prototype liner study. The liner was compacted at an average moisture content of 11.5 percent—1.5 percent wet of optimum as determined by the Standard Proctor test. The mean dry density of the liner was 1.84 g/cm^3—93 percent of the maximum Standard Proctor density.

The field-scale experiment began in April 1988 when the pond located on the liner was filled; 212 instruments (including tensiometers, gypsum blocks, pressure-vacuum lysimeters, and ambient environmental monitors) were used to measure various parameters in and around the liner. Infiltration rates were measured with large- and small-ring infiltrometers and a water balance for the liner.

At the beginning of the experiment, the tracers—bromide, *m*-TFMBA, *o*-TFMBA and PFBA—were added to the large-ring infiltrometers to monitor movement of water and solutes through the liner. Analysis of the first year of monitoring has provided the following information.

Infiltration properties

- Average infiltration fluxes were 7.9×10^{-8} cm/s, 5.0×10^{-9} cm/s, and 1.0×10^{-7} cm/s for the small-ring infiltrometers, large-ring infiltrometers, and pond-water balance, respectively.

- Flux data from the infiltrometers formed two statistically distinct populations. The small-ring infiltrometer data calculated from cumulative infiltration curves formed a lognormal distribution; the large-ring infiltrometer data consisted only of four widely scattered datum points.

- Geostatistical analysis (Kriging) of the small-ring infiltrometer flux data estimated a mean infiltration flux for the entire liner of 7.1×10^{-8} cm/s. Kriged estimates of infiltration fluxes for each quadrant of the liner ranged between 6.7×10^{-8} and 7.1×10^{-8} cm/s.

- An isotropic exponential variogram was found to best model the spatial relationship of the small-ring infiltrometer fluxes. Flux data are spatially uncorrelated at measurement distances greater than 1.3 m. This analysis and the small variances exhibited by the flux data suggest that the liner is homogeneous with respect to infiltration fluxes.

- Cumulative infiltration curves for the small-ring infiltrometers provided the best estimate of the steady infiltrability. These curves also revealed irregularities in infiltration rates that were interpreted as the result of leakage, changes in pond level, changes in barometric pressure, and changes in hydraulic conductivity of the liner itself.

- The remedial actions required during construction of the field-scale liner were reflected in the infiltration rates of six of the small-ring infiltrometers. Those infiltrometers adjacent to areas where slumping and dilation fractures formed had the highest infiltration rates.

- Hydraulic gradients in the field-scale liner fluctuated between 1.1 and 1.7. When steady-state conditions are achieved in the liner, the gradient should be approximately 1.3.

Saturated hydraulic conductivity of field-scale liner

- Hydraulic conductivities calculated using Darcy's law were 5.3×10^{-8} cm/s, 3.3×10^{-9} cm/s, and 6.7×10^{-8} cm/s for the small-ring infiltrometer, large-ring infiltrometer, and liner water-balance data sets, respectively.

- Hydraulic conductivities calculated using the Green-Ampt infiltration model were 3.8×10^{-8} cm/s, 2.4×10^{-9} cm/s, and 4.7×10^{-8} cm/s for the small-ring infiltrometer, large-ring infiltrometer, and liner water-balance data sets, respectively.

- All saturated hydraulic conductivities, regardless of the method of calculation or data set used, were below the USEPA maximum of 1.0×10^{-7} cm/s. The consistency and reproducibility of these data among the four quadrants of the liner indicated that the regulatory requirement for the saturated hydraulic conductivity was achievable.

Predictive methods (modeling)

- Fluid flow in the liner and drainage layer was numerically simulated using the one-dimensional unsaturated flow and transport models, SOILINER and CHEMFLO.

- The numerical code of SOILINER was used to calculate the relationship between flux and hydraulic conductivity. When observed flux data were inserted into the model, a corresponding hydraulic conductivity of 5.1×10^{-8} cm/s was obtained; this value is similar to the hydraulic conductivity values of 5.3×10^{-8} cm/s (calculated using Darcy's law) and 3.8×10^{-8} (calculated using the Green-Ampt model) from the small-ring infiltrometer data.

- Transit times were calculated by three of the analytical methods provided in the USEPA Technical Resource Document on liner design, construction, and evaluation; the results for each indicate the earliest time at which water is calculated to exit the bottom of the field-scale liner. The simple transit-time equation, which assumes steady-state saturated conditions, predicted the transit time to be 5.5 years. The modified transit-time equation, which adds suction at the base of the liner to the simple transit-time equation, predicted water breakthrough at 3.7 years. The Green-Ampt infiltration model predicted a transit time of 1.3 years. All these predictions assume that effective porosity equals total porosity and ignore dispersion and diffusion parameters.

- SOILINER predicted chemical breakthrough at 12.6 years, an unrealistic prediction. The model does not consider effects of effective porosity, dispersion, diffusion, attenuation, and reaction; therefore, meaningful contaminant transport results were difficult to generate with SOILINER.

- CHEMFLO predicted breakthrough of the tracers between 2.5 and 4.6 years. Because this model does not account for effective porosity, it may have overpredicted the time necessary for breakthrough to occur. The liner has not been ponded for that length of time, thus the accuracy of the model prediction cannot be judged.

- Flux and gradient values calculated by the flow and transport model were comparable to the fluxes and gradients observed in the liner. However, the model predicted steady state by 0.5 years, and the actual liner had not achieved steady state after an interval of more than 1 year. This difference is attributed to the models overestimating unsaturated hydraulic conductivity as a function of tension.

- The large fluctuation in heads and gradients may indicate that much of the liner is tension saturated and has a significant percentage of air in the soil pores. The liner has not reached steady state, so drainage from the base of the liner is not likely to be occurring. (Water has not been collected from the drains beneath the liner, a fact confirming that steady-state conditions have not been achieved.)

- Perimeter tensiometer data showed no evidence of lateral flow of water from the liner study area.

Environmental effects on instruments and liners

- Gypsum blocks buried in the liner did not provide meaningful data because the liner was initially at a soil-moisture content wetter than the designed working range of these instruments. Therefore, we conclude that gypsum blocks are inadequate for monitoring moisture movement in liner systems.

- Tension/head data in the liner appeared to be affected by atmospheric pressure and temperature fluctuations. Even after correcting for barometric pressure variation, we observed a cyclic pattern of pressure head: it is greatest in the summer and lowest in the winter. An increasing time-lag with depth in the liner indicated that the cyclic rise and fall of pressure head was at least partly caused by temperature changes in the liner.

- The effects of temperature and atmospheric pressure on the tension data made exact measurements of a wetting-front depth impossible. The apparent reaction of head values to the changes in temperature suggested that the liner was saturated to a depth greater than 20 cm, tension-saturated to a depth of a least 70 cm, and unsaturated at its base.

- The gage tensiometers located around the perimeter of the field-scale liner appeared to be affected by both temperature and barometric pressure. The trends in these tensiometers were similar to those observed in the pressure-transducer tensiometers.

Tracers

- Soil-water samples collected from the lysimeters in the field-scale liner 8 months after ponding showed that the tracers had not migrated vertically or laterally in sufficient concentration to be detected. One- and two-dimensional transport modeling confirmed that the tracers should not be detectable in the soil-water samples.

- Tracer data suggested that no preferential, lateral flow paths exist in the liner, either because they were eliminated during liner construction or were not intersected by the sampling devices.

- Laboratory batch adsorption results indicated that the tracers Br, *m*-TFMBA, *o*-TFMBA and PFBA were conservative; they did not sorb to the liner soil, nor did they appear to degrade with time. Microbial activity during the course of laboratory column studies did not alter the flow rates of water through the columns.

- Chemical interference in high-pressure liquid chromatography (HPLC) methods make the analytical detection of the tracers difficult at low concentration levels. Thus, the viability of using HPLC analytical methods for these tracers to monitor water flow in liner systems is questionable. Tritium was added to the pond in July 1989 to further study the movement of conservative tracers.

Preliminary Recommendations

Our experience on this project, a review of the literature, and direct observation of commercial liners have increased our concerns about the quality of liners in use today.

Construction of a soil liner is the most critical phase. Engineering geology practices are adequate for sampling and selecting of borrow materials used in construction of soil liners. The properties of the soil used to construct the field-scale liner deviated from initial predictions (based on field sampling) by less than 10 percent; densities were slightly less than estimated and plasticity indexes were slightly higher than estimated by the material selection process. The higher-than-estimated plasticity indexes may have resulted partly from the method of soil preparation.

Soil properties must be strictly specified and quality control rigidly maintained to ensure that a soil liner will be constructed to perform according to design criteria. Specifications for an acceptable soil must include not only a maximum value for laboratory and/or in situ hydraulic conductivity, but should also include moisture content at time of compaction, maximum clod size, and minimum density and plasticity requirements.

Soil moisture contents should be 1 to 3 percent wet of optimum, as determined by a Standard Proctor test. Liner materials should be processed before liner construction to ensure a uniform moisture content, reduce clod size to less than 5 cm in diameter, and remove all stones greater than 5 cm in diameter and as many smaller stones as practical.

Construction equipment must be large enough to fully compact the entire thickness of the lifts, and compactor feet must be at least as long as the compacted thickness of each lift and preferably as long as the loose lift plus the thickness of the loose material generated when compacted lifts are scarified. Compaction should continue on each lift until a prescribed minimum density is measured at a reasonable number of locations.

The numerical flow models used in this study are not very robust. SOILINER is particularly weak, in that it does not account well for ion transport. More sophisticated codes could be investigated as a replacement for SOILINER. However, numerical groundwater flow models (SOILINER, CHEMFLO) have been effective tools in analyzing the large data sets generated by this project. Used as predictive tools, they can help increase understanding of the soil-water physics of the liner. They can also indicate areas in which data may be unreliable, imprecise, or lacking. SOILINER simulations of water and tracer movement through the liner have demonstrated that our understanding of the hydraulic conductivity and soil-tension relationship in the liner is weak; however, the models have confirmed that the estimated saturated hydraulic conductivity based on measured infiltration fluxes and gradients is a reasonable value.

Transport rates through the liner can be affected by the physical state of the liner. Tensiometer results suggest that air is entrapped throughout the field-scale liner. The presence of the entrapped air can have significant effects on water movement through the liner. When two fluids such as water and air occupy a pore volume, the effective permeability of the soil to each is decreased. Effective permeability to one fluid may be 0 if no interconnected pores contain that fluid. Thus, the permeability to air may be 0, not allowing the escape of air, yet reducing the effective permeability to water. This condition can exist until the air is totally dissolved. This phenomenon can result in reduced water-transport rates.

However, increased transport rates could also be possible if the air is trapped in small isolated pores and water occupies the large pores. In this case, the reduction in effective permeability to water will be insignificant, but the reduction in effective porosity will increase transport rates. The liner will not reach "true" steady state until all entrapped air is dissolved. The effect of these phenomena on the performance of a soil liner needs to be evaluated.

Even liners that have low hydraulic conductivities can contain preferential pathways through which fluid flow is concentrated. The prototype liner had an estimated hydraulic conductivity of 3.6×10^{-8} cm/s, yet showed significant preferential paths: dyes penetrated 30 cm into the liner during the 50-day test, suggesting that breakthrough could have occurred at the bottom of the liner in less than 6 months. The main pathways were horizontal along lift interfaces. Infrequent fine fractures or other pathways can carry significant amounts of fluid through a liner; the occurrence of these pathways can be reduced only by strict design, construction, and quality control standards.

Measurement of in situ saturated hydraulic conductivity is necessary to determine the adequacy of the liner. Ideally, hydraulic conductivity tests should be performed on each lift after completion. Practically, a minimum of one conductivity test should be conducted on a small test pad constructed using the same QA/QC and design specifications as those used for the full-scale liner. Calculation of the saturated hydraulic conductivity from double-ring infiltrometer data is the most practical field test. Field infiltrometer tests should be conducted until a steady infiltration flux is achieved (so that the actual conductivity can be calculated) rather than just long enough to determine that the saturated hydraulic conductivity was less than the maximum regulatory value.

Soil liners can effectively contain contaminants when they are properly designed and constructed to meet performance expectations. Land burial of wastes is a commonly used waste management strategy. Soil liners are and will continue to be an integral part of many waste management programs. When properly applied, designed, and constructed, soil liners can effectively contain contaminants so that human health and the environment are protected.

1 CHARACTERIZATION AND SELECTION OF A SOIL MATERIAL FOR LINER CONSTRUCTION

The characteristics and performance of a soil liner are a function of the hydrological, geotechnical, and geochemical properties of the soil used in its construction. In Phase 1 of this study, three illite-rich glacial tills from five locations were chosen, on the basis of their anticipated physical characteristics, as potential candidates for construction of a liner. The tills were the Batestown, Snider, and Piatt of the Wedron Formation. The Batestown Till was sampled at three locations because its texture varies from a loam to a silt loam over the sampling area, while the remaining tills were each sampled at one location.

Selection criteria used to identify the most suitable soil for liner construction included saturated hydraulic conductivity, moisture/density relationships, moisture content, Atterberg limits, particle-size distribution, clay mineralogy, soil dispersion, cation exchange capacity, specific gravity, and uniformity. The proximity of the soil to the construction site in Champaign, Illinois, and the availability of the soil were other criteria considered.

Methods

■ Sampling

Two to three bulk samples weighing between 9 and 23 kilograms each were collected at each sampling location; a total of 14 bulk samples were collected from the five sites. Evenly distributed bulk samples were collected from tills that appeared to be texturally uniform over the sampling area. If significant differences occurred in texture, composite bulk samples were taken to incorporate the variations observed. The samples were then sealed in plastic bags to prevent excessive moisture loss.

The field moisture content of each bulk sample was measured immediately after collection. To obtain subsamples, we reduced the clod size of the 14 bulk samples by hand to pass a 4.75-mm sieve (fig. 1). The material greater than 4.75 mm was removed and weighed. The bulk samples were then split with a riffle sample splitter into representative subsamples of appropriate size. At the end of the sample preparation process, the moisture content of the bulk samples was within 0.2 to 2.6 percent of the field moisture content (an average decrease of 1.1 percent).

■ Particle-Size Distribution

Particle-size distribution of the soil samples was determined by standard pipette methods (Guy 1969) and by a Micromeritics® sedigraph X-ray autoanalyzer. The samples were initially separated by wet sieving into the sand (>53 μm) and the fine fractions (<53 μm). The sand-size fraction was air dried, then sieved using standard USGS methods (Guy 1969). Colloidal organic material was removed by heating the samples in chlorine bleach at 80°C.

■ Clay-Mineral Composition

The clay-mineral composition of the clay-sized fraction of the soil samples was determined using a Phillips Norelco® diffractometer with copper Kα radiation and a procedure described in Hughes and Warren (1989). This method used peak-area ratios among expandable clays (such as smectites), illite, and kaolinite combined with chlorite derived from a diffractrogram of an ethylene-glycolated sample. Illite was used as an internal standard and the summation of peak heights was used to derive quantitative estimates of the amount of each general clay type.

■ Moisture Content

The moisture content of the soil samples was determined by the conventional oven-drying method (ASTM D2216 [1982]). Also, a microwave oven method was used as a rapid means of

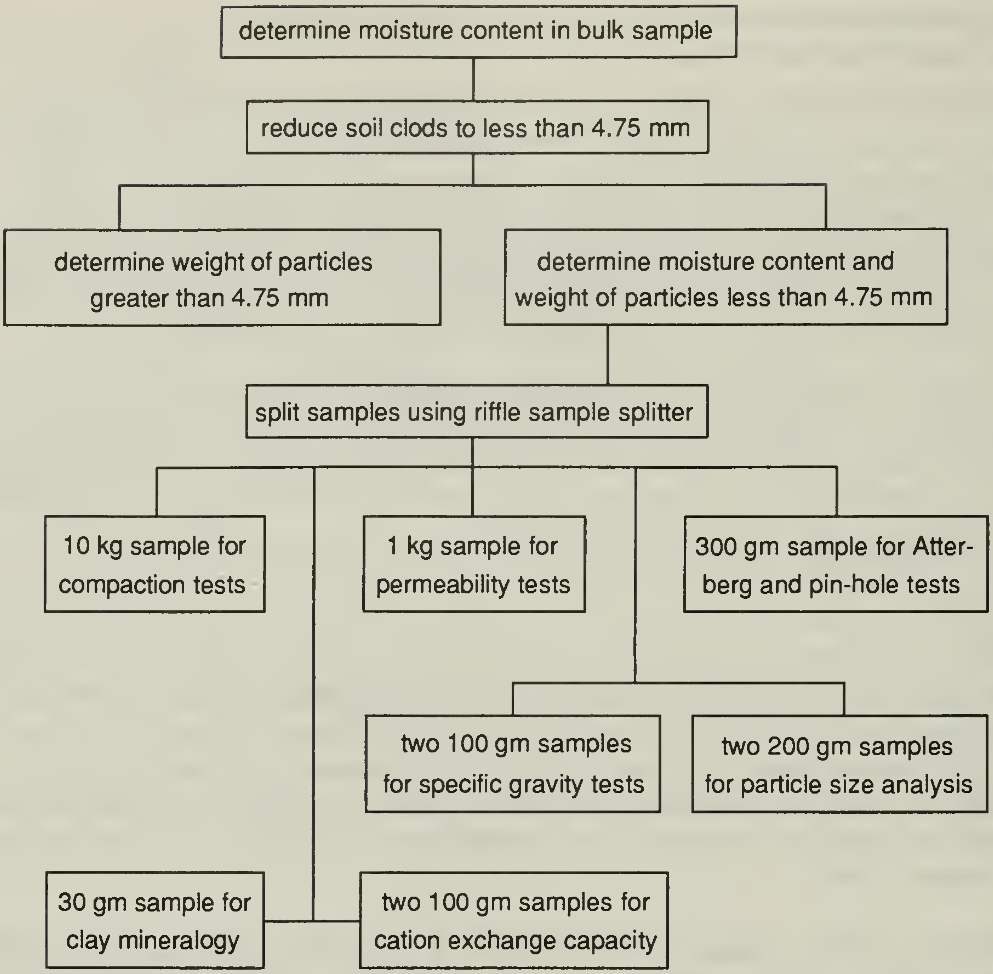

Figure 1 Flow chart for the sample preparation of the potential soil-liner materials.

obtaining moisture contents that could be used for the QA/QC program during liner construction (Lade and Nejadi-Babadai 1976, Carter and Bentley 1986). This method requires that a calibration curve (correlating moisture contents obtained by conventional oven and microwave methods) be developed for each soil.

- **Atterberg Limits, Moisture/Density Relationship**

The liquid and plastic limits and the moisture/density relationship for each soil were determined according to ASTM D4318 and a Standard Proctor compaction test (ASTM D698 A [1991]), respectively.

- **Specific Gravity**

The specific gravity of the soil samples was determined according to methods described by Lambe (1951).

- **Soil Dispersivity/Erodability**

The dispersivity of each soil was determined by double hydrometer and pinhole tests (Sherald et al. 1976). The particle-size distribution of a soil was determined by a standard hydrometer test (ASTM D422) in which the sample was dispersed using strong mechanical agitation and a chemical dispersant in the hydrometer bath. A second hydrometer test was made without strong agitation or a dispersant. The percentage of dispersion was then defined as the ratio of clay-sized particles of 5 µm, as measured in the two tests. The pinhole test involved flowing water through a 1.0-mm diameter hole in a soil that had been compacted using a Harvard miniature compaction method. The soil was considered dispersive if the water rapidly became cloudy and the hole quickly eroded.

■ Saturated Hydraulic Conductivity

Laboratory hydraulic conductivity tests were conducted using a falling-head permeameter that accommodated a small-diameter Harvard-cell sample mold (Herzog and Morse 1986). Samples were reduced to aggregate sizes of less than 2 mm and recompacted to a density duplicating that determined by Standard Proctor compaction tests. The soil sample was then saturated with permeant (tap water) to eliminate any entrapped air, and a known gradient was applied. Effluent from the cell was collected in a manometer, and the change in water level in the manometer was measured. The hydraulic conductivity was calculated on the basis of the area of the sample and the change in water level in the manometer between various measuring intervals.

■ Cation Exchange Capacity

Cation exchange capacity was determined by a sodium-saturation procedure (Jackson 1958, Sobek et al. 1978). Aliquots of a pH 8.2, 1N sodium acetate solution were repeatedly added to soil samples to replace exchangeable cations with sodium. The sodium was then removed from the exchange sites by repeated washings with a pH 7, 1N ammonium acetate solution. The cation exchange capacities of the soil samples were estimated by determining the concentrations of sodium in the NH_4OAc extracts. The exchanged sodium was quantified by inductively coupled argon plasma spectroscopy using a Jarrell-Ash 975 Plasma AtomComp®.

Results and Discussion

A suitable liner material must have the physical and geotechnical properties that limit the amount of leachate seeping from a waste management facility, so that the leachate does not (1) exceed the attenuation capacity of the hydrogeologic environment, and (2) does not enter the groundwater system. Selection of a liner material must balance factors related to environmental safety, construction operation, and economic feasibility. Unfortunately, there are few widely accepted guidelines for selecting a liner material. The principal selection criterion is that the soil can be compacted to achieve a low hydraulic conductivity (1×10^{-7} cm/s). In our study, selection of a suitable soil included (1) identification and sampling of potential borrow sources; (2) physical, geotechnical, and geochemical testing; and (3) evaluation and selection of the most suitable liner material.

■ Screening Criteria and Identification of Potential Borrow Sources

The characteristics of Quaternary deposits near the liner construction site were estimated from soil surveys, geological reports and maps, and engineering documents. On the basis of this information, texture classification, quantity, and uniformity of the soil as well as site accessibility and proximity to the construction site were chosen as criteria for screening potential sources.

Textural classification Soil material used in liner construction should have small clods. Daniel (1984) suggested that the hydraulic conductivity of a compacted soil decreases as the clod size decreases, assuming the same water content and compaction effort. If water must be added to the soil before liner construction to achieve an appropriate moisture content, uneven hydration and dehydration of large clods could result in significant differences in local densities and incomplete remolding of the clods during compaction. Sandy or silty soil materials are generally easier to excavate, process, and compact, but also yield a high hydraulic conductivity. Clayey soils have a low hydraulic conductivity, but are less workable. The ideal liner soil should contain enough sand or silt to be workable and enough clay to keep the hydraulic conductivity low. Soils that contain too much clay tend to fracture easily; optimum clay content appears to be between 15 and 40 percent. In this project, the liner material must be classified as SC, ML, CL, MH, or CH textures, as defined in the unified soil classification system (Weeks 1986).

Quantity and uniformity of the soil material A borrow source must have an adequate quantity of soil material to meet the design requirements.

Proximity to the construction site Hauling distance from the borrow source to the liner site directly affects the cost of liner construction. Economically desirable hauling distances are generally less than 10 miles, although hauling distances of up to 25 miles have been reported (USEPA 1988a). For this project, a maximum hauling distance of 30 miles was selected as a criterion.

We chose five potential borrow sources near Champaign, Illinois, that met the criteria. All of the sources were located in Wisconsian-age glacial deposits of the Snider, Batestown, and Piatt Till members of the Wedron Formation (Willman et al. 1975). These soils, commonly found in east-central Illinois, have been used as liner or cap materials for municipal waste landfills.

■ Physical, Geotechnical, and Geochemical Testing

Evaluation of the soils collected from the borrow sources were based on four specific soil properties (hydraulic conductivity, density/moisture content, Atterberg limits, particle-size distribution); whereas characterization of the samples taken from the selected borrow pits was based on 11 soil properties. The criteria selected can be categorized in terms of their relationship to regulations, liner construction, and long-term liner stability.

■ Regulatory Category

Hydraulic conductivity USEPA regulations state that a liner must have saturated hydraulic conductivities less than 1×10^{-7} cm/s. Studies indicate that conductivities determined in the laboratory are generally several orders of magnitude lower than those measured in the field. Therefore, we used a maximum criteria for a laboratory-measured hydraulic conductivity of 1×10^{-8} cm/s in the soil selection process.

■ Construction Category

Compaction/water content For a liner to function successfully, the soil must have a sufficient bearing capacity to carry the weight of the waste material and overburden and to prevent the formation of joints and fractures created by loading failure. Such fractures could become preferential flow paths for leachate, and thus decrease the ability of the liner to limit seepage from a waste disposal facility. A maximum dry density of 1.5 gm/cm^3 (95 lb/ft^3), as measured by the Standard Proctor test, was the minimum density considered acceptable for a potential soil liner.

A field water content 2 percent wet of optimum, as determined by Standard Proctor tests, was considered optimal. This water content was chosen because soils compacted wet of optimum generally exhibit lower hydraulic conductivities than those soils that are compacted dry of optimum (Cartwright et al. 1988). Soils that are too dry or too wet may incur extra costs in the soil preparation stage of liner construction.

Atterberg limits Atterberg limits provide empirical indications of the workability and curability of a soil. The lower the liquid limit and plasticity index of a soil, the more workable and easier it is to cure (obtain uniform moisture content and decrease clod size). Numerical guidelines based on the work of Daniel (1987) and Weeks (1986) were established for these properties. A plasticity index greater than 10 percent but less than 40 percent and a liquid limit greater than 25 percent was considered optimal.

Table 1 Potential soil materials for liner construction.

Snider Till Member		
Sample I.D.: SNID		
	Soil characteristics	Silty clay loam to clay loam, light olive-brown to gray-brown; calcareous, blocky, jointed
	Sample location	Roadcut surfaces of Emerald Pond area near Danville (two bulk samples)
Batestown Till Member		
Sample I.D.: BATEA		
	Soil characteristics	Loam to clay loam, light olive-brown to dark gray, calcareous
	Sample location	Stockpiled pile of borrow material frcm Urbana landfill (three bulk samples)
Sample I.D.: BATEB		
	Soil characteristics	Clay to silty clay loam
	Sample location	Roadcut surfaces near the Sangamon River Bridge along Illinois Route 47 (three bulk samples)
Sample I.D.: BATEC		
	Soil characteristics	Loam
	Sample location	River bank adjacent to the Mahomet Bridge along Interstate 74
Piatt Till Member		
Sample I.D.: PIAT		
	Soil characteristics	Coarse-grained and sandy loam, gray silty and sandy loam till somewhat similar to the overlying Batestown Till in appearance
	Sample location	River bank of a branch of the Sangamon River about ¼ mile southwest of the west gate of Lake of the Woods park near Mahomet (three bulk samples)

Particle-size distribution The particle-size distribution of a liner soil is also an indication of its workability and curability. Generally, reducing clod sizes and obtaining a homogeneous water content is difficult when soils have a high clay content. A soil with particles that are greater than 20 percent by weight and passes through a 4-µm sieve would rank highly as a potential liner material (Daniel 1987).

■ Stability Category

Other physical measurements that give an indication of the long-term performance of a liner can include clay-content index, expandable clay-mineral content, soil dispersivity, and cation exchange capacity. Although specific numerical criteria were not assigned to each of these factors, we considered these measurements in the material selection process.

■ Soil Property Evaluations

The results of the physical, geotechnical, and chemical tests for each of the till samples are summarized in table 2. The water content of the tills ranged from 9.6 to 15.5 percent. The ranking of the tills with respect to moisture content was BATEB>SNID>PIAT>BATEC>BATEA. Assuming that the soil should be compacted at 2 percent wet of optimum moisture (as determined by Standard Proctor compaction tests), we determined that the BATEA and SNID tills required the addition of water before construction. The field moisture content of the remaining samples was at least 1 percent greater than optimum moisture and thus would be likely to require little or no additional water before construction.

Table 2 Summary of the hydraulic, geochemical, and geotechnical test results for the potential liner soils.

Sample ID	Natural water content %	Specific gravity	Atterberg limits % L.L.	Atterberg limits % P.I.	Clay content index	CEC meq/100 g	Lab. K $\times 10^{-9}$ cm/s	Particle size % Sand	Particle size % Silt	Particle size % Clay	Compaction test τ_d	Compaction test W_{opt}	Unified classf. system	Clay mineralogy % Illite	Clay mineralogy % Chlor.	Clay mineralogy % Expand.
BATEA1	9.6	2.73	21.2	6.8	0.149	7.20	4.8	35.0	26.4	38.7	2.10	10.2%	CL-ML	64	10	26
BATEA2	10.6	2.74	22.6	8.7	0.200	8.57	4.0	33.0	30.0	37.1	2.06	10.6%	CL	63	10	27
BATEA3	10.9	2.74	19.4	5.5	0.191	13.96	6.8	37.8	23.0	39.2	2.07	10.1%	CL-ML	64	9	27
Mean	10.4	2.74	21.1	7.0	0.180	9.89	5.2	35.2	38.3	26.5	2.08	10.3%	—	64	10	27
SNID1	14.9	2.75	25.8	9.8	0.241	12.97	4.5	20.2	42.9	36.9	1.92	14.5%	CL	67	6	27
SNID2	14.9	2.75	26.0	9.0	0.201	12.27	7.0	21.3	40.0	38.7	1.88	15.1%	CL	68	7	25
Mean	14.9	2.75	25.9	9.4	0.221	12.60	5.8	20.8	41.4	37.8	1.90	14.8%	—	68	7	26
BATEB1	15.3	2.73	26.4	9.1	0.304	13.94	2.6	18.9	52.7	28.4	1.89	14.0%	CL	63	5	32
BATEB2	15.4	2.74	25.7	8.7	0.297	12.18	2.6	18.8	50.3	30.9	1.90	14.5%	CL	60	6	34
BATEB3	15.5	2.74	25.3	8.5	0.350	10.06	1.5	16.1	55.4	28.5	1.95	13.9%	CL	61	6	33
Mean	15.4	2.74	25.8	8.8	0.317	12.1	2.2	26.9	52.8	29.3	1.92	14.1%	—	61	6	33
PIAT1	11.9	2.73	17.4	4.2	0.125	14.15	8.5	32.8	45.4	21.8	2.04	10.8%	CL-ML	79	7	14
PIAT2	12.6	2.74	19.4	5.0	0.179	15.24	18.0	34.2	40.9	24.9	1.96	12.0%	CL-ML	66	5	29
PIAT3	13.3	2.74	19.4	5.7	0.121	14.88	8.5	34.9	40.8	24.3	2.03	10.7%	CL-ML	68	6	26
Mean	12.6	2.74	18.7	5.0	0.142	14.80	11.7	34.0	42.3	23.7	2.01	11.2%	—	71	6	23
BATEC1	12.6	2.73	17.4	4.5	0.135	6.04	4.0	31.6	44.8	23.6	2.09	9.7%	CL-ML	76	11	13
BATEC2	11.4	2.74	19.1	6.1	0.154	8.95	5.6	31.3	42.4	26.3	2.04	10.7%	CL-ML	77	10	13
BATEC3	13.0	2.74	20.3	6.3	0.161	13.78	3.2	31.5	39.7	28.8	2.00	11.7%	CL-ML	76	6	18
Mean	12.3	2.74	18.9	5.6	0.150	9.59	4.3	31.5	42.3	26.2	2.03	10.7%	—	76	9	15

L.L = liquid limit, P.I.= plasticity index, CEC = cation exchange capacity, K = saturated hydraulic conductivity, τ = dry density in g/cm^3, W_{opt} = optimum moisture content, Chlor. = chlorite, Expand. = expandables.

All of the soils met the selection criteria for dry density (table 2). In general, the BATEA samples had the highest maximum dry densities at the lowest moisture content, whereas the SNID samples had the lowest maximum densities at the highest moisture contents. Assuming that the greater the density the better a liner will perform (all other properties being equal), we concluded that the BATEA sample would be the most suitable material, even though water would have to be added to it before construction (fig. 2).

Laboratory-determined hydraulic conductivities for the till ranged from 1.5×10^{-9} to 1.8×10^{-8} cm/s. The ranking of the soils with respect to conductivity was BATEB<BATEC<BATEA <SNID<PIAT (table 2). All the materials had laboratory hydraulic conductivities less than the regulatory requirement. The mean conductivity for the PIAT samples (11.7×10^{-9} cm/s) exceeded the selection criteria of less than 1×10^{-8} cm/s; however, the mean conductivity for the PIAT sample was based on the average of three values, one of which is approximately one order of magnitude greater than the other two values. When this suspect datum point was not used, the soils all met the selection criterion.

Atterberg limits determined for all of the soils suggested that none of them would meet the selection criterion for plasticity index. The BATEA, PIAT, and BATEC samples also did not exhibit liquid limits that met the selection criterion (table 2 and fig. 3). Plasticity index values ranged from 4.2 to 9.8 percent with liquid and plastic limits ranging from 1.4 to 26.4 percent and 12.9 to 17.3 percent, respectively. The ranking of the soils with respect to both plasticity index and liquid limit was SNID>BATEB>BATEA>BATEC>PIAT.

Particle-size distribution for the potential liner materials is shown in table 2. All the soils except PIAT had less than 2-µm fractions greater than 20 percent, yet less than 40 percent, and met the selection criteria. The ranking of the soils with respect to the clay fraction was SNID>BATEB> BATEC>BATEA>PIAT. All the soils plotted as either CL or CL-ML (fig. 4).

Evaluation of the soils for specific gravity, clay-content index, cation exchange capacity, clay mineralogy, and dispersivity (table 2 and fig. 5)) indicated that these properties were similar in all the soils; therefore these parameters could not be used as selection criteria.

▪ Evaluation and Selection of Soil Material

The five potential soil materials were evaluated against the selection criteria established for this project. Laboratory measurements of the hydraulic conductivity of the PIAT sample indicated that this soil was undesirable, and it was therefore eliminated as a potential liner material. All the materials exceeded the particle size and compaction criteria. In general, the field moisture contents for all the materials were acceptable; the moisture content of the BATEB and BATEC samples were most satisfactory. None of the materials met the plasticity-index criteria, and only the SNID and BATEB materials met the liquid-limit criterion. We decided that the Atterberg-limit criteria could be relaxed, and all of the materials were acceptable on the basis of the relaxed criterion.

Although several quantitative guidelines were established for various geotechnical soil parameters, the soils in general had very similar properties, and except for the PIAT soil, all the materials were considered to be acceptable for use in liner construction. The ultimate selection decision was then based on economics. Hauling and material costs for the remaining four borrow soils were considered. On the basis of minimal hauling distance (<8 km) and the opportunity to obtain the soil at no cost other than transportation, we chose the BATEA soil as the soil material for the prototype liner.

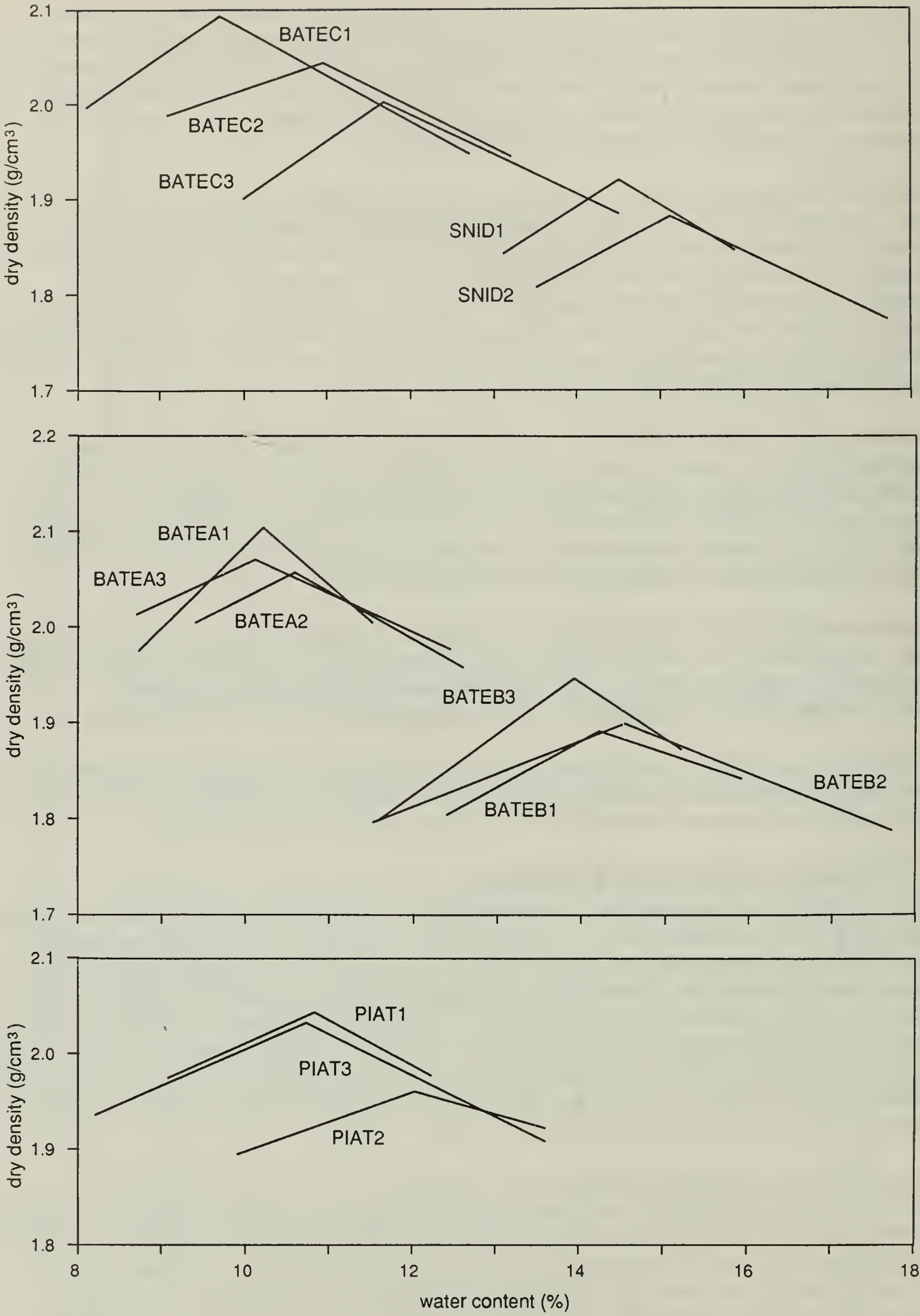

Figure 2 Standard Proctor compaction results for the potential soil-liner materials.

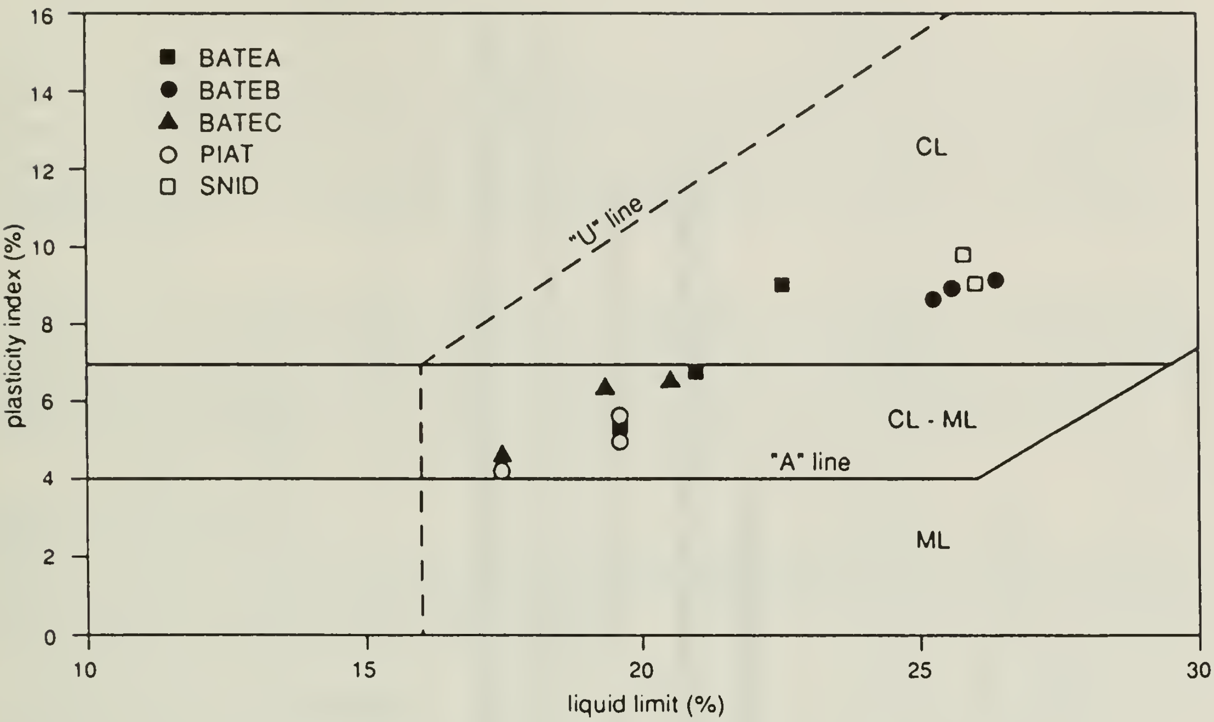

Figure 3 Casagrande's plasticity chart for the potential soil-liner materials.

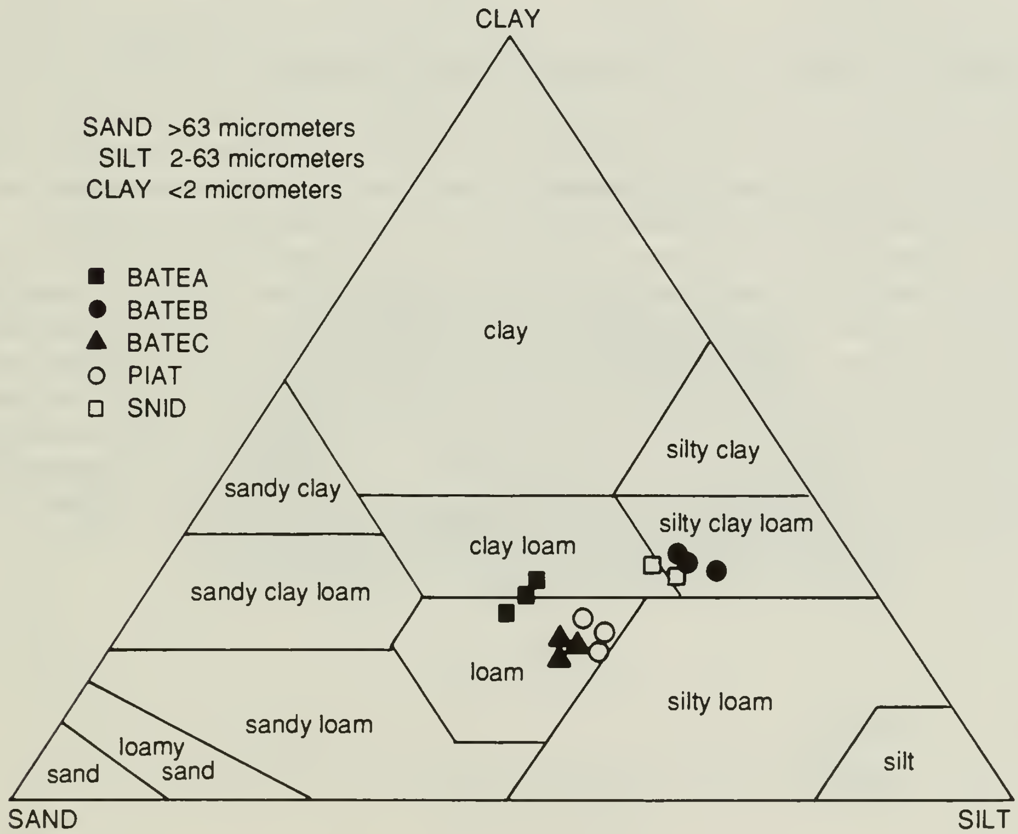

Figure 4 Unified soil textural diagram showing classification of the potential liner soils.

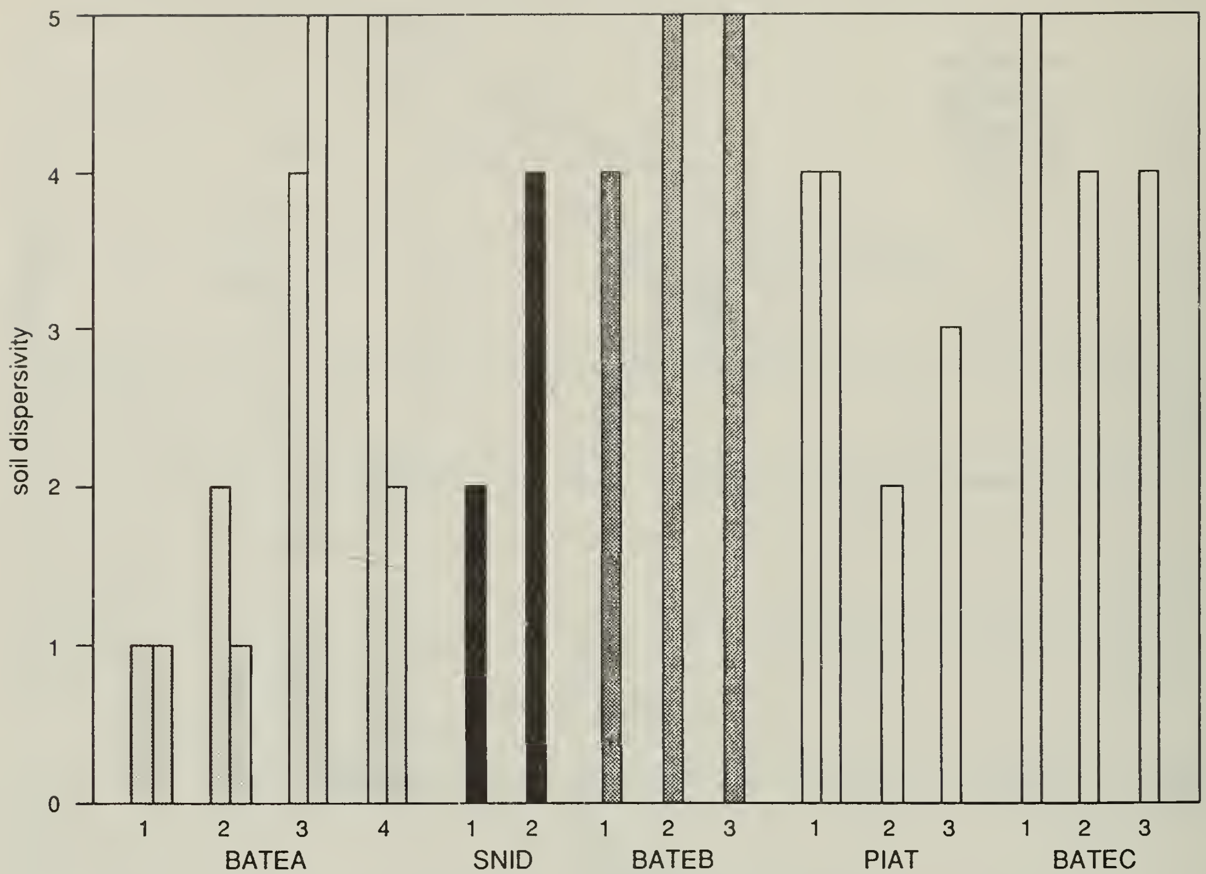

Figure 5 Dispersivity of the potential liner materials as determined by the pinhole test.

Summary

Qualitative selection criteria were established to evaluate soils as potential materials in which to construct soil liners. The soil properties assigned a numerical criterion were hydraulic conductivity, Atterberg limits, particle-size distribution, natural moisture content, and dry density. The hydraulic conductivity criterion eliminated one potential soil material. The Atterberg limits (plasticity index) criterion was relaxed because none of the materials achieved a plasticity index greater than 10 percent. Results of the liner construction (see chapters 3, 6, and 7) indicated that relaxing this criterion did not result in problems with liner construction; and performance, as determined through hydrologic monitoring, was adequate. The soils passed the remaining criteria for dispersivity, clay mineralogy, specific gravity, and cation exchange capacity; these properties did not differ significantly in the different soils to serve as selection criteria. The final selection decision was based on economic factors.

2 CONSTRUCTION AND MONITORING OF THE PROTOTYPE LINER

A prototype liner was designed and built to evaluate methods required to build, instrument and monitor a field-scale liner. Objectives of this phase of the project were to (1) evaluate potential construction problems that might arise when full-scale equipment was used; (2) evaluate the adequacy of vertically and horizontally installed instruments; and (3) determine whether the Batestown Till could be compacted to a hydraulic conductivity of less than 1×10^{-7} cm/s, as measured in situ.

The prototype project also provided training for the personnel involved later in the field-scale project. By analyzing and solving problems that arose during construction and monitoring of the prototype liner, we planned to eliminate at least some problems that would be encountered in construction of a field-scale liner and ensure that no major flaws in the construction and monitoring could jeopardize the success of the long-term project.

Preconstruction Tasks

Before the prototype liner could be constructed, three preliminary tasks had to be completed: prepare the site at which the prototype liner would be built, construct the liner's foundation, and prepare the soil to be used for the prototype liner.

■ Site Selection and Preparation

The site of the prototype liner was selected on the basis of proximity to the laboratories and offices of the Illinois State Geological Survey. Consequently, a site was chosen on the campus of the University of Illinois in Champaign, Illinois. Site preparation required that the area be well drained during the experiment and that the subgrade on which the prototype liner would rest have a bearing capacity that would support the liner and provide a stable nonyielding base on which a foundation could be built. The subgrade and the foundation would have to withstand the forces of full-scale compaction equipment. Construction of the drainage system required that existing drainage ditches at the selected site be modified and that new ditches be constructed so that runoff from the site would be channeled to existing outlets.

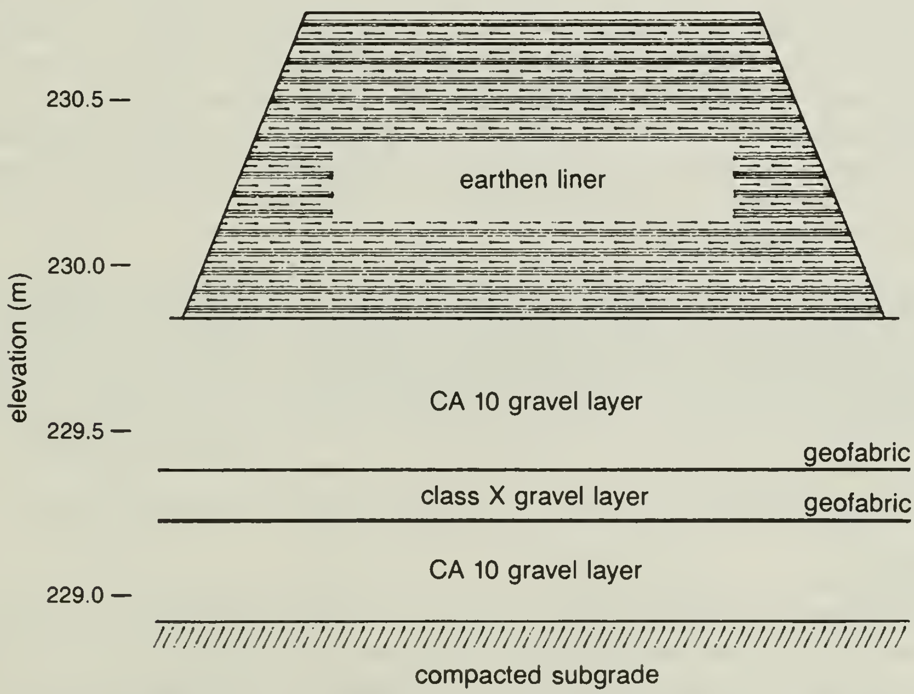

Figure 6 Foundation design to support the prototype and field-scale liners.

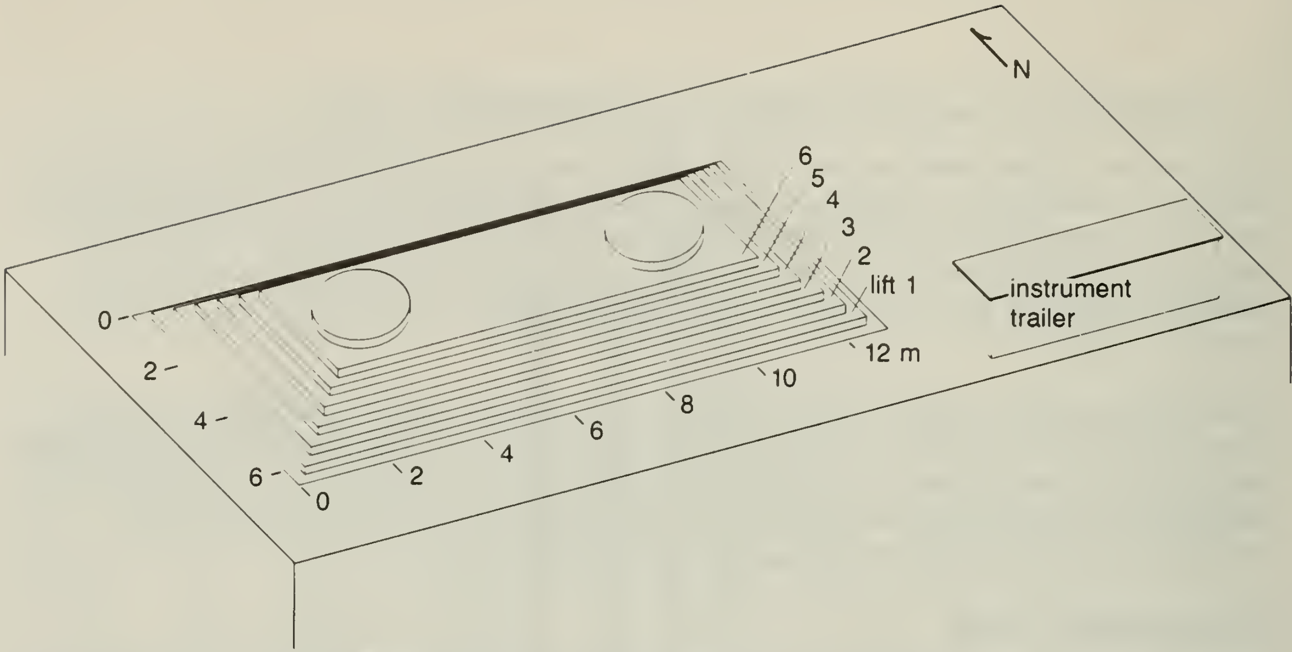

Figure 7 Diagrammatic view of the foundation, prototype liner, and grid system.

■ Foundation Construction

The foundation of the prototype liner was built to (1) provide a resistant nonyielding base on which the prototype and later field-scale liner could rest, (2) serve as a structural foundation upon which a shelter could be constructed to house the field-scale liner, and (3) divert surface drainage away from the liner facility.

The foundation was designed as a layered structure containing CA10/Class X/CA10 gravel layers (fig. 6). The CA10 gravel layers are made up of well-graded gravel compacted to a high bearing capacity; conversely, the Class X gravel layer is made up of poorly graded gravel that serves as a drainage layer. The thicknesses of the lower CA10, Class X, and upper CA10 layers are 30, 15, and 46 cm, respectively. A geofabric layer was placed above and below the Class X layer to provide additional strength and reduce the migration of fine particles into the Class X layer (such migration could reduce the efficiency of the drainage system). Each gravel layer was compacted in 8- to 10-cm lifts using a padfoot compactor (Hyster® C852A) that had feet 10 cm long and could deliver 22,680 Kg of force in the vibratory mode. The bottom of the Class X drainage layer (above the site drainage outlet) was graded about 0.2 percent from east to west to improve water flow from the drainage layer into the site drainage ditches. The final dimensions of the foundation were approximately 15 × 26 m, large enough to accommodate the prototype and field-scale liners and act as a structural foundation for the field-scale liner shelter.

■ Soil Preparation/Processing

Soil from the borrow source was transported to the liner site and stockpiled. No attempt was made to reduce the clod size of the material as it was stockpiled. Heavy rains during construction of the prototype liner made adjusting the moisture content of the soil impossible. Daniel (1984) showed that hydraulic conductivity of soils compacted wet of optimum, as determined by the Standard Proctor tests, was lower than those of soils compacted dry or at optimum; therefore, we concluded that the moisture content of the stockpiled soil was adequate, from a hydrogeologic perspective, for the construction of the prototype liner.

Liner Construction

Before the prototype liner was constructed, a grid system was established at approximately 30-cm intervals (in an x-y coordinate system) on the surface of the foundation to facilitate monitoring of compaction paths and placement of instruments (Troxler tubes, lysimeters, and tensiometers) buried within the prototype liner (fig. 7). A geofabric was also placed on the

Table 3 Summary of mean water content and coefficient of variation determined for each lift of the prototype liner.

	Moisture Content (%)							
	Microwave[b]		Seaman[c]		ASTM[d]		Core[e]	
Lift[a]	Mean	C.V.	Mean	C.V.	Mean	C.V.	Mean	C.V.
6	11.5	7.0	12.3	–	12.2	11.7	11.6	14.6
5	9.4	14.0	11.2	–	11.4	4.5	10.5	20.9
4	10.5	24.3	11.7	–	10.8	4.3	9.9	15.5
3	10.4	17.5	11.7	–	12.3	–	10.9	11.2
2	10.7	2.8	11.4	–	11.1	6.7	10.5	–
1	16.7	38.2	11.2	–	11.3	6.1	12.3	–
ALL	11.5	31.3	11.6	10.9	11.5	9.0	11.0	14.2

[a] 1 represents bottom lift of liner while 6 represents the top lift of liner.
[b] results of loose grab sample determined by a microwave method.
[c] results determined in situ using Seaman Nuclear density meter.
[d] results determined by drive cylinder method.
[e] results determined by volumetric core samples.

Table 4 Summary of mean dry density and coefficients of variation determined for each lift of the prototype liner.

	Dry Density (g/m^3)					
	Seaman		ASTM		Core	
Lift	Mean	C.V.	Mean	C.V.	Mean	C.V.
6	1.83	–	1.83	3.2	2.07	5.1
5	1.93	–	1.82	2.0	2.10	2.5
4	1.77	–	1.84	2.7	2.13	2.3
3	1.90	–	1.84	–	2.02	6.3
2	1.88	–	1.89	2.6	2.09	–
1	1.83	–	1.91	4.2	2.03	–
ALL	1.85	4.7	1.85	3.4	2.08	3.8

surface of the foundation so that prototype materials could be removed easily when this phase of the project was completed and construction of the field-scale liner began.

The prototype liner was constructed in a series of six lifts or layers; a front-end loader spread Batestown Till into 23-cm-thick layers. Although an attempt was made to reduce clod size by using a hand-held rototiller, it was ineffective in reducing clods to less than 15 cm in diameter. Relatively large rocks were removed from the till by hand so that no rock greater than 10 cm in diameter remained in each lift.

A padfoot compactor (Hyster® C852A) was used to compact the lifts to approximately 15 cm thick. The compaction paths overlapped each other by one-third to one-half of the path width; compaction progressed from the edge toward the center of the liner. The compactor passed over each lift a minimum of six times in the static mode and six times in the vibratory mode. Rototillers scarified the compacted surfaces to improve lift bonding. During the compaction operation, in situ density and moisture content were measured at a minimun of four locations for each lift. Density and moisture values were determined with a Seaman Nuclear® density

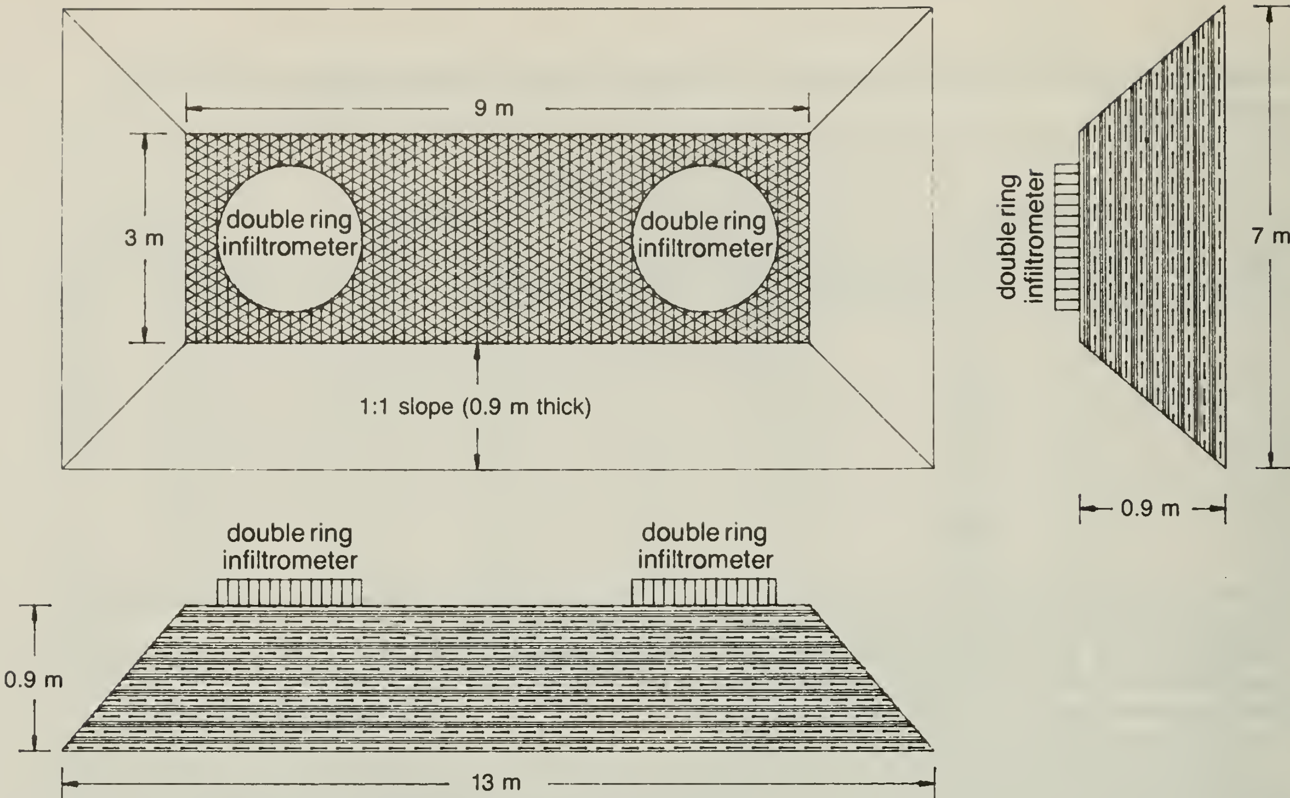

Figure 8 Plan and cross section view of the prototype liner.

meter; moisture content was also determined on grab samples by microwave and/or conventional oven methods. If lift densities did not exceed about 90 percent of maximum dry density, as determined by Standard Proctor tests, then additional compaction passes were made.

Once a lift met density specifications, two undisturbed volumetric core samples were collected from each of the four locations at which the measurements of in situ density and moisture content were made. Cores were weighed in the field and transported to the laboratory for analysis of bulk density and moisture content using the ASTM Drive Cylinder Method D2937.

After the prototype liner was completed, the perimeter of the liner was cut back to a 1:2 (vertical:horizontal) slope to provide structural support and eliminate the potential for desiccation of the edges of the liner. The final dimensions of the upper test surface of the liner were 3 × 9 × 0.9 m. Figure 8 provides the plan and cross section view of the completed prototype liner.

Liner Properties

Moisture contents determined using the microwave, Seaman Nuclear® density meter, and core methods are presented in table 3. The Seaman Nuclear and core results represent in situ moisture measurements after compaction; the grab samples were used to assess whether the moisture content of a lift was acceptable. Results indicated that, on the average, the liner was constructed 1 percent wet of the Standard Proctor optimum moisture content. The overall moisture content for the liner, as determined by the four methods, ranged from 11.0 to 11.6 percent, suggesting that the methods are comparable and accurately represent the moisture content in the liner. For individual lifts, moisture content ranged from 9.4 to 16.7 percent and appeared to be relatively uniform, as indicated by the relatively small coefficients of variation (ranging from 4.3 to 38.2). The higher variability in lift 1 was due to isolated wet spots. Lifts were subsequently constructed using drier and more thoroughly mixed material from the stockpile to eliminate variations in moisture content.

The average density for each lift ranged from 88 to 100 percent of the maximum Standard Proctor density (table 4). The one set of cores collected from the liner (labeled core in table 4) produced greater densities than did the other two data sets. The uniformity of the densities for the prototype liner is significant: densities ranged from 1.77 to 2.13 g/cm^3, regardless of the method used to make this determination; in situ measurements and extracted core samples generally produced similar results. The uniformity in densities for each lift is indicated by the small coefficients of variation (<7%), suggesting that the construction design for compaction of the liner was adequate for producing a homogeneous liner, with respect to density.

Instrumentation and Monitoring of the Prototype Liner

The hydrogeologic data obtained from the prototype liner provided the basis for establishing the design, construction, and monitoring protocols for the field-scale liner. Monitoring methods, hydraulic and morphologic properties, and recommendations regarding liner construction and instrumentation of the prototype liner have been published elsewhere (Albrecht and Cartwright 1989, Albrecht et al. 1989).

Conclusions regarding the hydraulic and morphologic properties of the prototype liner may be briefly summarized:

- The saturated hydraulic conductivity of the prototype liner was no more than 3.6×10^{-8} cm/s, meeting the USEPA conductivity requirement for soil liners of no more than 1×10^{-7} cm/s. Calculations were based on infiltration rates measured by large -1.5-m-diameter double-ring infiltrometers, assuming a Green-Ampt infiltration model.

- An average constant infiltration flux of 1.5×10^{-7} cm/s was achieved 2 to 3 weeks after the infiltration experiments began.

- Wetting front depths of 7.3 cm and 9.6 cm were calculated, assuming a Green-Ampt model, from infiltration volumes for each infiltrometer after 46 days of infiltration.

- Transit time for the wetting front to reach the bottom of the liner was predicted to be 3 years.

- Fluorescein and rhodamine WT dye patterns in the liner indicated that lateral flow had occurred between lifts as well as along clod-clod interfaces.

- Variable compaction was observed within lifts in the form of hard and soft layers of soil.

- Some horizontally installed instruments caused preferential flow paths between lift interfaces and were damaged during compaction.

Summary

The prototype liner was constructed using full-scale construction equipment. Moisture content and density of the liner appeared to be relatively homogeneous. Coefficients of variation indicate that moisture content was more variable than density in the liner. Densities of 90 percent of maximum, as determined by the Standard Proctor test, were achieved at moisture contents approximately 1 to 2 percent wet of optimum. The prototype liner met the construction design specifications.

3 CONSTRUCTION OF THE FIELD-SCALE LINER

A field-scale liner was designed to incorporate information derived from experience with the prototype liner and to allow for (1) the use of full-scale equipment and commonly used construction techniques, and (2) the need to determine the areal variability of the liner's hydraulic properties. The construction design thus incorporated instrumentation for evaluating the liner at various scales of measurement while still using standard engineering methods. The design of the liner included not only the soil liner, but also an underdrain system, pan lysimeters, drainage collection pits, a cutoff wall, a retaining wall, a catwalk, and a shelter to enclose the liner and these accessory components.

The liner design provided for construction of a 10 × 17 × 1 m area of compacted soil including a 7.3 × 14.6 × 0.9 m test area that was instrumented and ponded. Figure 9 shows the plan view and figure 10 shows a cross-sectional profile of the field-scale liner.

Underdrain and Pan Lysimeter Construction

■ Underdrain System

The function of the underdrain system is to collect water that has migrated down through the liner. The total volume of water collected in the underdrain system is a measure of the effluent flux of the liner and is used to estimate the saturated hydraulic conductivity of the overall liner. Data on the volume of water collected in the underdrains will provide additional information to determine the effects of measurement scale on estimating hydraulic properties.

The underdrain system is divided into four sections, each corresponding to one quadrant of the liner study area. A plan view and cross section of a section is shown in figure 11. The surface of the underdrain system is slightly larger than the entire study area, allowing a waterproof interface with the cutoff wall (fig. 10). Each underdrain section also has an independent drainage outlet to allow comparison of flow volumes from each quadrant of the liner.

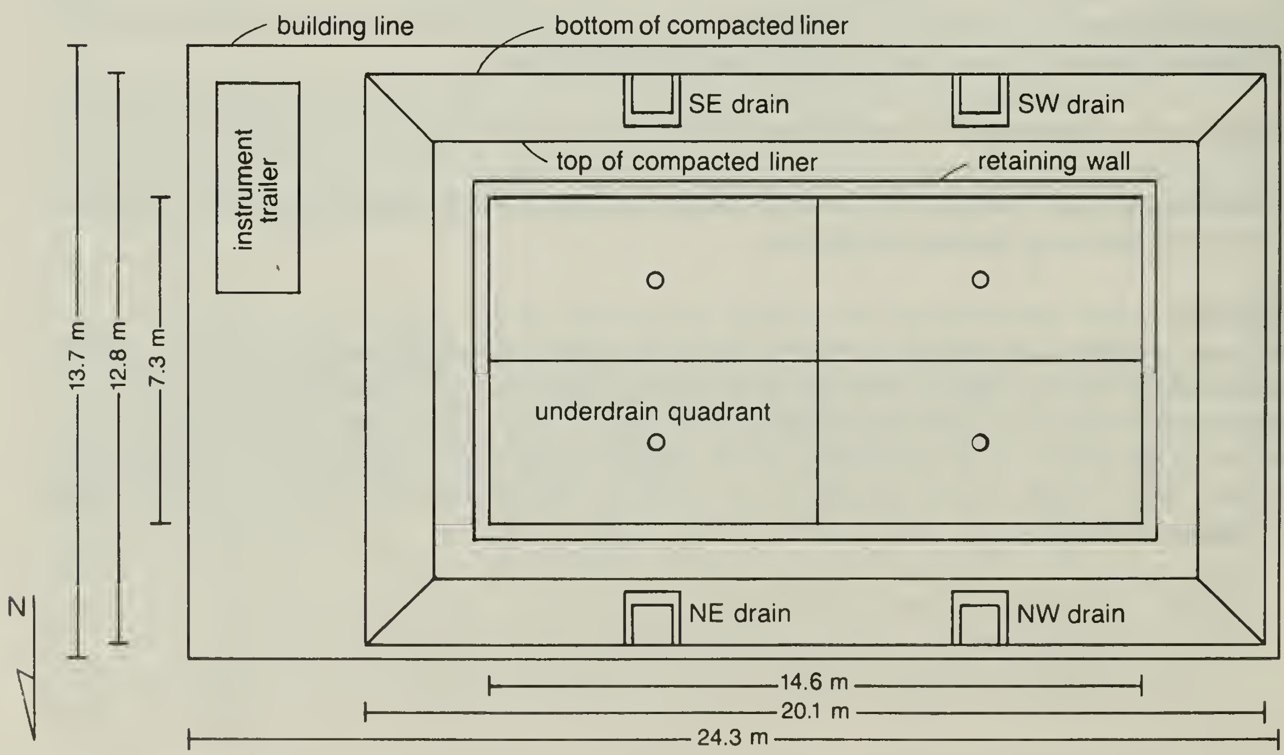

Figure 9 Plan view of the field-scale liner.

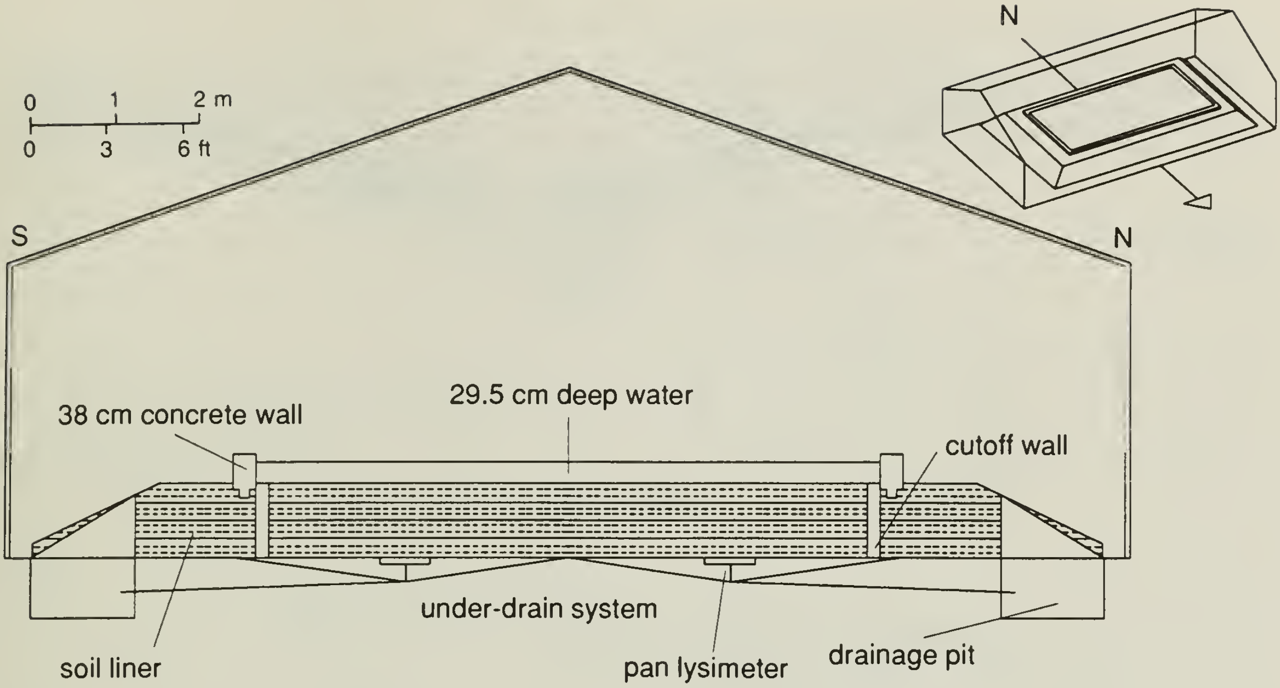

Figure 10 Cross section of the field-scale liner and accessory components.

Control points marking the position of the underdrain system were surveyed using a total station surveying instrument that combines an electronic distance meter and a theodolite. Surveyed locations were temporarily identified by hammering steel pins into the ground or marking the structure as construction proceeded. The corners of the liner and quadrants were surveyed and string lines were stretched between each of the quadrant corners to identify the boundaries of each quadrant.

The foundation subgrade of the liner quadrants was a 5-percent slope. Installing water drainage cups (fig. 12) and their outlet pipes required digging holes and trenches into the foundation subgrade. Holes 15 cm in diameter and 20 cm deep were dug in the center of each quadrant; trenches 10 cm wide were dug from each hole to the surveyed position of the drainage collection pits. The base of each trench was graded to a 2-percent slope so that water would flow from the drainage cups to the collection pits. Drainage cups were then installed in the holes and set in concrete to prevent any movement during liner construction. A 2-cm-OD (outside diameter) PVC pipe was connected to the drainage cup, placed in the trench, and connected to the appropriate location in the drainage pit. Flexible vinyl tubing was threaded through the drainage cup and PVC pipe. The trenches were then backfilled with CA-IO gravel and recompacted. The ends of the PVC pipe at each drainage pit were sealed with plastic tape and buried inside steel caissons to protect them during construction of the liner.

The underdrain system was constructed of five layers (fig. 13): from bottom up, a lower 3-cm layer of sand covered with geofabric, a 30-mil geomembrane of high-density polyethylene, a second 3-cm layer of sand and geofabric, and an upper layer of pea gravel (10 mm in diameter) graded to the liner foundation elevation.

- The sand layer was placed on the foundation subgrade surface and compacted with a walk-behind compactor; periodic surveying ensured that the design slope was maintained.

- Geofabric was placed on top of the sand layer. A hole was cut in the geofabric above each drainage cup to allow water to reach the drainage cup.

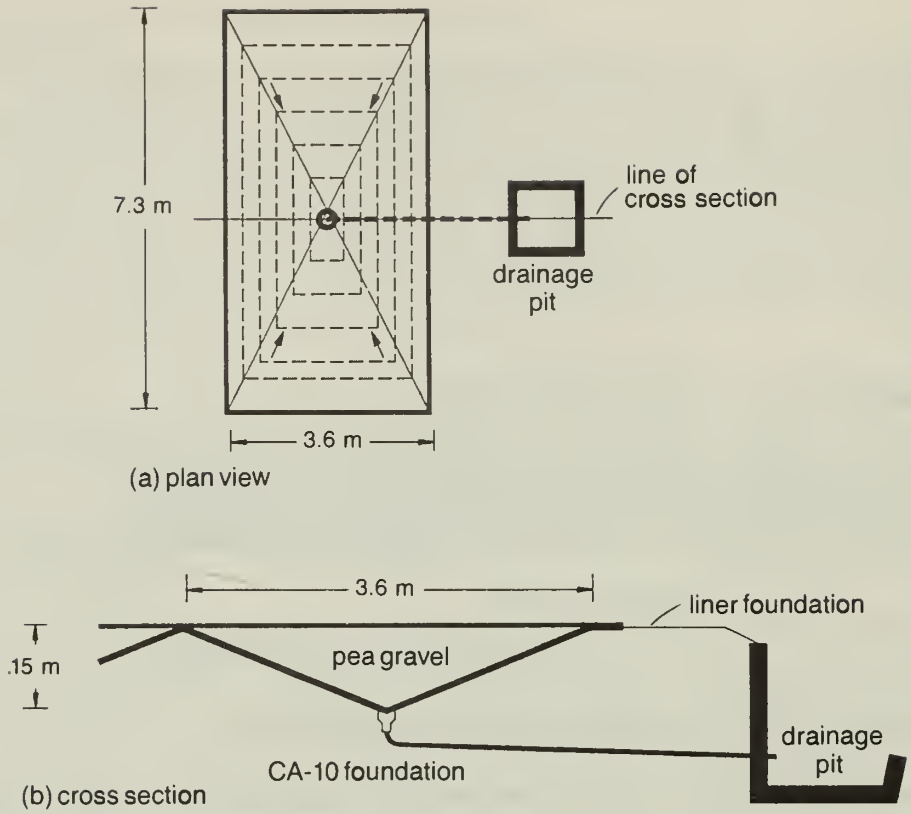

Figure 11 Plan and cross-section views of the underdrain system.

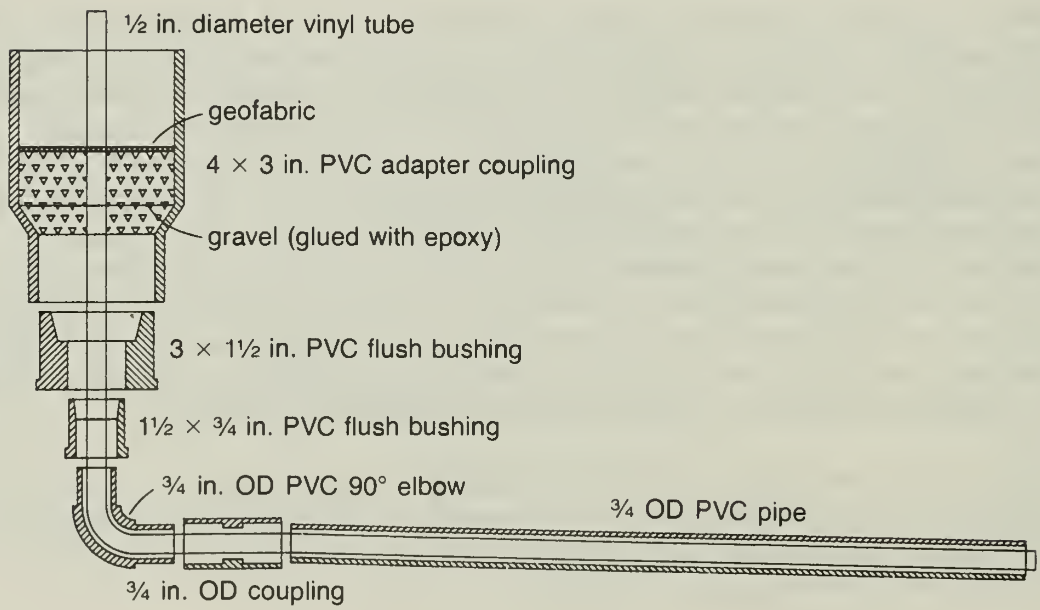

Figure 12 Design of drainage cups used in the underdrain system.

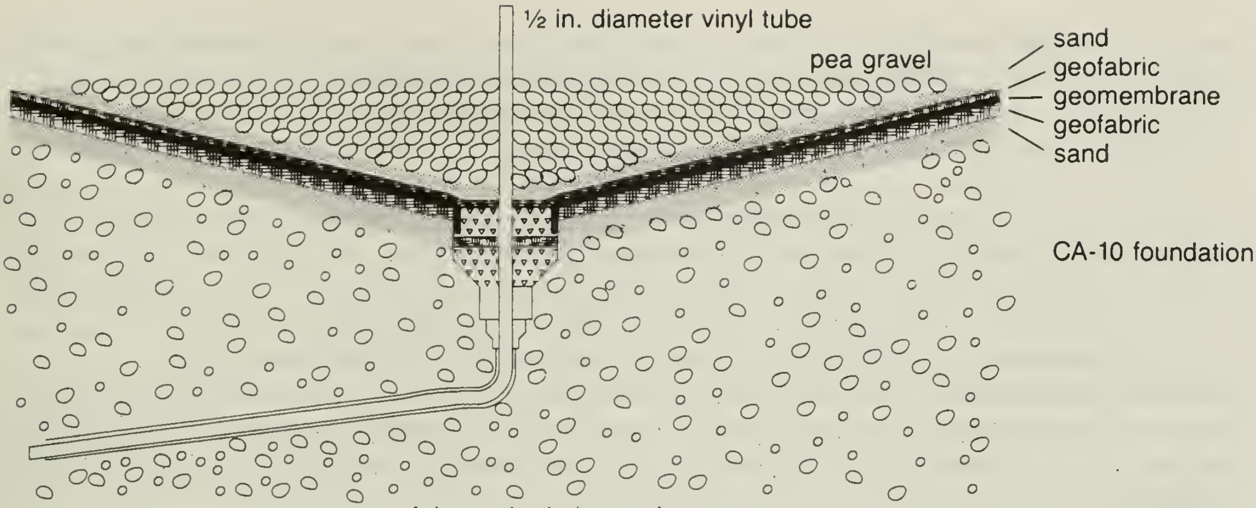

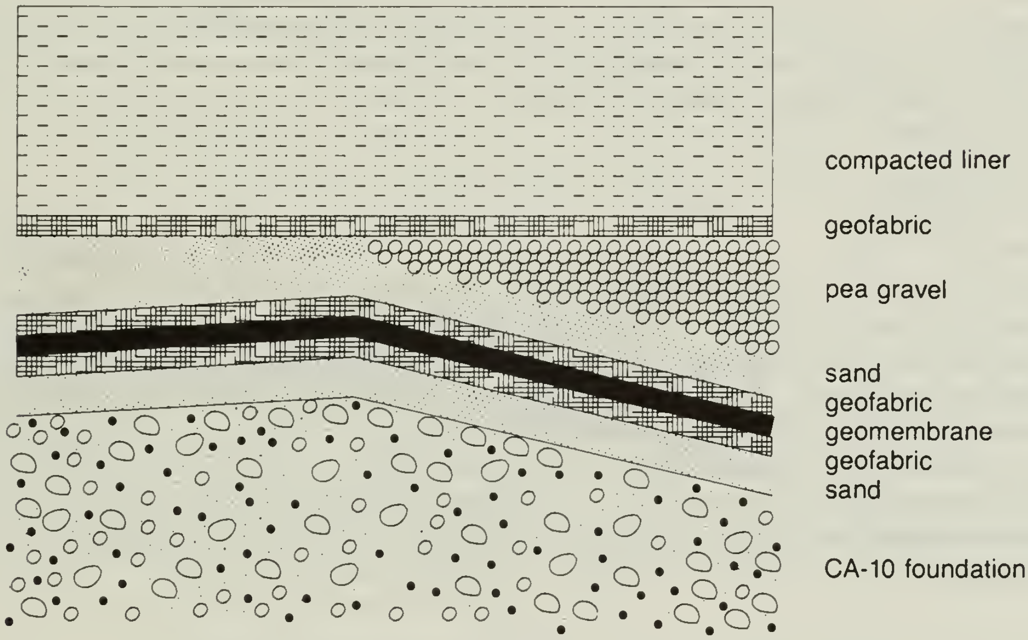

Figure 13 Composition of the underdrain system.

- A geomembrane layer was placed over the geofabric to serve as the lower confining layer of each underdrain section. We used four geomembrane sheets, each 4.3 × 7.9 m; each covered an underdrain quadrant and overlapped between quadrants. To connect the drainage cup to the geomembrane sheet, we cut the geomembrane radially and pushed it inside the cups. A mixture of epoxy and gravel was pushed into each drainage cup around the flexible tubing to seal the membrane inside and allow water to flow through the cup.

- A second layer of geofabric and a 3-cm layer of sand was placed on the geomembrane.

- Each collector was then filled with pea gravel (10 mm in diameter) level to the elevation of the liner foundation. The flexible tubing protruding from each drainage cup was protected during the addition of the gravel.

■ Pan Lysimeters

Four pan lysimeters were installed to provide an additional measurement of water flow through the liner directly beneath the large-ring infiltrometers. Because there is direct contact between the bottom of the liner and the lysimeter, there is minimal "dead space" in which water could collect, as compared to the extensive pore space in the underdrain system. Water migrating through the liner can move directly to the lysimeter, therefore increasing the resolution in determining when water and tracer breakthrough occurs.

Four pan lysimeters were constructed to the specifications shown in figure 14. A lysimeter was installed directly over the drainage cups near the top of each underdrain system. Each lysimeter was made with the lid of a 30-gallon metal garbage can. The lids were first covered with a layer of reinforced concrete 4 cm thick to prevent damage during compaction of the liner and to ensure a minimum of 5 percent grade sloping towards the center of each pan. A threaded PVC adapter was placed in the center of the lid and set in the concrete to serve as the drain. A layer of quick-curing liquid plastic was placed over the concrete. A mixture of epoxy and gravel was pushed into the adapter and a layer of geofabric was placed across the top of the drain to act as a filter.

A depression was made in the pea gravel of the underdrain system directly above each of the four drainage cups. Sufficient pea gravel was removed to allow the pans to be seated level with the top surface of the underdrain system. Each pan lysimeter drain was connected to the flexible tubing that had been threaded through the PVC collection tube and drainage cup of the underdrain system.

Liner Construction

■ Preparation of Soil

Preparing the soil before constructing the liner involved hauling, tilling, wetting, stockpiling, and curing the Batestown Till. Four hundred cubic meters of soil was excavated and hauled from the borrow source (Urbana landfill) to a storage area near the liner construction site. The soil was spread in layers as it was delivered to facilitate mixing and reducing clod size. The first loads of soil, spread and compacted by a bulldozer, made an 18×18×0.3-m working pad. A series of 15-cm-deep lifts were dumped on the working pad, then each lift was tilled with a Harvard® Rotavator HR-20 tiller. Tilling broke the large clods of soil into clods less than 5 cm in diameter and mixed the material thoroughly. Rocks larger than 5 cm in diameter were removed from the soil by hand.

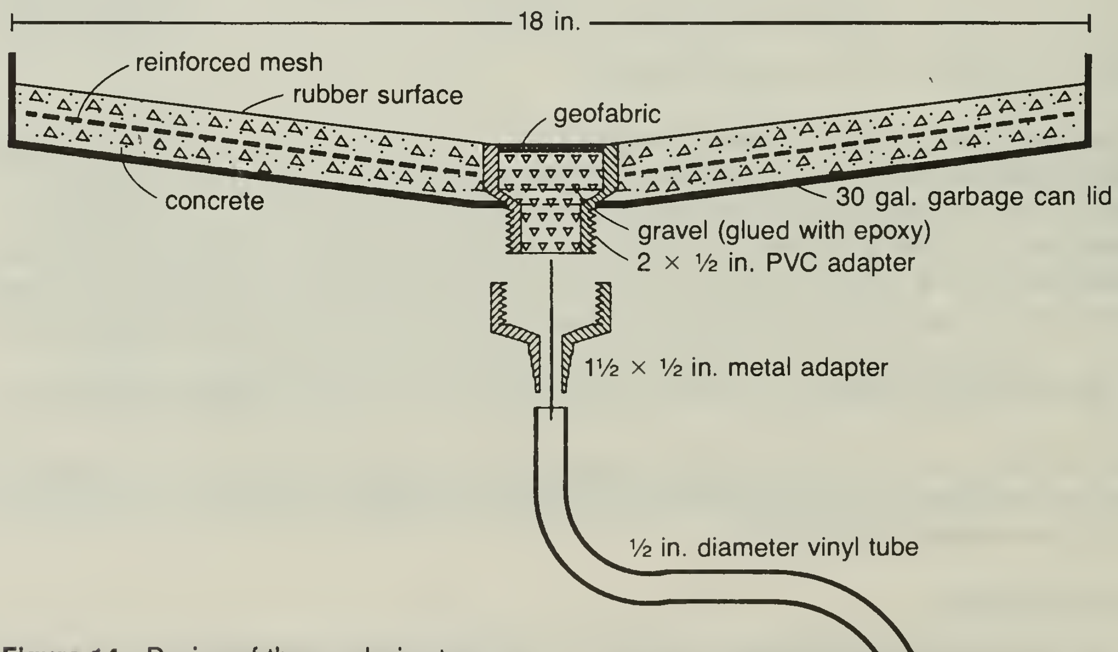

Figure 14 Design of the pan lysimeters.

Maintaining uniform moisture content was another purpose for tilling. When wetting the soil was necessary to meet design specifications, tap water was sprayed on the lift. The water, obtained from a nearby fire hydrant, was spread using a water truck and sprayer system. Water was added until the material reached a moisture content of approximately 12 percent (2 percent greater than optimum, as determined by Standard Proctor test results). Periodically, the moisture content of samples from each lift was tested using the microwave oven method. When the moisture content of each lift was satisfactory, the material was moved from the work pad to a storage area.

To ensure uniform moisture content in the till and to thoroughly hydrate the soil clods, we let the till (soil) cure for 3 weeks. The base of the storage area was lined with a polyethylene sheet to separate the processed soil from the untreated earth material and to prevent water movement into or from the soil. Soil was stockpiled to less than 2 m high to prevent large clods from forming at the bottom of the pile as it was squeezed by soil lying over it. The soil was then covered with polyethylene sheeting.

■ Soil Compaction and Construction QA/QC

Constructing the liner involved compacting the soil in layers or lifts. The prepared soil was trucked from the storage facility to the liner site. Soil samples were collected from each truckload, then combined to make a composite for each lift. Each composite sample was placed in a plastic bag, sealed, and stored in covered plastic garbage cans. Later, these samples were used for physical and chemical characterization of the soil. (Results are reported at the end of this section.)

The liner was constructed by compacting seven lifts with a Caterpillar® 815B compactor, a static load padfoot compactor with a rated operating weight of 20,037 kg; each foot was 20 cm long. To protect the underlying underdrain system and pan lysimeters, we made the first lift an uncompacted (loose), 31 cm thick. The uncompacted thickness of each remaining lift was 23 cm. The material was spread either by the scoop of the compactor or by the Harvard® Rotavator HR-20 tiller. Each lift was spread, retilled, then compacted to a thickness of 15 cm. Compaction of the first lift, using eight passes of the compactor, resulted in densities less than design standards. To more closely match these standards, the compactor had to make 12 passes. The total thickness of the seven lifts was 1.1 m.

Soil density and moisture content were used as QA/QC controls during construction of the field-scale liner. Moisture content was determined using the microwave-oven gravimetric method on grab samples of the loose soil before compacting each lift. Moisture-content data collected during construction of the prototype liner were used to correlate microwave and conventional oven-drying results. If the uncompacted soil did not have a moisture content between 11 and 12 percent, the soil was either wetted (most common occurrence) or allowed to dry and then retilled before compaction.

After a lift was compacted, a Seaman Nuclear® density meter was used to measure the density and moisture content at eight locations on the surface of each lift. The coordinate of each sampling location had been preselected and identified in the QA/QC plan on the basis of statistical analysis of density and moisture results from the prototype liner construction. Before measurements of the field-scale were made, a density/moisture calibration curve was constructed for the meter; samples collected during excavation of the prototype liner provided the basis for this calibration.

Results of the nuclear density tests during compaction of the liner are shown in table 5. The statistical analysis of the density results (table 6) indicate that the dry densities ranged from 90 to 95 percent of the maximum Standard Proctor density, or 93 to 97 percent of the density at

Table 5 Lift density and moisture data collected from the field-scale liner.

Date	Lift no.	Sampling locations (m) X	Y	Wet* density g/cm³	Water* density g/cm³	Dry density g/cm³	Water content %	Remarks
6/23/87	1	Standards						Okay
6/23/87	1	7.3	6.7	2.11	.194	1.91	10.1	After 8 passes.
6/23/87	1	7.3	6.7	2.11	.186	1.92	9.7	Meter not moved.
6/23/87	1	17.3	7.0	2.12	.242	1.88	12.9	
6/23/87	1	17.3	7.0	2.12	.238	1.88	12.7	
	Observation:	Moisture content was not homogenous. Dry density was low.						
	Decision:	Tilled and re-compacted (4 more passes).						
6/23/87	1	3.0	4.6	2.16	.214	1.94	11.0	Total 12 passes.
6/23/87	1	6.1	4.9	2.07	.203	1.87	10.9	
6/23/87	1	9.1	4.9	2.02	.229	1.79	12.8	
6/23/87	1	12.5	4.9	2.07	.224	1.84	12.2	
6/23/87	1	12.5	4.9	2.14	.224	1.91	11.7	Meter rotated 180°.
6/23/87	1	3.0	2.7	2.15	.218	1.83	11.9	
6/23/87	1	3.0	2.7	1.89	.200	1.69	11.8	Meter rotated 180°.
6/23/87	1	3.0	2.7	1.90	.197	1.70	11.6	Meter not moved.
6/23/87	1	6.1	2.4	2.16	.256	1.90	13.4	
6/23/87	1	12.5	2.4	2.12	.258	1.86	13.8	
6/23/87	1	9.1	2.4	2.01	.214	1.80	11.9	
	Observation:	No increase in density after 4 more passes. The reason might be (1) moisture was at wet of optimum or (2) the underneath gravel (for drainage) didn't have enough bearing capacity.						
	Decision:	More passes might cause bearing failure. Accepted! Because wet of optimum yields low K.						
6/23/87	2	Standards						Okay.
6/23/87	2	9.4	8.5	2.07	.218	1.85	11.7	After 12 passes.
6/23/87	2	14.0	8.2	2.09	.224	1.87	12.0	
6/23/87	2	18.8	7.6	2.11	.224	1.89	11.9	
6/23/87	2	18.8	7.6	2.05	.221	1.83	12.1	Meter rotated 180°
	Observation:	Density was still low. Soil was still wet.						
	Decision:	The lift was tilled and allowed to air dry for 2 hours before covering with plastic for the day.						
6/24/87	2	Standards						Okay.
6/24/87	2	4.3	6.5	2.10	.238	1.86	12.8	After 12 passes.
6/24/87	2	10.6	6.5	2.02	.218	1.81	12.0	
6/24/87	2	2.1	3.6	2.12	.221	1.90	11.6	
6/24/87	2	6.4	3.6	2.12	.221	1.90	11.6	
6/24/87	2	8.5	3.6	2.14	.224	1.92	11.7	
6/24/87	2	12.8	3.6	2.03	.224	1.82	12.4	
6/24/87	2	3.6	0.8	2.08	.218	1.87	11.7	
6/24/87	2	10.6	0.8	2.11	.238	1.87	12.8	
	Observation:	Average dry density was over 90% of the Proctor Maximum.						
	Decision:	Accepted! The 90% density was then assigned for the new compaction specification.						
6/24/87	3	Standards						Okay.
6/24/87	3	3.0	4.6	1.95	1.89	1.76	10.7	After 12 passes.
6/24/87	3	6.1	4.9	1.92	.211	1.69	12.4	
6/24/87	3	9.1	4.9	2.08	.218	1.86	11.7	
	Observation:	Density was too low.						
	Decision:	Recompacted (4 more passes).						
6/24/87	3	Standards						Okay.
6/24/87	3	12.5	4.9	2.04	.206	1.83	11.3	Total 12 passes.
6/24/87	3	3.0	2.7	2.03	.235	1.79	13.1	
6/24/87	3	6.1	2.4	1.97	.221	1.75	12.5	
6/24/87	3	10.1	2.4	2.10	.211	1.89	13.2	Meter rotated 180°
	Observation:	No increase in density after 4 more passes. Soil was still wet. In forecast, more rain is coming. Furthermore, the soil at stockpile was **very** wet.						
	Decision:	Tilled and allowed to dry. Cover with plastic overnight. Resume compaction activity next Monday (June 29). The soil stockpile must be reprocessed and dried.						
7/2/87	*Observation:*	Weather was bad. Rained every other day. Soil was too wet to compact.						
	Decision:	Postpone the compaction schedule to the week of July 6.						
7/7/87	*Observation:*	Weather was still bad. Forecast isn't good for a few weeks. Because of rain, the soil at stockpile is wetter. Reprocess to proper moisture content is necessary.						
	Decision:	Postpone the schedule to the week of August 3. Soil reprocessing begins July 13.						

Table 5 *(continued)*

Date	Lift no.	Sampling locations (m) X	Y	Wet* density g/cm³	Water* density g/cm³	Dry density g/cm³	Water content %	Remarks
8/5/87	3	Standards						Okay.
8/5/87	3	Standards						Okay.
8/5/87	3	12.5	4.9	1.95	.168	1.78	9.4	After 12 passes.
8/5/87	3	3.0	4.6	1.83	.179	1.65	10.8	
	Observation: Soil was too dry and density was low.							
	Decision: Water added, surface retilled, and recompacted.							
8/5/87	3	7.0	5.2	2.06	.179	1.88	9.5	After 12 passes.
8/5/87	3	3.0	4.6	1.95	.179	1.77	10.1	
8/5/87	3	3.0	2.7	2.00	.197	1.81	10.9	
8/5/87	3	6.1	2.4	1.90	.203	1.70	12.0	
8/5/87	3	12.5	2.4	2.02	.182	1.83	9.9	
8/5/87	3	12.5	4.9	1.86	.194	1.67	11.6	
8/5/87	3	9.1	4.9	1.96	.206	1.76	11.7	
8/5/87	3	9.1	2.4	1.98	.186	1.79	10.4	
	Observation: Although density was still low, there was no density increase after recompaction.							
	Decision: Accepted!							
8/5/87	4	4.3	6.5	2.04	.218	1.82	11.9	After 12 passes.
8/5/87	4	10.6	6.5	1.98	.194	1.79	10.8	
8/5/87	4	2.1	3.6	2.00	.200	1.80	11.1	
8/5/87	4	6.4	3.6	2.04	.186	1.86	10.0	
8/5/87	4	8.5	3.6	2.01	.221	1.79	12.3	
8/5/87	4	12.8	3.6	1.99	.182	1.81	10.1	
8/5/87	4	4.3	0.8	1.84	.176	1.66	10.6	
8/5/87	4	4.3	0.8	1.96	.186	1.77	10.5	Reprepared surface.
8/5/87	4	10.6	0.8	2.03	.200	1.83	10.9	
8/5/87	4	Standards						Okay.
	Observation: The Density was similar to that of the previous lifts.							
	Decision: Accepted!							
8/6/87	5	Standards						Okay.
8/6/87	5	3.0	4.6	2.00	.194	1.81	10.7	After 12 passes.
8/6/87	5	6.1	4.9	2.14	.214	1.93	11.1	
8/6/87	5	6.1	4.9	2.11	.214	1.90	11.3	Meter rotated 180°.
8/6/87	5	9.1	4.9	2.02	.277	1.74	15.9	Error by side effect.
8/6/87	5	9.1	4.9	2.09	.218	1.87	11.6	Cut the side off.
8/6/87	5	12.5	4.9	2.12	.245	1.87	13.1	
8/6/87	5	12.5	4.9	2.17	.259	1.92	13.5	Meter rotated 180°.
8/6/87	5	3.0	2.7	1.97	.200	1.77	11.3	
8/6/87	5	6.1	2.4	2.08	.206	1.88	11.0	
8/6/87	5	9.1	2.4	2.04	.197	1.85	10.6	
8/6/87	5	12.5	2.4	2.20	.218	1.99	11.0	
8/6/87	5	Standards						Okay.
	Observation: The density was similar to that of the previous lifts.							
8/6/87	6	Standards						Okay.
8/6/87	6	0.8	6.5	2.07	.197	1.87	10.5	After 12 passes.
8/6/87	6	0.8	6.5	2.14	.197	1.94	10.1	Meter rotated 180°.
8/6/87	6	7.3	6.5	1.76	.200	1.56	12.8	Error by side effect.
8/6/87	6	7.3	6.5	1.88	.203	1.66	12.2	
8/6/87	6	13.8	6.5	1.91	.173	1.74	9.9	
8/6/87	6	3.0	3.6	2.16	.221	1.94	11.4	
8/6/87	6	10.3	3.6	2.08	.211	1.87	11.3	
8/6/87	6	0.8	0.8	2.00	.197	1.80	10.9	
8/6/87	6	7.3	0.8	2.14	.242	1.90	12.7	
8/6/87	6	13.8	0.8	2.05	.218	1.83	11.9	
8/6/87	6	Standards						Okay.
	Observation: The density was similar to that of the previous lifts.							
	Decision: Accepted!							

* Determined from the ISGS density and moisture curves which were calibrated for the soil material used in the full-scale liner.

Table 6 Means and standard deviations of density and moisture contents of compacted lifts of the field-scale liner.

Lift no.	n[a]	Mean density g/cm³ [b]	s[c]	Percentage of Proctor density (at 9.9%)[d]	Percentage of Proctor density (at 11.3%)[e]
1	11	1.83	0.08	92	95
2	8	1.87	0.05	95	97
3	8	1.78	0.07	90	92
4	9	1.79	0.06	90	93
5	10	1.88	0.06	95	97
6	9	1.84	0.09	93	95
Overall	55	1.84	0.08	93	95

Lift no.	n	Mean moisture content (%)	s
1	11	11.9	0.7
2	8	12.0	0.7
3	8	10.8	0.9
4	9	10.9	0.8
5	10	11.5	1.0
6	9	11.2	1.0
Overall	55	11.4	1.0

[a] sample size
[b] $g/cm^3 \times 62.5 = lb/ft^3$
[c] standard deviation
[d] 9.9% is optimum moisture content for achieving a maximum Standard Proctor density of 1.98 g/cm^3
[e] 11.3% is approximate moisture content at which a Proctor density of 1.93 g/cm^3 was achieved

approximately 2 percent wet of the optimum moisture content. The densities were generally lower than the construction specification (95% of the maximum Proctor density). The densities may have been lower than expected because of (1) the design, which specified that the soil be compacted at a moisture content greater than wet of optimum, making it difficult or impossible for maximum densities to be achieved; and (2) the low bearing capacity of the pea gravel used in the underdrain system, so that the compaction effort was limited. Our assessment was that additional compaction could overcompact the soil, causing bearing failure and damage to the underdrain systems and pan lysimeters. Because density is a measure of the compaction efficiency and does not directly relate to the hydraulic properties of the material, 12 passes by the compactor were considered acceptable.

Cutoff Wall, Retaining Wall, Catwalk, and Shelter Construction

A cutoff wall was designed to limit lateral movement of water from the liner study area so that fluid flow would be vertical. Construction of the cutoff wall began by defining the location of the test area relative to the entire liner. Once the boundaries of the test area were located, a 15-cm-wide trench was cut, by machine, from the surface of the liner to the top of the foundation. Two 6-mil sheets and one 30-mil sheet of geomembrane were placed against the outside wall (the wall away from test area) of the trench, then the trench was backfilled with a mixture of 9-percent bentonite and 91-percent soil (fig. 15). The soil/bentonite mixture was placed into the trench in 8-cm lifts; each lift was lightly wetted and compacted using a compressed-air-operated jackhammer tamper. The tamper compaction effort was similar to effort applied in the Standard Proctor testing, and thus acceptable densities could be achieved in the cutoff wall. Technical data supplied by the manufacturer indicated that a soil mixture of 8.75-percent bentonite/91.25-percent would result in a reduction of the saturated hydraulic conductivity of a soil from 1×10^{-4} to 1×10^{-10} cm/s. We assumed that the hydraulic conductivity of the compacted bentonite/soil mixture would be one to two orders of magnitude less than that of the liner, and thus reduce or eliminate lateral movement of water.

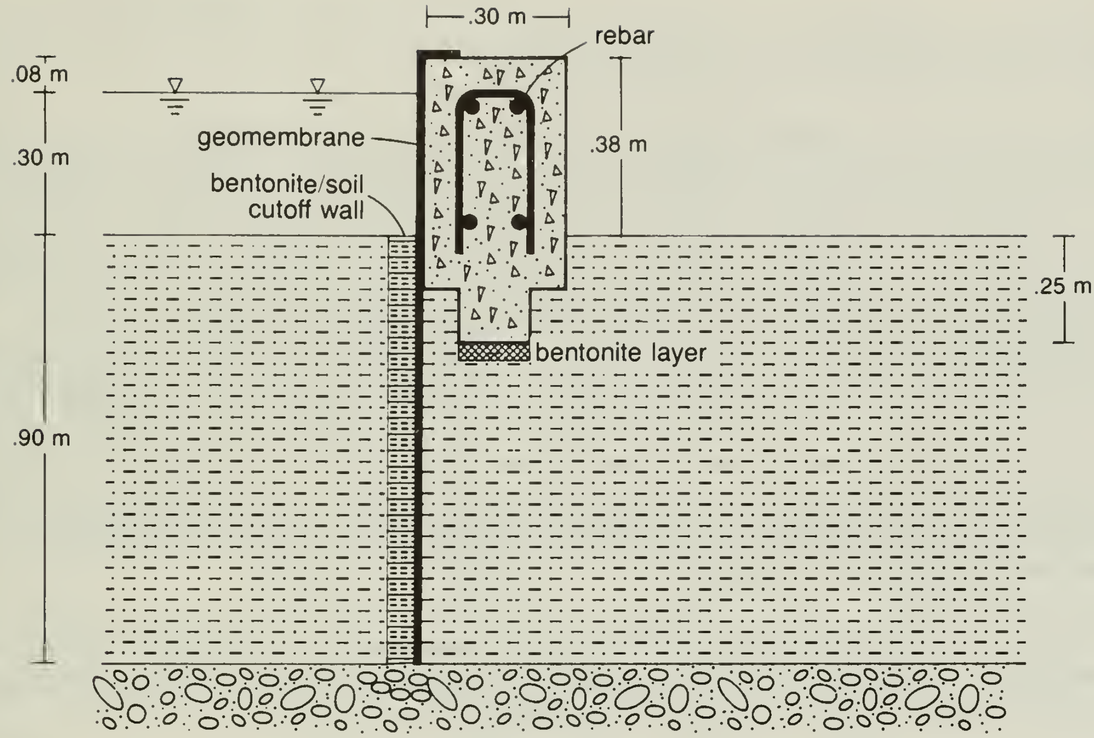

Figure 15 Design of the cutoff wall.

Slump failures or cracking occurred during cutoff-wall construction at three locations in the liner. A crack approximately 4 m long by 15 cm wide, running from the northeast corner towards the west and parallel to the trench, was excavated by removing an area of the liner 6 m long by 0.6 m wide. A small crack trending toward the west was observed in the northwest corner; this area was shored up to prevent slumping before filling of the cutoff trench. A third slump approximately 1.5 m long by 1.5 m wide occurred in the southwest corner of the liner. In these slumped areas, we excavated the soil with a backhoe, then recompacted it into the excavations exactly as we had filled the trench for the cutoff wall. When the cutoff wall was completed, the liner surface was graded to remove approximately the top 15 cm of soil. The final thickness of the liner was 0.9 ± .03 m.

Construction of the retaining wall required approximately 10 cubic meters of concrete. To expedite wall construction, we used a pumper truck to pump the concrete into the forms. The concrete was allowed to cure for 1 week before the forms were removed. When the retaining wall was completed, a cement-based waterproofing material (Thoroseal®) was brushed on the pond side of the wall.

A slot left by the forms between the concrete wall and the polyethylene sheets of the cutoff wall was filled with bentonite to minimize water seepage between the concrete/plastic interface. The bentonite was poured into the slot in lifts and periodically compacted with a metal rod.

The 30-mil polyethylene sheet installed as part of the cutoff wall was placed up and over the retaining wall. A soldering iron was used to seal the above-ground seams located at each corner and the punctures that developed during installation of the sheets. No attempt was made to seal the seams or punctures below the liner surface. After the holes in the sheet were repaired, a 5-cm-thick layer of bentonite was poured at the liner surface between the plastic and retaining wall. The sheet was then placed up and over the retaining wall. The wood sill was installed and the plastic fastened to the sill with staples.

The wood sill was attached to the top of the retaining wall. The sill design allowed for the attachment of a catwalk and the polyethylene sheet (geomembrane) of the cutoff wall, and for location of reference points for installing instruments.

A leak was detected in the liner slope outside the study area during the initial filling of the liner pond. We drained the pond and located the source of the leak. It occurred in the southeast corner of the pond when water traveled along a crease in the polyethylene sheet used as part of the cutoff wall. To remedy this problem, we dug a trench 20 cm wide by 13 cm deep along the inside of the concrete retaining wall (fig. 16). Geofabric was placed on the liner and the soil that had been excavated from the trench was temporarily placed on the geofabric. The polyethylene sheets were then cut off at the base of the trench. A bentonite slurry was poured on the bottom of the trench and a 20-mil sheet of PVC plastic was attached to the side of the trench. The excavated soil was mixed with bentonite and compacted into the trench, and the PVC plastic was placed over the compacted soil/bentonite mixture and attached to the sill of the retaining wall. The remaining excavated soil was placed on top of the PVC plastic and covered with geofabric to prevent soil dispersion onto the study surface. No detectable leaks have occurred since we refilled the pond.

Four drainage collection pits serve as water collection stations for the underdrain system and pan lysimeters. Constructing the four drainage pits consisted of excavating part of the liner slope and building a concrete block wall to stabilize the slope.

A catwalk built of trusses spanning the north and south retaining walls provides us with access to instruments at various locations. We also built a 13.7 × 24.4-m weatherproof shelter over the liner. Gas, water, electricity, and a gas-fired radiant heater were installed in the shelter.

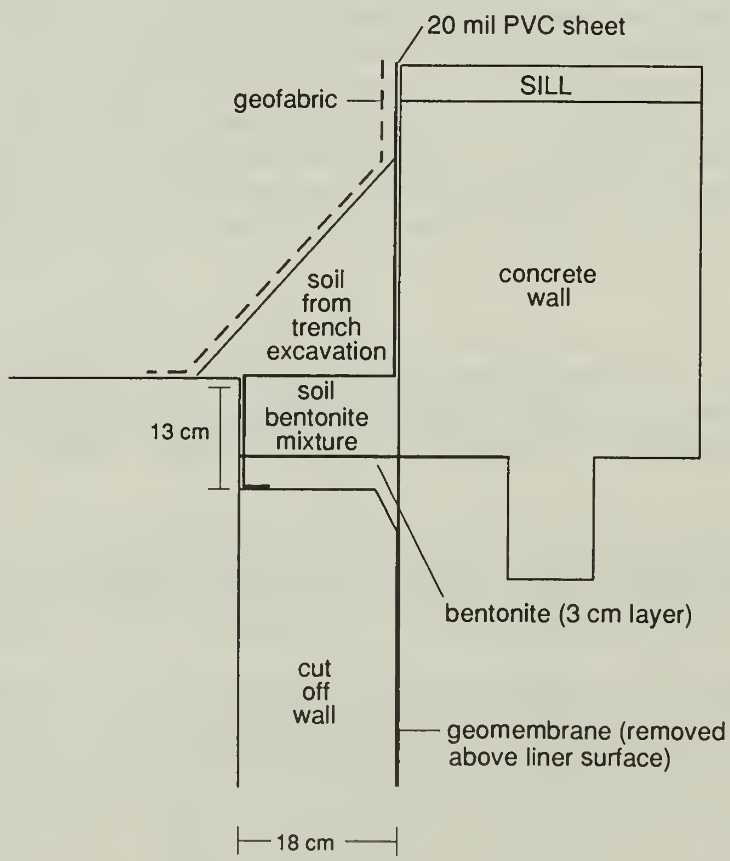

Figure 16 Remedial design of cutoff wall.

Geotechnical Evaluation of the Liner Soil

Geotechnical testing was conducted to determine whether the material selection process and prototype liner study could project the engineering characteristics of the final field-scale liner. Moisture content, density, Atterberg limits, and particle-size distribution were measured during each phase of the project. Fifteen auger samples were collected from the stockpiled soil used to construct the field-scale liner. Each sample consisted of 16 to 25 kg of soil obtained by combining four auger samples from each truckload of soil delivered to the construction site. Laboratory test results for these composite samples are shown in column 4 of table 7. Results from geotechnical testing of samples collected during the material selection and prototype liner phases are given in columns 1 and 2 (table 7); details about the collection of these samples can be found in chapters 1 and 2, respectively. Column 3 of table 7 presents the results of in situ measurements made during the field-scale liner construction.

Table 7 Summary of the geotechnical properties of the Batestown Till during various project phases.

Project phase	Material selection	Prototype liner	Field-scale liner	Lab tests of materials from field-scale liner	
Density (g/cm^3)					
X[a]	2.08	1.85[d]	1.84[d]	1.98[e]	1.94[f]
s[b]	0.02	0.08	0.08	0.01	0.02
CV[c] (%)	1.0	4.3	4.3	0.5	1.0
Moisture (%)	10.3	11.6	11.4	9.9	11.3
Atterberg limits					
Liquid Limit (%)					
X	21.1			23.3	
s	1.6			0.51	
CV (%)	7.6			2.2	
Plasticity index (%)					
X	7.0			10.1	
s	1.6			1.2	
CV (%)	22.9			11.9	
Particle size distribution[g]					
Sand (%)					
X	35.2	33.9		37.1	
s	2.2	1.1		1.4	
CV (%)	6.3	3.2		3.8	
Silt (%)					
X	38.3	35.4		33.1	
s	1.2	2.4		0.8	
CV (%)	3.1	6.8		2.4	
Clay (%)					
X	26.5	30.7		29.8	
s	3.2	2.9		0.7	
CV (%)	12.0	9.4		2.3	

[a] mean
[b] standard deviation
[c] coefficient of variation
[d] in-situ measurements
[e] standard Proctor dry densities at 9.9% moisture content
[f] standard Proctor dry densities at 11.3% moisture content
[g] sand < 2 mm and > 63 μm, silt < 63 μm and > 4 μm, clay < 4 μm

Laboratory-determined dry densities (Standard Proctor) and in situ (Nuclear Seaman) measured dry densities ranged from 2.08 to 1.84 g/cm^3 for all three project phases (table 7). The laboratory densities measured during the material selection phase of the project had the highest densities. In situ density measurements for the prototype and field-scale liner, averaged for all lifts, varied less than 0.1 g/cm^3 (6 lb/ft^3), and the average moisture contents were in close agreement (0.02%).

Average in situ densities of prototype and field-scale liners were 93 percent of the maximum laboratory-measured dry bulk density of the composite samples taken during liner construction. Measurements performed on samples collected during the material selection phase yielded densities approximately 5 percent greater than those determined from samples obtained during liner construction.

The plasticity index of samples collected during the material selection process was below the selection criterion set for the study (a plasticity index greater than 10%). However, the mean plasticity index of field-scale composite samples was 10.1 percent. The liquid limit of the samples used to construct the field-scale liner were approximately 2 percent higher than for those samples collected during the material selection phase.

The particle-size distribution of samples from all three project phases was relatively uniform. The clay fraction ranged from a high of 30.8 percent for the prototype samples to a low of 26.5 percent for the initial characterization samples. In general, differences in the percentage of sand, silt, or clay fractions varied less than 5 percent, indicating that the soil material used in all three project phases was relatively homogeneous.

Geotechnical tests performed on samples collected during all three phases of the project indicated that the soil samples were relatively uniform. Thus, the initial characterization of the soil material was adequate to predict the geotechnical properties of the field-scale liner.

4 LABORATORY DETERMINATION OF SOIL-MOISTURE CHARACTERISTIC CURVES

Soil-moisture characteristic curves were determined for 35 samples collected during excavation of the prototype liner. An averaged curve, determined on the basis of all samples, was used as input data for the numerical flow models. The curve provides the relationship between soil matrix pressure, which is measured in the liner, and volumetric moisture content of the soil. This curve is also used to calculate unsaturated hydraulic conductivity. As part of the test, bulk density and saturated moisture content (porosity) were also determined.

Methods

During excavation of the prototype liner, undisturbed soil cores contained in brass rings (5.7 cm in diameter by 3.0 cm high) and bulk soil samples were collected at the surface and at depths of 0.2, 0.3, 0.5, 0.6, 0.8 m at ten locations in each compacted lift (fig. 17). Soil cores were collected with a drop hammer core sampler (Soil Moisture Equipment Corp Model 200-A). At locations 1, 4, and 6 (fig. 17), soil cores were incorrectly sampled and were not analyzed.

Undisturbed soil cores and corresponding bulk samples were analyzed to determine the relation between moisture content and capillary pressure. Of the 42 correctly sampled cores, seven were either damaged during laboratory preparation procedures or were unusable because they contained large pebbles near their ends. The standard Tempe cell method (Reginato and van Bavel 1962) was used to obtain the pressure/moisture relationship over a pressure range of 0 to 860 cm of water. The dry end of this range is much greater than that experienced in the actual field-scale liner, because the liner was constructed at a high moisture content (11.4%) and moisture content continues to increase as water infiltrates into the liner. Therefore, we emphasized characterizing the high-moisture-content (low-pressure) range of the moisture-content/capillary-pressure relationship.

To fully characterize the moisture-content/pressure relationship, we used a pressure plate extractor and bulk samples to extend the characterization to 2,500 cm of water (ASTM D2325-68, ASTM D3152-72). This test was conducted on duplicate 25-gm samples that had been passed through a 2-mm sieve. We increased the pressure in the extractor incrementally from 1,000 to 2,500 cm of water and determined the moisture content of the samples gravimetrically at each increment.

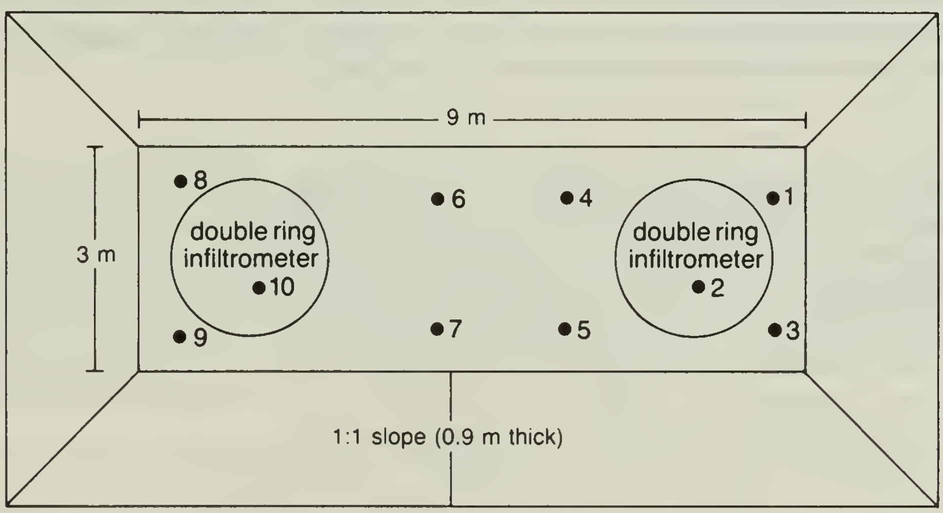

Figure 17 Plan view of the prototype liner showing sampling locations of the soil cores.

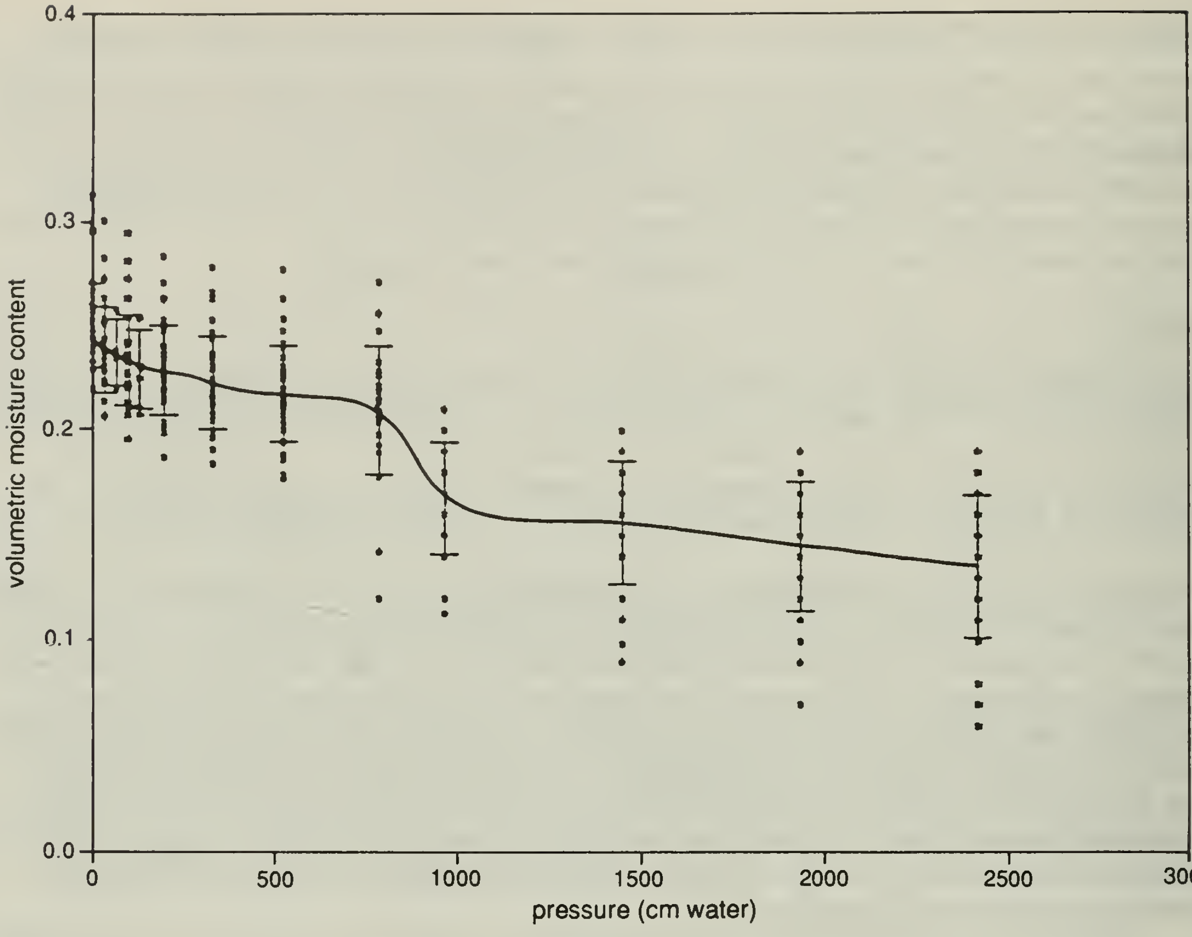

Figure 18 Soil-moisture characteristics curve for the Batestown Till. The solid line represents the average moisture content for a given pressure. The brackets represent one standard deviation about the mean. Datum points were generated by 35 core samples collected from the prototype liner.

Results

Results from the soil-moisture characteristic tests are plotted in figure 18. A solid line has been drawn through the mean value of volumetric moisture content at each increment in pressure. Error bars indicate one standard deviation from the mean. The mean value of saturation moisture content (porosity) is 0.250 cm^3/cm^3, with a standard deviation of 0.020 cm^3/cm^3. This value is plotted at a soil pressure of 0 cm of water in figure 18. The mean value of bulk density is 2.02 gm/cm^3, with a standard deviation of 0.047 gm/cm^3.

Summary

The soil-moisture characteristic curve shows a very slight decrease in volumetric moisture content for the initial pressures between 500 and 800 cm of water, then an abrupt decrease in moisture content between 800 and 1,000 cm of water. This shift is probably the result of a change in methods used (from the Tempe cell to the pressure plate extractor) and not a feature of the samples. However, the volumetric moisture content in the recompacted Batestown Till continued to decrease with increasing pressure throughout the test. The large standard deviations at high pressures also suggest that this continuing decrease in volumetric moisture content may be an artifact of the testing or sampling procedure.

5 INSTRUMENTATION OF THE FIELD-SCALE LINER

The performance of the field-scale liner is assessed in terms of (1) rate of water infiltration, (2) rate of wetting-front advancement, and (3) rate of tracer migration through the liner. Various instruments, including large- and small-ring infiltrometers, tensiometers, lysimeters, gypsum blocks, and evaporation pans are used to monitor the infiltration and movement of water and tracers through the liner. This chapter includes information about the liner monitoring plan and instrumental design, installation and monitoring procedures, and quality assurance methods associated with each task.

Monitoring Plan

The instrument monitoring plan was designed to allow for replication of measurements between liner quadrants and equal spacing of instruments in a rectangular grid design (fig. 19); 212 instruments were used to measure various parameters in and around the liner.

The numbers and locations of instruments were determined on the basis of (1) classical statistical estimates of sample numbers needed to estimate the mean of each physical and/or chemical property to within a specified degree of accuracy at a high confidence level; (2) geostatistical estimates of optimal sample numbers, particularly for hydraulic flux measurements, which tend to vary more than other physical properties and exhibit a high degree of spatial dependence; (3) measurement scale effects; and (4) provision for areal and vertical monitoring of the liner.

Coefficients of variation (CV) for moisture contents in naturally occurring soils have been reported to be between 12 and 50 percent, depending on the soil tension—where the variation in moisture content increases as soil tension increases (Warrick and Nielsen 1980). Results from the prototype liner study indicated that initial water contents, and hence tensions, are relatively uniform in a soil liner. Coefficients of variation for moisture contents in the prototype liner were generally less than 25 percent. Classical statistics were used to determine the number of samples required to estimate a mean within a predetermined error. Thus,

$$n = \frac{t^{*}_{(\alpha,n-1)}CV^2}{F} \qquad [1]$$

where n is the number of samples required to estimate the true mean to within F percent error from the sample mean at a given confidence level; t is the two-tailed Student's t-value for (n-1) degrees of freedom, and CV is the coefficient of variation (sample standard deviation divided by the sample mean) in percent (Snedecor and Cochran 1980). This equation is solved iteratively, since the value of t is a function of n. The method, based on the central limit theorem, assumes a normal population distribution, although it is commonly used for data that are not normal. Finite variance and random independent samples are also assumed. No accounting of spatial dependence can be made using this approach. Using a CV of 25 percent, we estimated the mean water content, and hence tension, of 24 samples to be within a 10-percent error at the 95-percent confidence level. Therefore, the use of 84 tensiometers, as specified in the monitoring plan, provided a conservative number of samples and allowed for instrument malfunctioning and breakage.

The optimum number of infiltrometers was determined on the basis of geostatistical results from a compacted soil liner study (Rogowski and Simmons 1988). Rogowski and Simmons developed a semivariogram for infiltration rates measured with 250 infiltrometers that were 30 cm in diameter. The semivariogram was used to calculate kriging variances (estimation variances), standard errors, and optimal sample numbers. Rogowski's results showed that

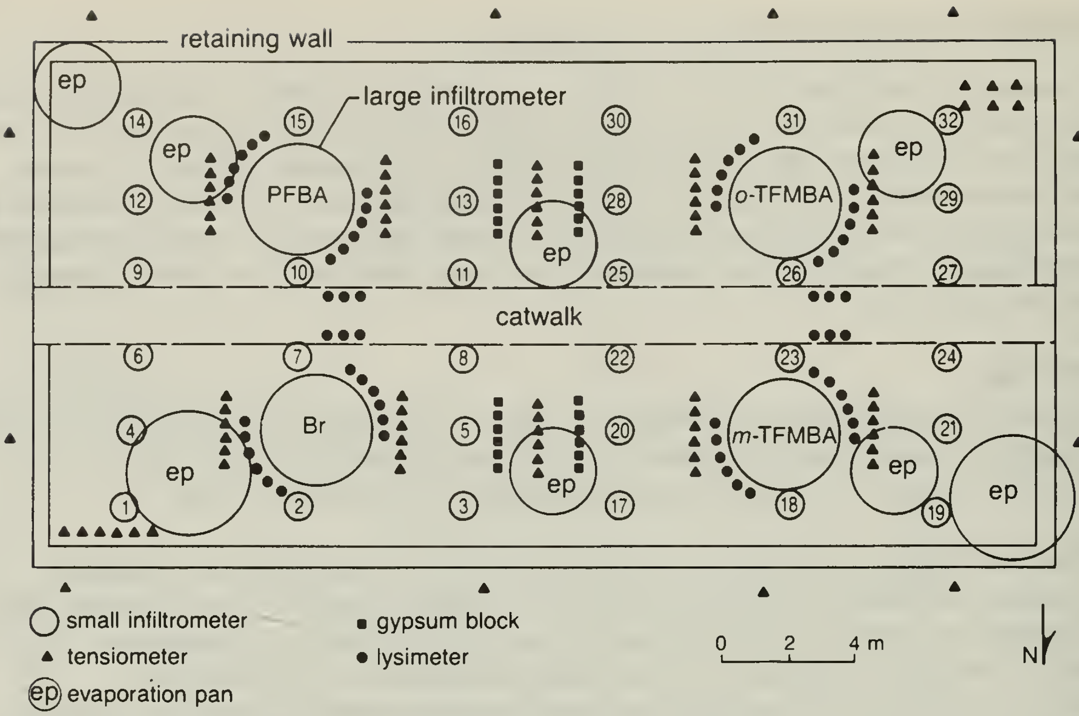

Figure 19 Plan view of liner showing locations of instruments.

about 50 samples provided an optimal number for estimating the mean infiltration rate; however, little increase in error was observed when the sample number was decreased to 30. These estimates suggested that 32 infiltrometers would be adequate for our monitoring.

Scale effects in estimating the hydraulic properties of the liner were considered in terms of both the relatively small dimensions of the soil liner as a whole and in terms of the sample volumes being measured by various monitoring instruments. Since the liner appears relatively homogeneous, as determined from density and water content, our sample number estimates for the instruments are thought to be conservative. Scale effects are evaluated by collecting in situ data at various scales. Increasing the sample volume will generally decrease variance so that fewer samples, incorporating a large area (i.e. large-ring infiltrometers), can be used to characterize the liner hydraulic properties. For example, in addition to the 32 small-ring infiltrometers (30-cm diameter), four large-ring infiltrometers (1.5-m diameter) and a mass water balance are continually being monitored to provide average infiltration rates for the entire liner. Extensive areal and vertical coverage by the monitoring instruments in the liner are illustrated in figure 19 and table 8.

Instrument Locations

The coordinates of each instrument on the liner were determined on the basis of a rectangular grid system. The abscissa and ordinate of the grid was considered the axis from the northeast to northwest and the northeast to southeast corners of the liner retaining wall, respectively. We marked the coordinate system and used a series of string lines and a plumb bob to determine the x and y coordinate of each instrument. The z coordinate was measured from the liner surfaceby lowering a ruler to the bottom of the hole into which each instrument was installed.

Instrument Design and Operation

■ Infiltrometers

The large-ring infiltrometers are fiberglass domes 1.5 m in diameter. Air was vented through two ports in the dome during installation. Since installation, one port has been used for routine maintenance to vent any gases that become entrapped in the dome, and the second port has

Table 8 Summary of instrumentation in the field-scale liner.

Instrument	Quantity	Location	Parameter measured
Large-ring infiltrometers	4	Center of each quadrant	Infiltration rates
Small-ring infiltrometers	32	8 per quadrant	Infiltration rates
Transducer tensiometers	66	2 nests per quadrant 1 nest in NE corner 2 nests along N-S center line	Soil-water tension
Gage tensiometers	18	SW corner and liner perimeter	Soil-water tension
Gypsum blocks	24	4 nests along N-S center line	Soil-water tension
Lysimeters	60	2 nests per quadrant 2 nests along E-W center line	Collect soil water for tracer analysis
Evaporation pans	8	Equally spaced in pond and liner perimeter	Evaporation rates

provided a connection for a water-infiltration monitoring device (intravenous (I-V) bag). These large-ring infiltrometers are designed specifically for use with soils that have low infiltration rates, generally in the range of 1×10^{-5} to 1×10^{-8} cm/s (Trautwein, personal communication, 1989). The small-ring infiltrometers are open-ended steel pipes 0.3 m in diameter and approximately 0.6 m high, with a port allowing connection to an I-V bag. The top of each pipe is covered with plastic to minimize evaporation; a small hole in the plastic permits pressure equilibration with the atmosphere. These small-ring infiltrometers were modified from the design used by Rogowski (1990) so that infiltration fluxes could be measured with I-V bags.

Operation of the infiltrometers is based on maintaining a constant head in each infiltrometer equal to the water level in the liner pond. The pond serves as the outer ring for all the infiltrometers to ensure vertical flow from the rings. As water infiltrates into the liner, water exits the I-V bag and moves into the infiltrometer to maintain a constant head. The bags are weighed periodically to determine weight loss, and the volume of water infiltrating into the liner from each infiltrometer is determined.

■ Pressure-Transducer Tensiometers

Pressure-transducer tensiometers were constructed with a sensing and monitoring component (fig. 20). The sensing component consists of two 1/8-inch OD (outside diameter) rigid polyvinyl tubes; one end of both tubes was epoxied to a single ceramic porous cup 1 inch long by 3/8-inch OD. Compression fittings were attached to the other end of the tubes to make air- and watertight connections with the monitoring devices (pressure transducers). The porous cups were placed at selected monitoring depths within the liner. One tube was sealed via a valve and the other was attached to the pressure transducer. The tubes and porous cup are periodically flushed with water to eliminate air that may become entrapped in the system.

The pressure-transducer tensiometers operate by allowing water to flow freely into or out of the porous cup at soil tensions that do not exceed the air-entry-tension (approximately 1,020 cm H_2O) of the cup. As water moves from the tubes into the unsaturated soil, a vacuum forms in the tubes and exerts a corresponding force on the flexible diaphragm of the pressure transducer. When the soil becomes saturated, water enters the porous cup, causing a negative tension (i.e., positive pressure). The pressure in the tube is measured against the force being

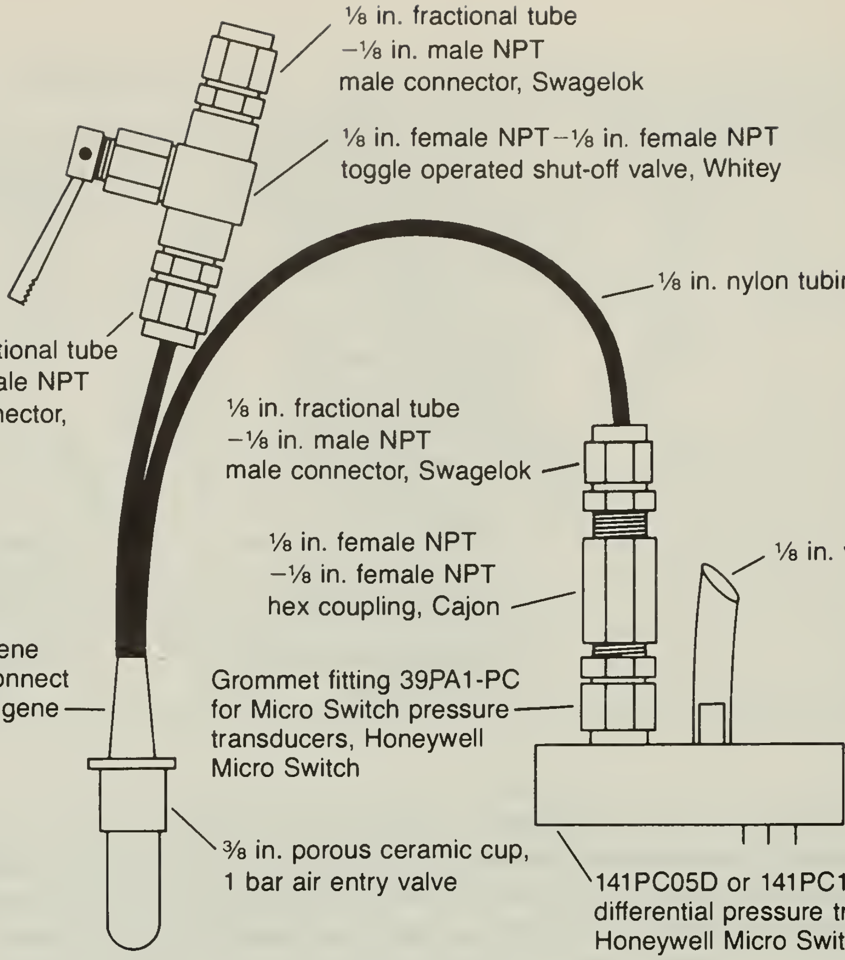

Figure 20 Design of pressure-transducer tensiometers.

exerted by the atmospheric pressure on the other side of the diaphragm. The difference in force results in the pressure-sensitive diaphragm flexing, which is converted into an electrical signal. After calibration of the transducer, this signal can be interpreted in terms of soil tension.

Pressure-transducer tensiometers can measure positive pressure head values equal to the height of the column of water over the tensiometer, and negative pressure head to -1,000 cm of water, depending on the type of transducer used with the tensiometer. Several external factors affect these measurements, however, including the pressure created by the column of water in the tube, air bubbles in the tubes, changes in atmospheric pressure, and changes in temperature. These factors are discussed in detail in chapter 6.

■ Gage Tensiometers

Used as supplemental instruments for monitoring the liner study area and perimeter, gage tensiometers operate on the same principle as transducer tensiometers. Operating in the range of 0 to 1,024 cm of water, their accuracy decreases as soil tensions approach 1,000 cm of water. The gage tensiometers were calibrated before installation into the liner by adjusting the gage to 0 as the ceramic cup of the tensiometer was saturated and submersed in water.

■ Pressure-Vacuum Lysimeters

Constructed to obtain soil water samples at selected monitoring depths in the liner, the lysimeters consist of a 2-inch-long and 1-inch-OD porous cup epoxied into 1/2-inch-OD PVC pipe (fig. 21). Rigid, 1/8-inch-OD polyvinyl tubing was threaded through the pipe until one end of the tube was near the bottom of the porous cup. A T-type fitting was screwed into the open end of the PVC pipe, and the small-diameter tube was threaded through one opening of the fitting. Thick-walled Tygon tubing 1/4 inch in diameter was attached to the other opening of the fitting. All connections were tested to ensure they were air and water tight.The length of each PVC pipe was adjusted to account for the location of the porous cup at different depths in the liner.

The lysimeters were operated by initially creating a vacuum on the lysimeter assembly by sealing off the small diameter tubing and connecting a vacuum pump to the Tygon tubing. The lysimeter was held under a vacuum of approximately 40 cm of water for 48 hours. The vacuum causes water to flow from the soil pores into the porous cup. The water is then removed from the cup by releasing the vacuum and placing a positive air pressure on the assembly, forcing the water in the cup to travel through the small-diameter tube into sample collection vials.

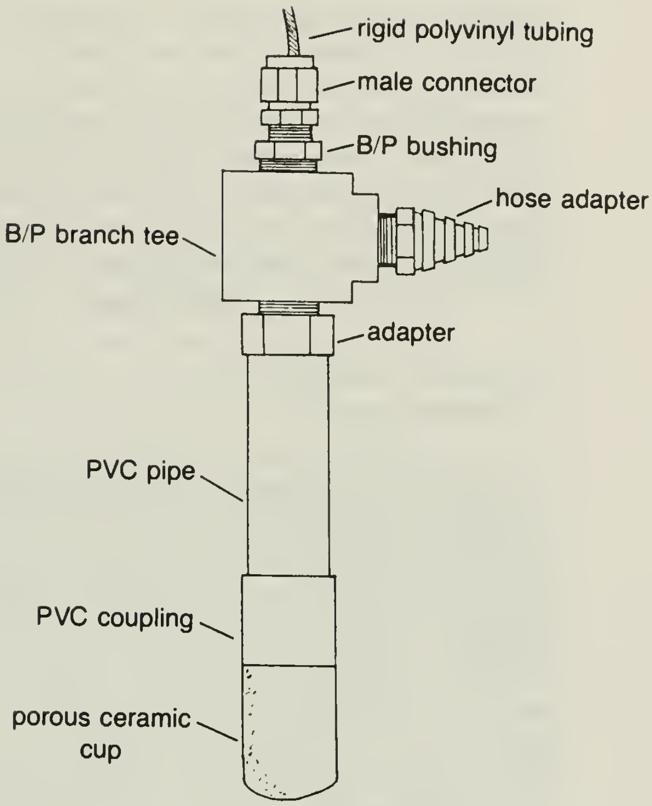

Figure 21
Design of pressure-vacuum lysimeters.

■ **Gypsum Blocks**

The gypsum blocks consist of two metal plates embedded into a block of gypsum ($CaSO_4$). Wires are attached to the plates so that changes in the electrical resistance of the gypsum between the two plates can be monitored. As the moisture content of the gypsum changes (coincident and in equilibrium with moisture changes in the surrounding soil), the electrical resistance of the gypsum is altered. Once these blocks are calibrated, soil moisture estimates can be made by monitoring changes in electrical resistance.

■ **Evaporation Pans**

The evaporation pans are metal cylinders 1.2 or 0.6 m in diameter and approximately 0.3 m tall; the bottom of each cylinder is sealed. Six pans were placed in the pond; the top of each pan is approximately 3 cm above the pond surface. The pans, equally spaced throughout the pond, allow monitoring of evaporation-rate variations within the pond. Two pans were placed on the perimeter of the liner. A stilling well, a device to measure water level, was placed in every pan. The evaporation rate from each pan is being determined by using a graduated cylinder to measure the volume of water added to maintain a constant water height in the pan. The total volume of water that evaporated from the pond over a given period of time was determined by summing data collected from the six pans in the pond.

Quality Assurance

Quality control measures were taken before installation of the instruments to ensure that the data generated would be reliable. All tensiometers and lysimeters were tested in the laboratory for air and water leaks around seals. All leaks were sealed, and the instruments were retested to verify proper operation. Calibration data for the transducers designed to be used as part of the tensiometers were obtained from the manufacturer.

Gypsum-block calibration was performed in the laboratory; 15 gypsum blocks were calibrated. With the exception of one gypsum block, the calibration results were similar. Twenty-four gypsum blocks were needed to implement the instrumentation plan for the liner. We assumed that the uncalibrated blocks would produce resistance values for a given suction similar to those of blocks that had been calibrated. A calibration curve incorporating the data from the 14 calibrated blocks was used to convert resistance measurement to soil tensions for all 24 gypsum blocks. All gypsum blocks and tensiometers were monitored in the liner prior to ponding to develop background data. Gypsum blocks that generated suspect data were replaced during this time. The pressure transducer of tensiometers that generated suspect data were electronically checked and replaced if necessary. If the transducer was functioning properly and the data were still suspect, the tensiometer was replaced.

Instrument Installation

■ Infiltrometers

One large-ring infiltrometer was installed in each quadrant of the liner. Each large-ring infiltrometer was centered over a pan lysimeter, approximately in the center of the quadrant. The infiltrometers were placed on the liner surface and the outline of the ring was painted on the soil. With the outline of the ring as a guide, we cut a trench 13 cm wide by 10 cm deep into the liner surface. The surface beneath each ring and the bottom elevation of each trench were checked to ensure that the ring would be level. After cheesecloth was placed over the liner surface to minimize soil dispersion in the infiltrometer, the average distance from the liner surface to the top of the sill was recorded. The trenches were filled with a slurry of cement and bentonite (90% cement and 10% bentonite by weight). The rings were pressed into the slurry and the top of each ring was set at a constant elevation (approximately 8 cm below the top of the sill). The slurry was then smoothed using a hand trowel and allowed to dry slowly to prevent cracking.

Thirty-two small-ring infiltrometers were installed in the liner by placing a thick steel plate on the top of each ring and using a sledge hammer to drive the rings into the soil. The bottom of each ring was driven to a depth of approximately 11 cm. Cheesecloth was loosely placed over the soil surface at each ring and anchored as the rings were driven into the ground. The liner material was recompacted around each ring by striking the soil surface with a sledge hammer to minimize preferential flow paths that may have been caused by the installation procedure. A thin layer of cement/bentonite slurry was spread around the ring-soil interface as a further means of reducing preferential flow paths.

■ Pressure-Transducer Tensiometers

The 70 pressure-transducer tensiometers installed in the liner are grouped in nests near each large-ring infiltrometer, between nests of gypsum blocks, and in the northeast and southwest corners of the liner (fig. 19). Each nest contains six tensiometers, with an instrument placed at depths of 10, 18, 33, 51, 69, and 89 cm below the soil surface of the liner. These depths correspond to locations within each of the six lifts of the liner.

Tensiometers were installed in 2.5-cm diameter holes created by driving a soil probe into the liner to the appropriate depth, then withdrawing it. The soil core was saved for backfilling of the hole. The depth of each hole in relation to the liner surface was measured and recorded. The porous cup of each tensiometer was covered with a soil slurry during the installation procedure. The slurry was made by grinding the soil cores through a 2-mm sieve and adding tap water until the soil was the consistency of paste. A small amount of the slurry was placed in the hole before installation of the tensiometers. A metal rod was used to guide the tensiometers down the holes. When the tensiometer reached the bottom of the hole, it was gently tapped to ensure a good contact between the porous cup and the soil. Slurry was added to completely cover the porous cup. Dry Enviro-Seal® (a polymer-treated flour bentonite) was then poured down each hole in short lifts and tightly packed by tamping with a metal rod. The Enviro-Seal, which extends from slightly above the porous cup to the liner surface, prevents preferential vertical water flow around the instruments.

Each transducer circuit was tested for continuity, consistent numbering, and null reading as it was connected to a corresponding tensiometer. Then each transducer was connected to the data logger with a three-wire extension cable labeled at each end to allow for wire identification. Before being connected to the data logger, each transducer was connected to a voltmeter and an 8.0-volt power supply to test for continuity and to confirm the wire labeling. The null value for the differential-type transducers was obtained when the measured pressure was equal to the reference pressure. During the null test, the measuring port was disconnected from the tensiometer, leaving the transducer open to the atmosphere. The output voltage from the transducer was then equivalent to a pressure difference of 0.0 psi. Design null value output of the transducers for an 8.0-volt power source is 1.000 VDC. The null values of the 70 tensiometers were recorded manually. The mean null value was 0.992 V, with a standard deviation of 0.025 V. Values ranged between 1.044 V and 0.939 V, resulting in a maximum error of 6.1 percent. Converting these values to pressure (in cm of water), instrument sensitivity is ± 9.3 cm of water. Standard deviation, maximum error, and instrument sensitivity values are approximately two times greater than values from factory calibration tests obtained for 52 of the instruments. The greater error found in the null values for the transducers installed at the liner (in comparison with that of the factory test values) is probably a result of a combination of factors inherent in field installation, including line losses, uncontrolled temperature, and supply voltage fluctuation. Line losses resulting from the resistance load of the extension wire and from field-installed electrical connections should be constant through time and not affect relative readings from individual instruments.

Operational procedures were adopted to minimize temperature fluctuations. Specifically, a thermostat-controlled electric heater and air conditioner were installed in the instrument trailer to maintain a constant operating temperature for the power supply and data logger. Electronic equipment is kept in the inner room of the trailer to further isolate the equipment from drafts. During the initial phase of installation, the heating system had not established a constant air temperature within the liner shelter (a constant shelter temperature minimizes temperature-induced errors). We have eliminated errors resulting from fluctuations in the power supply by instructing the data logger to record the power supply voltage as part of each instrument scan; we incorporate this value into subsequent pressure calculations.

After the null value test, the transducers were connected to the tensiometers and monitored by the data logger for approximately 2 weeks to obtain background values of soil tension throughout the liner prior to filling of the liner pond.

Two absolute-type pressure transducers (Microswitch® model 142PC15A) were installed in the liner shelter. These instruments are used to monitor atmospheric pressure and provide the reference pressure for the differential-type transducers. Testing of the absolute pressure transducers followed the same procedure used with the differential transducers; however, the test reading is local atmospheric pressure instead of the null value. A voltage divider in each absolute transducer output circuit was installed to ensure that transducer output voltages would be within the input range of the data logger.

■ Gage Tensiometers

Four gage tensiometers were installed in the southwest corner of the liner at depths of 33, 51, 69, and 89 cm. The installation procedure for these instruments was the same as for the transducer tensiometers, except that holes were made with a hand auger rather than with a soil probe. The auger was used to bore large-diameter (4-cm) holes to accommodate the larger diameter of the porous cup on the gage tensiometers.

Twelve gage tensiometers were installed around the periphery of the liner study area. These instruments, a warning/monitoring system to detect water leakage beyond the study area, were installed at a depth of 76 cm and spaced approximately 4.6 m apart. The installation procedure was the same as that used in the study area except that the holes were backfilled with silica sand (flour) rather than bentonite. The sand backfill allows monitoring of soil tensions for the entire 76-cm-deep soil profile rather than a specific depth.

- **Gypsum Blocks**

Twenty-four gypsum blocks were installed in the liner; the procedure was similar to that used with gage tensiometers. A hand auger was used to make the large-diameter (4-cm) holes required by the size of the gypsum blocks. A soil slurry was placed around each block before it was placed in the hole. The holes were then filled with dry Enviro-Seal. Each instrument circuit was tested for continuity and consistent numbering.

- **Pressure-Vacuum Lysimeters**

Sixty pressure-vacuum lysimeters were installed at depths of 10, 18, 33, 51, 69, and 89 cm in the liner. Twelve lysimeters (two nests) are located under the catwalk. The remaining eight lysimeter nests are around the periphery of each large-ring infiltrometer (two nests per infiltrometer) so that the nests are directly across from each other. Each lysimeter is 20 cm from the edge of the infiltrometer (fig 19).

All lysimeters were installed in holes made with a soil probe. Wet soil slurry identical to that used for installation of the gypsum blocks and tensiometers was used to coat the porous cup and also placed in the hole to ensure good contact between the lysimeter cup and the soil. Holes were backfilled with dry bentonite. All lysimeters were tested to make sure they would hold a vacuum.

- **Thermistors**

Two thermistors are used to monitor temperature fluctuations in the liner shelter. One thermistor, built into the data logger, records the temperature of the instrument room. The second thermistor (Campbell Scientific Inc.® (CSI) model 107) is located near the center of the liner shelter to monitor shelter temperature fluctuations.

- **Flow Meter**

A turbine-type totalizing flow meter (Omega Engineering Inc.® model FTB-4107P) was installed in the liner water-distribution system. The flow meter is rated at 76.0 liters/minute maximum flow and is accurate to ±1.0-percent reading at a minimum flow of 0.80 liters/minute. The totalizer is precise to 0.4 liters. A scaled pulse output, connected to the data logger, records flow with a precision of 4 liters.

- **Level switches**

Two liquid level switches (Omega Engineering, Inc.® model LV10) were installed to indicate water level in the liner pond. One switch was installed in normally open (NO) mode, the other in normally closed (NC) mode; each was connected to a colored light mounted on a rafter in the liner shelter to provide visual indication of pond level. The NO switch (green light) indicates adequate water level; the NC switch (red light) indicates low water level. The switches are sensitive only to pond-level fluctuations greater than 4 mm. A staff gage was mounted to the pond wall to visually record pond water levels. The staff gage is calibrated in 1-mm increments to provide accurate readings of water levels.

■ Data Logger

A CSI® model 21× data logger and peripheral equipment is used to monitor the output of the tensiometers, gypsum blocks, thermistors, and flow meter. The basic system was tested during monitoring of the prototype liner. Two 32-channel multiplexers (CSI® AM32) were added to the system to bring the total number of multiplexed analog input channels to 96. The system also includes 15 nonmultiplexed analog input channels and four pulse input channels. All 96 multiplexed channels are used by pressure transducers and gypsum blocks. Two analog input channels and one pulse input channel are also used, allowing for a total of 99 external data inputs. The data logger also records the day, hour, and minute of each recording as well as its own panel temperature and battery voltage.

6 SOIL MOISTURE AND TENSION PROFILES IN THE FIELD-SCALE LINER

Seventy pressure-transducer tensiometers, 18 gage tensiometers, and 24 gypsum blocks were installed in the field-scale liner to (1) provide soil-tension values for estimating the hydraulic gradient of the liner, (2) monitor the position of the wetting front, and (3) monitor changes in soil moisture content resulting from the movement of water through the liner (for description of installation techniques, liner locations, and monitoring procedures see chapter 5.

Total hydraulic head consists of three components: velocity head, elevation head, and pressure head (Freeze and Cherry 1979). *Velocity head* refers to the acceleration of the fluid. In most fine-grained materials, fluid velocity is very low, so the velocity head is considered negligible. *Elevation head* refers to the vertical position of a measurement point relative to some reference plane (datum); it is a measure of the potential energy of the fluid. *Pressure head* describes the fluid pressure and is measured as the height that a column of water will rise to in a manometer at the measurement point. For unsaturated conditions, the pressure head is negative. Tension is defined as the absolute value of the pressure head in the unsaturated zone.

An arbitrary 0 reference elevation was chosen; the bottom of the soil column (liner), soil surface, and surface of the pond are at elevations of 80, 170, and 200 cm, respectively.

Many fine-grained materials have a capillary zone in which most or all of the soil pore spaces are filled with water, even though the pressure head is negative. Such a soil may be referred to as tension saturated. In both the unsaturated and the capillary zones, the negative pressure head prevents flow to a piezometer, and thus a tensiometer is used to measure tension.

Results and Discussion

■ Gypsum Blocks

The gypsum blocks were installed to measure soil moisture, but also could have been used to estimate the tension in the unsaturated zone in soils with known moisture/tension relationships. However, in wet (0.0 to 0.1 bars) or tension-saturated soils, in which capillary water may fill the pore spaces of the gypsum, these instruments generate unreliable results. This was the case in the field-scale liner. Initial wet soil conditions caused capillary water to saturate the gypsum blocks, producing erratic and unreliable data. These instruments appear inadequate in liner monitoring plans. The use of gypsum blocks to measure water movement was thus terminated.

■ Tensiometer Data Reduction

The transducers electrically measure, in volts, the strain on a flexible diaphragm caused by the difference in pressure between the reference port (atmosphere) and the measurement port where the tensiometer water line is connected. The output voltage of each transducer was monitored via a data logger every 10 minutes and averaged so that a single output value was obtained every 24 hours. Because the voltage values have no physical meaning in terms of water content of the liner, voltages were converted to pressure via

$$P_n = \left(\frac{V_{out} \times 4.0}{V_{in}} - 1\right) \times B \qquad [2]$$

where

P_n = negative pressure (cm water)
V_{out} = transducer output (volts)
V_{in} = transducer power supply, approximately 4.0 volts, measured when transducer output is measured.
B = a transducer-dependent conversion factor: 210.9 for 15 psi and 70.3 for 5 psi transducers (cm H_2O).

To account for the pressure created by the weight of the column of water between the measurement point (transducer) and tensiometer cup, we corrected the pressure (P_n) via

$$T_r = P_n - C_w \qquad [3]$$

where T_r = raw tension (cm water)
C_w = column of water (cm water)

The raw tension values were converted to pressure at the tensiometer via

$$P_t = P_{atm} - T_r \qquad [4]$$

and smoothed via

$$\overline{P_t}(n) = \frac{\sum_{n=-14}^{n=14} P_t(n)}{29} \qquad [5]$$

where $\overline{P_t}(n)$ = average P_t at day n
P_t = absolute pressure at the tensiometer
P_{atm} = atmospheric pressure.

Atmospheric pressure was also measured every 10 minutes via the absolute transducers and averaged daily. A smoothed atmospheric pressure (ATM_{avg}) was obtained over the same 28-day interval as P_t. Finally, the averaged values of P_t were converted back to tension via

$$T_a = ATM_{avg} - \overline{P_t} \qquad [6]$$

where T_a = average tension, relative to atmospheric pressure.

Figure 22 shows values of T_r and T_a versus time for one of the 33-cm-deep tensiometers. A comparison of the magnitude of fluctuations for each line in the figure shows that the data-smoothing routine (dashed line) removed irregularities caused by short-term changes in atmospheric pressure.

■ External Effects on Tension Values

Air bubbles Air bubbles that form in the water lines between the tensiometers and transducers can reduce the pressure of the column of water, causing an overcompensation during data reduction and an apparent decrease in tension. That is, $C_w > C_{w\ actual}$ so that $T_r < T_{r\ actual}$ according to equation [3]. Air bubbles can also reduce vacuum pressure in the line, causing an apparent decrease in tension. Air bubbles were removed on a regular basis by flushing the tensiometer lines. Data from an individual tensiometer were not used if the shift in tension caused by removal of the air bubbles was greater than 20 cm.

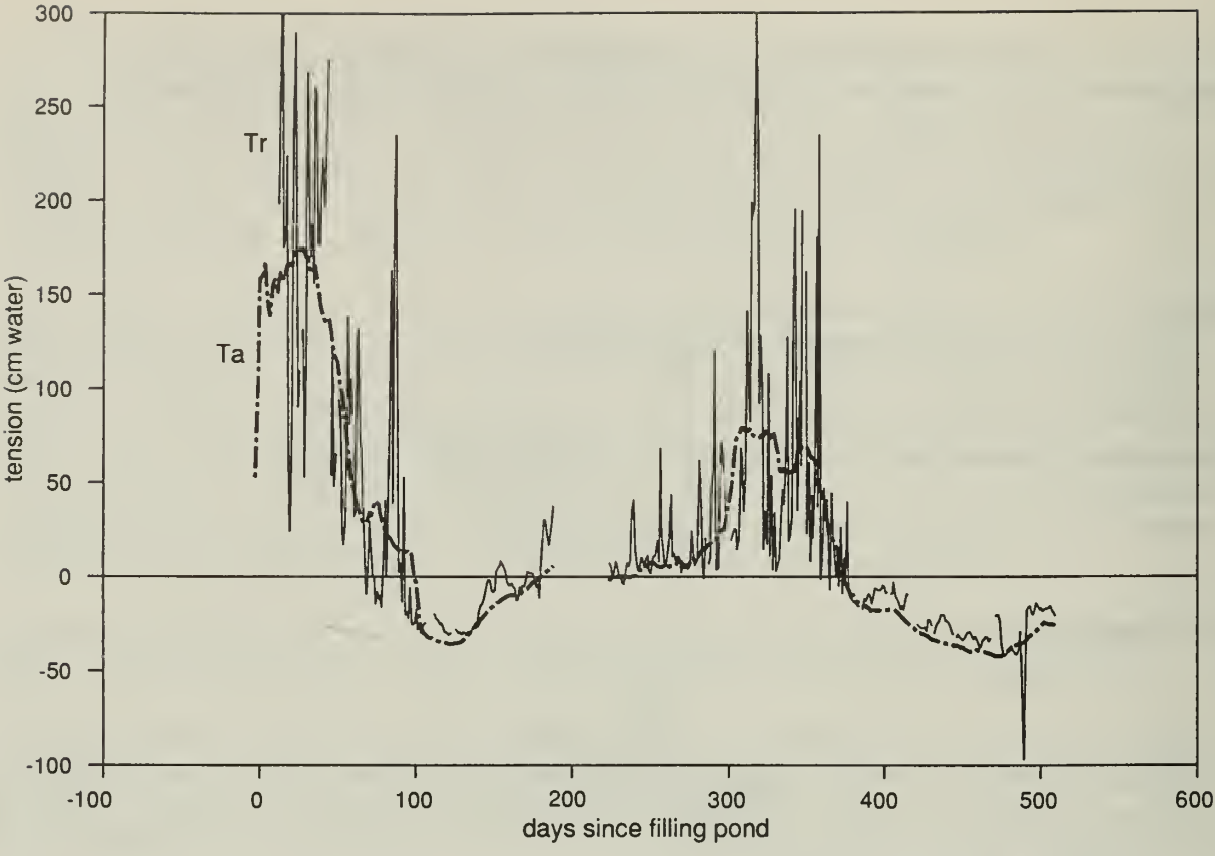

Figure 22 Raw (T_r) and averaged (T_a) tension for the 33-cm-deep tensiometer in nest SEE. Dashed and solid lines are raw and averaged tension data, respectively.

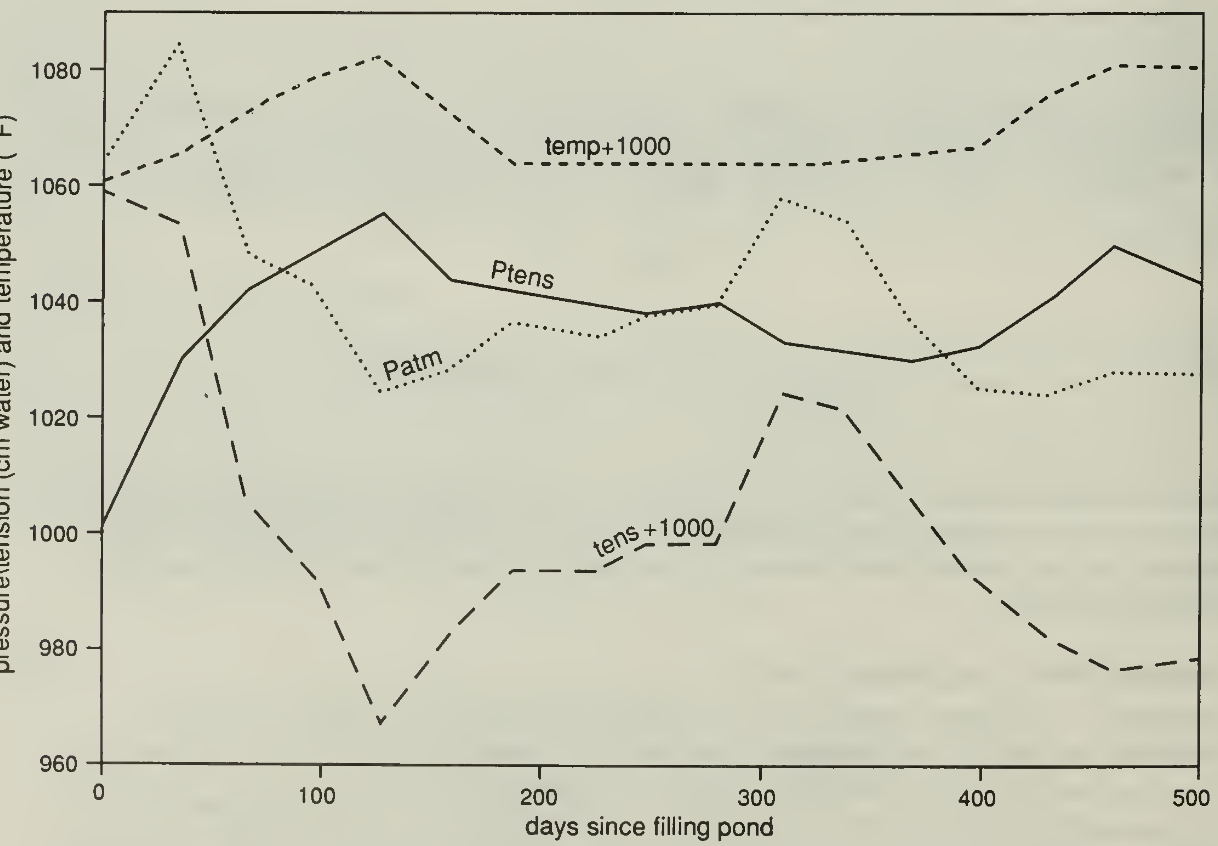

Figure 23 Comparison of air temperature and pressure to tension and pressure at the tensiometer. Tension and pressure at the tensiometer are an average for all valid datum points.

Null voltage Pressure transducers were designed to produce a "null" value of 1.000 volts when they were disconnected from the tensiometers because the pressure (atmospheric) applied to both sides of the diaphragm was equal. Testing of null voltage values on August 10, 1989, indicated that null values ranged from 1.170 to 0.879 volts. These anomalous null voltages resulted in shifts of 37.7 to -20.4 cm of water in calculated soil tension, respectively.

Null voltages ranging between 1.004 and 0.992 volts had been measured during instrument installation. This increased range in null voltage suggests the presence of uncompensated instrumental drift of about ±0.0045 V/month. A one-time correction was made by adding or subtracting the measured null shifts to the raw tension data of each respective tensiometer.

Atmospheric pressure and temperature Figure 23 represents the pressure at the tensiometer (P_{tens}) and tension (tension + 1,000), combined and averaged for all tensiometers regardless of monitoring depth or location in the liner.

Also shown on this graph are 28-day averages of atmospheric pressure and air temperature. Two relationships are apparent: First, the plot for tension closely resembles that for atmospheric pressure. Second, the plot for pressure at the tensiometers closely resembles that for air temperature. This suggests that air pressure and temperature are affecting the tensiometer data; however, it is unclear whether the changes in atmospheric pressure and temperature are actually affecting pressure heads in the liner, or whether they are affecting the ability of the instruments to measure heads in the liner.

Other researchers have noted that changes in atmospheric pressure affect soil pore water pressure when some of the pores contain entrapped air, a situation likely in the liner. Peck (1960a), Norum and Luthim (1968), and Turk (1975) have all suggested that pressure increases cause entrapped air to occupy less pore space in the soil, and pressure decreases cause entrapped air to expand and occupy more pore space. Thus a decrease in air volume caused by an increase in atmospheric pressure would increase tension, and vice versa. Turk (1975) suggested that this effect would be most apparent in fine-grained materials.

Smedema and Zwerman (1967) showed that when the capillary zone of a soil column contained more than 5-percent entrapped air, cooling of the column caused a significant lowering of the elevation at which the pressure head was equal to 0. The lowering of elevation was less significant when the volume of entrapped air was less than 5 percent of the total porosity. Their work, based on a theory from Peck (1960b), showed a positive relationship between temperature change and pressure head. Gardner (1955), observing a similar relationship, noted that the relative change was similar for both sand and muck. Thus as temperature falls, tension increases, and vice versa. This relationship is also observed with the liner data. Other researchers (Gatewood et al. 1950, Meyer 1960) reported decreases in saturated water levels with falling temperatures. These decreases would have resulted from increased tension in the unsaturated zone, and water would have been drawn from the saturated zone. Turk (1975) suggested that temperature changes have two long-term effects on soil moisture: (1) temperature changes affect surface tension near the soil surface, causing drainage of pores when temperature increases and increased tension when temperature decreases; and (2) temperature changes cause air entrapped in the soil pores to expand or contract. Thus an expansion of air caused by increasing temperature will decrease tension.

Tension data Tension values are dominated by atmospheric pressure trends. Because pressure at the tensiometer is apparently free of these effects, this parameter is used in the following discussion. In our study, heads are computed from the pressure data according to the following:

$$H = E_t + \overline{P_t} - 1{,}034 \qquad [7]$$

where
H = Head (cm)
E_t = Elevation of tensiometer (cm)
1,034 = Standard atmospheric pressure (cm)
$\overline{P_t}$ = average pressure at tensiometer (cm)

Adjusting heads calculated from the various tensiometers at various times to a "standard" atmospheric pressure allows comparison of relative head data from any tensiometer at any given time. However, because the reference pressure of 1,034 is an arbitrary standard, we could not determine the position in the liner where pressure head was equal to zero; thus it was not possible to determine precisely the position of the wetting front.

Figure 24 shows changes in average head with respect to time for each layer of tensiometers in the liner. A layer corresponds to the set of instruments installed at a given depth in the liner. Layers 1, 2, 3, 4, 5, 6 correspond to instruments depths of 10, 18, 33, 51, 69, and 89 cm, respectively. After ponding (day 0, fig. 24), head measured by tensiometers in layers 1 and 2 quickly rose to a maximum value of about 170 to 180 cm. Head in layer 1 and 2 became fairly constant approximately 60 days after the pond was filled. Head in layers 3 and 4 increased to about 140 cm approximately 90 to 120 days after liner ponding, respectively, then decreased to approximately 120 to 100 cm, where they have remained fairly constant. Head in layer 5 reached a maximum of about 100 cm during the 120 days after ponding and then stabilized to about 90 cm.

Head in layer 6 has been variable, reaching a maximum 100 cm during the 120- to 240-day period after ponding of the liner. Layers 3 to 6 all increased in head during the year after ponding.

The variability in head values in layers 3 to 6 suggests that temperature was affecting tension in the liner. From June to September of 1988 (90 to 180 days after ponding), when temperatures were high, head values were also relatively high, indicating low tension. During the winter months (> day 180), heads were lowest in these layers, indicating relatively high tension caused by cooling of the liner. A lag effect appeared to be operating, because layer 3 reached its highest and lowest head values 3 to 4 months before layer 6.

Temperature-induced tension variations are greatest when a soil contains entrapped air (Smedema and Zwerman 1967). The relatively constant head values observed in layers 1 and 2 suggested that these layers had little entrapped air and were probably saturated over most of the area of the liner. If we assume that the degree of head variability over time is related to the volume of entrapped air, then layers 3 and 4 would have slightly less entrapped air than layer 5, and layer 6 would have a relatively larger volume of entrapped air than layer 5. This relationship of head variation to temperature may suggest that layers 3 to 5 are nearly saturated and possibly within the tension-saturated zone. Layer 6 is probably unsaturated or at the fringe of the tension-saturated zone. On the basis of the tensiometer data, we estimated the wetting front to be at a depth between 18 and 33 cm 1 year after the liner pond was filled.

■ Gradients

When the liner reaches steady state, we anticipate that the final gradient will be approximately 1.3 cm/cm. This value assumes that total head at the upper surface will be equal to the elevation of the pond (200 cm) and that the pressure head at the base will be 0.0 cm. Thus, there will be a 120-cm change in head over a 90-cm distance, resulting in a gradient of 1.3 cm/cm.

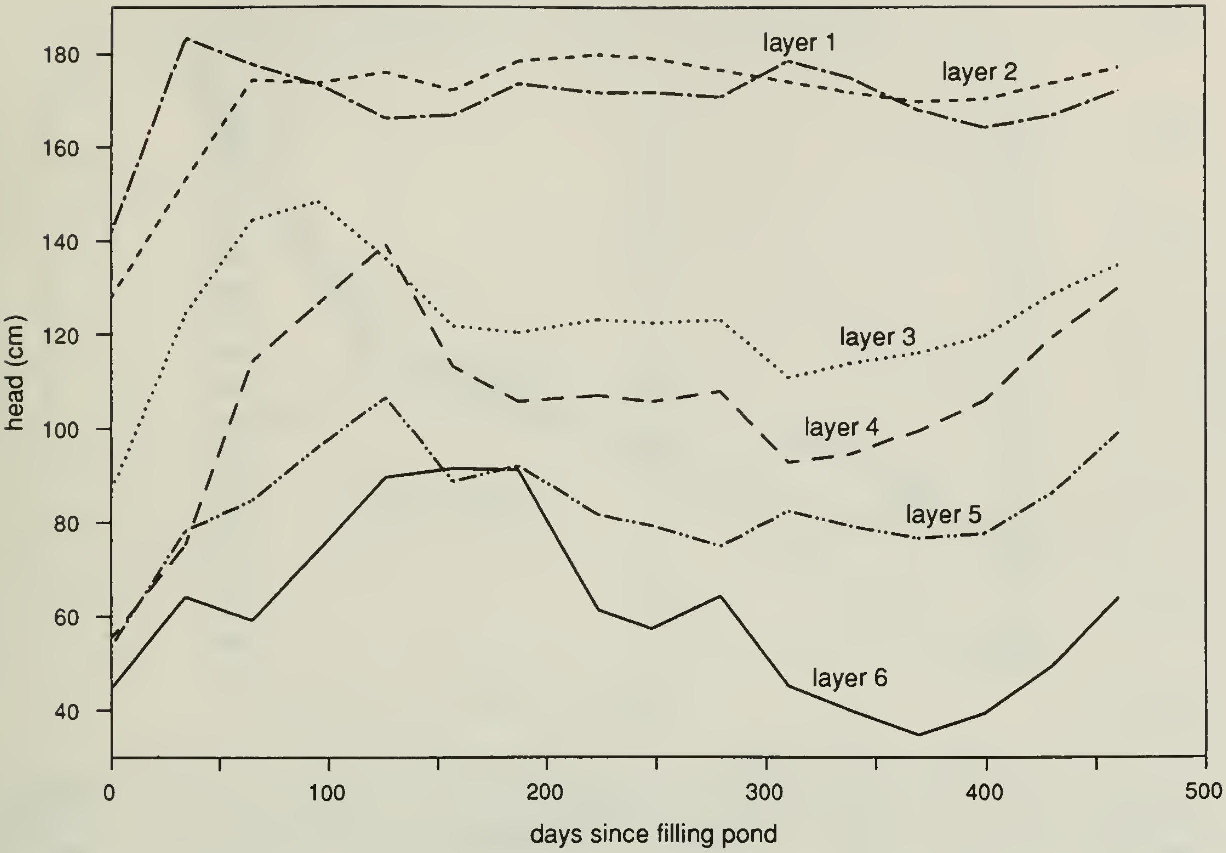

Figure 24 Average head for each layer of tensiometers corrected for atmospheric pressure. Depths of layers 1 to 6 are approximately 10, 18, 33, 51, 69, and 89 cm, respectively.

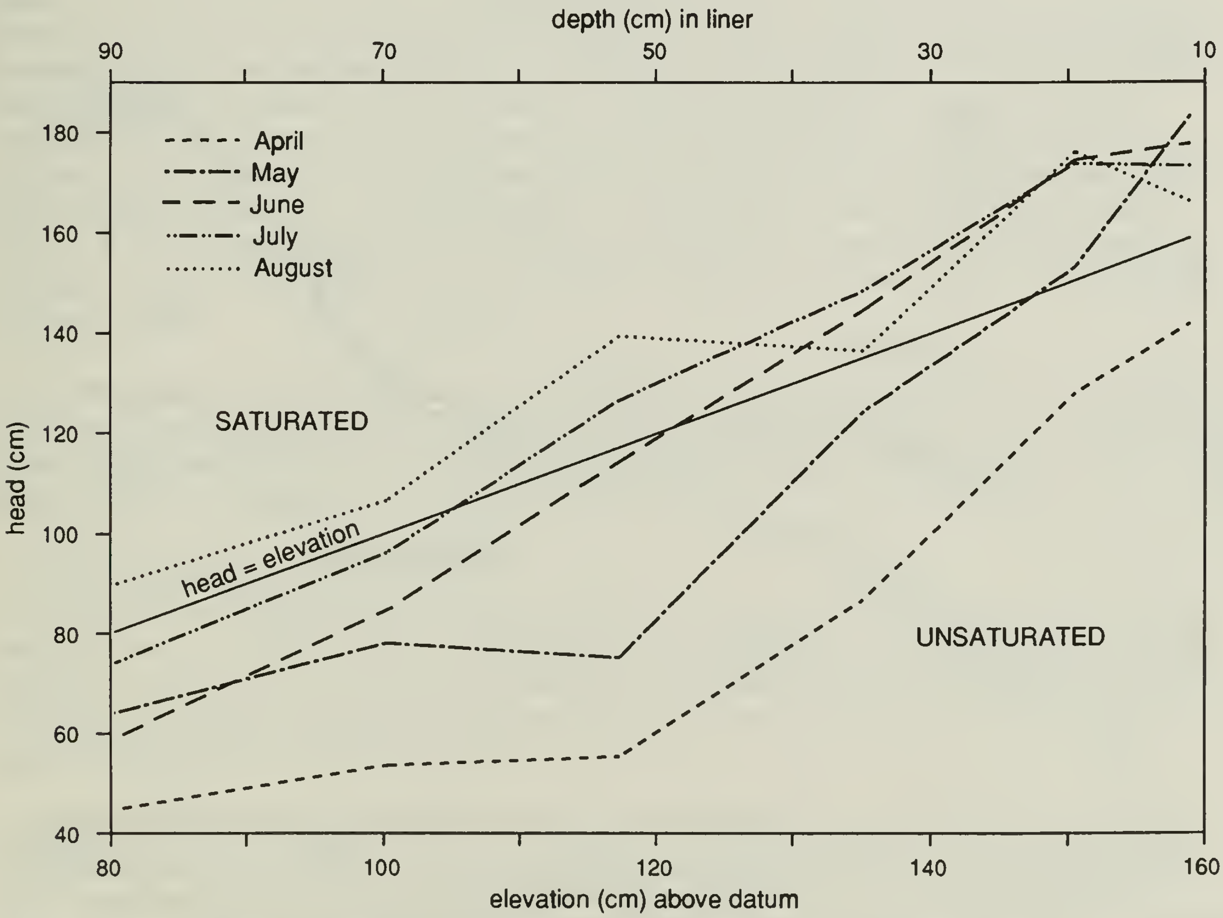

Figure 25 Changes in head relative to elevation for April 12, 1988, to August 12, 1988.

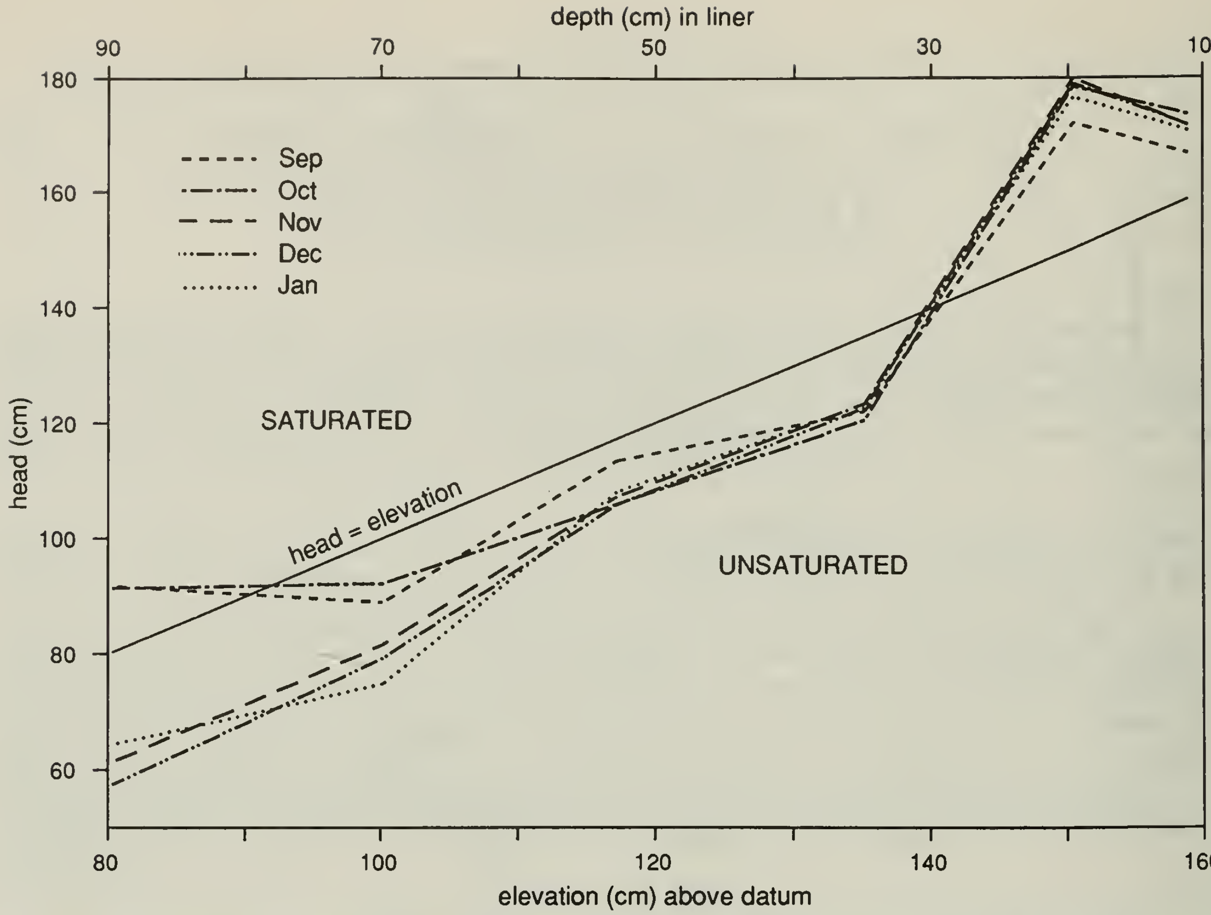

Figure 26 Changes in head relative to elevation for September 12, 1988, through January 12, 1989.

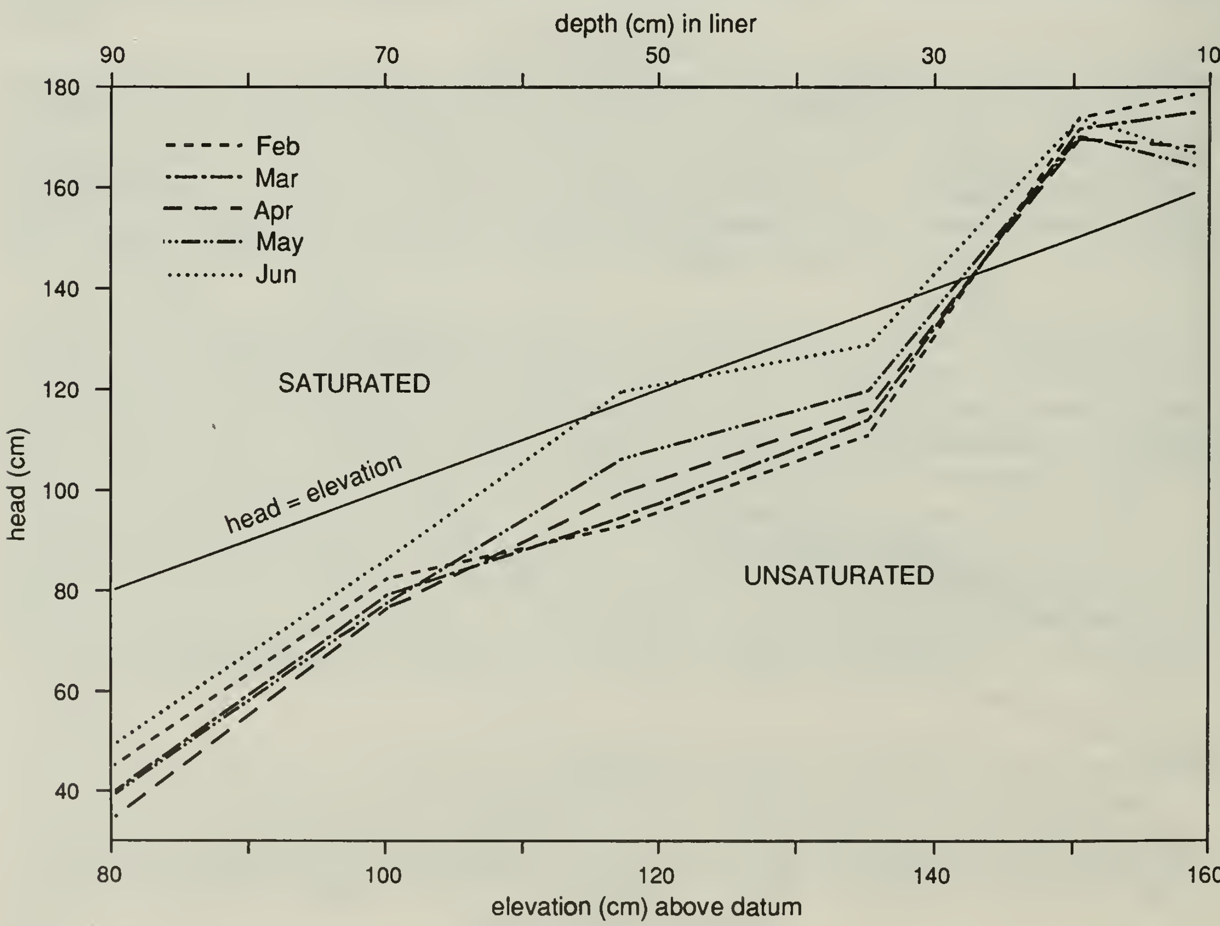

Figure 27 Changes in head relative to elevation for February 12, 1989, through June 12, 1989.

Table 9 Gradients for each month, since ponding, based on a 28-day average head centered on the twelfth of each month.

Month/year	Gradient	r^2
Apr 1988	1.28	0.87
May	1.50	0.88
Jun	1.60	0.99
Jul	1.35	0.99
Aug	1.05	0.92
Sep	1.11	0.86
Oct	1.19	0.83
Nov	1.53	0.94
Dec	1.58	0.95
Jan 1989	1.51	0.94
Feb	1.69	0.93
Mar	1.72	0.96
Apr	1.72	0.97
May	1.64	0.97
Jun	1.54	0.96
Jul	1.40	0.96
Aug	1.37	0.96

r^2 = squared linear correlation coefficient

Monthly hydraulic gradients were calculated by plotting average head for each layer versus the elevation of that layer in the liner. A regression line was then fit to the data and the hydraulic gradient for the entire liner was taken as the slope of that line. Table 9 shows the computed hydraulic gradient for the atmospheric pressure corrected data.

Figures 25 to 27 show the monthly head distribution from April 1988 through June 1989. The gradient increased until June 1988. Then increases in head in layers 4 to 6 caused a decrease in overall gradient until August 1988. During September and October, heads in layers 3 to 5 decreased while the head in layer 6 remained constant. No explanation exists for the high heads observed in layer 6 during September and October; these datum points may be anomalous. After October, the head in the deep tensiometers fell and the gradient increased until it reached a maximum of approximately 1.7 in April 1989. Since that time, the head in layers 3 to 6 increased, coincident with increasing temperatures, and caused the gradients to decrease. However, the gradient remained steeper during the summer of 1989 than during the summer of 1988.

The cyclic gradient variations are directly attributable to the cyclic trends in head in layers 3 to 6 (fig. 24). Head values in layers 1 and 2 have remained fairly constant over time, while head values in the lower layers have risen and fallen. When the heads in the lower layers are relatively high, the gradient is low, and vice versa.

■ Areal Distribution of Head Values

Areal trends were analyzed by examining head values measured on April 12, 1989, after the liner had been ponded for 1 year. Figure 28 shows the distribution of head in the liner at three elevations. Heads on that date were highest in the northwest quadrant of the liner and lowest in the northeast quadrant. At a depth of 63 cm, heads were 40 cm greater in the northwest quadrant than in the east third of the liner.

A computer-plotting routine that incorporated a minimum curvature method was used to draw cross sections of head distribution in the liner (fig. 29). These plots show that seepage in the liner is downward at a fairly uniform gradient everywhere except in the northeast quadrant. Heads on the south side were somewhat less than those on the north side.

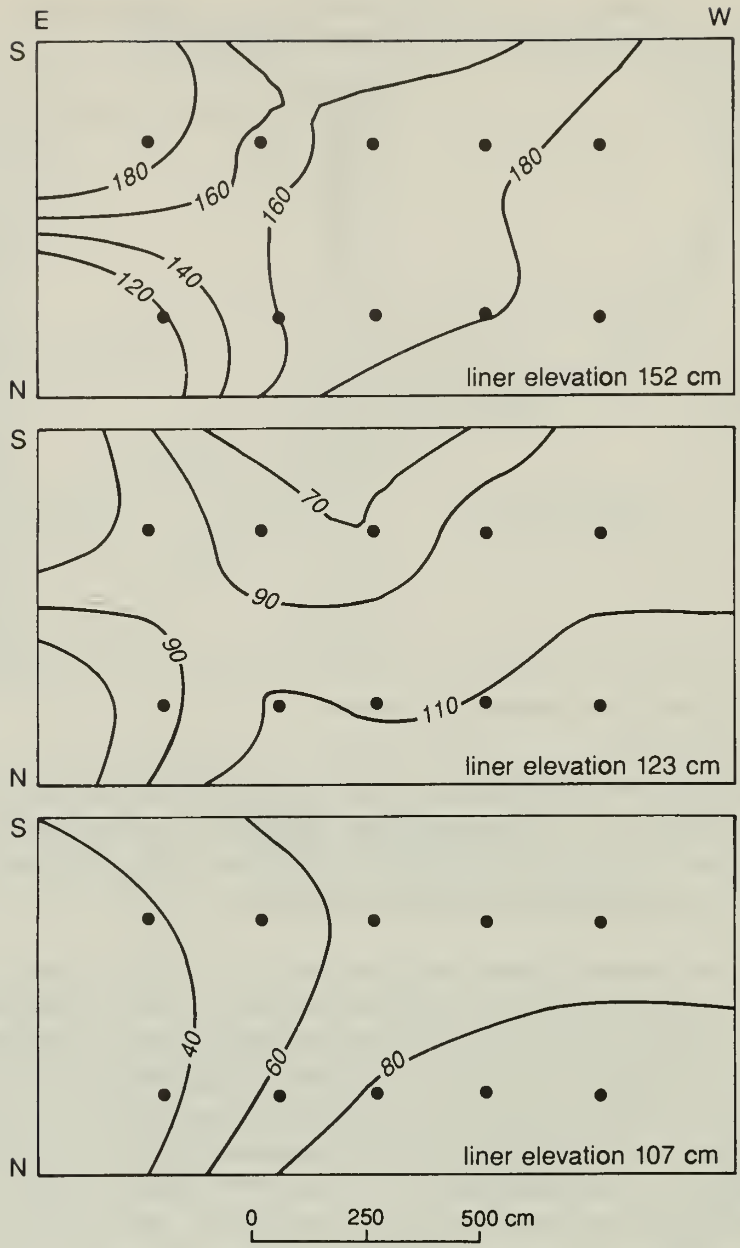

Figure 28 Equal-potential maps of head in the liner on April 12, 1989. Elevations of 152, 123, and 107 cm correspond to depths of 18, 47, and 63 cm.

Table 10 lists average gradients computed for each tensiometer nest on April 12, 1989. Gradient lines were completed by regressing (linear) head values relative to the elevation at which the head measurement was made in the liner for each nest of instruments. The gradient was the slope of the regression line. Gradients were computed by fitting a regression line through the change in head relative to the elevation data for each nest (fig. 30). The gradient is greatest along the south side of the liner and is least in the northeast quadrant.

■ Gage Tensiometer Data

Gage tensiometers are located around the perimeter and in the southwest corner of the liner. Tensiometers in the southwest corner of the liner monitor an area that slumped during construction of the cutoff wall and was recompacted by hand. Perimeter gage tensiometers that monitor soil tensions outside the liner study area are used to determine if lateral flow of water through the cutoff wall is occurring; their locations are shown on figure 19. (These tensiometers are numbered counterclockwise, beginning in the northeast corner of the site.)

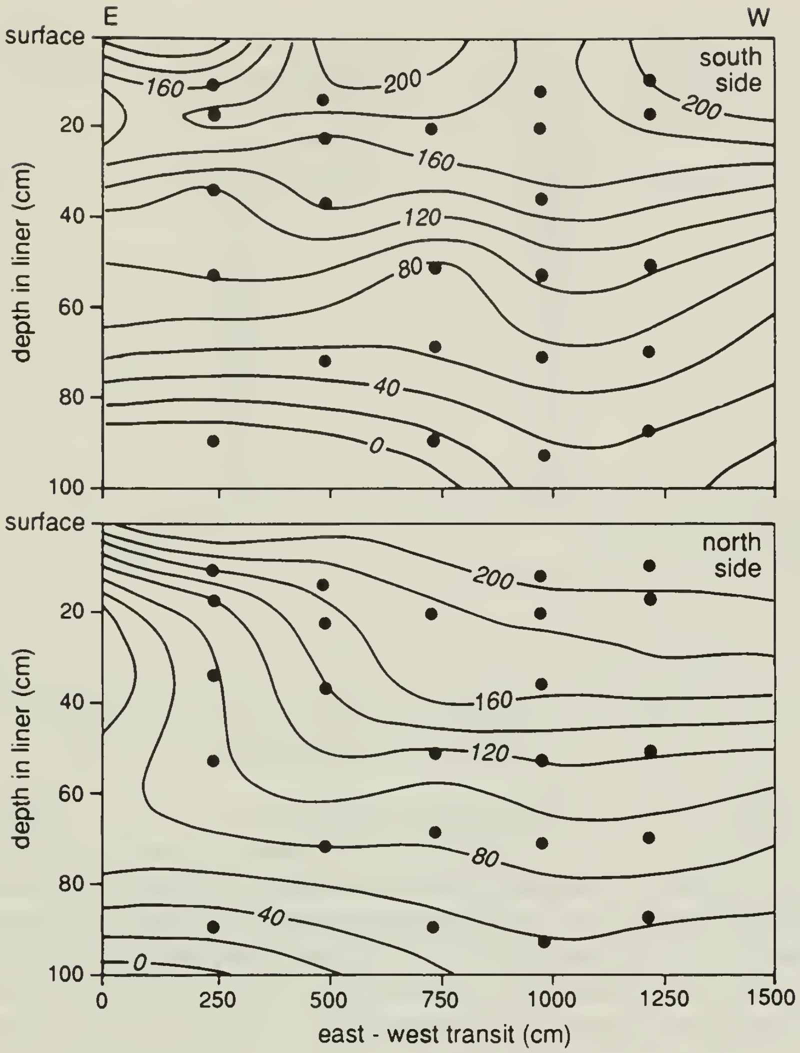

Figure 29 Cross-section views of head distribution in south half (top) and north half (bottom) of the liner on April 12, 1989.

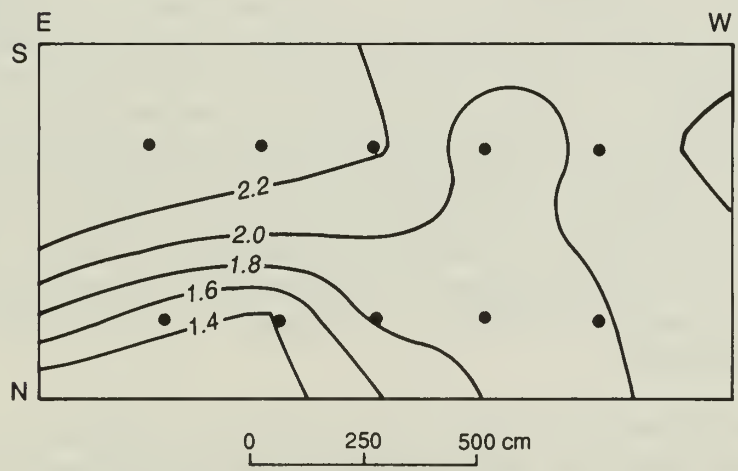

Figure 30 Contoured surface of liner gradient on April 12, 1989.

Table 10 Average gradients at each nest of tensiometers on April 12, 1989, 1 year after the liner was ponded; calculations/measurements were based on a regression of head (corrected for pressure) versus depth.

Nest	Gradient	r^2	a
NEE	1.48	0.83	5
NEW	1.36	1.00	3
NC	1.88	0.96	6
NWE	1.85	0.99	6
NWW	1.99	0.98	6
SEE	2.36	0.92	5
SEW	2.29	0.96	4
SC	2.25	0.94	4
SWE	1.82	0.97	6
SWW	2.12	0.99	5

a = number of datum points.
r^2 = squared linear correlation coefficient.

Background data were collected from the gage tensiometers from mid-January 1988 until the liner was ponded nearly 3 months later. During this time we checked the functioning of the tensiometers and allowed them to equilibrate before the liner pond was filled.

Data from the tensiometers in the southwest corner of the liner are shown in figure 31. Head in these tensiometers is simply $E_t + P_t$; no correction to a reference pressure was necessary. Tensiometer T-SW-C-13 gave erratic readings after installation and was replaced. Readings from the remaining tensiometers in the southwest corner were relatively stable after installation, except for some noise in the drier tensiometers immediately after ponding. These fluctuations may have been caused by the dryness of the soil because gage tensiometers lose accuracy as soil tension approaches 1,024 cm of water. Tensiometers T-SW-C-27a and T-SW-C-27b revealed wet conditions in layer 5, which was the wettest layer during construction of the liner. Because the exact size of the recompacted area was never measured, we do not know whether these instruments lie outside the slump area and thus cannot differentiate whether the recompacted area was also compacted very wet.

After liner ponding, the tensiometer data from the southwest corner generally show an increase in head, responding to the infiltration of water into the liner. The tensiometers at the 69-cm depth show an exception to this trend. Tensiometer T-SW-C-27a consistently produced "wet" (head near 80 cm) readings. Variations in these data follow the same seasonal oscillations as the transducer tensiometer data and appear to be inversely related to barometric pressure. Tensiometer T-SW-C-27b indicated rapid drying approximately 90 days after the pond was filled; tensions after this period were similar to those indicated by the other tensiometers in the cluster. The reason for this increased tension (decreased head) is unknown. Immediately after ponding, tensiometer T-SW-C-35b showed drier conditions than before ponding and the greatest fluctuations in readings; however, it too indicated a decrease in tension (increase in head) throughout the project.

All the gage tensiometers were installed to allow monitoring of soil tensions at depths equal to or greater than 31 cm. None of the gage tensiometers have indicated saturated conditions in the liner; thus the wetting front may not have yet reached the 33-cm depth. This observation agrees with data from the transducer tensiometers monitoring the remaining portions of the liner study area. An average downward gradient ranging between 1.2 to 1.7, one year after ponding, was calculated on the basis of head values measured by the gage tensiometers. This gradient is consistent with the gradients calculated from the transducer tensiometer data.

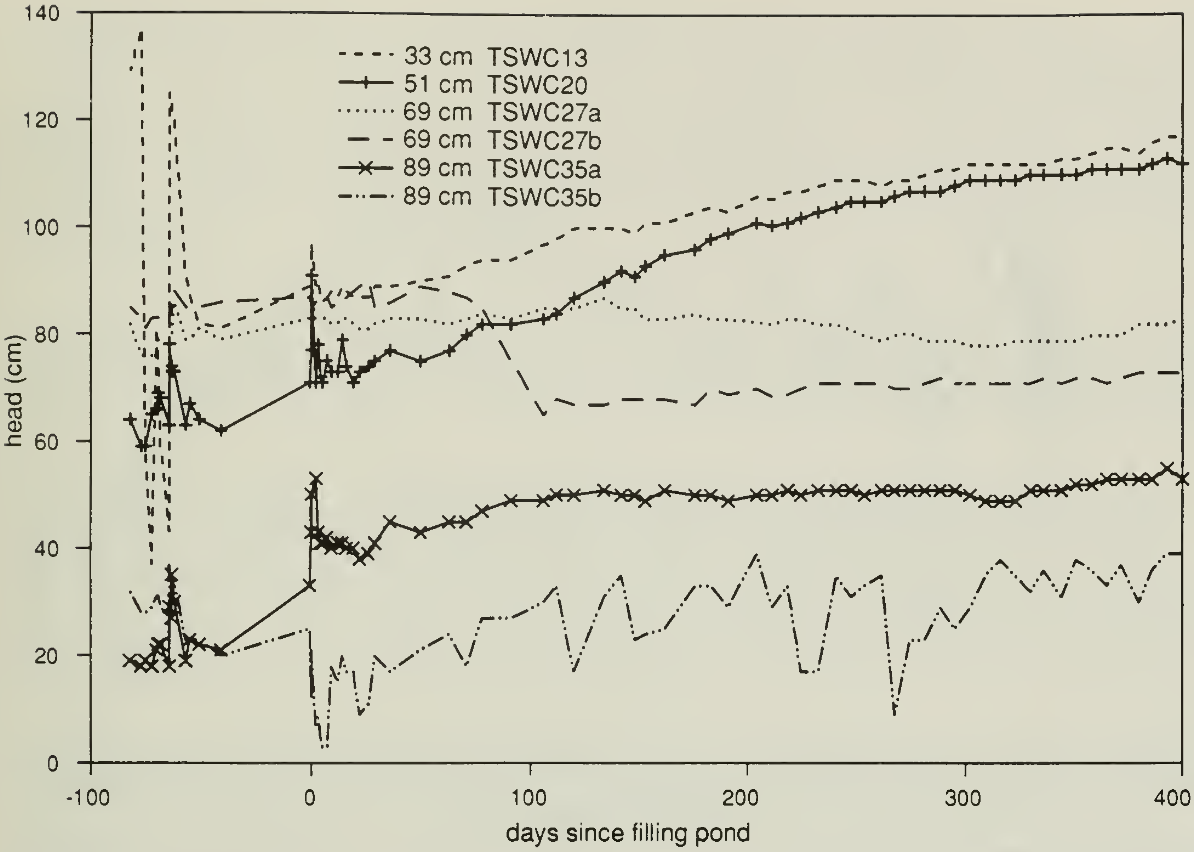

Figure 31 Head as determined by the gage tensiometers located in the southwest corner of the liner. The number represents the depth (in cm) of each tensiometer.

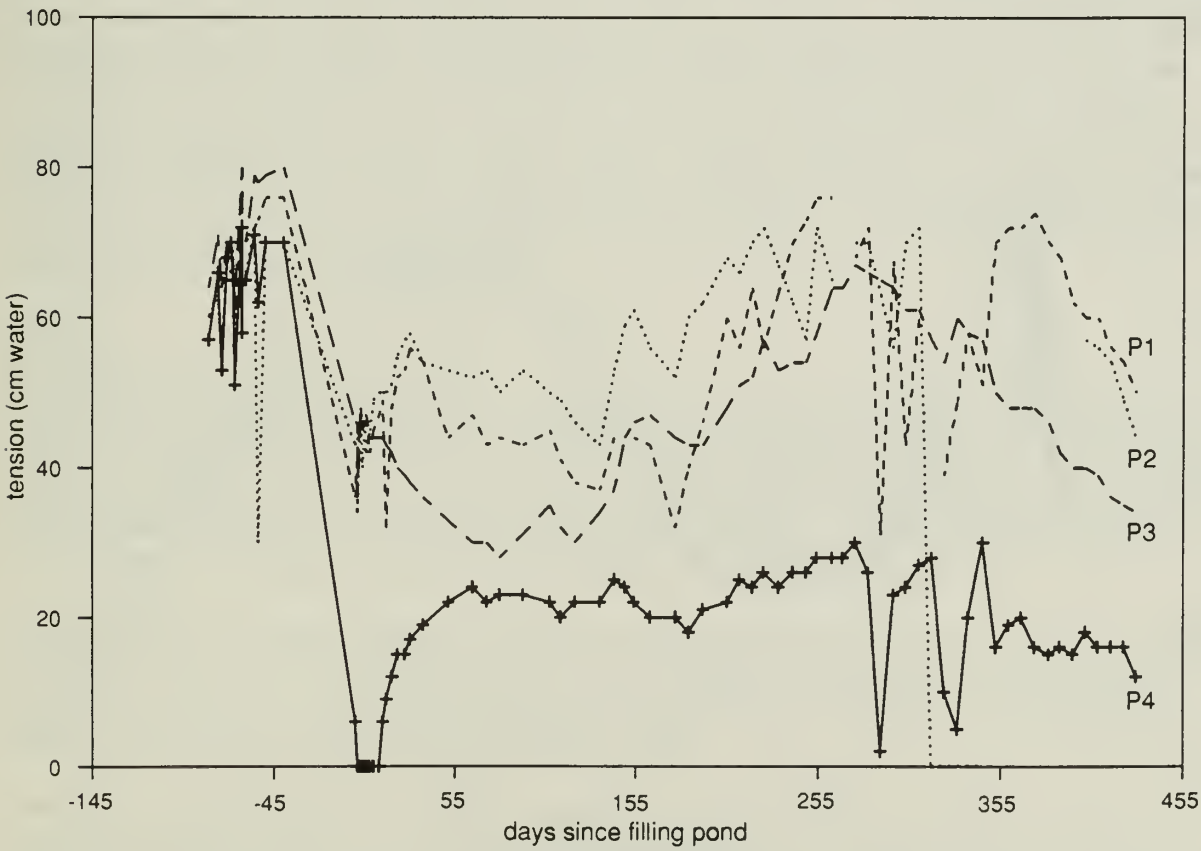

Figure 32 Soil tensions as determined by gage tensiometers around the north side of the liner perimeter. A letter/number represents each tensiometer.

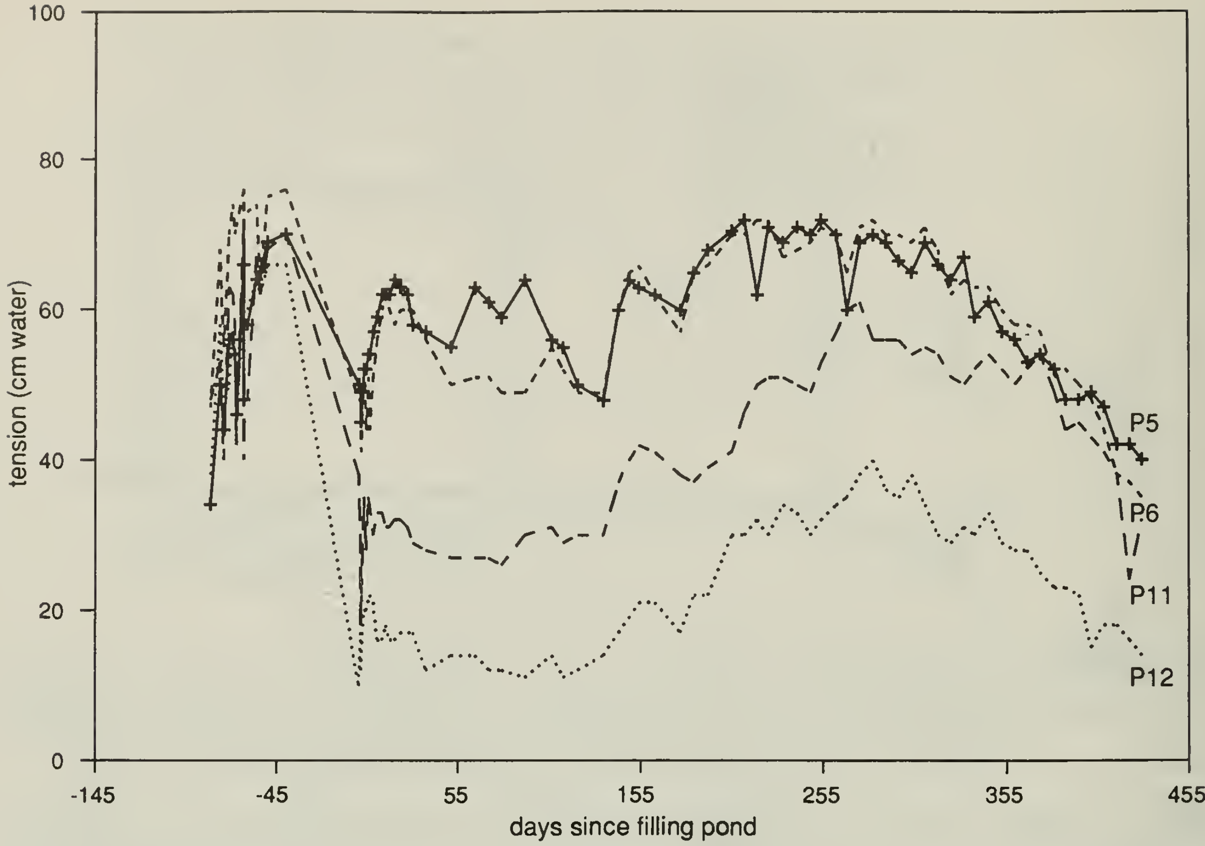

Figure 33 Soil tensions as determined by gage tensiometers around the west and east sides of the liner perimeter. A letter/number represents each tensiometer.

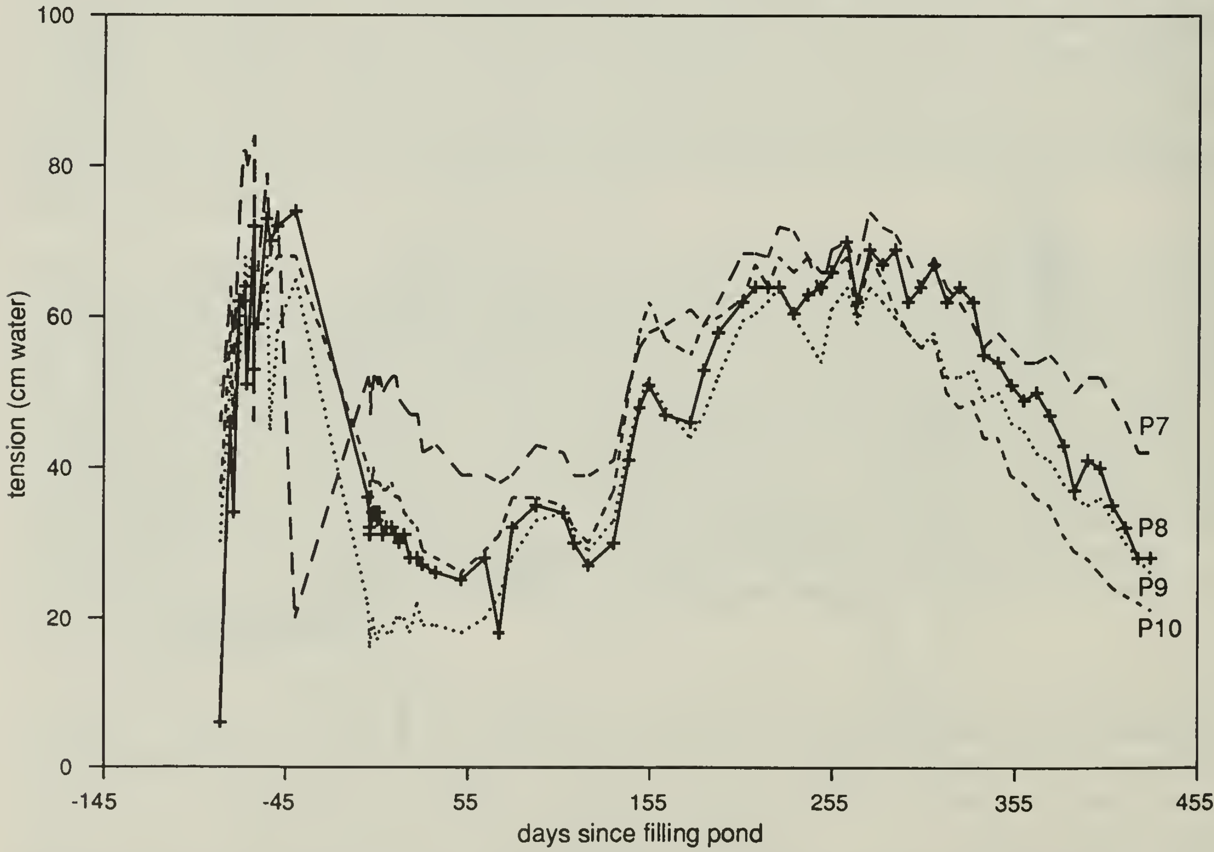

Figure 34 Soil tensions as determined by gage tensiometers around the south side of the liner perimeter. A letter/number represents each tensiometer.

Perimeter tensiometers were installed to detect water moving through the slurry wall. Perimeter tensiometer data are presented in figures 32 to 34. During the background monitoring period, readings from these tensiometers were high and relatively erratic. The liner apron (not in the study area) was not wetted during this time, a condition that may have resulted in the high tensions. Variability in the data may be partly due to the lack of accuracy the gage tensiometers have under very dry conditions. Tensiometer P10, which produced the most variable readings, was replaced.

The 45-day lapse in the tensiometer data shown in figures 32 to 34 corresponded to the period of liner repair. After repair began on the cutoff wall, the liner apron was kept moist to ensure against cracking and dessication of the apron soil. This accounts for the more stable values measured after the repair.

Tensiometer P2 began to produce readings of saturation as the liner was ponded. These readings did not indicate a leak; rather they suggested that the slurry backfill around the tensiometer had dried out so much that there was no longer good contact between the soil/sand and the ceramic cup. P2 was removed and replaced. A similar problem was noted in P3 in the spring of 1989. Again, inspection of the liner showed no evidence of a leak, and readings returned to normal after P3 was replaced.

Two striking features are evident in the perimeter tensiometer data. First, the data appear to follow a seasonal, cyclical pattern. This trend is most obvious in tensiometers P4 to P12 (figs. 32 to 34) and coincides with the trend in barometric pressure through the year (fig. 23). Increased barometric pressure coincides with increased soil tension—the same relationship recorded by the transducer tensiometers. The second feature is the erratic nature of the data, especially in P1 to P3 (fig. 32); this appears to be caused by relative temperature gradients in the liner shelter and by overall temperature fluctuations. The liner is heated by a radiant heater, the source of which is near P1. The heater is on the north side of the shelter and runs parallel to the north side of the liner, ending just past P3. Hence, tensiometers P1 to P3 are most influenced by the heater when it is running. This effect is especially evident from January through March (day 250 to 340, fig. 32), when the heater is running the most. The effect of relative temperature of the shelter is also evident. Tensiometers P5 to P10 are farthest from the heater and therefore are in the coldest parts of the liner apron. Tensions measured by these instruments are similar and generally higher (lower head) than tensions measured on the warmer half of the liner.

Summary

Tension/head in the liner appeared to be affected by atmospheric pressure and temperature fluctuations. Despite the correction for pressure, a cyclic pattern of pressure head occurred: head was greatest in the summer and lowest in the winter. An increasing time-lag with depth suggested that the cyclic rise and fall of pressure head was at least partly caused by changing temperatures in the liner. The pressure variations may be a result of external processes affecting the liner instrumentation. Further study is needed on this topic.

Because we are uncertain about the accuracy the tension data, we cannot compute an exact wetting-front depth. The apparent reaction of head values to the changes in temperature suggests that the liner is saturated to a depth of greater than 20 cm, tension-saturated to a depth of at least 70 cm, and unsaturated at its base.

Perimeter tensiometer data and visual inspection provide no evidence of lateral flow of water from the liner study area. The perimeter gage tensiometers also appear to be affected by temperature and barometric pressure. Trends in the data measured by these tensiometers are similar to trends observed in the data from the pressure-transducer tensiometers.

Hydraulic gradients were affected by the cyclic increase and decrease of heads in layers 3 to 6. Whereas the steady state gradient in the liner is expected to be approximately 1.3, observed gradients have fluctuated between 1.1 and 1.7.

Head was greatest in the northwest quadrant of the liner and lowest in the east third of the liner. The gradient on the south side of the liner was slightly greater than on the north side, except for the northeast quadrant, where it was much lower. If we assume that hydraulic conductivity is consistent throughout the liner, these data indicate that the greatest amount of seepage is occurring in the northwest quadrant and that the least seepage is occurring in the northeast quadrant.

Results of this analysis indicate that the liner has not yet reached steady state. The large fluctuation in heads and gradients may indicate that much of the liner is tension saturated, and that a significant percentage of air is entrapped in the soil pores. The low head values in layer 6 indicate that this layer is unsaturated or possibly approaching tension saturation, and thus drainage from the base of the liner is not likely to be occurring.

Air entrapped in the liner may have an effect on water movement through the liner. Freeze and Cherry (1979) state that unsaturated flow is a special case of multiphase flow. When two immiscible fluids occupy a pore volume, the effective permeability is decreased for each fluid because fewer pores contain air, and some pores containing air are no longer available as seepage pathways for water. In the case of the liner, the apparent hydraulic conductivity of the liner, which is calculated from the measured flux and gradient values, may be higher than the actual hydraulic conductivity. Flux is measured at the liner surface where the liner pores are totally filled with water. However, deeper in the liner, where air is still present, the hydraulic conductivity probably is lower, and will remain so until the air is dissolved into or displaced by water.

7 INFILTRATION MEASUREMENTS OF THE FIELD-SCALE LINER

The double-ring infiltrometer, a device commonly used in the field for determining the hydraulic conductivity of soil liners (USEPA 1988a), was used in this project. Infiltrometers are useful for measuring infiltration fluxes; however, they do not directly measure hydraulic conductivity. When ponding of water occurs above a soil or a soil liner, the rate of infiltration is initially high and dominated by the matric potential gradient. This initial capillary-dominated flux is unsteady because much of the infiltrating water fills empty voids until the soil storage capacity is reached. As the matric gradient decreases, the infiltration rate asymptotically decreases with time until a constant, gravity-induced infiltration rate is approached (fig. 35). The constant rate of infiltration signifies the achievement of steady-state infiltrability (as defined by Hillel 1982), dominated by gravity and directly proportional to the saturated hydraulic conductivity and hydraulic gradient.

The overall infiltration flux of the liner was also calculated using a water balance approach. To estimate the volume of water infiltrating the liner during a 1-year period, we subtracted the volume of water that evaporated from the pond from the amount of water required to maintain a constant pond level. The infiltration area of the liner (1.03×10^6 cm^2) is assumed to be the total study area minus the cumulative area covered by the large- and small-ring infiltrometers.

Saturated hydraulic conductivity values were necessary for calculating transit time for solute and water migrating vertically through the liner. To calculate saturated hydraulic conductivity (K_{sat}) from infiltration data, we first had to determine the hydraulic gradient and the extent of lateral flow. Hydraulic gradient was determined from tensiometer data (chapter 6) and lateral flow was considered to be negligible because of the experimental design.

Discussion

■ Cumulative Infiltration Plots

Cumulative infiltration curves for each infiltration ring and for the entire liner were used to determine steady-state infiltrability; cumulative infiltration volume was plotted against time

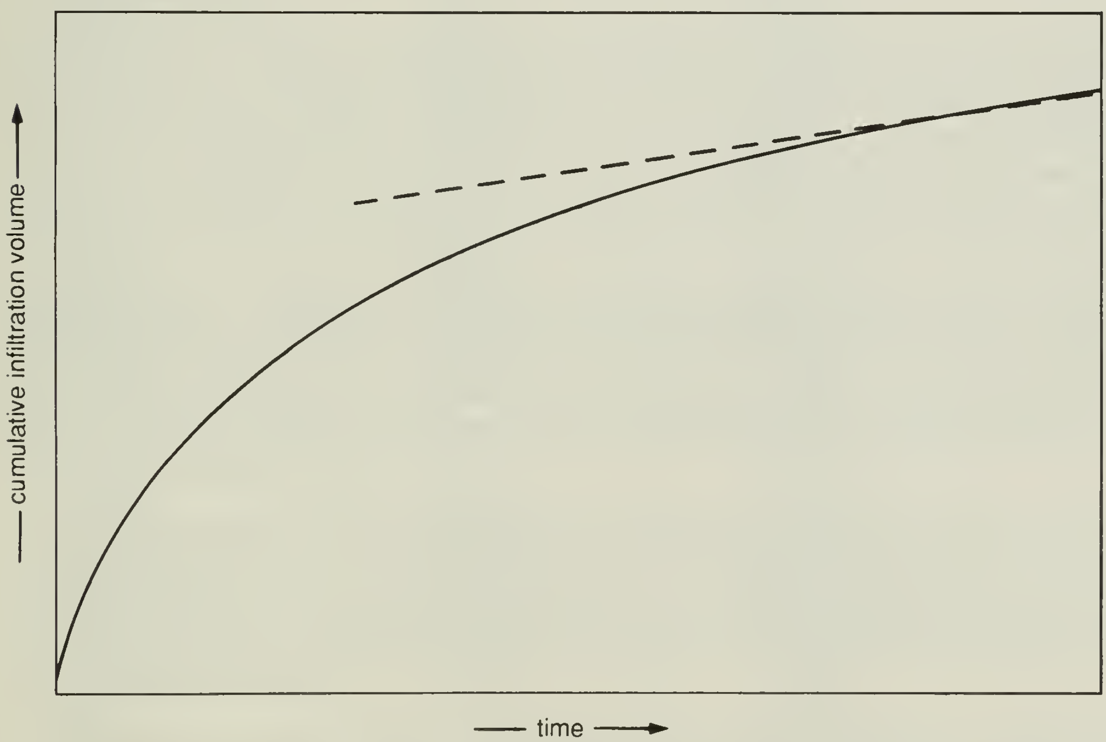

Figure 35 Idealized cumulative infiltration curve. Dashed line indicates achievement of steady-state infiltrability (modified from Hillel 1982).

subsequent to filling of the liner pond. Over time, the curve approached a relatively constant slope (between 25 to 40 days after ponding in this experiment) indicative of steady-state infiltrability. At steady-state infiltrability, the slope of the cumulative-infiltration curve is directly proportional to K_{sat}. As described by Cislerova et al. (1988), the steady-state infiltrability "represents the integral influence of the saturated hydraulic conductivities of particular layers of the soil profile, including the influence of macrostructures, preferential pathways, and anisotropy."

Regression equations The steady-state infiltrability of each of the ring-infiltrometers was determined by selecting the portion of the infiltration data that was constant or at steady state and regressing these cumulative infiltration volumes against time (1 year). The slope of the regression equation divided by the cross-sectional area of the infiltrometer represents the average infiltration flux for an entire year. Table 11 summarizes average infiltration fluxes and

Table 11 Summary of large-ring (LR) and small-ring (SR) infiltrometer infiltration fluxes and correlation coefficients for steady-state infiltrability.

Infiltrometer	Infiltration flux (cm/s)	r^2	Log of the infiltration flux (cm/s)
LR1	1.2×10^{-9}	0.98	−8.921
LR2	1.5×10^{-8}	0.99	−7.824
LR3	6.8×10^{-9}	0.97	−8.167
LR4	5.1×10^{-9}	0.98	−8.292
SR1	1.3×10^{-7}	0.98	−6.886
SR2	1.1×10^{-7}	0.99	−6.959
SR3	1.6×10^{-7}	0.99	−6.796
SR4	1.9×10^{-7}	0.99	−6.721
SR5	7.7×10^{-8}	0.99	−7.114
SR6	6.1×10^{-8}	0.99	−7.215
SR7	6.4×10^{-8}	0.99	−7.194
SR8	8.6×10^{-8}	0.99	−7.066
SR9	6.3×10^{-8}	0.98	−7.201
SR10	5.4×10^{-8}	0.99	−7.268
SR11	6.3×10^{-8}	0.99	−7.201
SR12	6.4×10^{-8}	0.96	−7.194
SR13	6.9×10^{-8}	0.99	−7.161
SR14	5.9×10^{-8}	0.95	−7.229
SR15	8.7×10^{-8}	0.99	−7.060
SR16	8.3×10^{-8}	0.99	−7.081
SR17	6.6×10^{-8}	0.99	−7.180
SR18	8.8×10^{-8}	0.99	−7.056
SR19	1.0×10^{-7}	0.99	−7.000
SR20	ND	ND	ND
SR21	6.9×10^{-8}	0.99	−7.161
SR22	6.4×10^{-8}	0.98	−7.194
SR23	6.2×10^{-8}	0.99	−7.208
SR24	7.7×10^{-8}	0.99	−7.114
SR25	7.9×10^{-8}	0.99	−7.102
SR26	5.1×10^{-8}	0.98	−7.292
SR27	8.3×10^{-8}	0.99	−7.081
SR28	6.6×10^{-8}	0.98	−7.180
SR29	1.2×10^{-7}	0.98	−6.921
SR30	9.3×10^{-8}	0.98	−7.032
SR31	4.0×10^{-8}	0.95	−7.398
SR32	1.5×10^{-7}	0.99	−6.824

r^2 = correlation coefficient squared
ND = not determined

correlation coefficients obtained when cumulative infiltration volumes were regressed against time for a duration of 1 year after the pond above the liner was filled.

We used a simple water balance approach for the 1-year period (April 1988 to April 1989) to determine the overall flux of the liner. During this period, 9,860 liters of water was added to the liner pond. Data from the evaporation pans indicated that 6,600 liters of water evaporated from the pond during this same period. We estimated that 3,260 liters of water infiltrated into the liner, resulting in an overall flux of 1.0×10^{-7} cm/s.

This rather simple approach to determining the water flux into the liner does not consider initial and steady-state infiltrability, anomalous data (e.g., sampling error), or changes in the infiltration rates over time. To evaluate these data (fig. 36), we used an approach similar to that used for infiltrometer data analysis, in which cumulative infiltration volume was plotted against time. This technique allowed us to estimate flux as well as to differentiate changes in the infiltration characteristics of the liner with time.

Figure 36 indicates that a three-fold increase in infiltration rate (inflection point of curve) occurred approximately 175 days after initiation of the experiment; the cause for the increase in infiltration is not known at this time. These data were collected weekly or bimonthly, and the lack of resolution in the data makes determination of the onset of steady-state infiltrability for the overall liner difficult.

On the basis of the infiltrometer data, we assumed that steady-state infiltrability was achieved after 39 days. Lines were regressed through the data from day 39 to 161 and from day 175 to 365. The equations of the regression lines are shown in figure 36. The slopes of the lines represent average infiltration rate in liters per day. An overall flux for the liner was determined by dividing the infiltration rate by the infiltration area. Fluxes of 4.6×10^{-8} cm/s and 1.5×10^{-7} cm/s were calculated for the initial and final slopes, respectively.

■ Infiltrometer Data

Small-ring infiltrometers The plots of the cumulative infiltration curves for the small-ring (SR) infiltrometers all showed short-term fluctuations in infiltration rates resulting from changes in barometric pressure and pond level. Infiltration data collected from 31 small-ring infiltrometers suggested that infiltration flux could remain constant, decrease, or increase with time after initial steady-state infiltrability was achieved. Because of suspected leakage of water into or out of the large-ring infiltrometers and SR-20, we will consider data from these infiltrometers separately.

Nineteen of the 31 small-ring infiltrometers exhibited a constant steady-state infiltrability for a period of at least 1 year (table 12). Infiltration rate fluctuations, as recorded, were short-lived and predominantly the result of changes in pond level and barometric pressure. Changes in infiltration rates similar to those observed in the latter part of the cumulative infiltration curves for the small rings were also observed in the cumulative infiltration curve developed from the water balance approach (fig. 36).

Five of the small-ring infiltrometers showed an increase in infiltration rate beginning between 140 and 183 days after ponding of the liner (table 12). The increase occurred during a period of relatively low barometric pressure (fig. 37) and during the same period in which a three-fold increase occurred in the infiltration rate for the whole liner, as calculated using the water-balance approach (fig. 36).

Infiltration rates of seven small-ring infiltrometers decreased abruptly (table 12 and fig. 37); infiltrometers 1 and 2 decreased on day 125, and infiltrometer 18 decreased on day 175 (the same week in which the liner's infiltration rate increased, as calculated using the water-balance

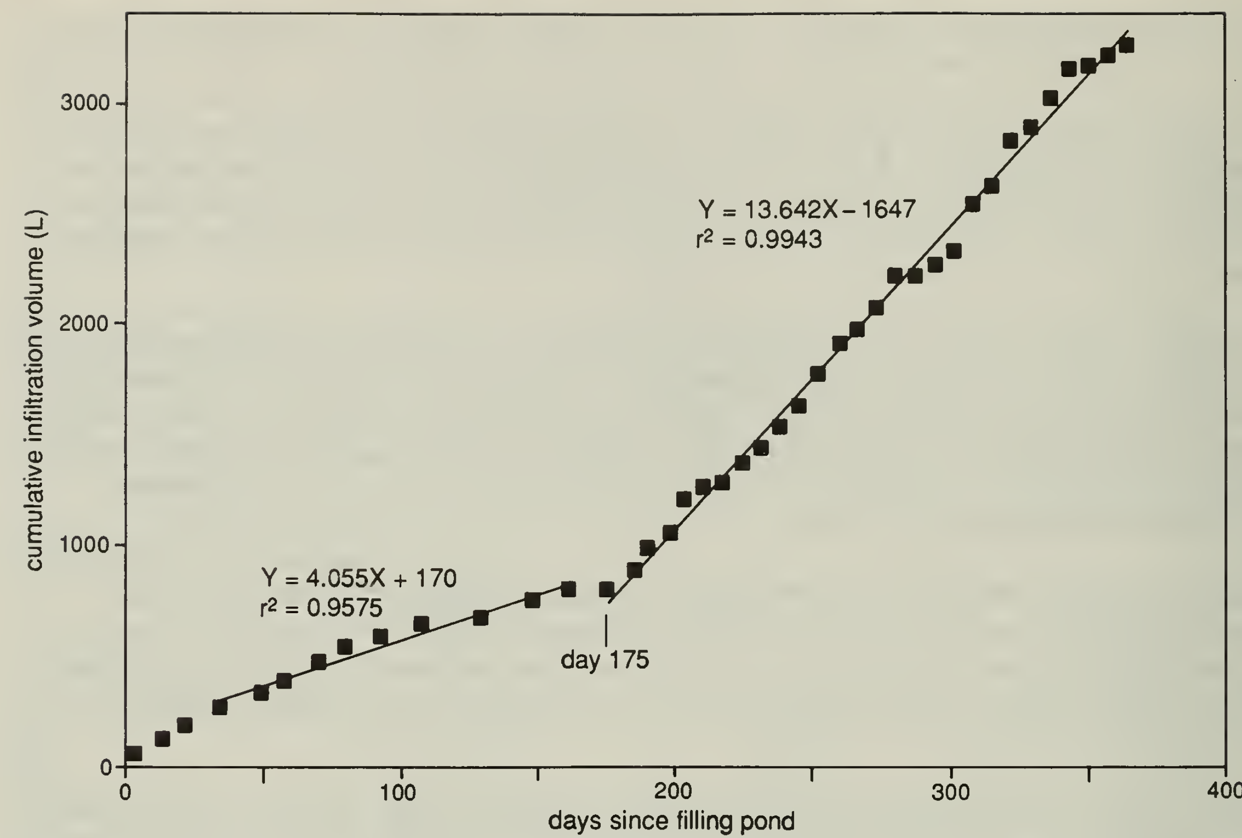

Figure 36 Cumulative infiltration volumes of the field-scale liner for a 1-year period, as determined by a water-balance approach.

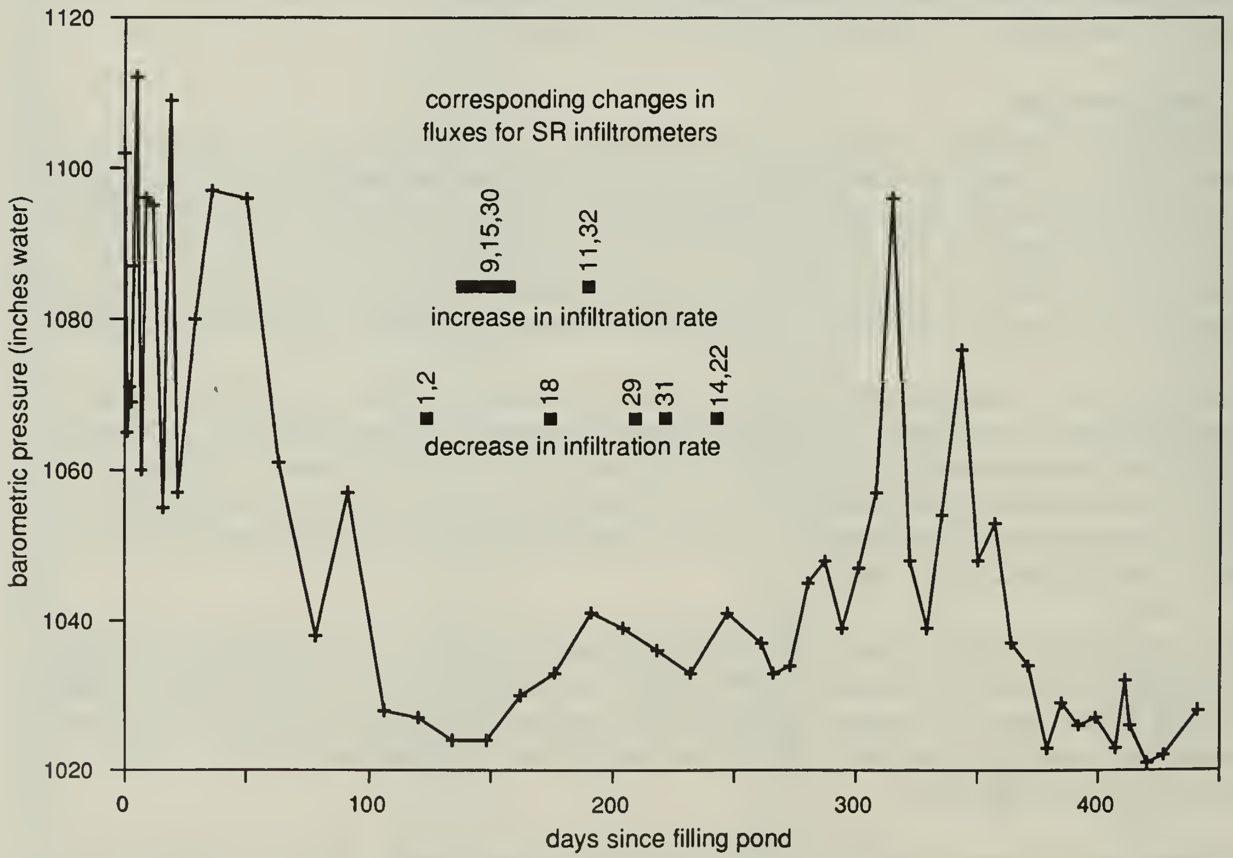

Figure 37 Average barometric pressure since the liner pond was filled and generalized indication of changes in infiltration rates for the small-ring infiltrometers.

Table 12 Summary of changes in steady-state infiltrability for the small-ring infiltrometers.

Infiltrometers	Flux (cm/s)	Flux 2 (cm/s)	Difference in infiltration
Constant infiltration flux			
3	1.6×10^{-7}		
4	1.9×10^{-7}		
5	7.7×10^{-8}		
6	6.1×10^{-8}		
7	6.4×10^{-8}		
8	8.6×10^{-8}		
10	5.4×10^{-8}		
12	6.4×10^{-8}		
13	6.9×10^{-8}		
16	8.3×10^{-8}		
17	6.6×10^{-8}		
19	1.0×10^{-7}		
21	7.0×10^{-8}		
23	6.2×10^{-8}		
24	7.7×10^{-8}		
25	7.9×10^{-8}		
26	5.1×10^{-8}		
27	8.3×10^{-8}		
28	6.6×10^{-8}		
Increase in infiltration flux			
9	2.1×10^{-8}	6.3×10^{-8}	4.2×10^{-8}
11	6.3×10^{-8}	1.0×10^{-7}	3.7×10^{-8}
15	5.9×10^{-8}	8.7×10^{-8}	2.8×10^{-8}
30	6.2×10^{-8}	8.3×10^{-8}	3.1×10^{-8}
32	6.4×10^{-8}	1.5×10^{-7}	8.6×10^{-8}
Decrease in infiltration flux			
1	1.3×10^{-7}	9.2×10^{-8}	3.8×10^{-8}
2	1.7×10^{-7}	1.1×10^{-7}	6.0×10^{-8}
14	5.9×10^{-8}	4.9×10^{-8}	1.0×10^{-8}
18	1.5×10^{-7}	8.8×10^{-8}	6.2×10^{-8}
22	7.9×10^{-8}	6.4×10^{-8}	1.5×10^{-8}
29	1.2×10^{-7}	8.0×10^{-8}	4.0×10^{-8}
31	6.5×10^{-8}	4.0×10^{-8}	2.5×10^{-8}

approach). The remaining four small rings decreased between 197 and 240 days after ponding (fig. 37). No relationship is apparent between barometric pressure and the decreases in infiltration rate. The variations in infiltration rates cannot be explained but are probably due to a combination of measurement errors and external perturbations on the liner and infiltrometers.

Large-ring infiltrometers Plots of the cumulative infiltration curves for the large-ring infiltrometers showed infiltration fluxes approximately one order of magnitude lower than those obtained for the small-ring infiltrometers (table 11). The infiltration flux data for the 31 small-ring infiltrometers and the four large-ring infiltrometers form two statistically distinct populations (fig. 38). The small-ring infiltration fluxes are log-normally distributed, on the basis of the Kolmogorow-Smirnow test of normality at the 95-percent significance level. A log-normal distribution of the infiltration data was expected on the basis of work by Rogowski (1972), Nielson et al. (1973), and Parkin et al. (1988), who had observed that soil hydraulic properties tend to follow a log-normal spatial distribution.

The geometric mean and standard deviation for the log of the average infiltration flux data from the set of large-ring and small-ring infiltrometers, measured from May 15, 1988, to June 15, 1989, are listed in table 13. This time period, which began approximately 1 month after the liner

Table 13 Geometric mean and standard deviation of log-transformed infiltration fluxes (cm/s) from large- and small-ring infiltrometers.

Infiltrometers	Mean log infiltration flux	Standard deviation	Geometric mean flux
Large-ring	−8.301	0.458	5.0×10^{-9}
Small-ring	−7.100	0.152	7.9×10^{-8}

pond was filled, corresponds to the date on which cumulative infiltration curves approached linearity with respect to time (attainment of steady-state infiltrability). The log infiltration fluxes of the 31 small-ring infiltrometers had a low variance, suggesting a relatively homogeneous distribution of the infiltration flux of the liner. The geometric mean infiltration fluxes were 5.0×10^{-9} and 7.9×10^{-8} cm/s for the large- and small-ring infiltrometers, respectively. The mean fluxes of the two infiltrometer data sets were statistically different at a 99.9-percent confidence level, as determined using a t-test. The reason for the difference between these two data sets is not known.

■ Perturbations to Ring-Infiltrometer Data

Leakage of large-ring infiltrometers Dye flow paths in the prototype liner indicated that the grout-soil interface is a likely preferential flow path for leakage of a large-ring infiltrometer; during excavation of the prototype liner (Albrecht et al. 1989), we found that bonding of the grout to the liner material and the fiberglass wall of the infiltrometer had not prevented the formation of preferential flow avenues. Entrained bubbles emanating from the surface of the field-scale liner outside and immediately adjacent to the large-ring infiltrometers were observed during operations to remove gas trapped inside the large rings. The entrained bubbles (believed to be biogenic in origin) indicated a connection between the inside of the large rings and the liner pond.

Evidence for gas formation and leakage was observed in all large-ring infiltrometers. The evolution of gas bubbles from the surface of the liner inside and outside the large rings is believed to be due to expulsion of gases formed under anaerobic conditions within the large rings and/or adjacent to the grout-liner interface. Preliminary analyses of the gas within the large rings showed a dominance of hydrogen sulfide and methane and a deficiency of oxygen, suggesting that anaerobic bacteria may be causing the gas buildup within the large rings.

Cumulative infiltration curves for large-ring infiltrometers Fluctuations in the large-ring cumulative infiltration curves corresponded to changes in barometric pressure. A relatively large but short-term increase occurred in the cumulative infiltration rate of LR-2 approximately 310 days after the pond was filled. At the same time, a large increase in barometric pressure occurred. LR-1 and LR-4 showed short-term increases just after day 350, during a transition between a high and low period of barometric pressure. These apparent changes in infiltration rate did not affect the long-term slope (i.e., infiltration rate) of the cumulative infiltration curves but could introduce errors into infiltration data collected over a relatively short period of time. It should be noted that these changes occurred before the gas bubbles were removed from the large rings; the bubbles probably contributed to the observed fluctuations in infiltration rate by increasing the sensitivity of the infiltrometers to changes in barometric pressure. Further research is being conducted to increase our understanding of the relationship between infiltration rate and barometric pressure in liner systems.

Small-ring infiltrometers Barometric pressure and pond-level fluctuations appear to affect infiltration measurements of the small-ring infiltrometers. Barometric pressure effects are observed in both short-term and possibly long-term infiltration data, whereas the effects of pond-level fluctuations are observed only in short-term data.

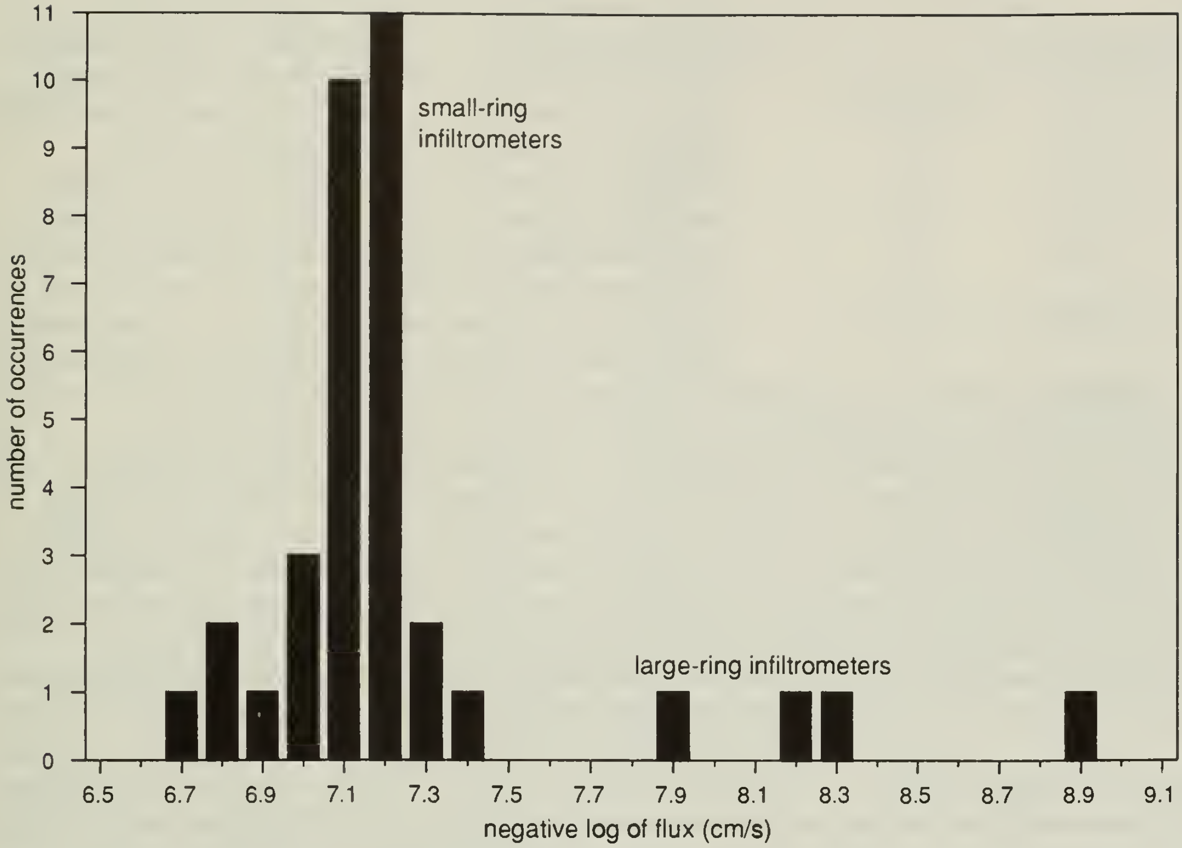

Figure 38 Histogram of the log of the fluxes for the infiltrometers.

Evidence for the effect of barometric pressure include inflections in cumulative infiltration curves that appear to coincide with changes in barometric pressure and a period of exceptionally high barometric pressure during the week of February 16, 1989, when most of the small-ring infiltrometers lost 100 gms of water in a 1-week period. The water loss during this week was approximately four times the average water loss per week; however, the high loss rate was short-lived and had no lasting effect on the slope of the cumulative water loss curve.

A possible explanation for the effects of changes in barometric pressure is that air became entrapped in the soil pores of the unsaturated zone; during wetting of the soil, the trapped air is particularly susceptible to changes in barometric pressure. Air trapped in the liner subsequent to ponding should be expected to affect the infiltration rates of the infiltrometers; the typical effect observed was an increase in infiltration rate as the air pressure increased. The volume of air trapped in the pore spaces of the soil tends to reduce the permeability of a saturated soil by as much as a factor of 30 (Christiansen 1944). Christiansen found that capillary forces were dominant at the wetting front, and that air trapped in pore spaces was immobilized, blocking some water flow through the soil. The same conclusions were drawn by Parlange and Hill (1976), Cislerova et al. (1988), Norum and Luthim (1968), Bianchi and Haskell (1966), Peck (1960b), and Turk (1975) in subsequent investigations. Norum and Luthim (1968), using a one-dimensional flow system in sand, found that when water moved into the soil, air was forced ahead of the wetting front. However, not all of the air within the soil was swept out with the wetting front, and trapped air bubbles within the soil had a considerable effect on the flow of water through the soil. The volume of air trapped in the soil is dependent upon pressure and temperature; consequently, barometric pressure changes can control the volume of trapped air in a soil and the permeability of the soil. For example, during periods of low barometric pressure, air in pore spaces expands and the effective porosity decreases, thereby decreasing the permeability of the soil.

Table 14 Lag intervals for the isotropic variogram.

Interval	Distance (m)
1	2.0
2	3.0
3	4.0
4	5.2
5	7.1
6	8.5

Changes in pond level Changes in pond level significantly affect the amount of water lost or gained in the I-V bags attached to the small-ring infiltrometers. Patterns of water gain in the I-V bags and decreases in water level of the pond (due to evaporation and infiltration) are cyclical and coincident. As the level of the pond decreases, the water level inside the small rings decreases to maintain a constant head across the infiltrometer boundary. For example, a 1-mm drop in the water level of the pond results in a 71-gram weight gain in the I-V bags attached to the small rings as the water level in the infiltrometer decreases to the pond level. An infiltration flux of 7×10^{-8} cm/s results from a water loss in a small-ring infiltrometer of 30 grams/week. Consequently, fluctuations in pond level tend to mask infiltration, but stringent quality control to maintain a constant pond level minimizes this problem. The pond is filled to a depth of 295 mm and not allowed to drop below 293 mm. To minimize pond-level effects on I-V bag weights, we adjust pond level on Tuesday and weigh the I-V bags on Thursday—the same days each week. This allows time for the rings and pond to equilibrate after the pond is refilled and ensures that the pond level is as constant as possible on all days when measurements are taken. Thus, although water loss and gain in the small rings is strongly affected by pond-level fluctuations, the cyclical nature of pond filling and bag weighing mitigates these effects.

Dummy-ring infiltrometers Four ring-infiltrometers similar in size and shape to the small-ring infiltrometers were built and placed in the liner pond on February 17, 1989. These rings, metal cylinders 20 and 36 cm in diameter, were sealed on the bottom to prevent infiltration. An I-V bag was attached to the cylinder (the same way the bags were attached to the small-ring infiltrometers). The cylinders, suspended just above the top of the liner surface, are referred to as "dummy-ring infiltrometers." They are affected by all factors affecting the small-ring infiltrometers except infiltration.

The dummy rings, three arbitrarily selected small-ring infiltrometers (SR 4, 13, 26), and all four large-ring infiltrometers were monitored daily (Monday through Friday) for 4 months. Cumulative infiltration for the dummy rings was 0 for the period; however, short-term water losses and gains in the I-V bags were apparent. The water loss/gain in the I-V bags of the small-ring infiltrometers and the dummy rings follow similar patterns, cyclical and closely related to pond-level changes. The large-ring infiltrometers are not usually affected by pond-level changes because they form a closed system below the surface of the liner pond. Initially, we believed that the water losses and gains in the dummy rings would correspond to fluctuations other than those of the infiltrometers, and therefore could be used to correct the small-ring data. However, the cyclical nature of the fluctuations and their correlation with pond level eliminated the need for correcting small-ring infiltration-rate data when the pond-filling and infiltrometer-monitoring schedule was followed. Careful monitoring of the pond level during infiltrometer measurement periods eliminated pond-level effects on the measurements.

■ Construction Effects and Instrument Malfunctions

The small-ring infiltrometers adjacent to areas in which remedial actions were required during construction of the cutoff wall had the highest infiltration fluxes. The six infiltrometers having the highest infiltration fluxes were SR-1, SR-2, SR-3, SR-4, SR-19, and SR-32; the geometric mean of the infiltration flux of these infiltrometers is 1.3×10^{-7} cm/s; whereas the geometric mean of the infiltration flux of the small-ring infiltrometers not adjacent to these areas is 7.1×10^{-8} cm/s.

A t-test performed at a 99.9-percent significance level showed that the means of the infiltration fluxes of the two sets of infiltrometers are significantly different. These results suggest that data

Table 15 Variogram estimates for various numbers of variogram directions and lag distances.

Variogram	Pairs	Average distance (m)	Variogram estimate
Isotropic	15	1.22	0.00365
	56	2.57	0.00900
	31	3.51	0.00907
	53	4.82	0.00968
	47	5.87	0.01217
	50	7.63	0.00657
0°	16	2.44	0.01241
	13	4.88	0.01391
30°	13	2.72	0.00909
	8	5.46	0.01619
60°	7	4.440	0.00717
90°	15	1.22	0.00365
	13	2.44	0.00453
	9	3.66	0.00843
120°	7	4.40	0.01190

collected from regions where slumping occurred are not representative of the overall liner. A likely explanation for the increased infiltration fluxes is the formation of preferential pathways adjacent to areas where lateral stress release and slumping had occurred.

One small-ring infiltrometer (SR-20) developed a leak during the monitoring period; data from this ring were not used in the data analysis.

■ Areal Distribution of Fluxes: Geostatistical Analysis of Infiltration Data

Estimates of the average value of the infiltration flux over portions of the liner were obtained by geostatistical analysis of the liner infiltration data; the USEPA geostatistical program GEO-EAS (Englund and Sparks 1988) was used. The mean value of each quadrant and the mean of the entire liner were estimated using the analysis. The following steps were taken to calculate the mean values for infiltration flux (Journel and Huijbregts 1978). A structural analysis consisting of the construction of experimental variograms, interpretation of the variograms, and selection of a theoretical variogram that best fit the structure of the data was performed. Using the analytical variogram, we then obtained the mean values via kriging. Data from SR-1, SR-2, SR-3, SR-4, SR-19, SR-20, and SR-32 were not used in this analysis because they were considered nonrepresentative of the liner.

Experimental variogram Several experimental variograms were calculated. Directional variograms were determined for five different directions that are 0°, 30°, 60°, 90°, and 120° with respect to the x-axis (the northeast corner of the liner is the origin; the x axis is the north side of the liner). An isotropic variogram was calculated with the aid of a scatter plot of the variogram couples (fig. 39). For each possible pair of datum points (infiltrometers), one-half the square difference of the infiltration flux is plotted relative to the distance between the two points. We determined the lag spacing from the distribution of datum points on figure 39 by choosing the lag intervals to include closely spaced groups of data and to avoid choosing an interval that contained only a few data pairs. The lag intervals chosen for the isotropic variogram are given in table 14; variogram estimates are presented in table 15. For the directional variograms, only datum points that fell within 10° of the specified angle were used in the calculations. The lags for the directional variograms were dictated by the instrument spacing. Variograms in the different directions (fig. 40) are quite dissimilar; however, only a few couples were available for the directional variogram calculations (table 15), and the scatter in the directional variograms may not be significant.

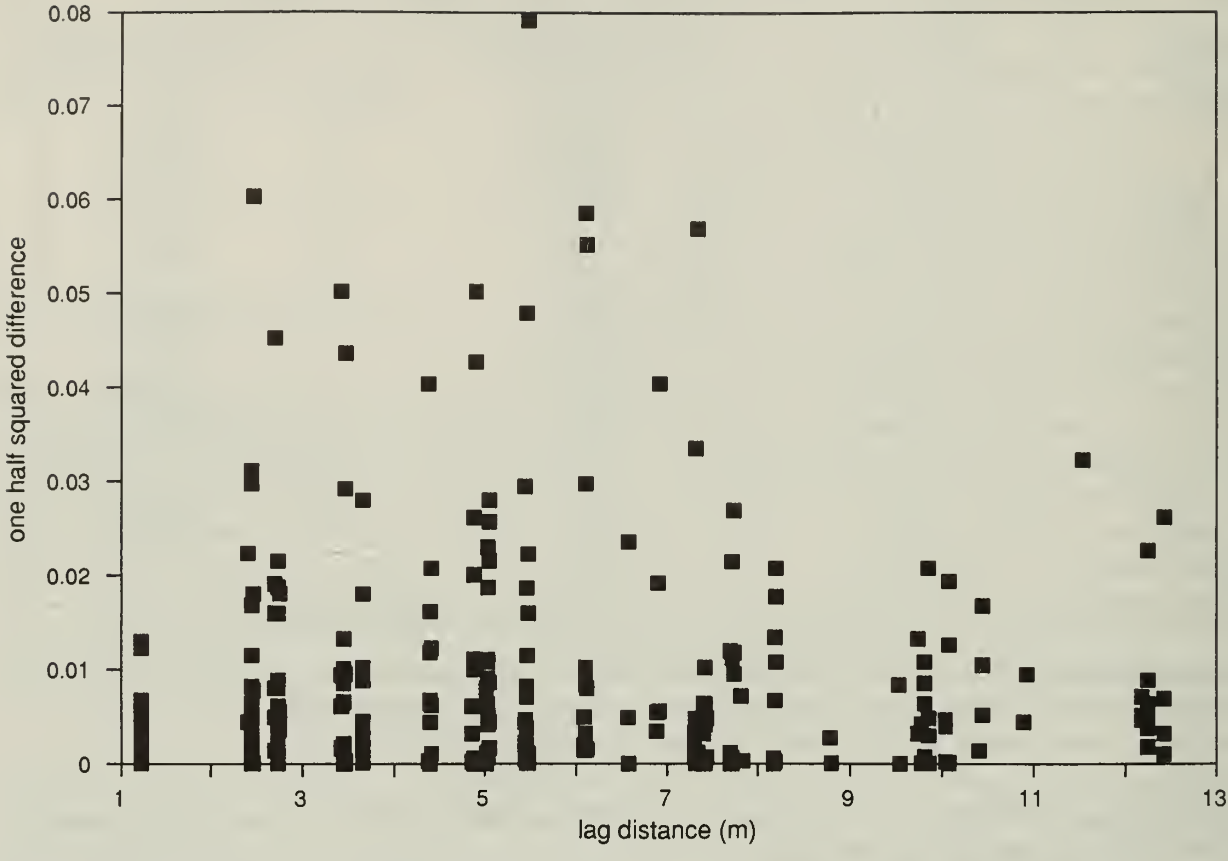

Figure 39 Scatter plot of variogram couples.

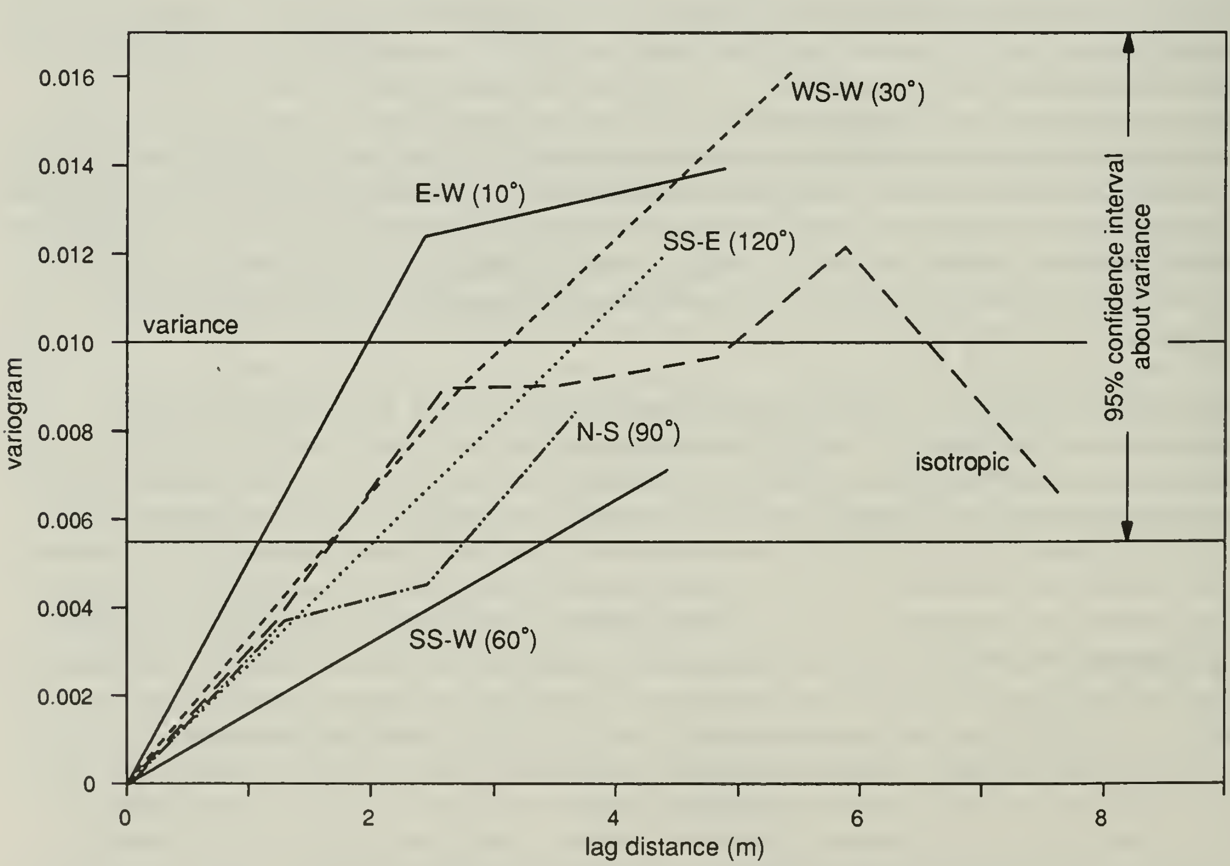

Figure 40 Semivariograms of small-ring fluxes for various directional orientations.

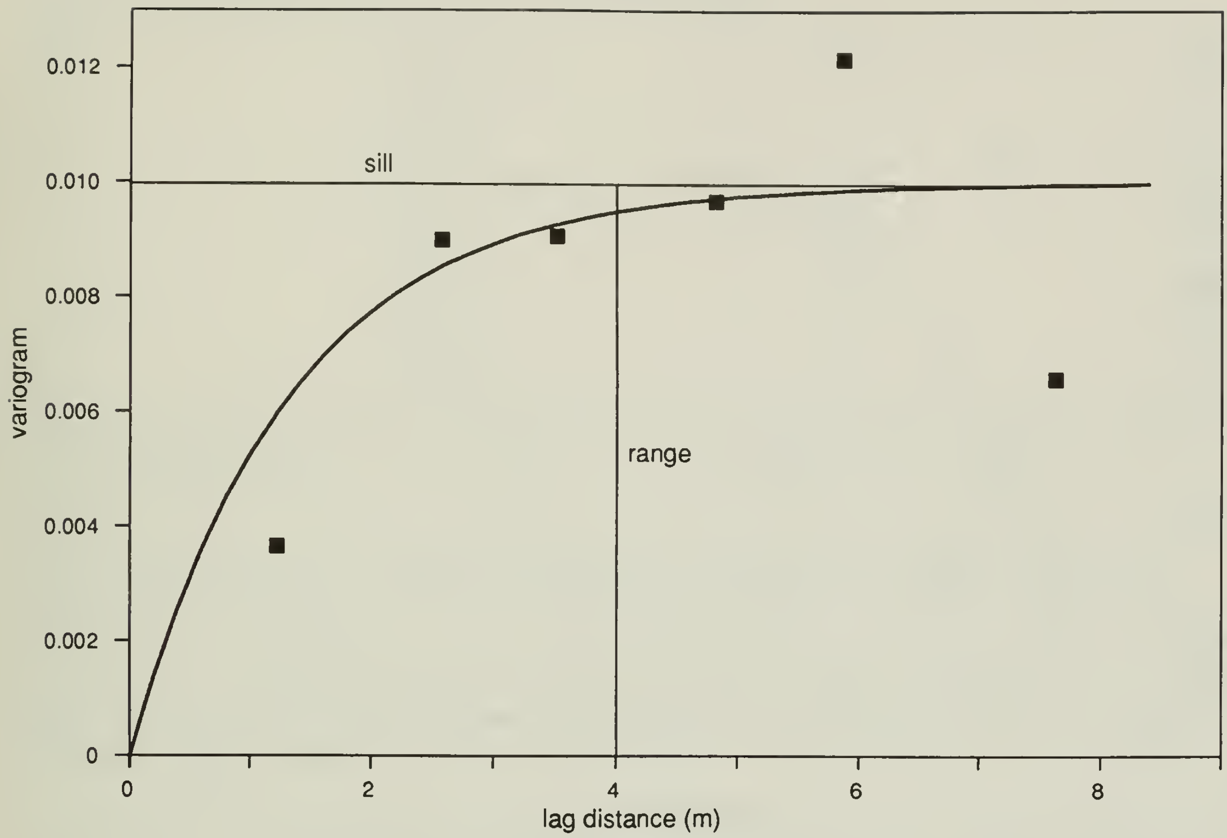

Figure 41 Model exponential variogram.

The 95-percent confidence interval for the sample variance (fig. 40) is large enough to include all the sample variogram values, except for one point at a lag distance of 5 m. Calculation of the confidence interval is based on the assumption that the infiltration values are independent and uncorrelated. In fact, the values are correlated, and Priestley (1981) has shown that in the case of a correlated random process with an exponential covariance, the confidence interval about the sample variance will be larger than if the samples were all uncorrelated. Hence the confidence interval shown in figure 40 is probably an underestimate of the uncertainty in the estimate of the variance. For a stationary random process, the sill of the variogram is expected to equal the variance; therefore, one would expect the sill value of the liner infiltration data to also be uncertain. Because the directional variograms were calculated with few pairs of datum points and are within the confidence interval of the variance, the directional variograms are deemed not statistically different from the isotropic variogram.

Theoretical variogram After an experimental variogram has been calculated, a theoretical variogram must be specified to obtain a kriged estimate of the liner properties. The choice of an appropriate theoretical variogram is not always straightforward. Three possible variogram forms, representing exponential, gaussian, and spherical models (Journel and Huijbregts 1978) are shown in figures 41 to 43. With these three models, ten possible variograms with different range and sill values were considered. The parameters of the ten possible variograms are given in table 16.

To determine the best variogram to use for kriging, we implemented two selection approaches. The first, known as validation (Journel and Huijbregts 1978, Englund and Sparks 1988), involved sequentially removing one datum point and using the remaining datum points to predict the missing value via kriging. For each datum point, we calculated the normalized error, defined as the measured value minus the predicted value divided by the square root of the

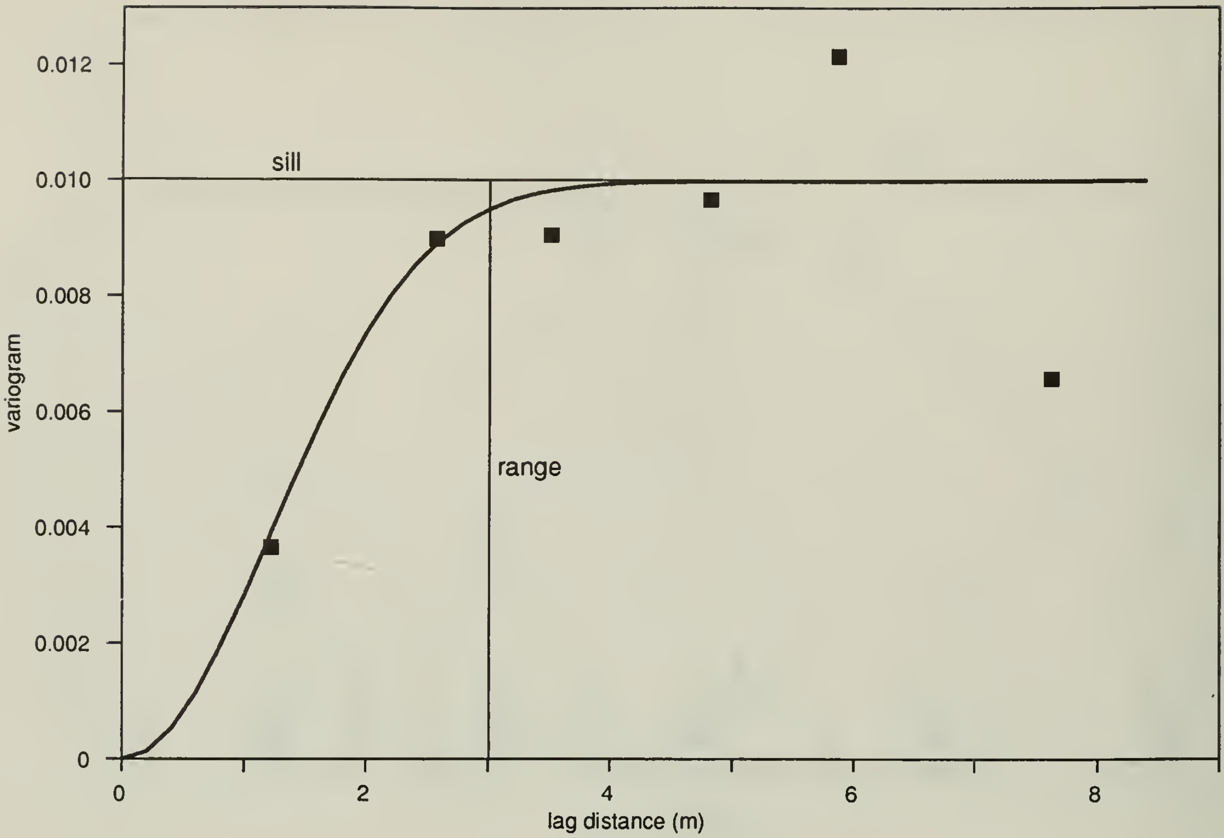

Figure 42 Model gaussian variogram.

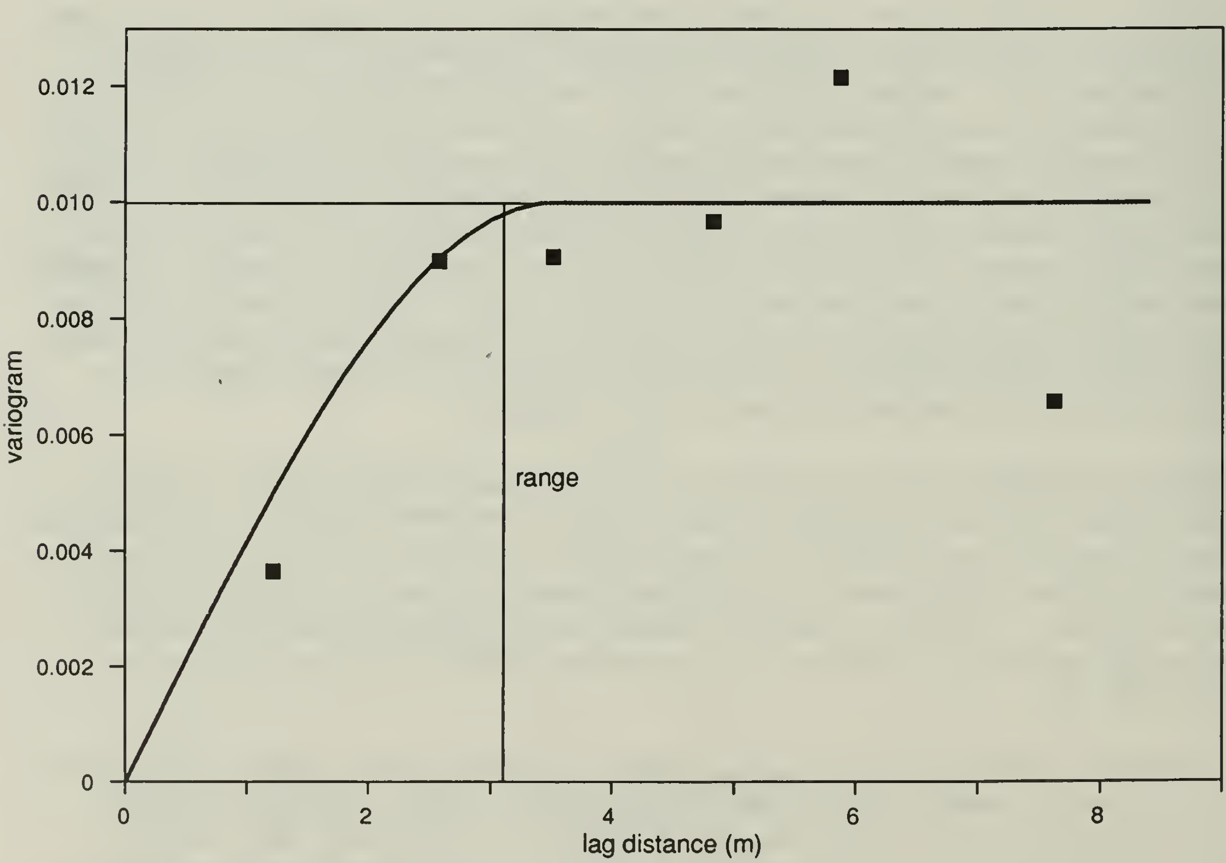

Figure 43 Model spherical variogram.

Table 16 Range and sill values for the ten variogram models.

Model	Variogram form	Range*	Sill
1	Exponential	4.0	0.01
2	Gaussian	3.0	0.01
3	Spherical	3.5	0.01
4	Exponential	7.0	0.012
5	Exponential	3.5	0.009
6	Spherical	6.0	0.012
7	Spherical	3.2	0.009
8	Spherical	4.0	0.01
9	Spherical	4.0	0.095
10	Spherical	4.5	0.01

*The range for the exponential and gaussian models is defined as the distance (in meters) at which the variogram reaches 95% of its sill value; for the spherical model it is the distance at which the variogram equals the sill value.

estimation variance. Validation was performed for each of the ten variograms listed in table 16. If the variogram model is a correct representation of the spatial variability, the average normalized error should have a value of 0 and a mean squared value of 1. In reality, the variogram is only an approximation of the spatial variability, and the best variogram for kriging is the one that most closely produces the mean and mean squared normalized error of 0 and 1. Table 17 presents the mean and mean squared values of the normalized error for the ten variogram models in table 16.

In a statistical sense, all the models would be acceptable because the mean and mean squared errors are not statistically different for 0 and 1. Nevertheless, ranking the variograms in table 16 on the basis of the results, as presented in table 17, and emphasizing the squared error more than the mean suggests that models 1, 3, and 5 were the best, models 4, 7, and 8 intermediate, and the rest were less desirable.

A second approach to ranking (Kitanidis 1986) different variogram models also used the predicted and measured infiltration flux values from each location for each variogram model. For each datum point, the absolute kriging error, defined as the absolute difference between the measured and predicted value, was calculated for each variogram model. For each datum point, the model that gave the smallest absolute kriging error was given a grade of 1, the second smallest a grade of 2, and so on. The overall grade of each model was the average of all the datum points. The model with the lowest grade was chosen as the best to fit the data. The three models with the lowest grade, beginning with the smallest, were 1, 3, and 7. Model 1 (exponential) was chosen as the best of the ten variogram models for kriging because it had the lowest mean squared normalized error and the lowest grade.

Discussion of variogram structure The best fit model variogram had a sill value approximately equal to the sample variance and a range of 4.0 m. The range is defined as the lag distance at which the variogram reaches 95 percent of its sill value. The correlation scale, defined as the lag distance at which the variogram reaches 63 percent of the sill value, was about 1.3 m. Datum points separated by distances greater than the correlation scale can be considered uncorrelated. For the small-ring infiltrometers, only adjacent points in the north-south direction can be considered correlated. Analysis of the variogram indicated that the sample grid was well designed to capture the variability of the infiltration over the surface of the liner. A denser grid would produce highly correlated measurements, and each value would contribute little new information. A less dense grid would have run the risk of missing some zone of the liner with a significantly higher or lower infiltration rate than that of the liner as a whole. For this liner, the variability in measured infiltration was very small; thus the mean infiltration rate for the liner can be determined within relatively narrow bounds.

Table 17 Mean and mean squared error from validation of the ten variogram models.

Model	Mean	Mean squared error
1	0.025	1.029
2	−0.011	1.522
3	0.029	1.120
4	0.021	1.143
5	0.027	1.048
6	0.020	1.384
7	0.028	1.134
8	0.034	1.196
9	0.035	1.227
10	0.032	1.278

Table 18 Calculated geometric and kriged mean infiltration fluxes (cm/s) for each quadrant of the liner.

Quadrant	Geometric mean	Kriged mean
Northeastern	7.1×10^{-8}	6.9×10^{-8}
Southeastern	6.7×10^{-8}	6.7×10^{-8}
Northwestern	7.0×10^{-8}	7.0×10^{-8}
Southwestern	7.2×10^{-8}	7.1×10^{-8}

Mean infiltration flux for entire liner The geometric mean infiltration flux for the entire liner was given previously as 7.1×10^{-8} cm/s. The kriged estimate of the mean infiltration flux was 7.1×10^{-8} cm/s. This estimate was calculated with the USEPA geostatistical analysis package, GEO-EAS, using the 25 infiltration flux values and a 4 × 4 grid of prediction points.

Quadrant estimates of infiltration flux The mean infiltration flux of each quadrant was estimated in two ways. First, the geometric mean of measurements within each quadrant was computed; then the quadrant values of infiltration flux were estimated by kriging, using variogram model 1 (exponential). Using GEO-EAS, we derived the quadrant average values of infiltration flux. Only measurements within a quadrant were used to predict the mean value of the quadrant. The geometric mean and kriged mean values are given in table 18.

The geometric mean and kriged mean values for the four quadrants are similar. The mean infiltration flux is nearly the same over the entire liner except for the southeast quadrant, where the infiltration flux is slightly lower.

■ Hydraulic Conductivity Estimates

Use of cumulative infiltration curves for calculating K_{sat} Infiltrometers used commercially for characterizing the hydraulic properties of liners are monitored until the measured infiltration rates satisfy regulatory requirements or until steady-state infiltrability is achieved, whichever comes first (Daniel and Trautwein 1986). This technique assumes vertical groundwater flow and a hydraulic gradient of 1.0. Monitoring of these infiltrometers generally requires 1 or more weeks. Although the monitoring may indicate that a liner meets regulatory requirements, even if the test terminates before steady-state infiltrability is achieved, such tests do not yield an accurate measurement of K_{sat} (Daniel and Trautwein 1986). Monitoring the infiltrometers until they achieve steady-state infiltrability and calculating the infiltration rate from the slope of the cumulative infiltration curve is a more accurate means of determining the K_{sat} of a liner. Although this method may require monitoring the infiltrometers for at least 2 months, a longer test period should alleviate problems associated with fluctuations in barometric pressure and sudden changes in temperature, and should also allow for monitoring of more than the top few centimeters of the liner. The results of this technique should yield a more representative K_{sat} for the liner as a whole.

Darcy's law The easiest method available for calculating the hydraulic conductivity of the liner is through the use of Darcy's law. This method assumes that all flow through the liner is saturated. In simple terms, Darcy's law can be written as $Q = -K_{sat} I A$, where Q is the discharge, K_{sat} is the saturated hydraulic conductivity, I is the hydraulic gradient, and A is the cross-sectional area of flow. Solving for K_{sat} produces $K_{sat} = -Q/(AI)$. Q/A is the measured steady-state infiltration rate per unit area; in Darcy's law, Q/A is negative because flow is downward. The average hydraulic gradient value for the liner, determined from the tensiometer data after 1 year of ponding, was 1.5. Hydraulic conductivity values for the liner calculated from four sets of infiltrometer data are shown in table 19. The hydraulic conductivity values calculated from all sets of data were less than 1×10^{-7} cm/s; the maximum flux measured (regardless of instrument type or location) produced a conductivity slightly exceeding 1×10^{-7} cm/s.

When the entire thickness of the liner becomes saturated, the hydraulic gradient will decrease to 1.3. Even at this lower gradient, if infiltration rates remain constant, hydraulic conductivity ranges between 5.5×10^{-8} in areas not affected by cutoff-wall construction, to 1.0×10^{-7} cm/s in areas affected by the construction. Data generated by the LR-infiltrometers were ignored in calculation of these values. Therefore, all sets of infiltrometer data should meet the hydraulic conductivity requirement for soil liners ($<1 \times 10^{-7}$ cm/s).

Green-Ampt approximation The Green and Ampt (1911) equation for soil infiltrability (the first introduced) is still widely used. Their approximation assumes the wetting front is sharp, the matric potential at the front is constant, and the wetted zone is uniformly wet and of constant hydraulic conductivity. The sharpness of the dye front in the prototype-liner phase of this project (Albrecht et al. 1989) indicated that the assumption of a sharp wetting front is reasonable.

This approximation differs from the simple use of Darcy's law in that the depth of the wetting front, instead of a measured hydraulic gradient, is required for the calculation. Given these assumptions, the analytical solution to vertical infiltration produces an equation that resembles the Darcy equation:

$$K = i\left(1 + \frac{h + \psi_f}{L_f}\right)^{-1} \qquad [8]$$

Table 19 Infiltration fluxes and hydraulic conductivity values determined from infiltrometer data using Darcy's law and Green and Ampt approximation.

Infiltrometers	Infiltration flux (cm/s)	Darcy K_{sat} (cm/s)	Green and Ampt K_{sat} (cm/s)	n
All small rings	7.9×10^{-8}	5.3×10^{-8}	3.8×10^{-8}	31
Small rings not affected by construction	7.1×10^{-8}	4.7×10^{-8}	3.4×10^{-8}	25
Small rings affected by construction	1.3×10^{-7}	8.7×10^{-8}	6.2×10^{-8}	6
Large rings	5.0×10^{-9}	3.3×10^{-9}	2.4×10^{-9}	4
Water balance	1.0×10^{-7}	6.7×10^{-8}	4.7×10^{-8}	1
Maximum flux	1.9×10^{-7}	1.3×10^{-7}	9.0×10^{-8}	1

Table 20 Values used for the parameters in different transit-time prediction methods.

Transit-time prediction method	Saturated hydraulic conductivity K_{sat} (cm/s)	Total porosity, η	Moisture suction potential $\psi(\theta)$	Initial moisture content θ_i	Transit time (yrs) min	max
Simple transit-time equation	2.4×10^{-9} (min) 1.3×10^{-7} (max)	0.33			5.5	296
Modified transit-time equation	2.4×10^{-9} (min) 1.3×10^{-7} (max)	0.33	55 cm		3.7	202
Green-Ampt wetting-front model	2.4×10^{-9} (min) 1.3×10^{-7} (max)	0.33	7 cm	0.21	1.3	71

The bracketed term is the hydraulic gradient, h is the ponding depth, ψ_f is the matric potential at the wetting front, L_f is the depth to the wetting front, and i is the steady-state infiltration flux. The matric potential ψ_f was measured to be 7 cm by tensiometers located just at the wetting front (33 cm deep).

The depth of the pond was 29.5 cm. After 1 year of ponding, tensiometer data suggest that the wetting front was at a depth between 18 and 33 cm, and an estimate based on the water-balance approach indicated that the wetting front should have been 26 cm below the liner surface. To provide the more conservative estimate of saturated hydraulic conductivity, we used a 33-cm wetting front depth in these calculations. K_{sat} estimates using the Green and Ampt assumptions for the same five data sets as were used in the Darcy approximation are given in table 19. Because the average measured hydraulic gradient was 1.5 and the calculated gradient was approximately 2, the values calculated from a simple use of Darcy's law are approximately 30 percent higher than those calculated by the Green and Ampt method.

Transit time predictions An important objective of this project is to determine the accuracy of methods used to predict transit time. Water did not break through at the bottom of the liner during the first year of monitoring, nor have soil-water samples contained detectable concentrations of tracers. Therefore, after the first year of monitoring, the predictions cannot be verified, only compared.

The USEPA (1988a) suggested seven methods to predict water and solute movement through a soil liner. Two are numerical methods, which are discussed in chapter 9. Three of the remaining five, all simple analytical solutions, are discussed in this section. These three methods include the simple transit time equation, the modified transit time equation, and the Green-Ampt wetting-front model. The parameters required for each model are given in table 20. The conductivity values used in the models represent the highest and lowest calculated by either Darcy's law or the Green and Ampt approximation. (Using both conductivity values provides a minimum and maximum time when breakthrough should occur.) In our project, a total porosity (η) of 0.33 was determined from the average liner density (1.84 g/cm^3) and a particle density of 2.74 g/cm^3. The porosity term for each of the models was assumed to equal total porosity rather than effective porosity. The time predicted by the models for a solute to break through is increased by using the total porosity, rather than the effective porosity. We used the total porosity value because of the lack of measured effective porosities in the liner and because we were following USEPA recommendations (1988a).

Simple transit-time equation This equation assumes that the liner has always been saturated and drains freely at the bottom; that there is steady-state one-dimensional flow; and that dispersion and adsorption are neglected. Transit time was calculated as

$$t = \frac{\eta d}{v} = \frac{\eta d}{K_{sat}} \frac{d}{(h + d)} \qquad [9]$$

where d is the liner thickness (90 cm), h is the depth of the liner pond (29.5 cm), v is the Darcian velocity, and all other parameters are as defined previously. On the basis of this equation, we predicted tracer transit time through the liner to be between 5.5 and 296 years, depending upon which K_{sat} was used.

Modified transit-time equation The modified transit time equation (Cogley et al. 1984) includes suction potential at the bottom of the liner, and thus recognizes that the liner is not in a completely saturated condition. All other assumptions of the simplified transit time equation remain the same. Modifying equation [9] yields

$$t = \frac{\eta d}{v} = \frac{\eta d}{K_{sat}} \frac{d}{(h + \psi + d)} \qquad [10]$$

where ψ is suction potential at the bottom of the liner (55 cm, per tensiometer data). The modified transit time method estimated breakthrough between 3.7 and 202 years.

Green-Ampt wetting-front model The Green-Ampt infiltration model assumes piston flow and can be used to predict the time it will take for the wetting front to reach a prescribed depth in the liner. If the wetting front depth is assumed to be at the base of the liner, the model predicts the time of water breakthrough,

$$t = \frac{\theta_s - \theta_i}{K_{sat}} \left[L_f - (h + \psi_f) \ln \left(1 + \frac{L_f}{h + \psi_f} \right) \right] \qquad [11]$$

All parameters are defined above, except that L_f (the depth to the wetting front at breakthrough) equals the liner thickness (90 cm); ψ_f is 7 cm, based on tensiometer data just below the wetting front; θ_i is 0.21; and θ_s equals the total porosity. A breakthrough estimate of 1.3 years produced by using the largest hydraulic conductivity from all the data sets represents the earliest time in which water will exit the bottom of the liner. The use of the smallest Green-Ampt estimated hydraulic conductivity (2.4×10^{-9} cm/s) produced a breakthrough estimate of 6.8 years, and the estimated conductivity for the entire liner (4.7×10^{-8} cm/s) estimated breakthrough at 3.6 years.

The tensiometer data suggested that the wetting front was at a depth of about 30 cm after 1 year of ponding. The tensiometer data reflect the actual liner performance and suggest that water should break through in approximately 3 years, if the rate of water movement in the liner is assumed to be constant with respect to time. The Green-Ampt breakthrough estimate of 3.6 years (based on overall conductivity) for the wetting front to reach the bottom of the liner appears to be consistent with actual data.

Summary

Cumulative infiltration curves for the small-ring infiltrometers provided an estimate of the steady-state infiltrability. In addition, these curves revealed irregularities in infiltration rates that were interpreted as measurement errors caused by leakage, changes in pond level, changes in barometric pressure, and changes in the hydraulic conductivity of the liner itself. The infiltration data, based on all of the small-ring infiltrometers, show that the K_{sat} of the liner is 3.8×10^{-8} cm/s. This value is well below the K_{sat} of 1.0×10^{-7} cm/s required by the USEPA. The consistency and reproducibility of these data among the four quadrants of the liner suggest that the regulatory requirement for the saturated hydraulic conductivity is achievable.

Instruments that need to be grouted into place have leaked because of poor bonding between the grout and the liner material. Thus, if ring infiltrometers are grouted into place and do leak, the resulting infiltration data may underestimate the infiltration rate of the liner. This may be the problem with the large-ring infiltrometers, which yielded infiltration fluxes that are an order of magnitude lower that those of the small-ring infiltrometers. The small-ring infiltrometers provided the most reliable and areally reproducible infiltration data; this statement is partly supported by the K_{sat} value calculated using the water-balance approach (i.e., 3.8×10^{-8} cm/s for the small rings, as compared to 4.7×10^{-8} cm/s for the water-balance calculations).

The shortcomings of the small-ring infiltrometers include their susceptibility to changes in pond level and to barometric pressure. However, problems with pond-level fluctuation can be overcome if the pond is filled and the rings are monitored on a regular basis (e.g., on the same days every week). Changes in barometric pressure affect the infiltration rate but are of no consequence in the long term because barometric pressure fluctuations are cyclical in nature, and because the effects of barometric pressure appear to be transient.

The data from the infiltrometers form two statistically distinct populations. The small-ring infiltrometer data, as calculated from cumulative infiltration curves, form a lognormal distribution; the large-ring infiltrometer data consist of only four relatively widely scattered datum points.

The large-ring infiltrometer data may not be useable because of suspected leakage of the rings along the grout-liner interface. This leakage may explain the order of magnitude difference between the small-ring and large-ring infiltration-rate data. In addition, gases collected within the large rings—apparently generated by anaerobic bacteria growing within the large ring and/or along the grout-liner interface—may also affect the large-ring infiltration-rate data.

The impact of remedial actions conducted as a result of problems encountered during construction of the liner have shown up in the infiltration fluxes of six of the small-ring infiltrometers. Small rings adjacent to areas where slumping and dilation fractures formed have the highest infiltration fluxes of the infiltrometers. The soil macrostructures formed in the liner probably account for the increased permeability. The rings adjacent to recompacted areas were not considered representative of the liner and thus were not used in the kriging calculations.

Construction-related problems, as reflected in the data set, indicate several practices that should be avoided during the construction phase of a liner. Because of the compressive forces applied to the liner during construction, trenching and/or excavations in the liner subsequent to its construction can lead to stress-release features, such as dilation fractures, and even collapse. Dilation fractures associated with such excavations could result in the increase in the infiltration rate in or adjacent to the areas where the excavations occurred.

The final calculations for the hydraulic properties of the liner indicate that the most representative hydraulic conductivity of the liner, as determined by applying Darcy's law and the Green-Ampt model to water-balance data, were 6.7×10^{-8} cm/s and 4.7×10^{-8} cm/s, respectively. Transit times were calculated by three methods. Using the simple transit time equation, transit time was predicted to be 5.5 years. The modified transit time equation estimated the transit time to be 3.7 years. Finally, the Green-Ampt wetting-front model estimated water breakthrough between 1.3 to 71 years after filling the pond.

8 TRACERS FOR MONITORING WATER MOVEMENT IN THE FIELD-SCALE LINER

Tracers were added to the large-ring infiltrometers of the field-scale liner to monitor the movement of water through the liner. Tracers are widely used to determine water flow rates and directions in porous media (Biggar and Nielsen 1960, 1962, Horton et al. 1985). Several compounds have been suggested for tracing water movement through soil (Bowman 1984a, USEPA 1985). Laboratory experiments were performed on tracers considered for use in the liner study to determine whether the movement of the tracer through the Batestown Till (liner material) would be a valid indication of water flow.

The tracers examined included *m*-trifluoromethyl benzoic acid (*m*-TFMBA), *o*-trifluoromethyl benzoic acid (*o*-TFMBA), pentafluorobenzoic acid (PFBA), bromide (as KBr), and tritiated water. The primary objective was to ascertain whether the tracers would be retarded by adsorption onto the soil. Consequently, batch adsorption experiments were conducted to measure the extent to which tracers had been adsorbed from solution onto the soil under steady-state conditions.

A secondary objective was to determine whether soil microorganisms indigenous to the soil affect the transit times of the tracers. We hypothesized that microorganisms might influence the apparent transit times by (1) chemically altering the tracers so that analytical procedures would fail to detect breakthrough, and (2) decreasing soil porosity due to blockage by microbial cells and/or microbially excluded exocellular gums. Column experiments were designed so that transit times of the tracers through sterile and nonsterile soil could be compared.

Methods

■ Batch Adsorption Tests

Batch adsorption tests were conducted according to procedures given in Roy et al. (1991). These procedures provide the data required to (1) select an appropriate soil-to-solution (ss) ratio, (2) determine an appropriate equilibration time, and (3) construct adsorption isotherms.

A series of soil-to-solution ratios were tested to assess the capacity of the Batestown till to adsorb the tracers Br, *o*-TFMBA, *m*-TFMBA, and PFBA. Thirty-five milliliters of a solution containing Br, *o*-TFMBA, *m*-TFMBA and PFBA, each at an approximate concentration of 20 mg/L, was added to 50-mL polyethylene centrifuge tubes. An equivalent weight (on an oven-dry basis) of till was added to each centrifuge tube. Eight soil-to-solution ratios were tested. The slurries were allowed to mix for 24 hours on a National Bureau of Standards rotary tumbler. The pH of each solution was taken after 24 hours, and the solutions were centrifuged for 30 minutes at 16,000 rpm. The centrifugate was then decanted and stored in 30-mL glass scintillation vials. Analysis of the samples by high-pressure liquid chromatography (HPLC) was performed within 48 hours following procedures given in Bowman (1984b).

In conjunction with determining an appropriate equilibration time, the stability of the tracers in contact with the Batestown till was also assessed. After selecting a soil-to-solution ratio, we prepared a series of soil/tracer slurries in 50-mL centrifuge tubes. The slurries were agitated for up to 81 days, and tracer concentrations were measured periodically in the slurries. The concentrations measured at the various times were than compared to the original tracer concentration.

■ Column Tests

Liner soil was passed through a 1.4-mm sieve and divided into two portions. The moisture content (9.8%) required to achieve the maximum dry density of the soil had been determined by Standard Proctor tests (chapter 1). Attempting to attain this moisture content for two separate samples proved to be extremely tedious because one sample was sterilized and could

Table 21 Description of soil treatments, packed soil densities, and tracer solutions added to columns.

Column No.	Treatment of soil	Moisture content (%)	Density (g/cm^3)	Density adjusted to 9.8% moisture (g/cm^3)	Porosity	Pore volume (cm^3)	Tracer solution
1	untreated	11.1 ± 0.3	2.09	2.06	0.24	22	A
2	untreated	11.1 ± 0.3	2.09	2.06	0.24	22	A
3	untreated	11.1 ± 0.3	2.09	2.06	0.24	22	B
4	sterile	10.6 ± 0.8	2.18	2.16	0.20	18	B

A = *m*-TFMBA, *o*-TFMBA, PFBA, Br
B = *m*-TFMBA, *o*-TFMBA, PFBA

not be left open to the air for fear of microbial contamination. After many weeks of attempting to adjust the moisture content, we decided to proceed with column packing. One portion of the soil was equilibrated in a sealed jar to a moisture content of 11.1 ± 0.3 percent. The second portion of soil was sterilized by autoclaving at 121°C for 2 hours on each of 2 successive days and equilibrated in a presterilized jar with sterile distilled water until the soil reached a moisture content of 10.6 ± 0.8 percent. Soil moisture, calculated as a percentage of dry weight, was determined after triplicate samples were dried at 105°C to a constant weight.

Tracer preparation Solutions of tracers were prepared by adding 47.5-mg *m*-TFMBA, 47.5-mg *o*-TFMBA, and 53.0-mg PFBA to 1 liter of distilled water. The final concentration of each of these three compounds was 0.25 mM. We added 0.1-mL tritiated water (specific activity 4.64 µCi/mL) to this solution and sterilized the mixture by passing it through a 0.2-µm filter. Final activity was 1056 ± 30 dpm.

This solution was divided into two portions. One portion was maintained aseptic ("B"); the other received KBr to a final concentration of 0.5 mM ("A"). Bromide was omitted from the tracer solution used to test the ability of microorganisms to influence transit time in order to ensure that microbial degradation of the organic tracers would not be inhibited by Br-toxicity. Table 21 indicates the tracer solution added to each column.

Radioactivity was determined in triplicate with 200 to 500-µL aliquots in a 4-mL OptiFluor Scintillation Cocktail (Packard)®. Radioassays were performed using a Packard® 2000 CA computer-aided liquid scintillation counter. Sample quenching was determined by comparing the transformed index of the ^{133}Ba external standard to that on a computer-stored quench curve. Sealed commercial tritium standards and blanks were included in each run to validate the quench curve.

Column preparation Four Anspec® 3500 series LC columns (2.5 × 40 cm) were packed, 1 cm at a time, to the 15-cm mark with preweighed aliquots of soil in an attempt to achieve a uniform density of 2.08 g/cm^3. Column volumes were measured by closing off the bottom end of each column and filling it with water. The volume at the 15-cm mark was 91.5 mL. Table 21 shows the actual densities of the packed soil, as determined from column volume and total weight of the packed soil; it also lists the densities adjusted to 9.8-percent moisture content.

To test the effects of microbial activity on transit time, we maintained one column under sterile conditions. Before the column was packed with sterilized soil, it was equipped with a microfilter constructed from a glass serum bottle packed with wool; then it was sterilized by autoclaving at 121°C for 15 minutes. The column packer was autoclaved before use and handled in an aseptic manner.

After the columns were packed and connected to a gas manifold, 100 mL of tracer solution was added to the headspace, and the columns were pressurized to 2.04 atmospheres. Presterilized, vented, tared, Teflon®-sealed Balch tubes were connected by means of Vacutainer needles (Beckton-Dickinson®) to the base of each column to collect the effluent. The volume of effluent collected was determined gravimetrically, assuming a specific density of 1.0 g/cm^3. Five-hundred microliter aliquots were assayed for radioactivity. The effluent was diluted 1:10 and assayed for the four individual tracers using high-pressure liquid chromatography (HPLC).

Isolation of fluorobenzoic acid degraders The following salt medium was used as the basal medium for enrichment cultures on a per-liter basis: $(NH_4)_2SO_4$ 1.0 g; $MgSO_4 \cdot 7H_2O$, 0.5 g; K_2HPO_4 0.28 g; KH_2PO_4 0.28 g; KCl, 0.15 g; $CaCl_2 \cdot 2H_2O$, 0.15 g; $MnSO_4 \cdot 7H_2O$, 0.01 g; $FeSO_4 \cdot 7H_2O$, 0.01 g. The basal medium was sterilized by autoclaving at 121°C, and cooled. One of three filter-sterilized fluorobenzoic acid derivatives, PFBA, *o*-TFMBA, or *m*-TFMBA, was then added to make a final concentration of 100 mg/L. In some cases enrichment cultures were amended with yeast extract (0.025 g/L), which provided an enriched food source.

One set of enrichment cultures consisting of the three types of media was inoculated with 10-percent sludge (by volume) from the Champaign-Urbana Sanitary District. A second set was inoculated with 10-percent topsoil (by volume) from the borrow source for the liner soil. Cultures were incubated on a gyrator shaker at 150 rpm at 28°C. After 2 weeks, these initial enrichments served as inocula (1% by volume) for secondary enrichments in the same media. After approximately 4 weeks, the secondary cultures were used as inocula for a third set of enrichments. At the same time, these cultures were streaked on plates containing the same media solidified with Noble agar (1.5%). Many isolates appeared. Two of the most vigorously growing colonies from each medium were restreaked to obtain pure cultures. To ensure that the isolates were growing on the fluorobenzoic acids rather than some other component of the media, we also streaked plates with the fluorobenzoic acids omitted.

Results and Discussion

Table 22 illustrates the soil-to-solution ratios used and the pertinent data of the experiment. Results of the soil-to-solution ratio experiment (fig. 44) suggest that none of the tracers are

Table 22 Soil solution ratio data for *m*-TFMBA, *o*-TFMBA, Br, and PFBA.*

ss ratio (g/mL)	Soil wt. (g)	Equilibrium concentration (mg/l) *m*-TFMBA	*o*-TFMBA	Br	PFBA	pH	EC (μmhos/cm)
1:4	8.75	20.6	20.8	19.9		8.09	607
1:10	3.50	20.2	20.0	19.6		8.33	332
1:20	1.75	21.0	21.0	20.6		8.45	224
1:40	0.875	20.7	20.5	18.9		8.61	170
1:60	0.583	20.9	20.7	20.0		8.63	154
1:100	0.350	20.5	20.4	19.8		8.60	151
1:200	0.175	20.7	20.4	20.1		8.58	126
1:500	0.700	20.7	20.4	20.4		8.53	123
1:4	8.75				19.6	8.25	541
1:10	3.50				20.1	8.58	248
1:20	1.75				20.2	8.81	180
1:40	0.875				20.1	9.03	112
1:60	0.583				20.1	9.17	82
1:100	0.350				19.8	9.20	84
1:200	0.175				20.0	9.26	67
1:500	0.070				20.4	9.34	41

* The volume of solute solution added to each sample was 35 mL. Initial solute concentrations were 20.7, 20.5, 19.9, and 19.8 mg/L for *m*-TFMBA, *o*-TFMBA, Br, and PFBA, respectively.

Table 23 Percentage of each tracer adsorbed and relative concentrations of each tracer as determined from the soil-to-solution data.

ss ratio (g/mL)	Percent adsorbed			
	m-TFMBA	*o*-TFMBA	Br	PFBA
1:4	0.48	−1.46	0.0	1.01
1:10	2.42	2.44	1.56	−1.52
1:20	−1.45	−2.44	−3.52	−2.02
1:40	0.0	0.0	5.03	−1.52
1:60	−1.00	−0.98	−0.50	−1.52
1:100	1.00	0.49	0.50	0.00
1:200	0.00	0.49	1.01	−1.01
1:500	0.00	0.49	−2.51	−3.03

ss ratio (g/mL)	C/C_0			
	m-TFMBA	*o*-TFMBA	Br	PFBA
1:4	0.995	1.015	1.000	0.990
1:10	0.976	0.976	0.985	1.015
1:20	1.015	1.024	1.035	1.020
1:40	1.000	1.000	0.950	1.015
1:60	1.010	1.010	1.005	1.015
1:100	0.990	0.995	0.995	1.000
1:200	1.000	0.995	1.010	1.010
1:500	1.000	0.995	1.025	1.030

Percent adsorbed = $(C_0 - C/C_0) \times 100$
C_0 = initial solute concentration
C = final solute concentration

Table 24 Kinetic data for *m*-TFMBA, *o*-TFMBA, Br, and PFBA using a ss ratio of 1:4; the experiment was performed at room temperature (≈ 21°C) and at a pH of 8.2.

Time of contact (hrs)	Rate of change (%)			
	m-TFMBA	*o*-TFMBA	Br	PFBA
1	—	—	—	—
24	8.0	3.9	2.9	2.5
48	3.3	4.7	5.1	2.5
72	1.4	1.0	2.9	1.0

Time of contact (days)	C/C_0			
	m-TFMBA	*o*-TFMBA	Br	PFBA
0.04	1.06	1.01	0.99	1.01
1	1.08	1.04	1.03	1.03
2	1.05	0.99	0.98	1.00
3	1.06	1.00	1.01	1.01
7	1.05	0.98	0.94	0.98
14	1.07	1.00	0.87	0.99
46	1.01	0.99	0.93	1.02
81	1.02	1.12	1.40	1.01

Rate of change (%) = $((C - C_1)/C) \times 100$
C = solute concentration at time *t*
C_1 = solute concentration at time $t + 24$ hours

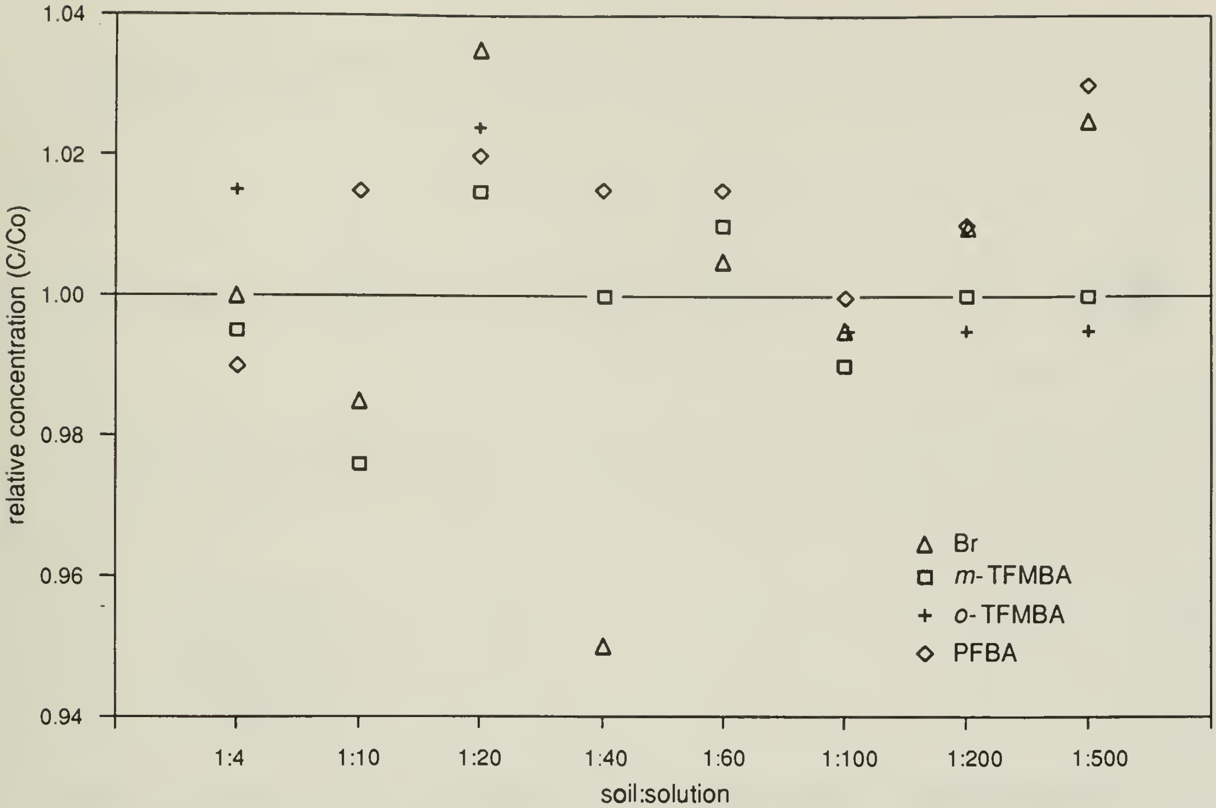

Figure 44 Adsorption of the tracers at various soil-to-solution ratios.

being adsorbed to any significant extent by Batestown till. The scatter in the data exhibited in figure 44 represents analytical variability in detecting small differences (<1 mg/L) in tracer concentrations between stock and experimental solutions.

The methods outlined in Roy et al. (1991) were followed in conducting the adsorption tests; however, deviation from the procedure was necessary. The procedure recommended selection of a soil-to-solution ratio in which 10 to 30 percent of the solute is sorbed by the adsorbent. The soil-to-solution ratio is then used in the remaining experiments to determine kinetics and construct isotherms. In the tracer studies, no tracer exhibited greater than 5-percent adsorption at any soil-to-solution ratio (table 23). We chose a ratio of 1 to 4 (mass/volume) for the kinetic studies because it best approximates the ratio likely to be found in the liner, yet still allows adequate mixing of the solution.

■ Kinetic Experiments

Kinetic studies were undertaken to determine when equilibration was reached in the adsorption of the tracers by the soil. Table 24 presents the results of this experiment. The operational definition of equilibrium (Roy et al. 1991) occurs when there is less than a 5-percent rate of change of the solute concentration per 24-hour reaction period.

All tracers (except *m*-TFMBA) exhibited less than a 5-percent change in concentration after 24 hours. Thus 24 hours was defined as the equilibrium time. Kinetic studies were continued over an 81-day period to ascertain if long-term exposure of the tracers to the soil resulted in their adsorption or degradation. Figure 45 presents the results of the kinetic study in terms of relative concentration (C/C_o, where C is the tracer concentration after a given time, and C_o is the initial tracer concentration). The values of C/C_o are close or equal to 1, a fact that suggests no analytically discernable adsorption or degradation of the tracers was occurring.

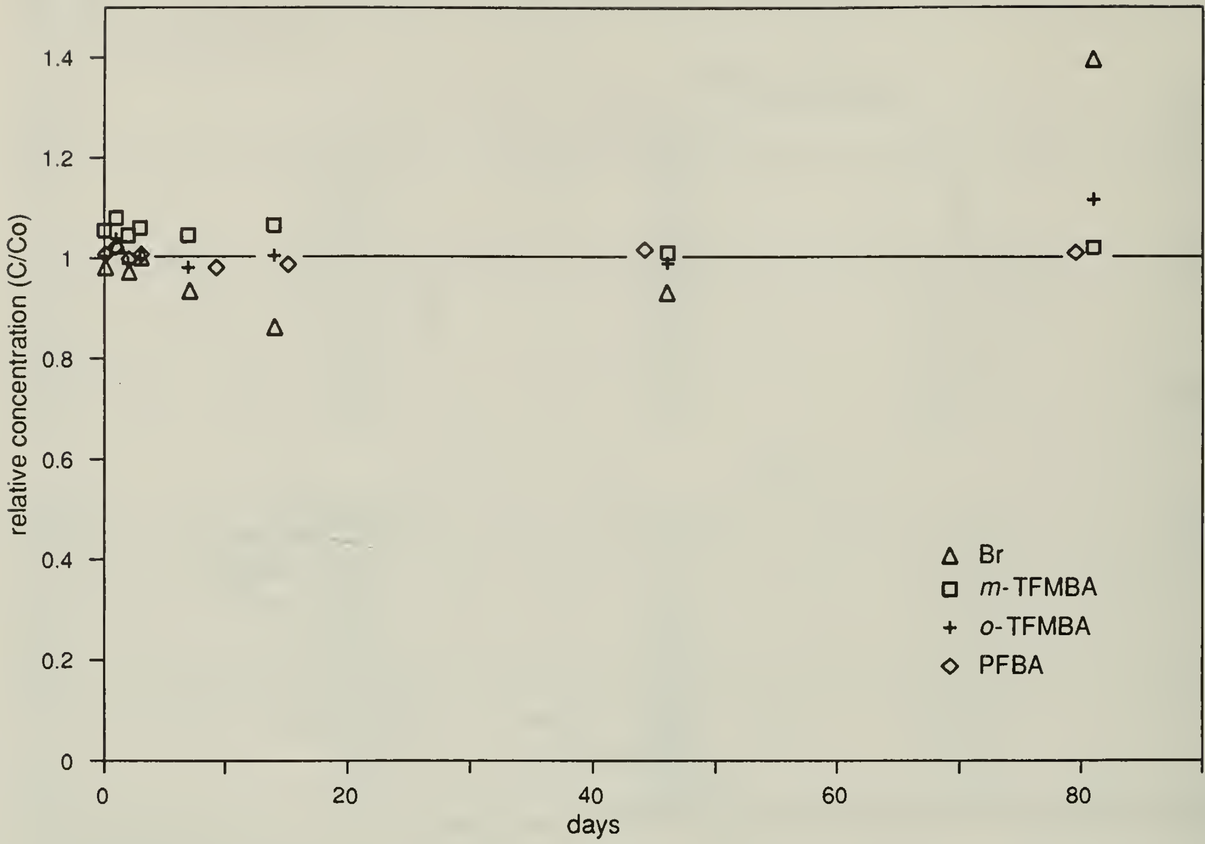

Figure 45 The relative concentration of the tracers at various contact times between the till and the tracer solutions.

Generally, the data for *m*-TFMBA plots above C/C_o values equal to 1, a fact that suggests the experimental tracer concentration is greater than the initial concentration (fig. 45). The use of soil/deionized water blanks indicated that some analytical interferences by unknown components in the solution apparently may result in greater than initial concentrations.

A correction factor for Br of approximately 2.7 mg/L was subtracted from the data to account for the interference by the sample matrix. The other tracers showed no significant interferences; however, the variability in the analysis or minor interference may account for the plotting of C/C_o values greater than 1. Bowman (1984b), who developed and used the HPLC procedure in tracer quantification, also observed C/C_o values greater than 1. For the purposes of this study, the data are adequate to demonstrate that the tracers are not being significantly adsorbed by the soil.

■ Isotherm Construction

To provide additional data on tracer adsorption, we constructed isotherms for each tracer using data from the soil-to-solution ratio experiment. Figures 46, 47, 48, and 49 show the isotherms for the tracers *m*-TFMBA, *o*-TMFBA, Br and PFBA, respectively. The isotherm data showed, as did the soil-solution ratio data and the kinetic data, that the tracers were not adsorbed by the Batestown till.

A linear regression of the data was attempted to obtain a numerical value for the K_d of each tracer. The K_d is a distribution coefficient that describes the partioning of the tracers between the solution phase and the liner soil material (the Batestown Till) at equilibrium. The distribution coefficient is defined as dS/dC, where S is equal to X/M (the amount adsorbed per mass of adsorbent), and C is the equilibrium concentration of the tracers. The value of the K_d is the

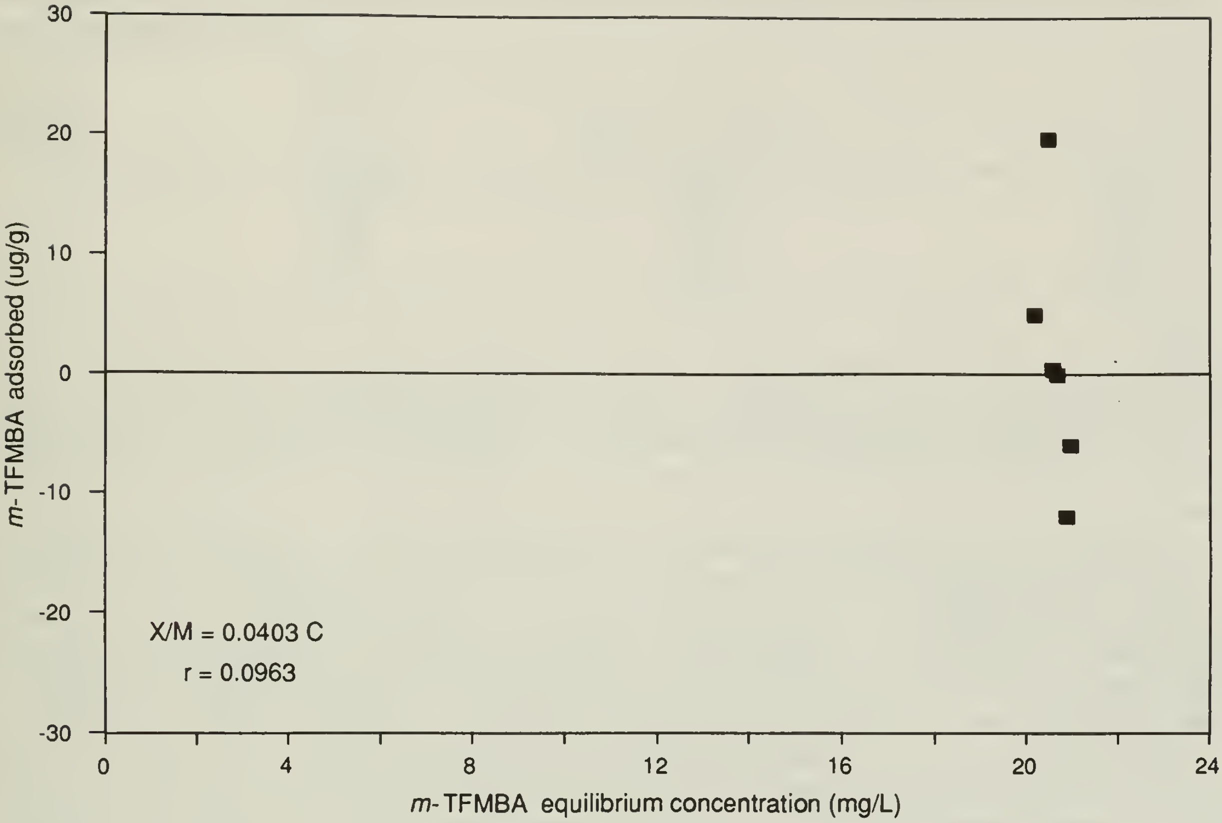

Figure 46 *m*-TFMBA adsorption by Batestown till at 21°C and pH 8.3.

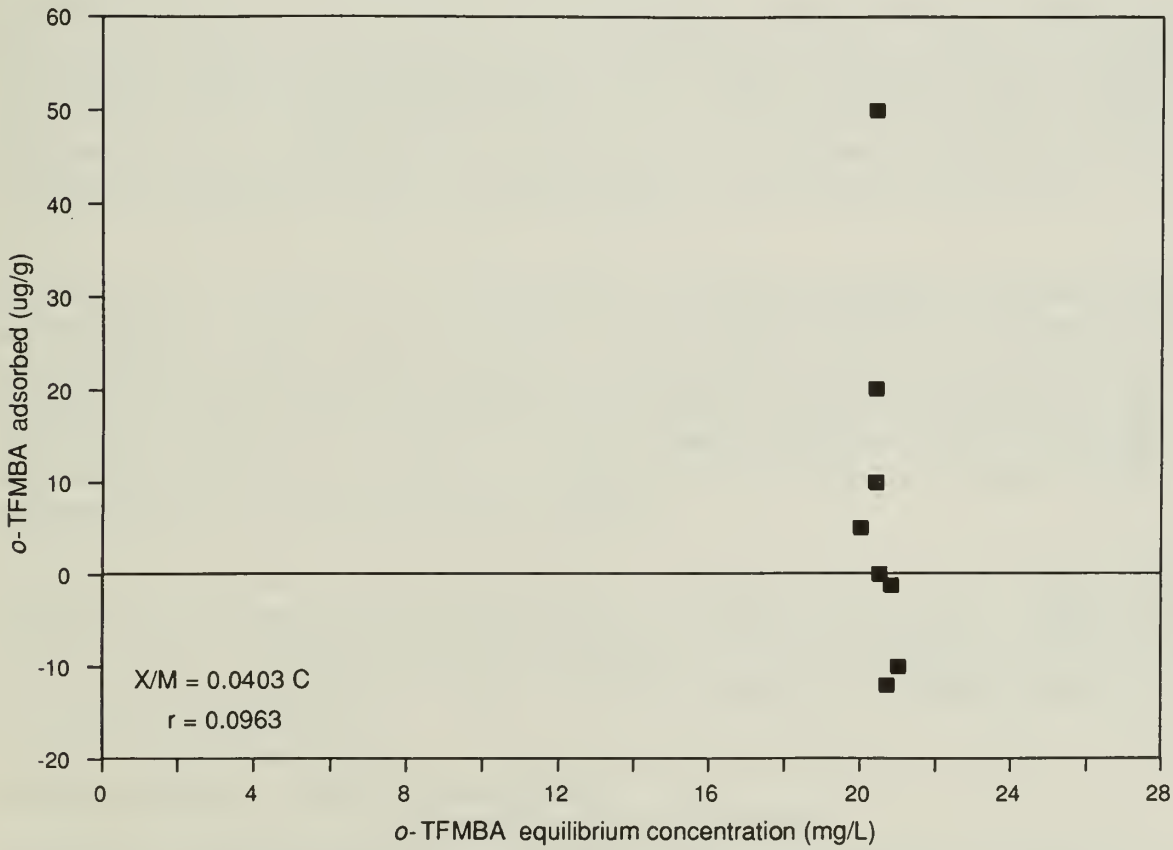

Figure 47 *o*-TFMBA adsorption by Batestown till at 21°C and pH 8.3.

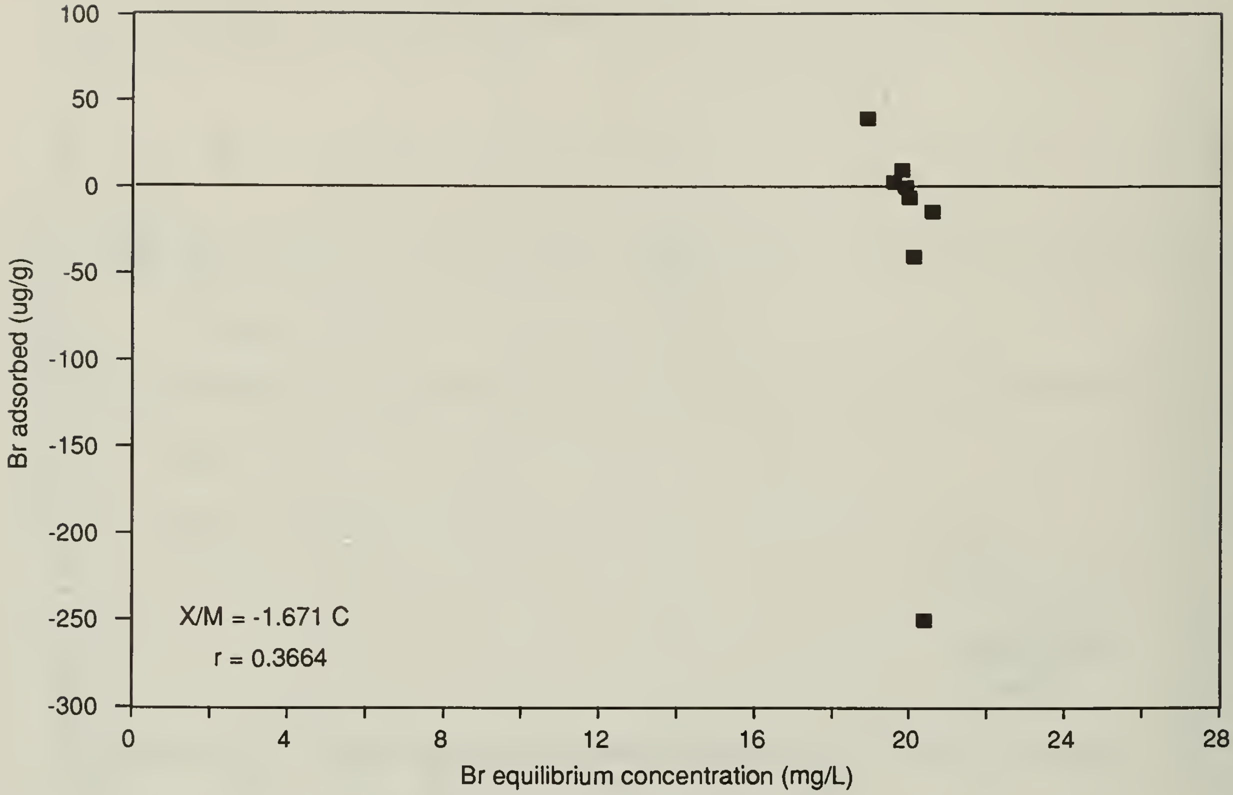

Figure 48 Bromide adsorption by Batestown till at 21°C and pH 8.3.

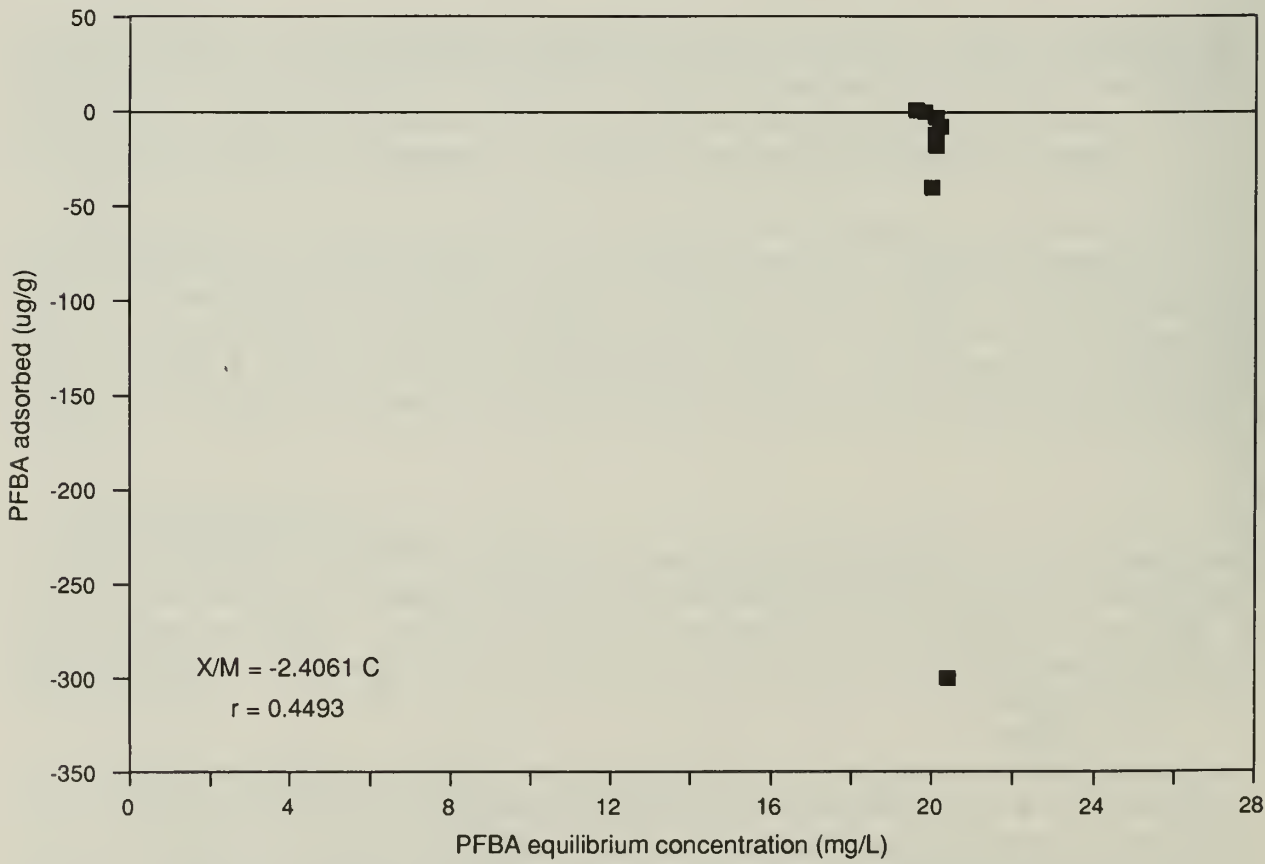

Figure 49 PFBA adsorption by Batestown till at 21°C and pH 8.3.

Table 25 Flow rates through columns, and squared coefficients of correlation between flow of water and movement of tracers.

Column number	Flow rate mL/h	r^2 (T_2O vs. *m*-TFMBA)	r^2 (T_2O vs. PFBA)
1	0.052	0.9945	0.9747
2	0.038	0.9944	0.9444
3	0.029	0.9840	0.9810
4	0.043	0.9987	0.9649

slope of the adsorption isotherm. The adsorption data were regressed so that the "line of best fit" for the isotherm was statistically forced through 0. In all cases, the K_d value (slope of line) was close to 0, suggesting no adsorption of the tracers. The correlation coefficients are low (<0.5) for all isotherms, indicating that the line of best fit is statistically not significant.

Statistical analysis of the data to determine if the r values are significantly different from 0 at the 0.05 level of significance showed that in all cases the correlation coefficients are not different from 0. Statistical evaluation of the coefficients suggests that there is no correlation between the amount adsorbed and the equilibrium concentration of the tracers. As can be seen in figures 46 to 49, the data are actually a cluster of datum points around a single equilibrium concentration, again suggesting no adsorption; thus the construction of a line through the data was unrealistic. The determination of a numerical K_d value was not possible using standard isotherm modeling techniques. For the purposes of modeling tracer movement in the liner material, the K_d value is considered equal to 0.

■ Determination of Breakthrough Curves

Breakthrough curves of the tracers in the column experiments are shown in figures 50 to 53. These curves show the concentration in the column effluent relative to the initial concentration (C/C_o) and in relation to time and cumulative volume of water exiting the column. Table 25 shows that the flow rates varied from a high of 0.052 mL/h to a low of 0.029 mL/h. In spite of this, data for each column are similar when expressed on the basis of volume. In each case, the relative concentration of T_20 was approximately 50 percent after 20.0 ± 1.08 mL (approximately 1 pore volume) of effluent was collected.

Bromide and *o*-TFMBA could not be determined in the collected effluents until near the end of the experiments because of the presence of interfering compounds that were released from the soil as the tracer solution passed through the columns. These unknown compounds were apparently no longer present in the final effluent samples from each column because the relative percentage of the two tracers was approximately 100 percent. However, because identification of the HPLC peaks was uncertain, conservation of these two tracers during passage through the soil may be open to question.

Because of these interferences, determination of datum points for Br- and *o*-TFMBA were impossible, and these data are not shown. Bowman (1984b) used the HPLC program to study these tracers in a sandy soil that had been purged of interferences with many volumes of water prior to the tracer experiments. Therefore, it is not surprising that interfering compounds were not encountered in his study.

■ Microbiological Effects on Transit Times

The flow of tritium through the sterile column (fig. 53) was similar to its flow through the corresponding nonsterile column (fig. 50 to 52), a fact suggesting that soil porosity had not

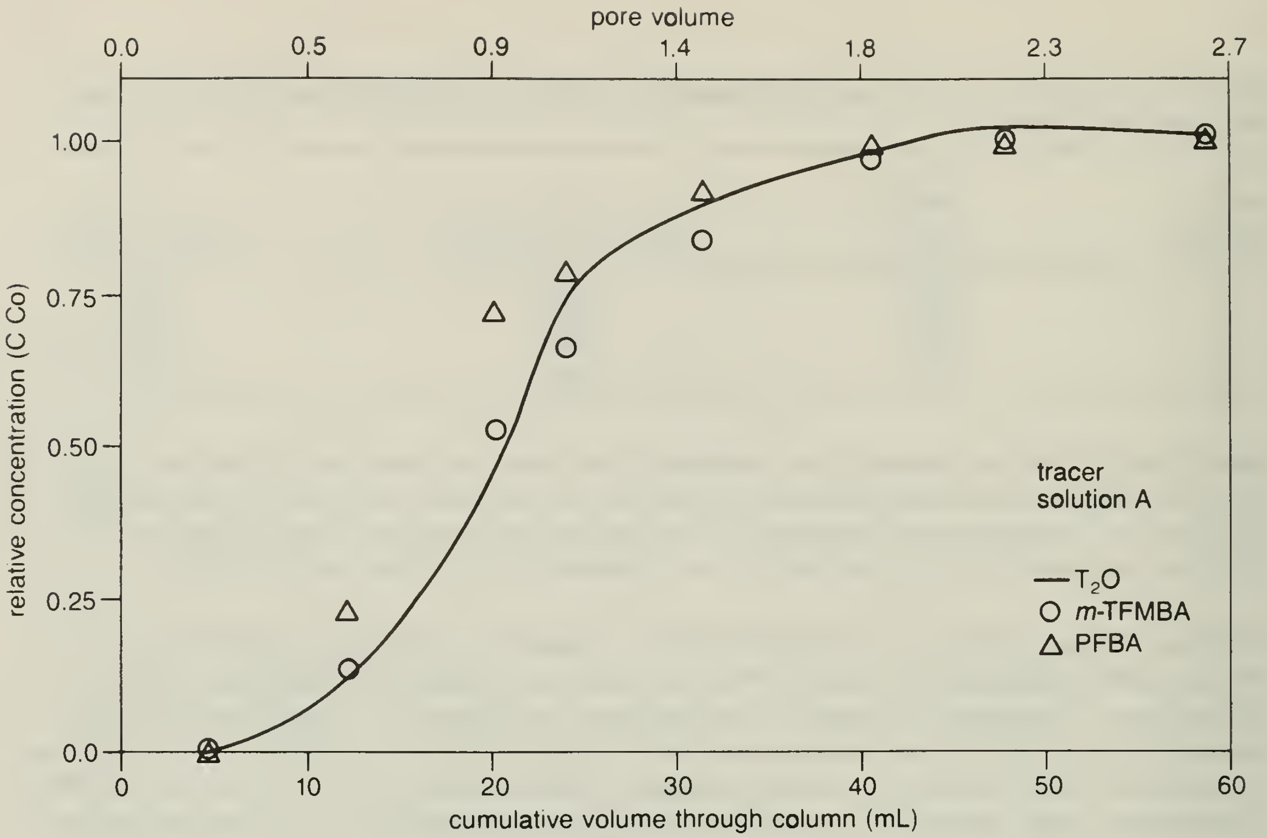

Figure 50 Movement of tritiated water, *m*-TFMBA, and PFBA through a nonsterile soil column. The tracer solution also contained *o*-TFMBA and Br.

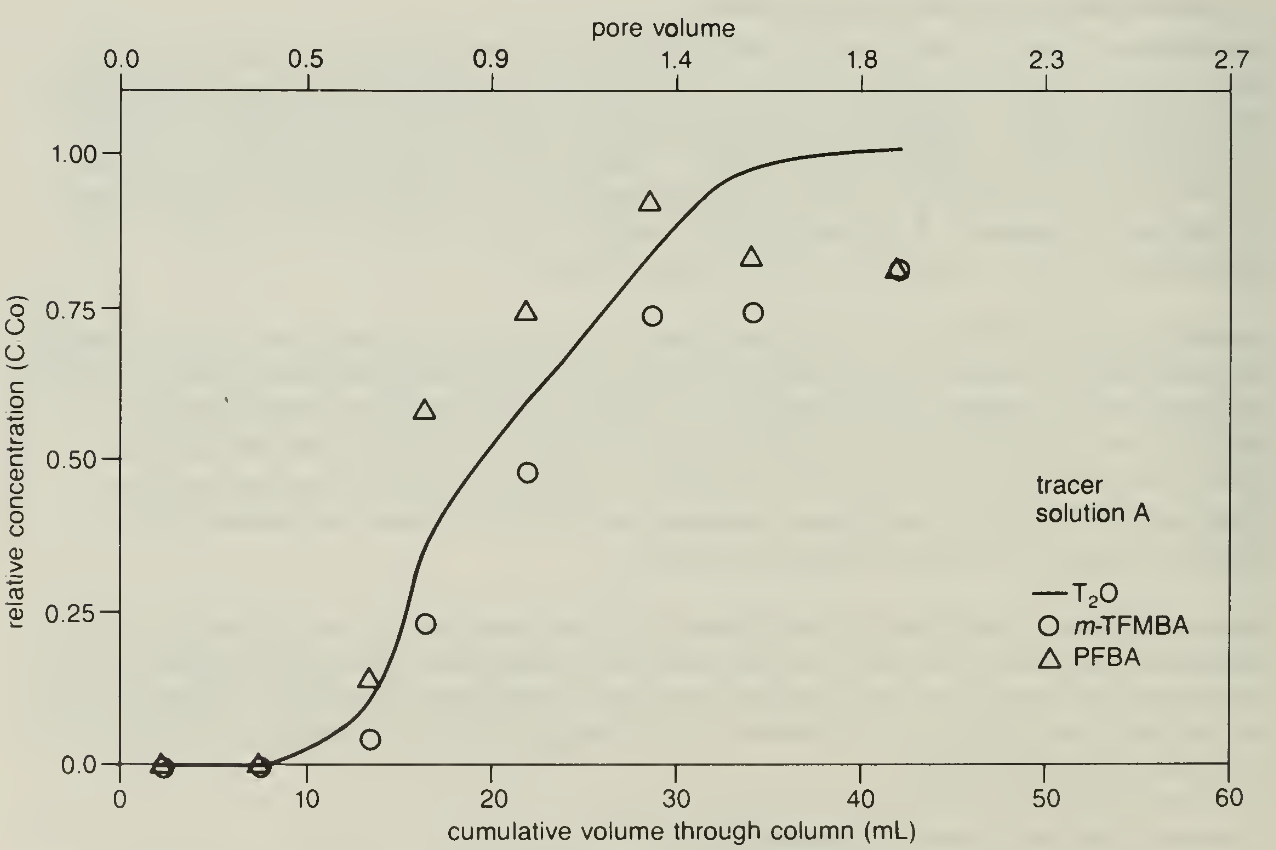

Figure 51 Movement of tritiated water, *m*-TFMBA, and PFBA through a second nonsterile soil column. The tracer solution also contained *o*-TFMBA and Br.

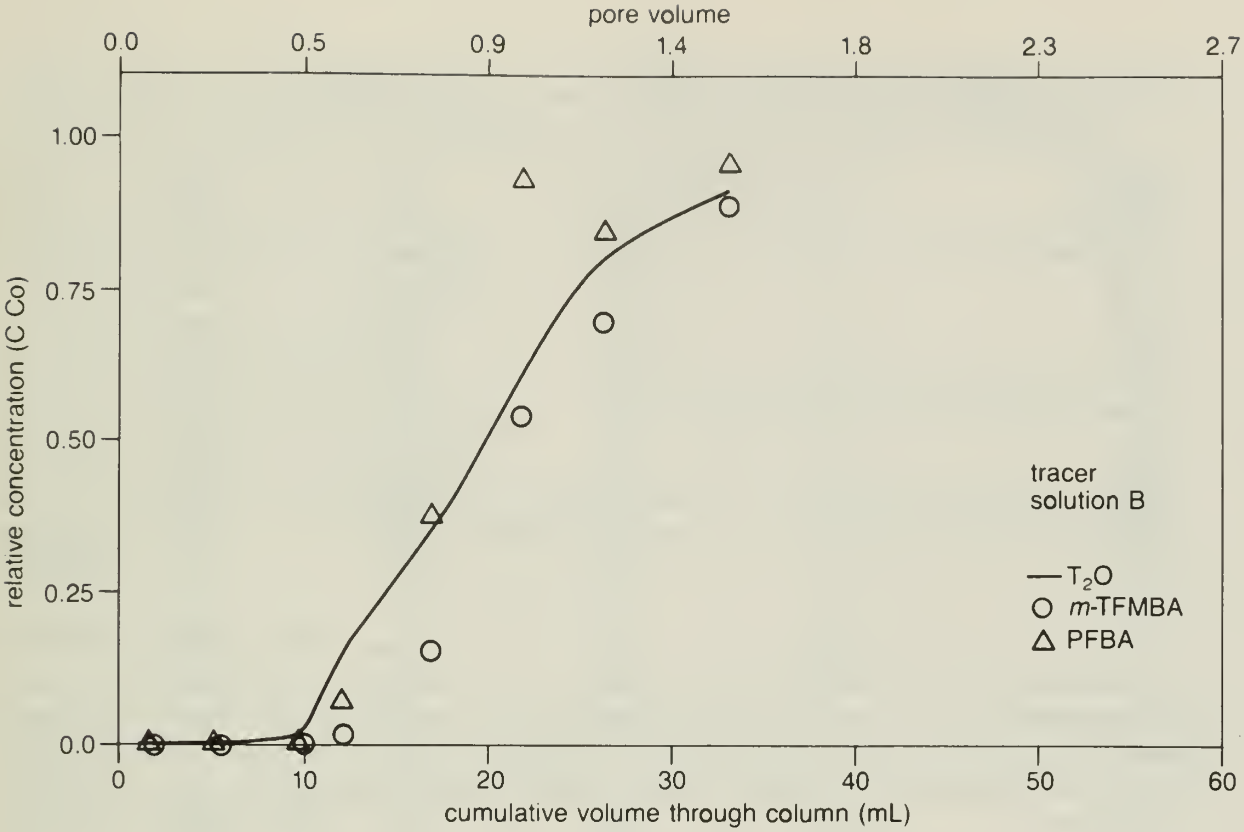

Figure 52 Movement of tritiated water, *m*-TFMBA, and PFBA through a nonsterile soil column. The tracer solution also contained *o*-TFMBA and Br.

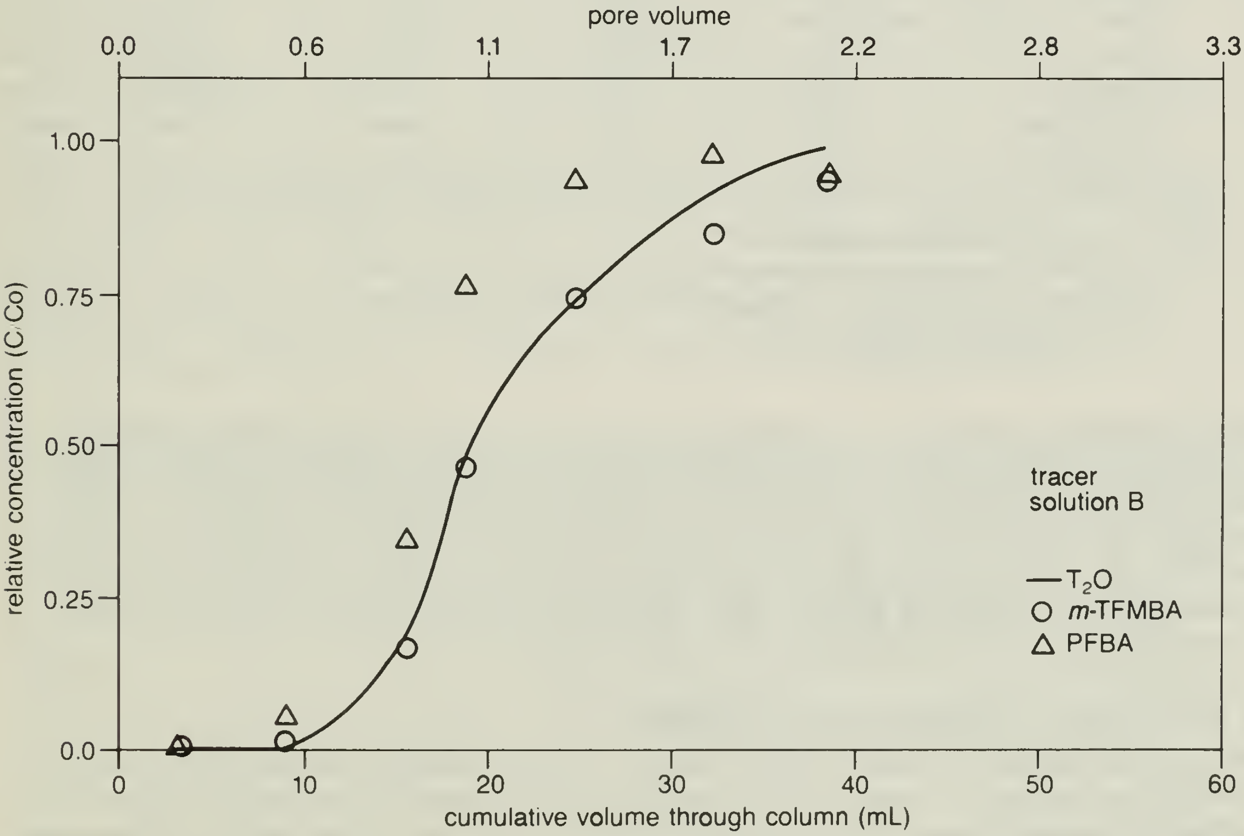

Figure 53 Movement of tritiated water, *m*-TFMBA, and PFBA through a sterile soil column. The tracer solution also contained *o*-TFMBA.

Table 26 Quality assurance data for the HPLC tracer analytical method.

Date analyzed	Concentration (mg/L)			
	m-TFMBA	*o*-TFMBA	Br	PFBA
Actual conc.	5.35	5.05	5.08	5.00
3/2/87	5.17	5.22	5.22	N/A
3/2/87	5.18	5.28	5.24	N/A
3/2/87	5.31	5.47	5.28	N/A
3/3/87	5.11	5.26	5.05	N/A
3/3/87	5.28	5.45	5.27	N/A
3/5/87	5.49	5.14	5.04	4.47
3/9/87	5.30	4.99	4.89	4.34
3/9/87	5.46	5.20	5.09	4.50
3/13/87	5.70	5.48	5.48	5.37
3/13/87	5.43	5.17	5.26	5.22
X	5.34	5.27	5.18	4.78
S	0.179	0.160	0.166	0.477
CV (%)	3.35	3.03	3.21	9.98
% accuracy	0.19	3.03	1.97	4.40
n	10	10	10	5
Actual conc.	21.4	20.2	20.3	20.0
3/13/87	22.2	21.6	21.7	21.0
3/13/87	21.7	20.7	21.0	20.2
3/13/87	22.0	21.3	21.4	20.9
3/13/87	20.7	19.5	19.8	19.2
3/13/87	21.7	20.5	20.8	20.2
X	21.6	20.7	20.9	20.3
S	0.578	0.798	0.724	0.730
CV (%)	2.68	3.85	3.46	3.60
% accuracy	0.93	2.47	2.96	1.50
n	5	5	5	5

X = mean
S = standard deviation
CV = coefficient of variation (S/X) × 100
% accuracy = ((Actual conc. − Analyzed conc.)/Actual conc.) × 100
n = number of samples
N/A = not analyzed

been changed by microbial activity during the course of the experiments. Tracers apparently had not been adsorbed or degraded in either column, thus we assume that no microbial alteration had occurred during residence in the soil. Repeating these studies a number of times would be necessary to detect any minor differences in water flow and transit time and conservation of the tracers. The possible introduction of organic material into the soil under field conditions could conceivably produce other results. If microbial growth were stimulated, soil pores could become blocked by cells and/or exocellular gums.

■ Isolation of Fluorobenzoic Acid Degraders

Isolation of a bacterium capable of using any one of the fluorobenzoic acid derivatives as a growth substrate was unsuccessful. As indicated by growth on solid media with fluorobenzoic acid derivatives omitted, all potential isolates grew at the expense of trace organic compounds present in the Noble agar used to solidify the media, rather than on the tracers. This does not mean that biodegradation of these compounds is impossible, however, one would not expect it to be rapid. Conservation of the tracers in the column studies supports this conclusion.

Failure to detect $^{14}CO_2$ evolution from radio-labeled fluorobenzoic acid derivatives incubated in soil or sludge cultures would prove biostability. Because cometabolism by microbial consortia is often the route by which these compounds are eventually used by soil microorganisms, isolation of a pure culture might be impossible. Radio-labeled compounds were not used in these studies because the cost of custom synthesis is extremely high and difficult to justify, particularly when both the column studies and the efforts to isolate degraders suggested that biological alteration of these compounds did not occur or was negligible.

Table 27 Summary of tracer concentrations in lysimeter samples 8 months after liner ponding; 48 samples were analyzed.

Concentration (mg/L)	Percent of samples
<0.1	46
0.1–0.5	38
0.5–1.0	10
>1.0	6

At a concentration of 0.5 mg/L, C/C_0 is less than 1 percent.

■ Quality Control Data

Quality control data illustrating the HPLC analytical procedures precision and accuracy are presented in table 26. The data represent standards analyzed over a 5-day period. This period corresponds to the time in which the samples from the ss ratio and kinetic experiments were analyzed. In general the precision and accuracy of the method is ±4 percent for *m*-TFMBA, *o*-TFMBA, Br, and PFBA.

■ Field-Scale Liner Study

The four tracers evaluated in the laboratory studies are being used to monitor water movement in the field-scale liner. Bromide, PFBA, *m*-TFMBA, and *o*-TFMBA were placed in large-ring infiltrometers 1, 2, 3, and 4, respectively (see chapter 5 for infiltrometer locations). Initial concentrations (C_o) were 90.3, 61.2, 72.4, and 73.8 mg/L for *m*-TFMBA, PFBA, Br, and *o*-TFMBA, respectively. Soil-water samples are collected quarterly from the suction lysimeters located around the infiltrometers. Analysis of these samples for the tracers by HPLC has proved difficult because of chemical interferences in the samples. We assumed that a tracer was detected in the sample if a chromatographic peak had a retention time within ±0.3 minute of a standard. Without additional methods to identify these peaks, absolute confirmation is not possible at these low concentration levels. We anticipate that when tracer concentrations in the soil water samples exceed 2 mg/L (determined on the basis of the magnitude of the interferences), interferences will be minimized, and quantification and identification of the tracers will be more reliable.

Evaluation of tracer movement in the liner was based on soil-water samples collected from the lysimeters 8 months after the liner pond was filled. Although 60 lysimeters are being used in the liner study, no water was collected in 12 of them. Data on all the tracers from the 48 samples available were grouped for analysis. Table 27 presents a summary of the results of the tracer analysis; the samples are grouped according to apparent concentration range. Eighty-four percent of the samples contained tracers at apparent concentrations of less than 0.5 mg/L, resulting in C/C_o values of less than 1 percent. Generally, interpretation of tracer behavior is based upon results when C/C_o is approximately 50 percent (C/C_o = 0.5). Because of these low concentrations, determining the effects of dispersion, diffusion, and retardation on tracer movement in the liner is currently not possible. The low concentration of tracer (<1.5 mg/L) in these samples suggests that the lysimeters have not detected or intersected preferential flow paths or that lateral flow paths from the infiltrometers do not exist. No liner effluent water has been collected in the underdrain system, so tracers have not been detected at the bottom of the liner. Analysis of these data with respect to sampling depth also indicated no trends. Data on the movement of tracers are inconclusive because of analytical interferences and very low concentrations of tracers.

■ Solute Modeling

Preliminary solute modeling was performed to ascertain if the negative results (no detection of tracer after 8 months of ponding) of the tracer analysis could be predicted and/or anticipated. A one-dimensional steady-state flow model (Ogata and Banks 1961) was used to predict the potential movement of the tracers through a saturated soil with a hydraulic conductivity similar to that of the liner. This scenario represents tracer movement through the soil directly beneath the large-ring infiltrometers after liner saturation. Again assuming saturation of the liner, we used a two-dimensional model, PLUME, to predict the movement of the tracers laterally in the liner.

The one-dimensional model solves the generalized differential equation that describes the change in solute concentration as a function of time at steady-state conditions in a saturated homogeneous material (Freeze and Cherry 1979, Bear 1972). The analytical solution for the change in solute concentration is given by

$$\frac{C}{C_o}(x,t) = \frac{1}{2}\left[\operatorname{erfc}\left(\frac{x-t^*}{2\sqrt{D_x t^*}}\right) + \exp\left(\frac{Vx}{D_x}\right)\operatorname{erfc}\left(\frac{x+Vt^*}{2\sqrt{D_x t^*}}\right)\right] \qquad [12]$$

where $C/C_o(x,t)$ = the ratio of the solute concentration C at time t and distance x to the initial solute concentration C_o

erfc = the complementary error function

V = the mean water velocity (cm/sec); $V = K_{sat} i/\eta_e$ where K_{sat} is the saturated hydraulic conductivity, η_e is the porosity, and i is the hydraulic gradient

D_x = the dispersion coefficient (cm^2/sec) along flow path x; $D_x = \alpha V + D^*$ where α is the dispersivity (cm) and D^* is the diffusion coefficient in water (cm^2/sec)

t^* = the retarded time t/R (actual time divided by the retardation factor)

x = the distance of migration (cm).

The following parameters were used for the model: $K_{sat} = 4 \times 10^{-8}$ cm/sec; i = 1.7; $n_e = 0.3$; $K_d = 0$, which leads to R=1 and t=t*; x = 91 cm (thickness of the liner); C_o = 90.3, 61.2, 72.4, and 73.8 mg/L for *m*-TFMBA, PFBA, Br, and *o*-TFMBA, respectively; $D^* = 7.4 \times 10^{-6}$, 7.2×10^{-6}, 7.4×10^{-6}, and 18.7×10^{-6} cm^2/sec *m*-TFMBA, PFBA, *o*-TFMBA and Br, respectively.

The model predicted the concentration of each tracer at the bottom of the saturated soil at five time periods (fig. 54). These results suggest that tracers will not reach concentrations above analytical detection at the bottom of the soil for a minimum of 2 years, and that concentrations will not reach a C/C_o = 0.5 level for approximately 10 years. A concentration profile was constructed from the model output showing the anticipated concentration of the tracers at various depths in the saturated soil (fig. 55). Because this is a one-dimensional model, these concentrations are for soil water directly below the tracer source (large-ring infiltrometers). Regardless of the tracer, the model predicts that 1 year after ponding, concentrations at approximately the 50 cm depth would be significantly above the analytical detection limit (>3 mg/L), so detection should be relatively easy. Results of the analyses of soil water collected

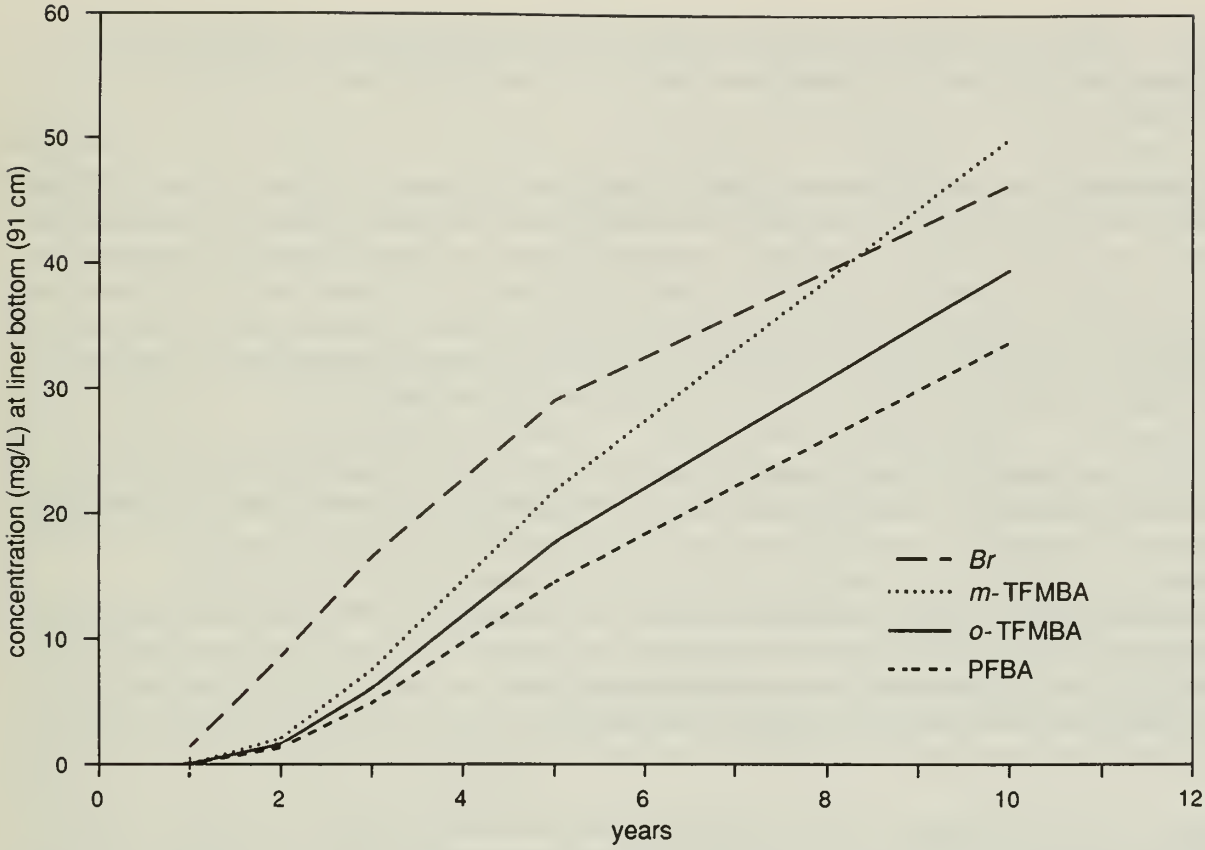

Figure 54 Estimated concentration (mg/L) of the tracers at the bottom of a saturated soil column at various times after introduction of tracers.

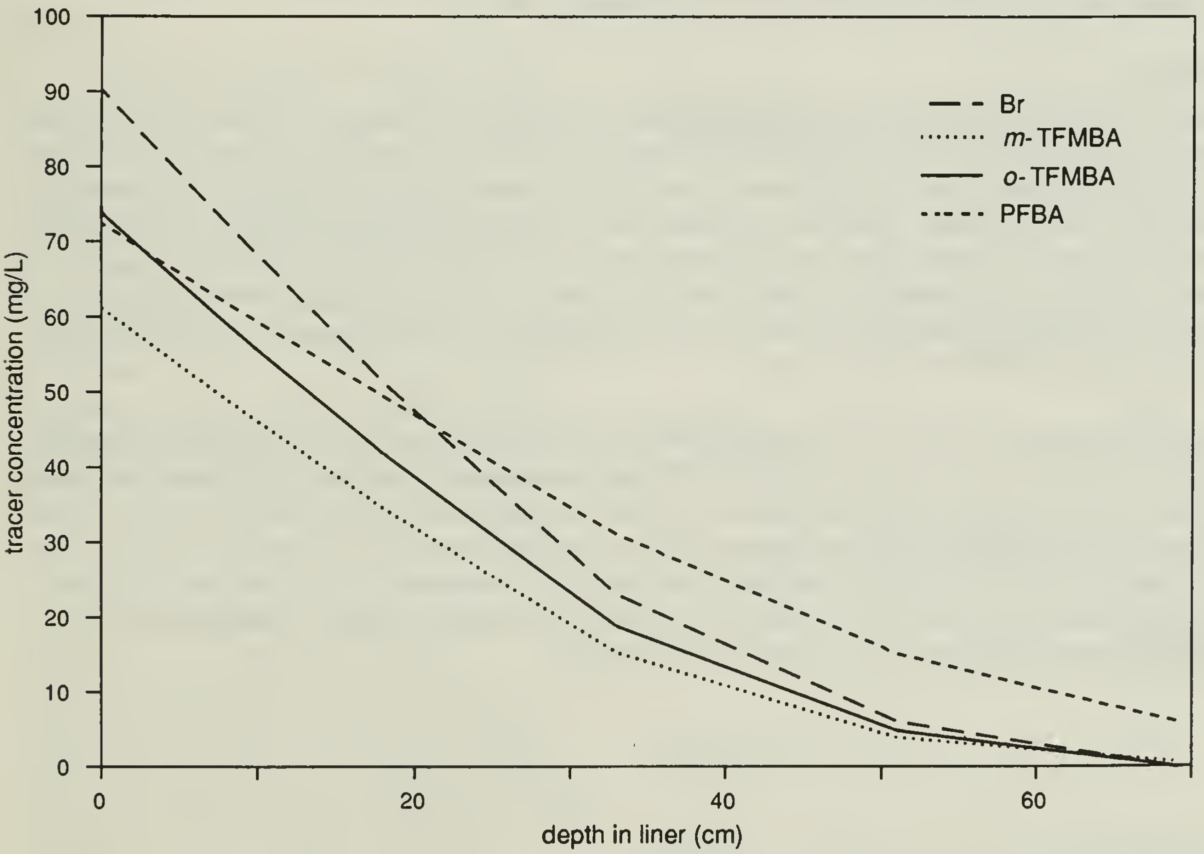

Figure 55 Estimated concentrations (mg/L) of the tracers at various depths within a saturated soil column 1 year after introduction of the tracers.

from the lysimeters indicate that lateral movement of the tracers has been minimal, since measured concentrations are a minimum of one order of magnitude less than model predictions.

A two-dimensional model that uses a solution to the general transport equation similar to that of the one-dimensional model, was used to estimate the lateral movement of the tracers (Bumb et al. 1984). The model solution is the basis of the two-dimensional solute transport computer program PLUME (version 2.0, Insitu, Inc., Laramie, Wyoming). The model assumed a saturated isotropic soil in which hydraulic conductivity in the y and z directions was equal. The dispersion coefficient in the y direction was assumed to be 15 percent of that in the z direction, and the dispersivity was assumed to be 10 percent of the liner thickness (91 cm).

This model was used to estimate lateral movement of the tracers, assuming that the top centimeters (wetting front estimates are between 18 and 40 cm) of the liner are saturated, even though the soil liner was not initially saturated. This estimation was made because the lysimeters are offset from the large-ring infiltrometers (the sources of the tracers) by approximately 18 cm, so that the tracers have to move laterally from the tracer source to the sampling location. PLUME simulations suggested that lateral movement of tracers after 1 year would not be sufficient to reach the suction lysimeters, and even after 10 years the tracers would have a marginal chance of migrating laterally to the suction lysimeters. These results agree with the observed results to date.

The goal of the tracer portion of this study was to monitor water movement through the liner. If the modeling predictions are correct, water movement will be difficult to assess by the use of this experimental design and tracers. To provide more definitive data on water movement through the liner, we added a new tracer, tritiated water, to the liner pond in July 1989. At this time, there are no results on tritium movement through the liner.

Summary

Laboratory batch adsorption results indicate that the tracers (*o*-TFMBA, *m*-TFMBA, PFBA, and Br) are conservative; they do not sorb to the Batestown till, nor do they appear to degrade with time. Microbial activity during the course of the column studies did not alter the flow rates of water through the columns. However, problems with analytical detection using HPLC make the viability of using these tracers to monitor water flow in liner systems questionable. All four tracers appeared to be reasonably well conserved during passage through the soil columns; however, coefficients of correlation with water flow could only be calculated for *m*-TFMBA and PFBA because of analytical difficulties.

Soil-water samples collected from the lysimeters in the field-scale liner 8 months after ponding indicate that the tracers have not migrated vertically or laterally in sufficient concentrations to be detected. One- and two-dimensional solute models confirm the observed results that the tracers should not be detectable in the soil-water samples. The tracer results do suggest that preferential, lateral flow paths in the liner either were not intersected by the sampling devices or were eliminated during liner construction. The addition of tritium to the liner pond may give more information as to the flow regime through the liner.

9 ONE-DIMENSIONAL NUMERICAL MODELING OF THE FIELD-SCALE LINER

Two models, SOILINER and CHEMFLO, were used to estimate the time required for water and tracers to break through the field-scale soil liner. The models also were used to estimate saturated hydraulic conductivity of the liner by determining the conductivity value required for input into the model to produce a flux value equal to that measured in the liner. The accuracy of these models to predict transit times through soil liners was evaluated by comparing model predictions to field measurements.

The numerical codes of both models use the Richards equation to predict one-dimensional flow and transport of a nonreactive tracer through unsaturated soils. Input requirements for both models include (1) a mathematical approximation of a soil moisture characteristic curve, (2) a mathematical relationship between hydraulic conductivity and moisture content, (3) values for saturated hydraulic conductivity and moisture content (4) upper and lower boundary conditions, and (5) initial moisture conditions. In addition, CHEMFLO allows input of chemical transport parameters such as dispersivity and diffusion.

SOILINER can simulate flow and transport in a layered soil system; however, this code does not incorporate adsorption, degradation, dispersion, or diffusion into its particle-tracking algorithm. Instead, it tracks the movement of a particle of contaminant through the system by advection only. In essence, it tracks the point where the relative concentration (C/C_o) of a nonadsorbed, nondegraded, nondiffused contaminant is 0.50. A complete description of the model is given in Johnson et al. (1986).

CHEMFLO (Nofziger et al. 1989) simulates flow and transport for one soil layer. The effects of dispersion, diffusion, and degradation on transport may be used with this model. CHEMFLO computes the concentration profile of the contaminant in the soil at regular intervals.

Methods

■ Conceptual Model and Model Setup

The conceptual model used in SOILINER is shown in figure 56. The top layer, consisting of 80 variably spaced nodes, represents 91 cm of compacted soil. A middle layer of 12 nodes represents drainage gravel. The thickness of the drainage layer was varied from 1 to 20 cm. The lower layer of four nodes represents the undisturbed natural soil under the liner system. The assumption was that saturated conditions occur at depth within this lower soil, which was modeled at thicknesses of 1 to 200 cm.

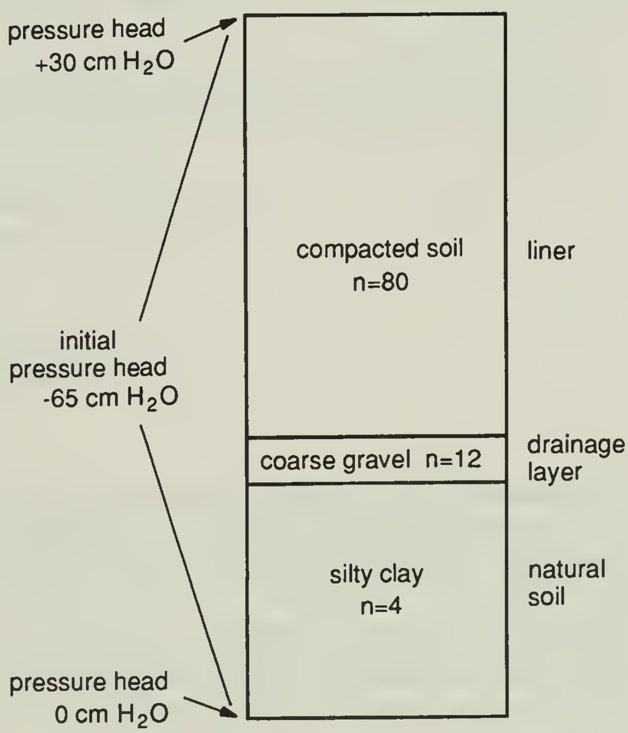

Figure 56 Conceptual model of a one-dimensional liner system. The number of SOILINER nodes to represent each soil is denoted by n.

The gravel layer in the field-scale liner was underlain by a geomembrane. The preferred method to model this feature would be as a no-flow boundary; however, this type of boundary could not be used with SOILINER. Therefore, a constant head boundary within a lower soil layer was used. The primary purpose of this lower layer was to maintain unsaturated conditions in the gravel layer without setting a constant head zone in the gravel layer. Preliminary modeling showed that a constant head boundary in the gravel affected the change in tension values in the upper (liner) model layer; however, placing the constant head boundary in the lower layer did not significantly affect tension changes in the liner layer. Because the primary purpose of the modeling was to study the change of tension values in the upper (liner) layer caused by a stress change (filling the pond) at the upper boundary, we decided to model the liner with a constant head boundary in the underlying soil.

The conceptual model for CHEMFLO consisted of 91 cm of liner material. Node spacing for this model was 1 cm. Because this code is not designed for use with layered material systems, the gravel and underlying layer modeled with SOILINER were not needed.

▪ Moisture Characteristic Curves

The equations used to relate soil moisture to tension were determined, using laboratory data, from soil cores collected from the prototype liner (fig. 18). SOILINER uses equation [13] as described by Clapp and Hornberger (1978) to relate soil moisture to tension. CHEMFLO allows a choice from several soil moisture-tension equations contained in the code. The experimental data were best simulated by equation [14] (van Genuchten 1980), and thus this equation was incorporated into CHEMFLO simulations.

$$\begin{aligned} \psi &= \psi_s W^{-b} \qquad (0 \le W \le W_i) \\ \psi &= -m(W - n)(W - 1) \qquad (W_i \le W \le 1) \end{aligned} \qquad [13]$$

where

ψ = soil tension

W = water content (θ/θ_s)

W_i = critical W

$$n = 2W_i - \left(\frac{\psi_i b}{mW_i}\right)^{-1}$$

$$m = \left(\frac{\psi_i}{(1 - W_i)^2}\right)\left(\frac{\psi_i b}{W_i(1 - W_i)}\right)$$

where ψ_i, W_i describe the inflection point on the moisture characteristic curve

$$\begin{aligned} \theta &= \theta_r + \frac{\theta_s - \theta_r}{(1 + \alpha\psi^n)^m} \qquad \psi < 0 \\ \theta &= \theta_s \qquad \psi > 0 \end{aligned} \qquad [14]$$

Parameters in the Clapp and Hornberger equation [13] were varied, and four soil-moisture characteristic equations were used with SOILINER. Two equations represented the liner soil: one the drainage layer, and one the soil underlying the drainage layer.

Figure 57 shows the characteristic curves calculated by SOILINER for the liner material. The equation for the moisture characteristic curve of soil A was derived according to the method outlined in the SOILINER documentation. The equation for soil B was empirically derived from laboratory data to achieve a best fit when soil tension was less than 816 cm of water. The characteristic curve computed for soil A fit the complete set of laboratory data better than the curve computed for soil B; however, soil B better represented the laboratory data when tensions were less than 816 cm of water. Observed tensions in the liner have been below 816

Table 28 Data input to generate soil-moisture characteristic curves for soils A, B, and C in SOILINER. Soil moisture equations modified from Clapp and Hornberger (1978), hydraulic conductivity equation from Campbell (1974). Equations are listed in SOILINER documentation (Johnson et al. 1986).

Soil	b	W_i	ψ_i	ψ_s
A	7.97	0.84	−816.00	−42.1
B	10.4	0.84	−816.00	−130.
C	10.4	0.92	−116.63	−49.0

Table 29 Data input to generate soil-moisture characteristic curve for the drainage layer in SOILINER. Soil moisture characteristic equation is from King (1965), hydraulic conductivity relationship from Mualem (1978), and input data from Johnson et al. (1983).

Soil	θ_r	n	P_o	β	ϵ	σ
Gravel 1b	0.017	3.03	5.436	−4.44	0.749	1.189

Table 30 Data input to generate soil-moisture characteristic curves for CHEMFLO. Soil characteristic equation is from van Genuchten (1980), hydraulic conductivity relationship is equation 5 from Nofziger (1985). CHEMFLO soil CF approximates SOILINER soil B. K_α and K_n describe coefficients used to compute a hydraulic conductivity/moisture curve.

Soil	θ_r	n	m	α	K_α	K_n
CF	0.20	1.42	0.30	0.0106	1.00×10^{-4}	18.934

cm of water, so the soil characteristic curve for soil B was considered a better representation than soil A of in situ conditions in the liner. Table 28 lists the values input to the Clapp and Hornberger equation for soils A and B, as well as for soil C, which represents the material underlying the drainage layer. Soil C was described by Johnson et al. (1986) as a silty clay.

The equation for the soil characteristic curve of the drainage gravel used for SOILINER was reported in Cartwright et al. (1988). They used equation [15] from King (1965) to calculate a soil-moisture characteristic curve for coarse gravel (table 29). Figure 58 shows the computed soil characteristic curves for the drainage layer and for soil C.

$$\theta = \theta_s \left[\frac{\cosh\left(\left(\frac{\psi}{P_0}\right)^{\beta} + \epsilon\right) - \sigma}{\cosh\left(\left(\frac{\psi}{P_0}\right)^{\beta} + \epsilon\right) + \sigma} \right] \qquad [15]$$

The set of equations available in CHEMFLO did not include the Clapp and Hornberger equation [13]. Therefore, we used the equation [14] from van Genuchten (1980) because it resulted in characteristic curves similar to the curves computed with the Clapp and Hornberger equation (fig. 59). Figure 59 presents the soil-moisture characteristic curves calculated by SOILINER (soil B) and by CHEMFLO (soil CF), as compared to the laboratory-measured water content, for the tension range between 0 and 1000 cm water. Table 30 lists the input data used with the van Genuchten equation to determine the soil moisture curve for soil CF.

■ Relationship of Hydraulic Conductivity to Soil Moisture

Hydraulic conductivity is a function of soil moisture content, which is a function of tension. Therefore, an equation to relate hydraulic conductivity to soil moisture content was necessary to

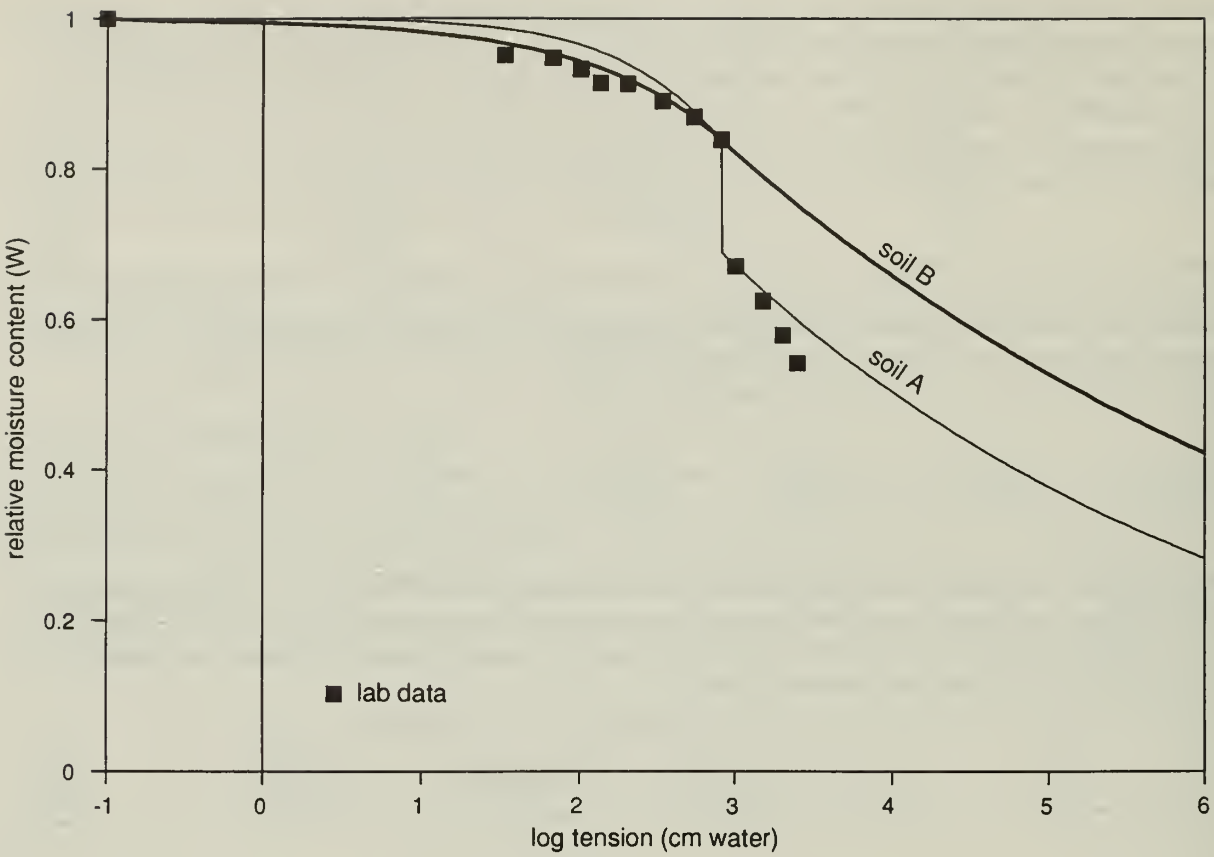

Figure 57 Soil-moisture characteristic curves for SOILINER soils A and B, and prototype liner data.

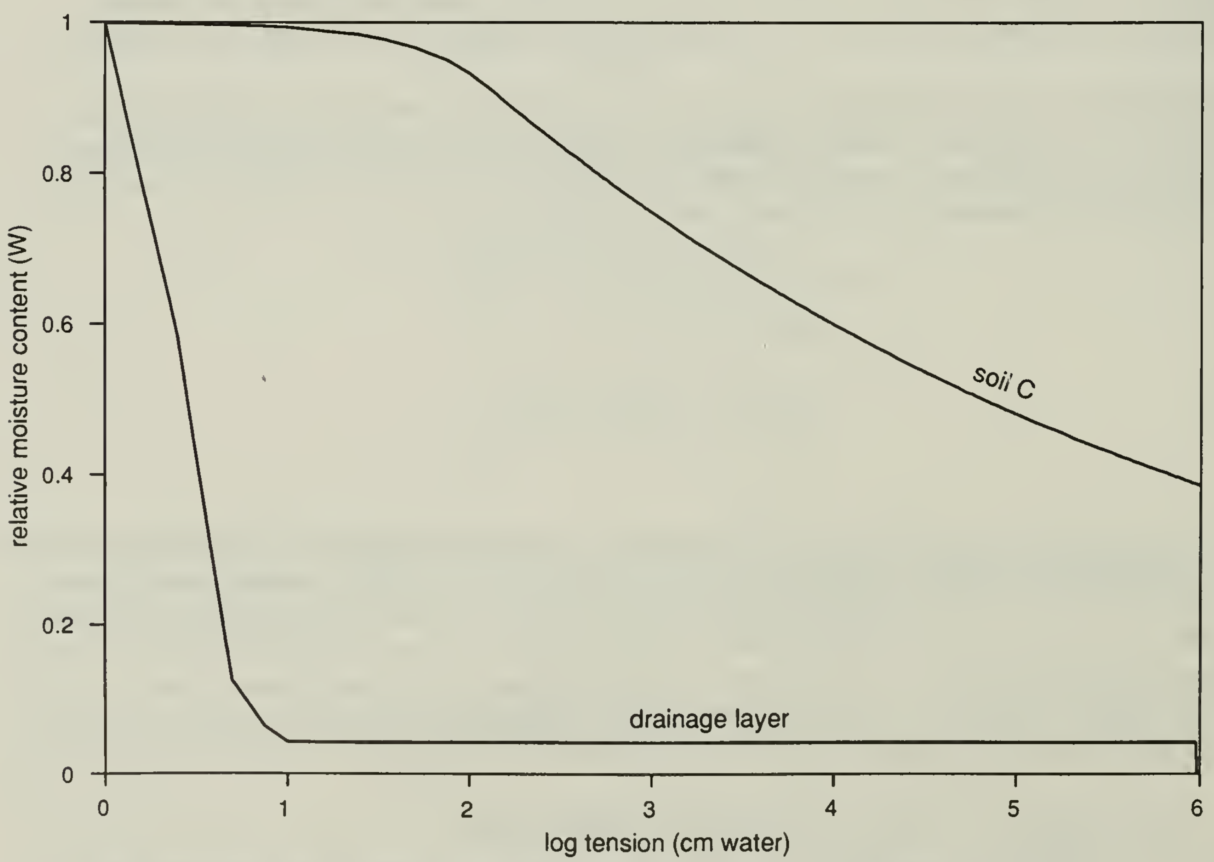

Figure 58 Soil-moisture characteristic curves for SOILINER soil C and the drainage layer.

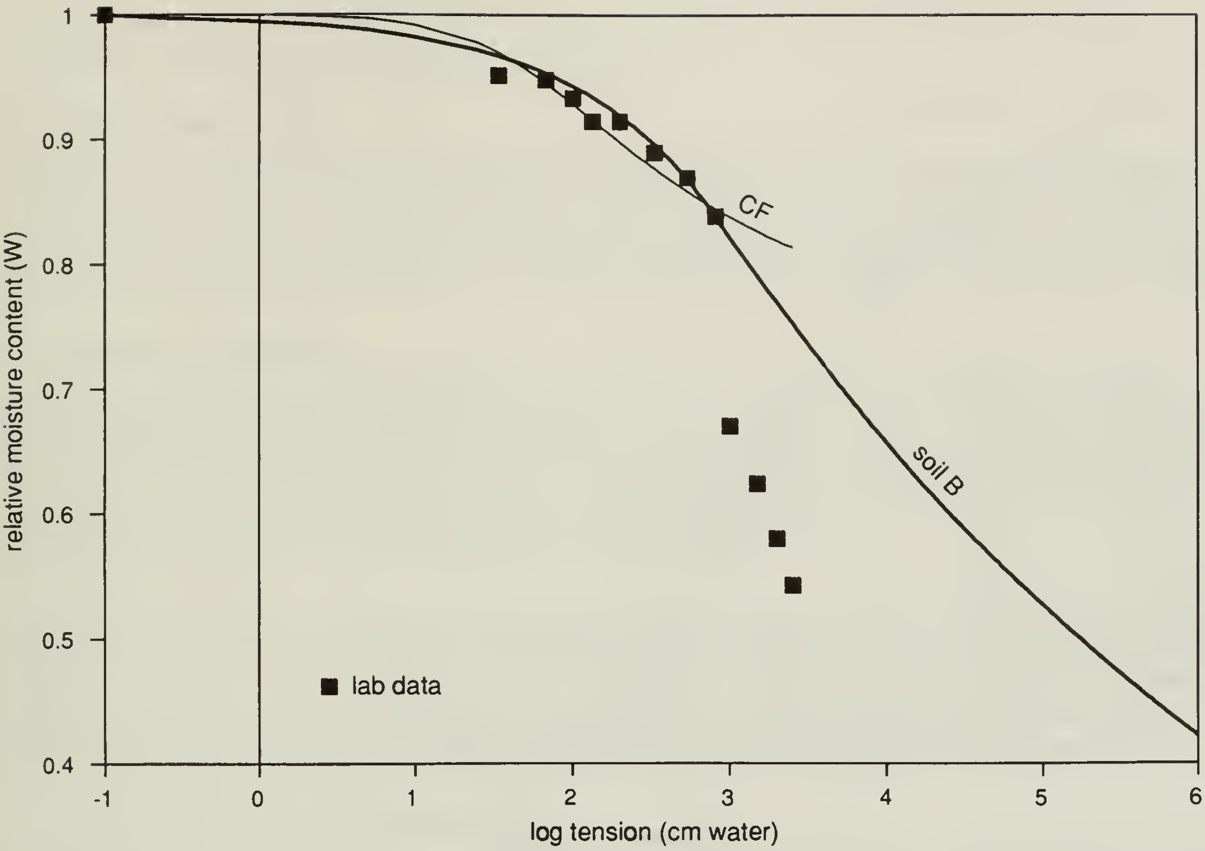

Figure 59 Soil-moisture characteristic curves for SOILINER soil B and CHEMFLO soil CF.

model water movement through the liner. This relationship was developed for SOILINER soils A, B, and C using equation [16] by Campbell (1974). Hydraulic conductivity/tension relationships for the underdrain gravel were derived by equation [17], as given in Mualem (1978). CHEMFLO utilized equation [18] by Nofziger (1985) to compute the hydraulic conductivity/tension relationship for soil CF. Input parameters for the hydraulic conductivity functions are listed in tables 28 to 30. The relationship of hydraulic conductivity to tension, derived from these equations, is shown in figures 60 and 61.

$$K = K_s W^{(2b+3)} \qquad [16]$$

$$K = K_s \left(\frac{\theta - \theta_r}{\theta_s - \theta_r} \right)^n \qquad [17]$$

$$K = \alpha \theta^n \qquad [18]$$

■ Saturated Hydraulic Conductivity and Soil Moisture Content

Values for saturated hydraulic conductivities and moisture content were based on experimental data. The saturated hydraulic conductivity value of 4×10^{-8} cm/s used for the liner material was similar to the conductivity values calculated from all the small-ring infiltration fluxes and the gradient data available at the time the modeling was performed. A saturated moisture content (porosity) value of 0.25 was based on laboratory tests on material extracted from the prototype liner. This moisture content value was lower than the values estimated for the field-scale liner (0.33), but it was used in the model because it had been incorporated into equations used for

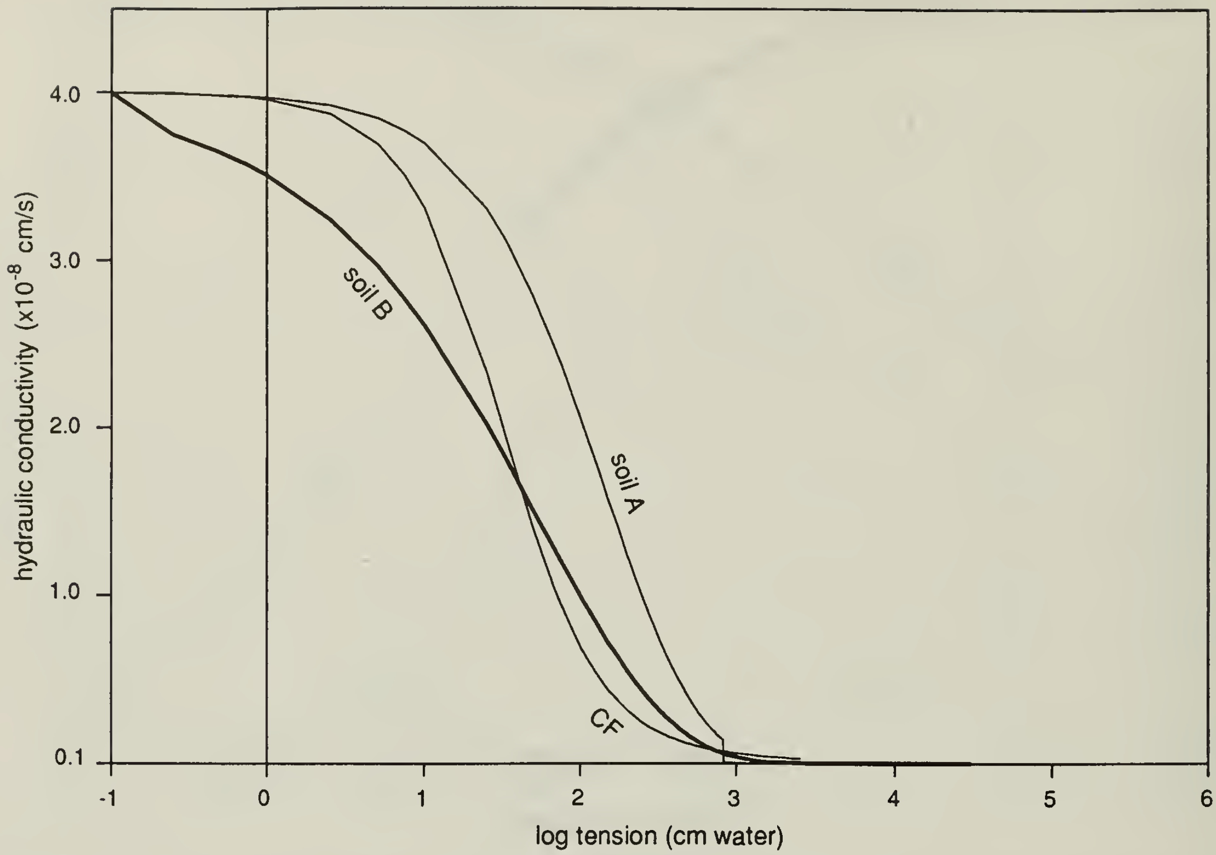

Figure 60 Hydraulic conductivity curves for SOILINER soils A and B, and CHEMFLO soil CF.

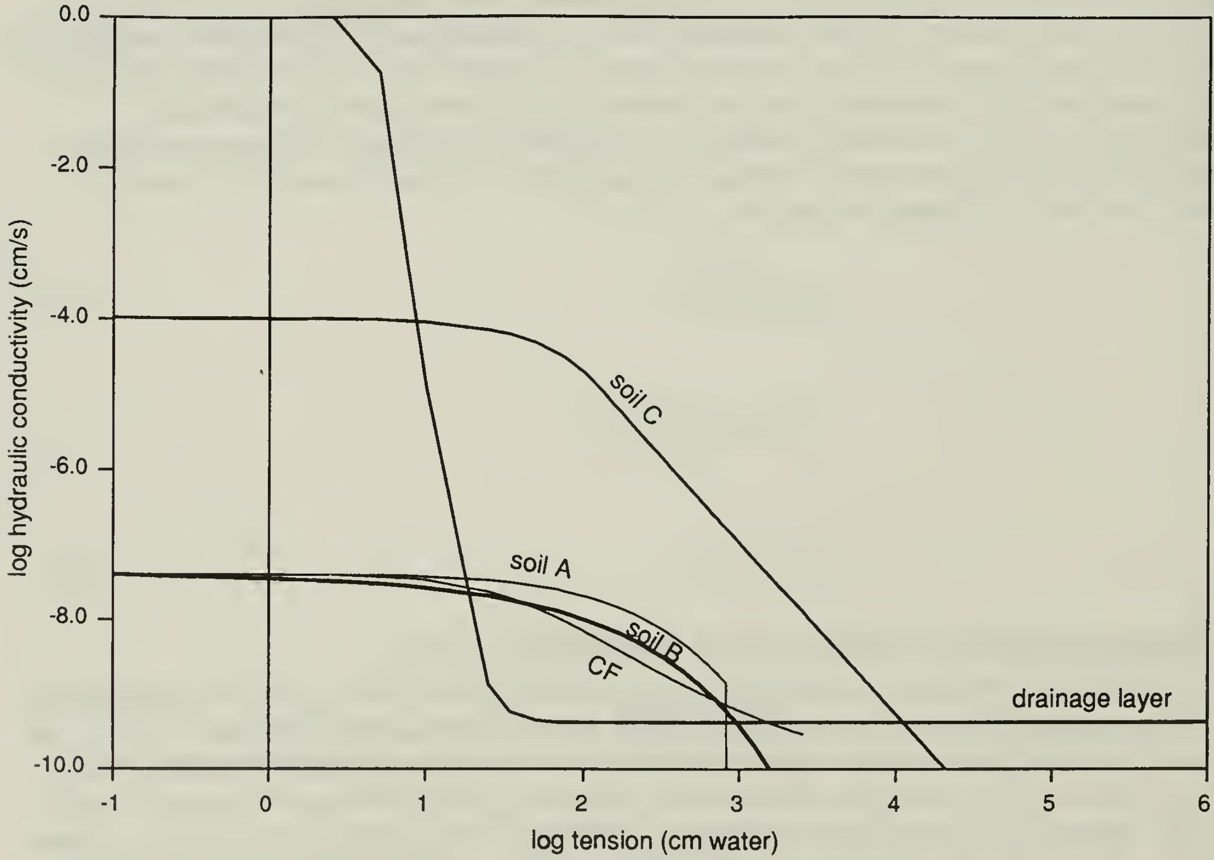

Figure 61 Hydraulic conductivity curves for all soils modeled.

constructing the moisture characteristic curves. However, a range of values for these parameters was used for the sensitivity analysis.

■ Initial Pressure Head

The value for initial pressure head in the liner was taken from the average tension recorded April 9, 1988, 3 days before the liner was ponded. Average tension on that day for 240 reporting points was 64.7 cm, with a standard deviation of 47.8. The maximum value recorded was 287 cm; the minimum was 4.4 cm. Initial pressure head input to the models was –65 cm.

■ Boundary Conditions

The upper boundary condition used in SOILINER to simulate the liner experiment was a constant pressure head of 30 cm. This boundary represents the water in the pond overlying the liner. The lower boundary condition for the model was a constant pressure head of 0.0 cm, simulating the water table in the soil beneath the drainage layer. Sensitivity analysis showed that the lower boundary had little effect on SOILINER results.

The upper boundary condition used in CHEMFLO was also a constant pressure head of 30 cm. The lower boundary was assigned a mixed boundary condition: the flux was 0.0 cm/s until a pressure head of –15 cm was calculated, after which the boundary was converted to a constant pressure head of –15 cm. This procedure allowed flow results comparable to those from SOILINER, which computed a steady state head of –15 cm at the base of the liner soil.

■ Contaminant Transport Parameters

SOILINER tracks the advective movement of a particle through the flow system and does not account for any transport parameters other than those used to compute water movement. CHEMFLO allows the use of both dispersivity and diffusion; little information existed for either of these parameters. Maximum dispersivity was estimated by CHEMFLO, assuming that dispersivity is one-tenth the migration distance. In the liner experiment, maximum migration distance is 91 cm, so the maximum dispersivity value used in the model was 9.0 cm. Diffusion coefficients were taken from Freeze and Cherry (1979), who state that typical diffusion coefficients for clayey geologic deposits range from 10^{-10} to 10^{-11} m^2/s. Specific diffusion coefficients used for this model were 3.6×10^{-3} and 3.6×10^{-4} cm^2/hr.

Model Output

Table 31 provides the model parameter values used in each computer simulation. Figure 62 shows the pressure-head distribution computed by SOILINER for simulation B_3 at times of 0.0, 0.2, and 0.48 years. The system reached steady state at 0.48 years. (Steady state is defined as the flux of water entering the liner equal to the flux exiting the bottom.) In this run, as in all other runs, the base of the liner did not become saturated. Cartwright et al. (1988) obtained similar results when modeling a fine-grained material over a coarse-grained drainage layer. Additional output obtained from SOILINER included the time when steady-state flow was achieved, the depth of the wetting front at steady state, the time when particle breakthrough occurred, and the flux at steady state. Output obtained from CHEMFLO included the time when steady-state flow was achieved, the depth of the wetting front at steady state, breakthrough times for C/C_o = .001 and 0.5, and the steady-state flux. These results are discussed separately in the following sections.

Discussion

■ Sensitivity Analysis

Because of the uncertainty with regard to the values assigned to the input parameters of the models, we performed a sensitivity analysis in which one parameter was varied while all others

Table 31 Results of the SOILINER sensitivity analysis. For each set of data, one parameter was varied while the others were held constant. Run B3 was considered the control simulation.

Run	Liner soil	K_s (cm/s)	θ_s	K_s/θ_s	Thickness (cm)	Initial head (cm)	Boundary conditions (head) upper (cm)	Boundary conditions (head) lower (cm)	Steady-state time (yrs)	Wetting front depth (cm)	Break through time (yrs)	Flux (cm/s)
A Saturated hydraulic conductivity of the liner soil (Soil B), varied from 1×10^{-6} to 1×10^{-9} cm/s.												
B9		1×10^{-6}				−65	30	0	0.026	76	0.5	1.4×10^{-6}
B6		1×10^{-7}				−65	30	0	0.18	73	5.0	1.4×10^{-7}
B3		4×10^{-8}				−65	30	0	0.48	73	12.6	5.6×10^{-8}
B10		2×10^{-8}				−65	30	0	0.95	73	25.1	2.8×10^{-8}
B7		1×10^{-8}				−65	30	0	1.82	73	50.2	1.4×10^{-8}
B11		5×10^{-9}				−65	30	0	3.9	73	100.0	7.1×10^{-9}
B8		1×10^{-9}				−65	30	0	17.8	72	501	1.4×10^{-9}
B Saturated moisture content of the liner soil (Soil B), varied from 0.15 to 0.30.												
B13			0.30			−65	30	0	0.56	73	15.1	5.6×10^{-8}
B3			0.25			−65	30	0	0.48	73	12.6	5.6×10^{-8}
B12			0.20			−65	30	0	0.39	73	10.0	5.6×10^{-8}
B14			0.15			−65	30	0	0.30	73	7.5	5.6×10^{-8}
C Initial pressure in all three soils, varied from −30 to −200 cm.												
B17						−30	30	0	0.39	73	12.7	5.6×10^{-8}
B3						−65	30	0	0.48	73	12.6	5.6×10^{-8}
B15						−112	30	0	0.54	73	12.5	5.6×10^{-8}
B16						−200	30	0	0.60	73	12.3	5.6×10^{-8}
D Thickness of the drainage layer, varied from 1 to 20 cm.												
B18b					1	−65	30	0	0.43	76	12.7	5.6×10^{-8}
B18c					3	−65	30	0	0.45	75	12.6	5.6×10^{-8}
B3					6	−65	30	0	0.48	73	12.6	5.6×10^{-8}
B18a					20	−65	30	0	0.50	73	12.5	5.6×10^{-8}
E Saturated hydraulic conductivity of the drainage layer, varied from 1.0 to 1×10^{-3} cm/s.												
B3		1×10^{-0}				−65	30	0	0.48	73	12.6	5.6×10^{-8}
B19b		1×10^{-1}				−65	30	0	0.48	75	12.6	5.6×10^{-8}
B19a		1×10^{-3}				−65	30	0	0.66	79	12.7	5.5×10^{-8}

Table 31 *continued*

Run	Liner soil	K_s (cm/s)	θ_s	K_s/θ_s	Thickness (cm)	Initial head (cm)	Boundary conditions (head) upper (cm)	lower (cm)	Steady-state time (yrs)	Wetting front depth (cm)	Break through time (yrs)	Flux (cm/s)
F Saturated moisture content of drainage layer, varied from .41 to .50.												
B3			0.41			−65	30	0	0.48	73	12.6	5.6×10^{-8}
B20			0.50			−65	30	0	0.46	72	12.5	5.7×10^{-8}
G Saturated hydraulic conductivity of the base soil (Soil C), varied from 1×10^{-3} to 1×10^{-5} cm/s.												
B21a		1×10^{-3}				−65	30	0	0.48	73	12.6	5.6×10^{-8}
B3		1×10^{-4}				−65	30	0	0.48	73	12.6	5.6×10^{-8}
B21b		1×10^{-5}				−65	30	0	0.48	73	12.6	5.6×10^{-8}
H Saturated moisture content of the base soil (Soil C), varied from 0.20 to 0.49.												
B3			0.49			−65	30	0	0.48	73	12.6	5.6×10^{-8}
B22			0.20			−65	30	0	0.48	73	12.6	5.6×10^{-8}
I Thickness of the base soil (Soil C) and depth to water table, varied from 5 to 200 cm.												
B23a					1	−65	30	0	← failed to converge →			
B23b					5	−65	30	0	0.42	76	12.7	5.6×10^{-8}
B3					12	−65	30	0	0.48	73	12.6	5.6×10^{-8}
B23c					200	−65	30	0	0.68	75	12.5	5.6×10^{-8}
J Pressure at lower boundary varied from 0.0 (water table) to −112.5 (unsaturated) cm.												
B3						−65	30	0	0.48	73	12.6	5.6×10^{-8}
B24a						−65	30	−65	0.52	73	12.5	5.6×10^{-8}
B24b						−65	30	−112.5	0.61	75	12.5	5.6×10^{-8}
K Previous runs repeated, using soil A instead of soil B as the liner soil.												
B3	B			4×10^{-8}		−65	30	0	0.48	73	12.6	5.6×10^{-8}
A9	A			1×10^{-6}		−65	30	0	0.0088	66	0.49	1.5×10^{-6}
A6	A			1×10^{-7}		−65	30	0	0.088	64	4.84	1.5×10^{-7}
A5	A			4×10^{-8}		−65	30	0	0.23	62	12.0	5.9×10^{-8}
A7	A			1×10^{-8}		−65	30	0	0.85	62	47.9	1.5×10^{-8}
A13	A			0.30		−65	30	0	0.28	62	14.4	5.9×10^{-8}
A12	A			0.20		−65	30	0	0.19	62	9.63	5.9×10^{-8}
A15	A					−112	30	0	0.28	62	11.9	5.9×10^{-8}
A16	A					−200	30	0	0.34	62	11.8	5.9×10^{-8}

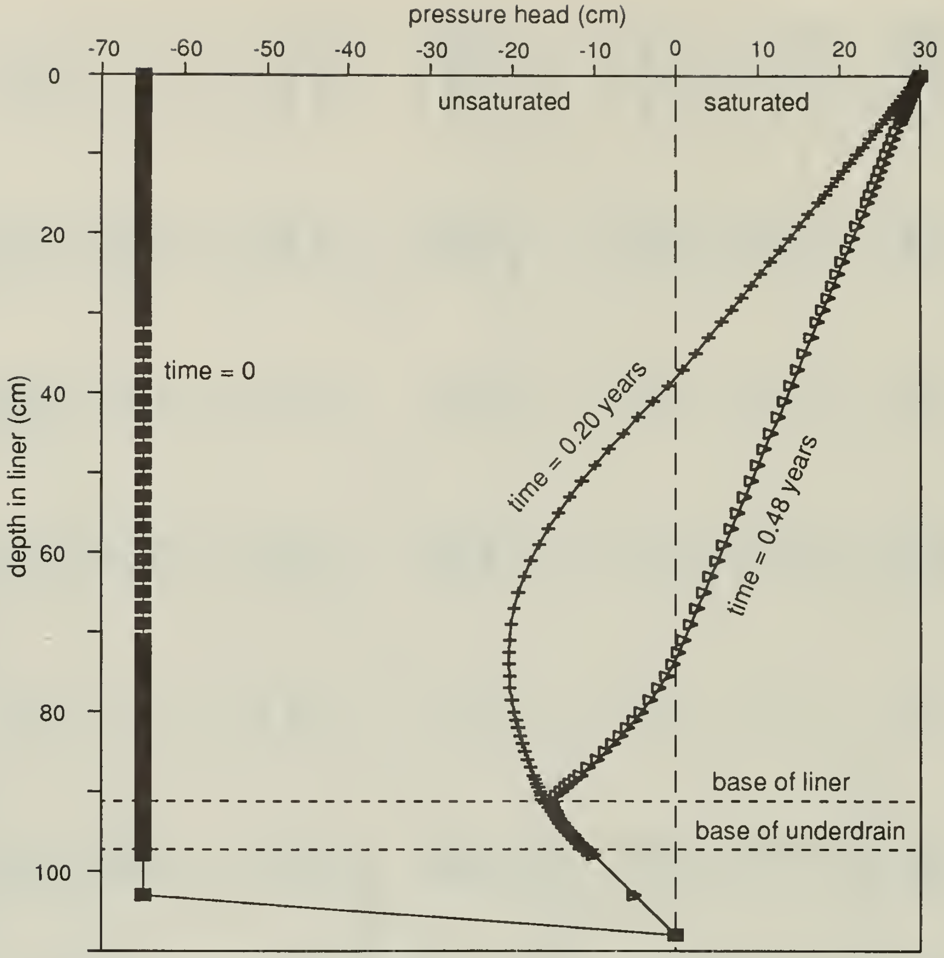

Figure 62 Pressure head as predicted by SOILINER for simulation B3. Steady-state flow was achieved at time = 0.48 years. (Table 31 shows parameter values used in B3.)

were held constant (results are given in table 31). SOILINER simulation number B3 was considered the control for this analysis because the parameters input to that run, using soil B, were the best estimates for the given data. Results were as follows:

- Seven simulations were made using soil B (table 31A), in which the saturated hydraulic conductivity of the liner material was varied from 1×10^{-6} to 1×10^{-9} cm/s. The time required to reach steady state and breathrough, as well as the breakthrough flux, all proved to be sensitive to the hydraulic conductivity value used to represent the liner material. As hydraulic conductivity was decreased, the time required to attain steady state and breakthrough increased, and the flux decreased.

- In four simulations, the saturated soil moisture content of the liner material was varied from 0.15 to 0.30 (table 31B). Predictions of the time to reach steady state and breakthrough were sensitive to this parameter; time increased as saturated moisture content increased.

- Changes in initial pressure of the entire system (table 31C) only slightly affected the predictions of the time to reach steady state and breakthrough. Steady-state and breakthrough times were directly and inversely proportional, respectively, to decreases in the initial soil pressure.

- Model results were relatively insensitive to changes in thickness, saturated hydraulic conductivity, and saturated moisture content of the drainage layer and the lower layer (table 31D-J.)

- The soil-characteristic equation used in the model affected results (table 31K). When soil A was used as the liner soil, and all other parameters were equal to the soil B simulations, the time required to reach steady state was decreased by half, the wetting front depth was reduced from about 73 to about 62 cm, breakthrough time was reduced by about 5 percent, and flux was increased by about 5 percent.

■ Hydraulic Conductivity

The strong correlation between the computed steady-state flux and modeled hydraulic conductivity (fig. 63) allows an alternate method of determining the liner's hydraulic conductivity. Direct measurements of infiltration and gradient have been used to compute a flux value for the liner of 7.1×10^{-8} cm/s. This field-observed flux value may be used with the model results to back-calculate a hydraulic conductivity value. This back-calculation is made by locating the point on figure 63 where the modeled flux is equal to the observed flux, and by finding the corresponding hydraulic conductivity value. Figure 63 indicates that a modeled flux of 7.1×10^{-8} cm/s would require soil B to have a hydraulic conductivity of 5.1×10^{-8} cm/s.

This conductivity calculation assumes that the flux is for a steady-state flow system. In reality, no water has been collected at the base of the liner, so it must be assumed that the liner is not at steady state. The observed flux value is probably higher than it will be when the system reaches steady state because the hydraulic gradient will decrease as the liner becomes increasingly saturated. When this graphical method of determining hydraulic conductivity is used with the lower flux value that should occur after the system reaches steady state, the resulting hydraulic conductivity value will be correspondingly lower.

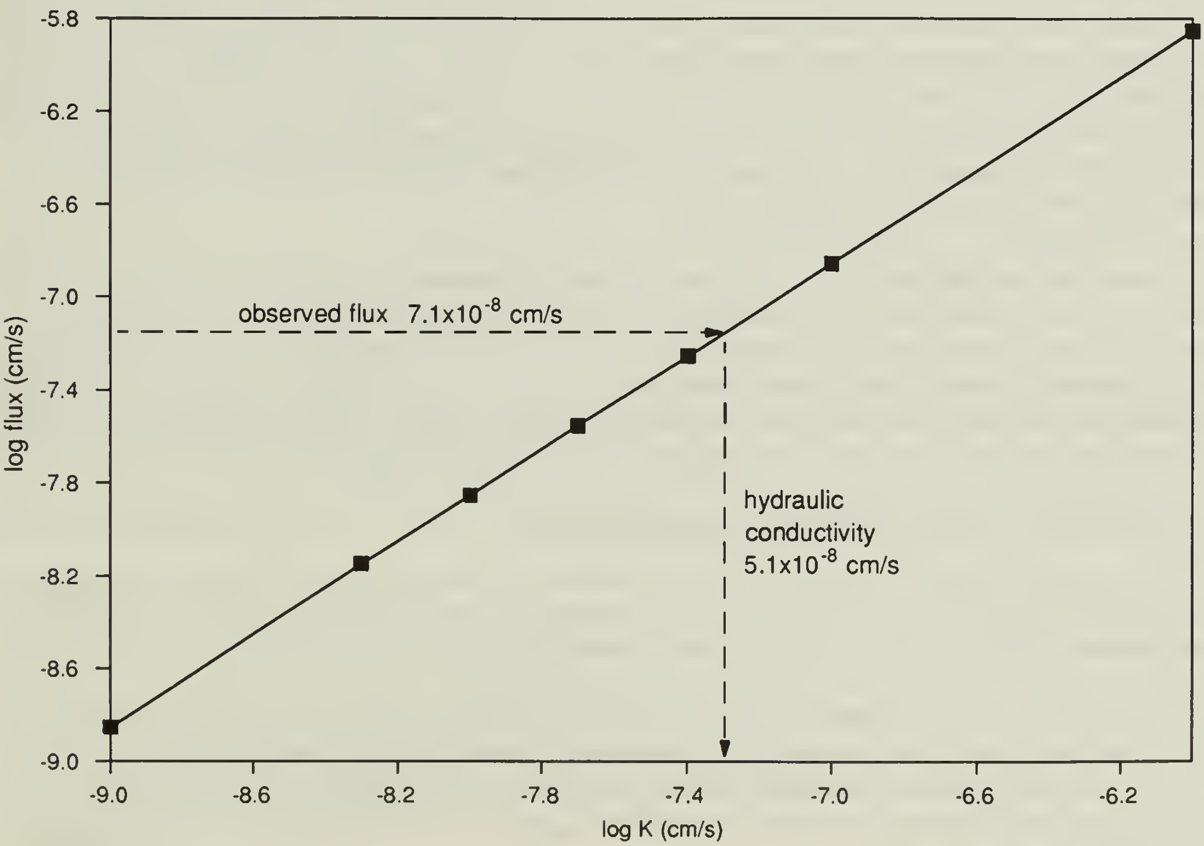

Figure 63 Predicted flux as a function of hydraulic conductivity for SOILINER soil B. The linearity of this relationship (r^2 = 1.0) allows a determination of hydraulic conductivity from the measured liner flux.

Table 32 CHEMFLO predictions of breakthrough time for a nonadsorbed contaminant flowing through 91 cm of compacted soil.

Run	Diffusion (cm^2/hr)	Dispersivity (cm)	Steady state (yr)	depth (cm)	Breakthrough (yrs) A[1]	Breakthrough (yrs) B[2]	Flux (cm/s)
Control	0.0	0.0	.69	67	10.5	12.4	5.8×10^{-8}
T2	3.6×10^{-4}	9.0	.69	67	3.1	11.2	5.8×10^{-8}
T1	3.6×10^{-3}	9.0	.69	67	2.5	10.9	5.8×10^{-8}
T4	3.6×10^{-3}	4.5	.69	67	3.3	11.3	5.8×10^{-8}
T5	3.6×10^{-3}	2.0	.69	67	3.9	11.5	5.8×10^{-8}
T6	3.6×10^{-3}	0.9	.69	67	4.4	11.7	5.8×10^{-8}
T7	3.6×10^{-3}	0.45	.69	67	4.5	11.7	5.8×10^{-8}
T9	3.6×10^{-3}	0.2	.69	67	4.6	11.7	5.8×10^{-8}
T3	3.6×10^{-3}	0.1	.69	67	10.0	12.4	5.8×10^{-8}

[1] $C/C_0 = 0.001$
[2] $C/C_0 = 0.5$

■ Chemical Breakthrough

The sensitivity of CHEMFLO to flow parameters was not determined because the model was only used to predict transport time through the liner. The SOILINER predictions of transport time are large because it only predicted C/C_o = 0.50 for a nondispersed, nondiffused contaminant. CHEMFLO allowed dispersion and diffusion parameters to be included, and also determined breakthrough concentrations other than C/C_o = 0.50.

For this analysis, the flow boundaries of CHEMFLO were set so that flow would be similar to that predicted by SOILINER in simulation B3. The time at which steady state is reached (0.69 years) and the depth of the wetting front predicted by CHEMFLO (67 cm) differed from the time and depth predicted by SOILINER (0.48 years and 73 cm) by more than 5 percent; however, the fluxes (5.8×10^{-8} cm/s and 5.6×10^{-8} cm/s, respectively) predicted by the two models were within 5 percent. When dispersion and diffusion values were set at 0.0, the CHEMFLO breakthrough time for C/C_o = 0.50 was within 5 percent of breakthrough time (12.4 and 12.6 years, respectively) predicted by SOILINER.

The results of the CHEMFLO runs are listed in table 32. When dispersion and diffusion values were set at 0.0, breakthrough (defined as C/C_o = 0.001) occurred 10.5 years after ponding. When a relatively high dispersivity value of 9 cm was used, breakthrough occurred between 2.5 and 3.1 years, and breakthrough concentrations of C/C_o = 0.50 occurred at 10.9 to 11.2 years, depending on the diffusion coefficient. For all dispersivity values greater than 0.1 cm, the time for breakthrough was estimated to be 2.5 to 4.6 years after ponding.

■ Comparison of Model Results to Observed Data

The ultimate test for any model is its ability to reproduce observed data. Table 33 lists model predictions and observed values for flux, time required to reach steady state, time required for breakthrough (C/C_o = 0.001) to occur, and hydraulic gradient.

The flux and hydraulic gradient predictions agree reasonably well with observed data. As the liner system approaches steady state, the observed flux will probably decrease, becoming closer to the modeled flux. The agreement of modeled flux and gradient to observed data indicates that the saturated hydraulic conductivity value of 4×10^{-8} cm/s used in the model is a valid estimate for the liner.

Table 33 Comparison of computed flux, hydraulic gradient, steady state, and breakthrough to observed values. Computed values are from SOILINER run B and its CHEMFLO equivalent.

	Modeled	Observed
Flux (cm/s)	5.6×10^{-8}	7.1×10^{-8}
Hydraulic gradient	1.45	1.4–1.7[1]
Steady state (time in years)	0.48	[2]
Breakthrough (time in years)	2.5–4.6	[2]

[1] gradients since August 1988.
[2] has not occurred.

The model apparently fails in its prediction of the time required for steady state to be reached. Steady state is achieved in the model well before it has occurred in the liner, a fact suggesting that one or more model parameters may be in error. When the soil B moisture characteristic curve was used in the model, realistic increases in saturated moisture content and decreases in initial pressure head could not cause the model to predict a time of more than 1 year to reach steady state. A longer time to reach steady state could be predicted only if the hydraulic conductivity were reduced. However, the saturated hydraulic conductivity value used in the model appears to be accurate because both the flux and hydraulic gradient agree closely with the gradient observed in the liner. Therefore, an error in the calculation of the unsaturated hydraulic conductivity is probable; it may be due to an error in calculation of the soil-moisture characteristic curve and/or to entrapped air in the liner.

A soil-moisture characteristic curve error could be attributed to either of two causes: (1) the soil from the prototype liner, which the soil B characteristic curve was fitted to, may be different from the soil of the field-scale liner; or (2) the soil B characteristic curve used in the model was a drying curve. Although the liner soil is becoming wetter, the soil B characteristic curve used in the model was generated using parameters determined from a soil that was drying. In the case of hysteresis, for a given tension a soil becoming drier will have a greater moisture content than a soil becoming wetter (Hillel 1982); thus the hydraulic conductivity of the drying soil at that pressure is greater than the hydraulic conductivity of the wetting soil. In this case, at any given tension, the unsaturated hydraulic conductivity value used by the model was too large because the model used a drying curve. Unfortunately, a wetting soil characteristic curve was not determined for the liner soil (see chapter 4) so this case could not be modeled.

Entrapped air in the liner might also account for the lower unsaturated hydraulic conductivity in the liner in comparison with the model calculated value. In this case, two nonfluids or slowly mixing fluids (air and water) exist in the liner, each with its own apparent hydraulic conductivity. If part of the pore volume otherwise available for water flow is occupied by air, the apparent hydraulic conductivity of water is less than if entrapped air was not present.

Summary

Fluid flow in a liner and drainage layer has been numerically simulated using the one-dimensional unsaturated flow and transport models, SOILINER and CHEMFLO. These models demonstrate that the flux through the liner is sensitive to the hydraulic conductivity of the liner material. Comparison of the observed flux to model calculated fluxes and corresponding hydraulic conductivities indicated that the gradient-flux-based hydraulic conductivity value of 4×10^{-8} cm/s is reasonable.

Modeled flux and gradient values were comparable to the flux and gradient observed in the liner. However, the model predicted steady state by 0.5 years, whereas the liner had not achieved steady state after an interval of more than 1 year after ponding. Most of this difference probably can be attributed to the use of a drying soil-moisture characteristic curve in the model rather than a wetting curve.

SOILINER cannot give realistic predictions of chemical movement because it does not use transport parameters such as dispersion, diffusion, and attenuation. Thus, it is difficult to determine any meaningful solute transport results with SOILINER.

Breakthrough predicted with CHEMFLO occurred between 2.5 and 4.6 years. Because the liner has not been ponded for that length of time, we cannot judge the applicability of the model prediction to the liner.

Groundwater flow models are effective tools because the results may show areas in which data are inadequate. The SOILINER simulations of moisture movement through the liner have demonstrated that we do not fully understand the relationship of hydraulic conductivity to tension in the liner. However, the model has confirmed that our value of saturated hydraulic conductivity was reasonable, given the observed gradient and flux values.

REFERENCES

Acar, Y. B., and S. D. Field, 1983, Organic leachate effects on the structural stability and hydraulic conductivity of clay liners (proposal): Louisiana State University, Baton Rouge, LA., 11 p.

Albrecht, K. A., and K. Cartwright, 1989, Infiltration and hydraulic conductivity of a compacted earthen liner: Ground Water, v. 27, p. 14-19.

Albrecht, K. A., B. L. Herzog, L. R. Follmer, I. G. Krapac, R. A. Griffin, and K. Cartwright, 1989, Excavation of an instrumented earthen liner: Inspection of dyed flow paths and soil morphology: Hazardous Waste and Hazardous Materials, v. 5, p. 269-279.

American Society for Testing and Materials, 1982, Standard method of laboratory determination of moisture content of soil, *in* Annual Book of ASTM Standards, Part 19, Soil and Rock; Natural Building Stones: American Society of Testing and Materials, Philadelphia, PA, p. 347-350.

American Society for Testing and Materials, 1991, Annual book of ASTM standards, Section 4: Construction, Volume 4.08: Soil and Rock; Building Stones; Geotextiles: American Society of Testing and Materials, Philadelphia, PA. 1155 p.

Anderson, J. L., and J. Bouma, 1973, Relationships between saturated hydraulic conductivity and morphometric data of an argillic horizon: Soil Science Society of America, Proceedings, v. 37, p. 408-413.

Bear, J., 1972, Dynamics of fluids in porous media: American Elsevier, New York, p. 764.

Bianchi, W. C., and E. E. Haskell, Jr., 1966, Air in the vadose zone as it affects water movement beneath a recharge basin: Water Resources Research, v. 2, p. 315-322.

Biggar, J. W., and D. R. Nielsen, 1960, Diffusion effects in miscible displacement occurring in saturated and unsaturated porous materials: Journal of Geophysical Research, v. 65, p. 2887-2895.

Biggar, J. W., and D. R. Nielsen, 1962, Miscible displacement: II. Behavior of tracers: Soil Science Society of America, Proceedings, v. 26 p.125-128.

Bowman, R. S., 1984a, Evaluation of some new tracers for soil water studies: Soil Science Society of America Journal, v.48, p. 987-993.

Bowman, R. S., 1984b, Analysis of soil extracts for inorganic and organic tracer anions via high performance liquid chromatography: Journal of Chromatography, v. l285, p. 467-477.

Brown, K. W., and D. C. Anderson, 1982, Effects of organic solvents on the permeability of clay soils (draft report): Texas A&M University, Texas Agricultural Experiment Station, College Station, TX, 153 p.

Bumb, A. C., C. R. McKee, J. M. Reverand, J. C. Halepaska, J. I. Drever, and S. C. Way, 1984, Contaminants in groundwater: Assessment of containment and restoration option: Conference of Management of Uncontrolled Hazardous Waste Sites, Hazardous Materials Control Research Institute, Washington, DC, p. 378-414.

Campbell, G. S., 1974, A simple method for determining unsaturated conductivity from moisture retention data: Soil Science, v. 117, p. 311-314.

Carter, M., and Bentley, S. T., 1986, Practical guidelines for microwave drying of soils: Canadian Geotechnical Journal, v. 23, p. 598-601.

Cartwright, K., T. H. Larson, B. L. Herzog, T. M. Johnson, K. A. Albrecht, D. L. Moffett, D. A. Keefer, and C. J. Stohr, 1988, Trench Covers to Minimize Infiltration at Waste Disposal Sites: Illinois State Geological Survey, Champaign, IL, Circular 541, 88 p.

Chen, H. W., and L. O. Yamamoto, 1987, Permeability tests for hazardous waste management unit clay liners, *in* D.J.A. van Zyl, S. R. Abt, J. D. Nelson, and T. A. Sheppard (editors), Geotechnical and Geohydrological Aspects of Waste Management: Lewis Publishers, Chelsea, Michigan, p. 229-244.

Christiansen, J. E., 1944, Effects of entrapped air upon the permeability of soils: Soil Science, v. 58, p. 355-365.

Cislerova, M., J. Simunek, and T. Vogel, 1988, Changes of steady-state infiltration rates in recurrent ponding infiltration experiments: Journal of Hydrology, v. 104, p. 1-16.

Clapp, R. B., and G. M. Hornberger, 1978, Empirical equations for some soil hydraulic properties: Water Resources Research, v. 14, p. 601-604.

Cogley, D. R., D. J. Goode, and C. W. Young, 1984, Review of the transit time equation for estimating storage impoundment bottom liner thickness: Appendix A, *in* A. J. Goode and P. A. Smith: U.S. Environmental Protection Agency, Cincinnati, OH, EPA/530-SW-84-001, p. A-1 to A-32.

Daniel, D. E., 1981, Problems in predicting the permeability of compacted clay liners: Symposium on Uranium Mill Tailings Management, Fort Collins, CO, p. 665-675.

Daniel, D. E., 1984, Predicting hydraulic conductivity of clay liners: Journal of Geotechnical Engineering, v. 110, p. 285-300.

Daniel, D. E, D. C. Anderson, and S. S. Boynton, 1984, Fixed-wall vs. flexible-wall permeameters: Journal of Geotechnical Engineering, v. 110, no. 2, p. 285-300.

Daniel, D. E., and S. J. Trautwein, 1986, Field permeability test for earthen liners, *in* S. P. Clemence (editor), Use of In Situ Tests in Geotechnical Engineering: American Society of Civil Engineers, New York, NY, p. 146-160.

Daniel, D. E., 1987, Earthen liners for land disposal facilities, *in* Geotechnical Practice for Waste Disposal, ASCE Specialty Conference, Proceedings, GSP No. 13 ASCE, New York, NY, p. 21-39.

Daniel, D. E., and K. W. Brown, 1988, Landfill liners: How well do they work and what is their future? *in* J. R. Gronow, A. N. Schofield, and R. K. Jain, Land Disposal of Hazardous Waste: Ellis Horwood Limited, West Essex, England, p. 235-244.

Dunn, R. J., and J. K. Mitchell, 1984, Fluid conductivity testing of fine-grained soils: Geotechnical Engineering, v. 110, no. 11, p. 1648-1665.

Elsbury, B. R., G. A. Sraders, D. C. Anderson, J. A. Rehage, J. O. Sai, and D. E. Daniels, 1990, Field and laboratory testing of a compacted soil liner: U.S. Environmental Protection Agency, Risk Reduction Engineering Laboratory, Cincinnati, OH, EPA/600/S2-88/067, 139 p.

Ely, R. L., G. L. Kingsbury, M. R. Branscome, L. J. Goldman, C. M. Northeim, J. H. Turner, and F. D. Mixon, 1983, Performance of clay caps and liners for disposal facilities (draft): Grant 68-03-3149 to Research Triangle Institute, U.S. Environmental Protection Agency, Cincinnati, OH, 292 p.

Englund, E., and A. Sparks, 1988, GEO-EAS (Geostatistical Environmental Assessment Software) Users Guide: U.S. Environmental Protection Agency, Environmental Monitoring Systems Laboratory, Las Vegas, NV, EPA/600/4-88/033A, 119 p.

Freeze, R. A., and J. A. Cherry, 1979, Groundwater: Prentice-Hall, Englewood Cliffs, NJ, 604 p.

Foreman, D. E., 1984, The effects of hydraulic gradient and concentrated organic chemicals on the hydraulic conductivity of compacted clay: M.S. thesis, University of Texas at Austin, 346 p.

Gardner, R., 1955, Relation of temperature to moisture tension of soil: Soil Science, v. 79, p. 257-265.

Gatewood, J. S., T. W. Robinson, B. R. Colby, J. D. Hem, and L. C. Halpenny, 1950, Use of bottomland vegetation in lower Safford Valley, Arizona: U.S. Geological Survey, Water Supply Paper 1103, 210 p.

Green, W. H., and G. A. Ampt, 1911, Studies on soil physics: I. Flow of air and water through soil: Journal of Agricultural Science, v. 4, p. 1-24.

Guy, H. P., 1969, Laboratory theory and methods for sediment analysis, *in* Techniques of Water-Resources Investigations of the United States Geological Survey, Book 5, Chapter C1: United States Printing Office, Washington, DC.

Herzog, B. L., and Morse W. M., 1986, Hydraulic conductivity at a hazardous waste disposal site: Comparison of laboratory and field determined values: Waste Management and Research, v. 4, p. 177-187.

Hillel, D., 1982, Introduction to soil physics: Academic Press, New York, 364 p.

Horton, R., M. L. Thompson, and J. F. McBride, 1985, Estimating transit times of noninteracting pollutants through compacted soil materials: Eleventh Annual Research Symposium on Land Disposal of Hazardous Waste, Proceedings, U.S. Environmental Protection Agency, Cincinnati, OH, EPA/600/9-85/013, p. 275-282.

Hughes, R. E., and Warren, R. L., 1989, Evaluation of the usefulness of earth materials by X-ray diffraction, *in* R. E. Hughes and J. Bradbury (editors), The 23rd Annual Forum on the Geology of Industrial Minerals, Proceedings: Illinois State Geological Survey, Champaign, IL, Illinois Minerals 102, 105 p.

Jackson, M. L., 1958, Soil Chemical Analysis: Prentice-Hall, Englewood Cliffs, NJ, p. 65-66.

Johnson, R. A., E. S. Wood, R. J. Wood, and J. Wozmak, 1986, SOILINER model-documentation and user's guide (version 1): U.S. Environmental Protection Agency, Office of Solid Waste, Cincinnati, OH, Public Comment Draft, EPA/530-SW-86-006, 193 p.

Journel, A. G., and C.J. Huijbregts, 1978, Mining geostatistics: Academic Press, 600 p.

King, L. G., 1965, Description of soil characteristics for partially saturated flow: Soil Science Society of America Journal, v. 29, p. 359-362.

Kitanidis, P. K., 1986, Geostatistics in ground water analysis: Applied estimation of spatial functions, *in* Short course on Stochastic and Geostatiscal Analysis in Ground Water Modeling, Notes, September 15-19, 1986: International Ground Water Modeling Center, Indianapolis, IN, 80 p.

Lade, P. V., and Nejadi-Babadai, H., 1976, Soil drying by microwave oven (section 1): American Society for Testing and Materials, Special Technical Publication 599, p. 320-340.

Lambe, T. W., 1951, Soil Testing for Engineers: John Wiley and Sons, Inc. New York, 165 p.

Mason, D. D., J. F. Lutz, and R. G. Peterson, 1957, Hydraulic conductivity as related to certain soil properties in a number of great soil groups—sampling errors involved: Soil Science Society of America, Proceedings, v. 21, p. 554-561.

Meyer, A. F., 1960, Effect of temperature on ground-water levels: Journal of Geophysical Research, v. 65, p. 1747-1752.

Mitchell, J. K., and J. S. Younger, 1967, Abnormalities in hydraulic flow through fine-grained soil: American Society for Testing and Materials, Philadelphia, PA, Standard Technical Publication 417, p.106-139.

Mualem, Y., 1978, Hydraulic conductivity of unsaturated porus media-generalized macroscopic approach: Water Resources Research, v. 14, p. 325-334.

Nielson, D. R., J. W. Biggar, and K. R. Ehr, 1973, Spatial Variability in Field-Measured Soil-Water Properties: Hilgardia, v. 42, p. 215-259.

Nofziger, D. L., 1985, Interactive simulation of one-dimensional water movement in soils—user's guide: University of Florida, Institute of Food and Agricultural Sciences, Circular 675, 56 p.

Nofziger, D. L., K. Rajender, and P. Y. Su, 1989, CHEMFLO: One-dimensional water and chemical movement in unsaturated soils: U.S. Environmental Protection Agency, Robert S. Kerr Environmental Research Laboratory, Ada, OK, EPA/600/8-89/076, 106 p.

Norum, D. I., and J. N. Luthim, 1968, The effects of entrapped air and barometric fluctuations on the drainage of porous mediums: Water Resources Research, v. 4, p. 417-424.

Ogata, A., and R. B. Banks, 1961, A solution of the differential equation of longitudinal dispersion in porous media: U.S. Geological Survey, U.S. Government Printing Office, Washington, DC, Professional Paper 411-A, 7 p.

Olson, R. E., and D. E. Daniel, 1979, Field and laboratory measurements of the permeability of saturated and partially saturated fine-grained soils: Permeability and Groundwater Contaminant Transport, Symposium: American Society of Testing and Materials, Philadelphia, 67 p.

Parkin, T. B., Meisinger, J. J., Chester, S. T., Starr, J. L., and Robinson, J.A., 1988, Evaluation of statistical estimation methods for lognormally distributed variables: Soil Science Society of America Journal, v. 52, p. 323-329.

Parlange, J. Y., and Hill, D. E., 1976, Theoretical analysis of wetting front instability in soils: Soil Science, v. 122, p. 236-239.

Peck, A. J., 1960a, The water table as affected by atmospheric pressure: Journal of Geophysical Research, v. 65, p. 2383-2388.

Peck, A. J., 1960b, Change of moisture tension with temperature and air pressure: theoretical: Soil Science, v. 89, p. 303-310.

Priestley, M. B., 1981, Spectral analysis and time series: Academic Press, San Diego, p. 890.

Quigley, R. M., 1990, Clay barriers for mitigation of contaminant impact: Evaluation and design, *in* Volume II—Clay/leachate compatability laboratory and field diffusion: University of Western Ontario, London, Ontario, Canada, 273 p.

Reginato, R. J., and C.H.M. van Bavel, 1962, Pressure cell for soil cores: Soil Science Society of America Proceedings v. 26, p. 1-3.

Rogowski, A. S., 1990, Relationship of Laboratory and Field Determined Hydraulic Conductivity in Compacted Layer: U.S. Environmental Protection Agency, Risk Reduction Engineering Laboratory, Cincinnati, OH, EPA/600-2-90/025, 204 p.

Rogowski, A. S., and D. E. Simmons, 1988, Geostatistical analysis of field hydraulic conductivity in compacted clay: Mathematical Geology, v. 20, p. 423-446.

Rogowski, A. S., 1972, Watershed physics: Soil variability criteria: Water Resources Research, v. 9., p. 1015-1023.

Rowe, R. K., 1990, Clay barriers for mitigation of contaminant impact: Evaluation and design, *in* Volume I—Modeling and its role in the geotechnical design of barriers: University of Western Ontario, London, Ontario, Canada, 300 p.

Roy, W. R., I. G. Krapac, S.F.J. Chou, R. A. Griffin, 1991, Batch type procedures for estimating soil adsorption of chemicals: U.S. Environmental Protection Agency, Technical Resource Document, EPA/530-SW-87-006-F.

Sherald, J. L., Dunnigan, L. P., Decker, R. S., and Steele, R. F., 1976, Pinhole test for identifying dispersive soils: American Society of Civil Engineers, Journal of the Geotechnical Engineering Division, v. 102, no. GT1, p. 69-85.

Smedema, L. B., and P.J. Zwerman, 1967, Fluctuations of the phreatic surface, 1. Role of entrapped air under a temperature gradient: Soil Science, v. 103, p. 354-359.

Smith, R. M., and D. R. Browning, 1942, Persistent water-unsaturation of natural soil in relation to various soil and plant factors: Soil Science Society of America, Proceedings, v. 7, p. 114-119.

Snedecor, J. B., and W. G. Cochran, 1980, Statistical Methods, 7th edition: The Iowa State University Press, Ames, 507 p.

Sobek, A. A., W. A. Schuller, J. R. Freeman, and R. M., Smith, 1978, Field and laboratory methods applicable to overburdens and mine soils: U.S. Environmental Protection Agency, Industrial Environmental Research Laboratory, Cincinnati, OH, EPA-600/2-78-054, 204 p.

Turk, L. J., 1975, Diurnal fluctuations of water tables induced by atmospheric pressure changes: Journal of Hydrology, v. 26, p. 1-16.

U.S. Environmental Protection Agency, 1979, Design and Construction of Covers for Solid Waste Landfills: Municipal Environmental Research Laboratory, Cincinnati, OH, EPA-600/2-79-165, 249 p.

U.S. Environmental Protection Agency, 1985, Introduction to Ground-Water Tracers: Robert S. Kerr Environmental Research Laboratory, Ada, OK, EPA/600/2-85/022, 201 p.

U.S. Environmental Protection Agency, 1987, Hazardous Waste Management System: Minimum Technology Requirements: Federal Register, 40CFR part 264 and 265, v. 52, no. 74, p. 12566-12569.

U.S. Environmental Protection Agency, 1988a, Design, construction, and evaluation of clay liners for waste management facilities: Risk Reduction Engineering Laboratory, Cincinnati, OH, EPA/530-SW-86-007F, 502 p.

U.S. Environmental Protection Agency, 1988b, Lining of waste containment and other impoundment facilities: Risk Reduction Engineering Laboratory, Cincinnati, OH, EPA-600/2-88/052, 711 p.

U.S. Environmental Protection Agency, 1990, Seminars—Design and construction of RCRA/CERCLA final covers: Office of Research and Development, Washington, DC, CERI-90-50, 209 p.

van Genuchten, M. Th., 1980, A closed-form equation for predicting the hydraulic conductivity of unsaturated soils: Soil Science Society of America Journal, v. 44, p. 892-898.

Warrick, A. W., and D.R. Nielsen, 1980, Spatial variability of soil physical properties in the field, *in* D. Hillel (editor), 1980, Applications of Soil Physics: Academic Press, Inc., New York, NY, p. 319-339.

Weeks, O. L., 1986, Liner systems used for the containment of solvents and solvent-contaminated hazardous wastes: Open file report for the Environmental Institute for Waste Management Studies, University of Alabama, Tuscaloosa, AL, p. 28-29.

Willman, H. B., E. Atherton, T. C., Buschbach, C. Collinson, J. C. Frye, M. E. Hopkins, J. A. Lineback, and J. A. Simon, 1975, Handbook of Illinois Stratigraphy: Illinois State Geological Survey, Champaign, IL, Bulletin 95, p. 228-229.

Zimmie, T. F., J. S. Doynow, and J. T. Wardell, 1981, Permeability testing of soils for hazardous waste disposal sites: Tenth International Conference on Soil Mechanics and Foundation Engineering, Stockholm, Sweden, Proceedings, v. 2, p. 403-406.